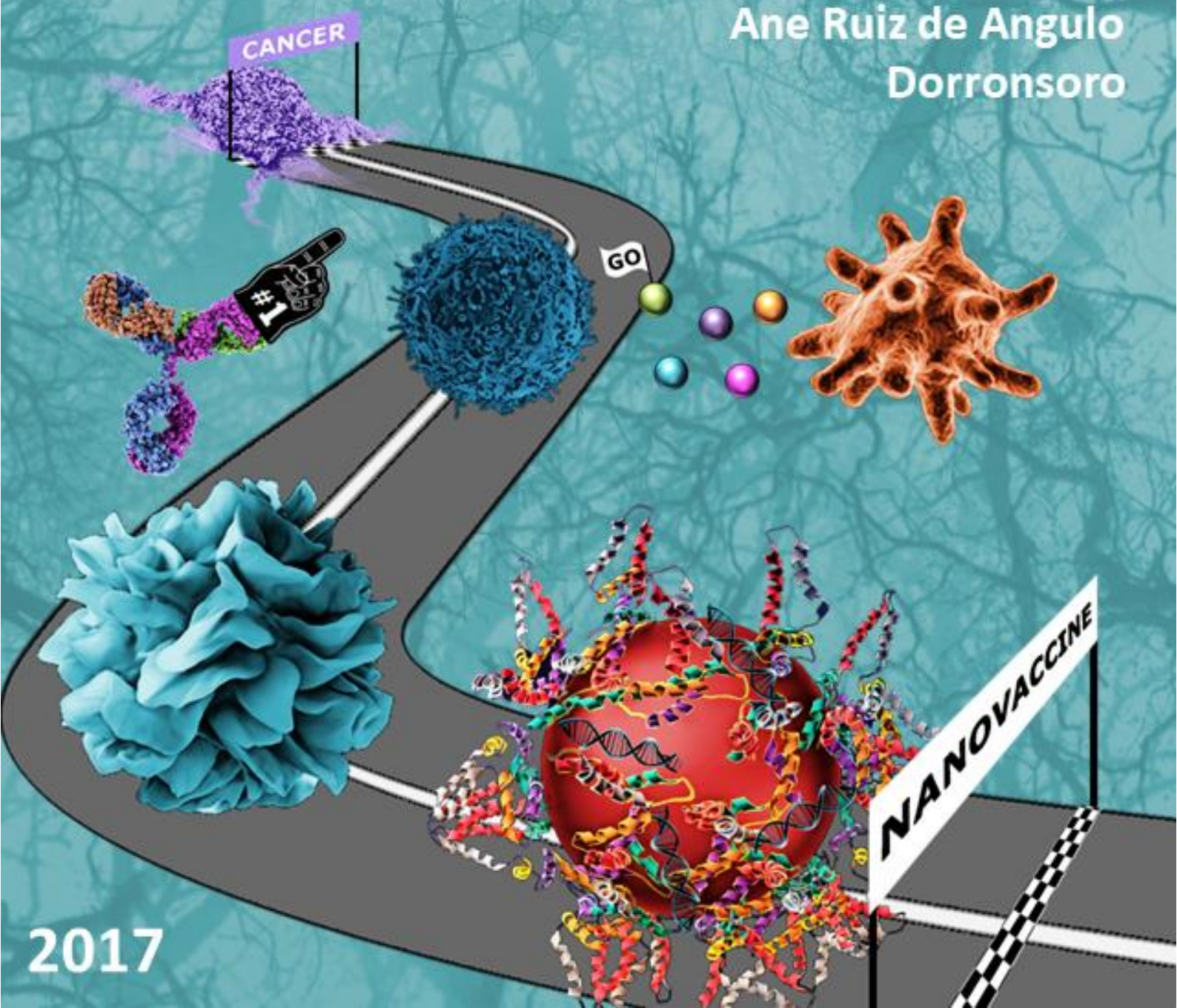


Modular magnetite-filled nanomicelles for multimodal imaging-guided development of effective anticancer vaccines



UPV EHU

Ane Ruiz de Angulo
Dorronsoro




2017

**AUTORIZACION DEL DIRECTOR DE TESIS
PARA SU PRESENTACION**

Prof. Juan Carlos Mareque Rivas con N.I.F.: 33281019-L como Director de la Tesis Doctoral: “Modular magnetite-filled nanomicelles for multimodal imaging-guided development of effective anticancer vaccines”, realizada en el Programa de Doctorado en “Biología Molecular y Biomedicina” por la Doctoranda Doña. Ane Ruiz de Angulo Dorronsoro, autorizo la presentación de la citada Tesis Doctoral, dado que reúne las condiciones necesarias para su defensa.

En San Sebastián, a 18 de mayo de 2017

EL DIRECTOR DE LA TESIS

Fdo.: 

**AUTORIZACION DEL PONENTE DE TESIS
PARA SU PRESENTACION**

Prof. Miguel Ángel Trueba Conde como Ponente de la Tesis Doctoral: “Modular magnetite-filled nanomicelles for multimodal imaging-guided development of effective anticancer vaccines” realizada en el Programa de Doctorado en “Biología Molecular y Biomedicina” por la Doctoranda Doña. Ane Ruiz de Angulo Dorronsoro, y dirigida por el Prof. Juan Carlos Mareque Rivas autorizo la presentación de la citada Tesis Doctoral, dado que reúne las condiciones necesarias para su defensa.

En Bilbao, a 29 de mayo de 2017

EL PONENTE DE LA TESIS



Fdo.: Prof. M. Trueba


**AUTORIZACION DE LA COMISIÓN ACADÉMICA DEL
PROGRAMA DE DOCTORADO**

La Comisión Académica del Programa de Doctorado en “Biología Molecular y Biomedicina” en reunión celebrada el día 10 de mayo de 2017, ha acordado dar la conformidad a la presentación de la Tesis Doctoral titulada: “Modular magnetite-filled nanomicelles for multimodal imaging-guided development of effective anticancer vaccines” dirigida por el Prof. Juan Carlos Mareque Rivas y presentada por Doña. Ane Ruiz de Angulo Dorronsoro adscrita al Departamento de Bioquímica y Biología Molecular.

En Bilbao, a 29 de mayo de 2017

EL MIEMBRO DE LA COMISIÓN ACADÉMICA RESPONSABLE DEL
PROGRAMA DE DOCTORADO

Fdo.:


Prof. M. Yrujo

AUTORIZACION DEL DEPARTAMENTO


El Consejo del Departamento de Bioquímica y Biología Molecular en reunión celebrada el día 30 de mayo de 2017 ha acordado dar la conformidad a la admisión a trámite de presentación de la Tesis Doctoral titulada “Modular magnetite-filled nanomicelles for multimodal imaging-guided development of effective anticancer vaccines” dirigida por el Prof. Juan Carlos Mareque Rivas y presentada por Doña. Ane Ruiz de Angulo Dorronsoro ante este Departamento.

En Bilbao, a 30 de mayo de 2017

VºBº DIRECTOR/A DEL
DEPARTAMENTO

Fdo.: 

SECRETARIO/A DEL
DEPARTAMENTO


Fdo.: JOSE LUIS NIÉVA

ACTA DE GRADO DE DOCTORA
ACTA DE DEFENSA DE TESIS DOCTORAL

DOCTORANDA DOÑA: Ane Ruiz de Angulo Dorronsoro

TITULO DE LA TESIS: "Modular magnetite-filled nanomicelles for multimodal imaging-guided development of effective anticancer vaccines"

El Tribunal designado por la Comisión de Postgrado de la UPV/EHU para calificar la Tesis Doctoral arriba indicada y reunido en el día de la fecha, una vez efectuada la defensa por la doctoranda y contestadas las objeciones y/o sugerencias que se le han formulado, ha otorgado por _____ la calificación de: *unanimidad ó mayoría*

SOBRESALIENTE / NOTABLE / APROBADO / NO APTO

Idioma/s de defensa (en caso de más de un idioma, especificar porcentaje defendido en cada idioma):

Inglés (100 %)

En _____, a ___ de _____ de 2017

EL/LA PRESIDENTE/A,

EL/LA SECRETARIO/A,

Fdo.:

Fdo.:

Dr/a: _____

Dr/a: _____

VOCAL 1º,

VOCAL 2º,

VOCAL 3º,

Fdo.:

Fdo.:

Fdo.:

Dr/a: _____

Dr/a: _____

Dr/a: _____

LA DOCTORANDA,

Fdo.: _____

Modular magnetite-filled nanomicelles for multimodal imaging-guided development of effective anticancer vaccines

PhD Thesis

to obtain the Doctor of Philosophy degree in
Molecular Biology and Biomedicine
at the University of the Basque Country (UPV/EHU)

by

ANE RUIZ DE ANGULO DORRONSORO

Donostia, 2017

Thesis Supervisor: Prof. Juan Carlos Mareque Rivas (Theranostic Nanomedicine laboratory, CIC biomaGUNE)

University Tutor: Prof. Miguel Ángel Trueba Conde (Department of Biochemistry and Molecular Biology, Faculty of Science and Technology, University of Basque Country (UPV/EHU))

Funding Agencies

This thesis was economically supported by Spanish Ministry of Economy and Competitiveness (grants PRI-PIBIN-2011-0812, CTQ2014-54761-R and MAT2013-48169-R), the Department of Industry of the Basque Country (grant ETORTEK) and Gipuzkoako Foru Aldundia (Exp 63/15). The PhD studentship and the stay in the laboratory of Dr. Dennis Christensen at Statens Serum Institut were financed by Department of Education, Language Policy and Culture of the Basque Government.

Table of contents

Abbreviations	i	
Laburpena	iii	
Summary	ix	
Chapter I	Introduction	
1.1.	Immune system as weapon against cancer	3
1.1.1.	Immune system role in cancer suppression and promotion	7
1.1.2.	Cancer immunotherapies	11
1.2.	Constructing anticancer subunit vaccines	16
1.2.1.	Antigen	18
1.2.2.	Adjuvant	19
1.2.3.	Carrier	21
1.3.	Nanomedicine in anticancer therapy	24
1.3.1.	Anticancer therapies using IONPs	25
1.3.2.	State of the art anticancer nanovaccines	26
1.4.	Justification and objectives of this research	30
	References	32
Chapter II	Design, synthesis and characterisation of the PEGylated IONP-filled nanovaccine	
2.1.	Introduction	55
2.1.1.	Physicochemical properties and synthesis of IONPs	55
2.1.2.	Water solubilisation of IONPs	57
2.1.3.	Biofunctionalisation of IONP-filled micelles	59
2.1.4.	Labelling of IONP-filled micelles	60
2.2.	Results and discussion	63
2.2.1.	Synthesis of IONP-based micelles	63
2.2.2.	Attachment strategy of CpG ODNs	64
2.2.3.	Attachment strategy of model antigen OVA	68
2.2.4.	Development of the multimodal imaging contrast agent	72
2.3.	Conclusions	77

2.4.	Supporting information of Chapter II	79
	References	80
Chapter III	<i>In vitro</i> and <i>in vivo</i> trafficking and biodistribution of the constructed nanovaccines	
3.1.	Introduction	87
3.1.1.	Multimodal imaging	87
3.1.2.	Intracellular fate of NPs	89
3.1.3.	<i>In vivo</i> biodistribution of NPs	90
3.2.	Results and discussion	93
3.2.1.	<i>In vitro</i> and <i>in vivo</i> trafficking of the micelles by optical imaging	93
3.2.2.	<i>In vivo</i> biodistribution of the micelles by nuclear imaging	97
3.3.	Conclusions	111
3.4.	Supporting information of Chapter III	112
	References	114
Chapter IV	Application of the designed IONP-filled micelles as anticancer nanovaccines	
4.1.	Introduction	121
4.1.1.	Anticancer immunity	121
4.1.2.	Challenges for enhancing antitumour immunity using NPs	122
4.2.	Results and discussion	127
4.2.1.	<i>In vitro</i> and <i>in vivo</i> immunostimulatory activity of the CpG-IONP micelles	127
4.2.2.	<i>In vivo</i> immunization studies with CpG- and OVA-IONP micelles	131
4.2.3.	Anticancer activity of CpG- and OVA-IONP micelles	141
4.3.	Conclusions	148
4.4.	Supporting information of Chapter IV	150
	References	155
	Summary of results	163
	Experimental section	165
	Acknowledgements	185
	Curriculum Vitae	187

Abbreviations

ADCC	Antibody-dependent cell-mediated cytotoxicity	DSPE-aPEG (2000)	1,2-distearoyl-sn-glycero-3-phosphoethanolamine-N-[amino(polyethylene glycol)-2000]
APC	Antigen-presenting cell	DSPE-cPEG (2000)	1,2-distearoyl-sn-glycero-3-phosphoethanolamine-N-[carboxy(polyethylene glycol)-2000]
AuNP	Gold nanoparticle	EDC	1-Ethyl-3-[3-dimethylaminopropyl]carbodiimide hydrochloride
BCA	Bicinchoninic acid	ELISA	Enzyme-linked immunosorbent assay
BiTE	Bispecific T cell engager	EMA	European medicine agency
BMDC	Bone marrow derived cells	EPR	Enhanced permeability and retention
CpG ODN	Cytosine-phosphate-guanine oligodeoxynucleotide	FDA	Food and drug administration
CTL	Cytotoxic T lymphocyte	FITC	Fluorescein isothiocyanate
DAMP	Damage-associated molecular pattern	ICP-AES	Inductively coupled plasma-atomic emission spectrometry
DCs	Dendritic cell	Ig	Immunoglobulin
DDD	Drug discovery and development	IL	Interleukin
DLS	Dynamic light scattering	INF-γ	Interferon gamma
DNA	Deoxyribonucleic acid	IONP	Iron oxide nanoparticle
DOTA	1,4,7,10-tetraazacyclododecane-1,4,7,10-tetraacetic acid	ISCOM	Immunostimulating complex
DOTAP	1,2-dipalmitoyl-3-trimethylammonium-propane	LN	Lymph node
DPPE-mPEG (2000)	1,2-Dipalmitoyl-sn-glycero-3-phosphoethanolamine-N-[methoxy (polyethylene glycol)-2000]	LPS	Lipopolysaccharide
DPPE-Rho	1,2-dipalmitoyl-sn-glycero-3-phosphoethanolamine-N-(lissaminerhodamine B sulfonyl)	mAb	Monoclonal antibody
		MFI	Mean fluorescence intensity
		MHC	Major histocompatibility complex

Abbreviations

MOF	Metal-organic framework	QD	Quantum dot
MPLA	Monophosphoryl lipid A	RES	Reticuloendothelial system
MRI	Magnetic resonance imaging	RNA	Ribonucleic acid
NHSS	N-hydroxysulfosuccinimide (sodium salt)	siRNA	Small interfering RNA
NK	Natural killer	SLO	Secondary lymphoid organ
NP	Nanoparticle	SPECT	Single-photon emission computed tomography
OVA	Ovalbumin	TAA	Tumour-associated antigen
PAMP	Pathogen-associated molecular pattern	T_{CM}	Central memory T cell
PDI	Polydispersity index	TCR	T cell receptor
PEG	Polyethylene glycol	T_{EM}	Effector memory T cell
PEG-PL	PEGylated phospholipid	TEM	Transmission electron microscopy
PET	Positron emission tomography	Th	T helper
pI	Isoelectric point	TLR	Toll-like receptor
PLGA	Poly(lactic-co-glycolic acid)	TNF-α	Tumour necrosis factor alpha
PO	Phosphodiester	UCNP	Upconverting nanoparticle
PRR	Pattern recognition receptor	VLP	Virus-like particle
PS	Phosphorothioate		

Laburpena

Minbizia gaixotasun bat bera baino, gaixotasun multzo zabal batek osatutako gaixotasuntzat har daiteke. Faktore ezberdinek eragin dezakete gaixotasun honen sarrera, bai kanpo- eta baita barne-faktoreek, alegia. 2012an minbiziak 14 milioi pertsonari erasan zien mundu osoan. Tamalez, tumore bakoitza bakarra eta berezia da, eta honek tratamendu orokor eta eraginkorra aurkitzea erronka zaila bilakatzen du. Gaur egungo terapiak, kimioterapiak eta erradioterapiak kasu, estrategia bakarra erabiltzen dute tumore-zelulen kontra: gehien bikoizten diren zelulei erasotzen diete. Ehun osasuntsuekin alderatuta, zelula gaiztoek hazte-tasa handiagoa dute, eta sentikorragoak dira, beraz, terapia konbentzionalen eraginei. Hala ere, hainbat ehunek bizona osoan zehar hazte-tasa altua mantentzen dutenez, kimio- eta erradioterapiak albo-kalte larriak eragiten dituzte ehun osasuntsu hauengan ere.

Minbiziaren kontrako terapia konbentzional hauen albo-kalte hauek saihestu nahian, ikerkuntzak tratamendu eta terapia alternatiboen bila sakonki dihardu, horien artean immunoterapia. Terapia mota hau immunitate-sistemak berezkoak dituen espezifikotasunaz eta indarrak baliatzen da. Honela, eraso zelula tumoralen kontra zuzentzen da espezifikoki, albo-kalteak murriztuz. Immunoterapia mota ezberdinak garatu dira azken hamarkadetan, bi talde orokorretan sailkatu daitezkeelarik: 1) terapia 'pasiboak', ezaugarri antineoplasikoak dituzten terapiak; eta 2) terapia 'aktiboak', norbere erantzun immunea indartu eta minbiziaren aurka bideratzen dituzten estrategiak. Terapia aktiboen artean, 'txerto subunitarioak' aurkitzen dira, minbiziaren kontrako etorkizun oparoa iragarri dutenak, hain zuzen ere. Txerto mota hauek mikrobio osoa (edo, minbiziaren kasuan, zelula tumoral osoa) inokulatu ordez, zati antigeniko eta adjuvanteak erabiltzen ditu soilik. Formatu subunitario honek txertoa osatzen duen zati bakoitza aldatu eta hobetzeko aukera ematen du, non erantzun immune osoa eta eraginkorra lortzea ahalbidetzen duen.

Antigenoa eta adjuvantea eskuarki garraio-sistemekin batera administratzen dira, molekulak babestu ez ezik, haien efektuak itu-organora hel daitezzen. Orain arte ezagutzen ditugun txerto askok aluminio-gatzak erabiltzen dituzte bi funtzio betetzeko, adjuvante eta garraiatzaile gisa. Substantzia hauek oso eraginkorrak dira antigorputzek

bideratutako erantzun immunea, erantzun humorala delakoa, sustatzeko baina infekzio askoren kontra oso garrantzitsuak diren arren, antigorputzek ez dute minbizien kontrako babesean paper nagusia betetzen immunitate-sistemaren baitan. Hain zuzen ere, ehun tumoralak seinالاتu eta suntsitzeko zelula zitotoxikoetan oinarritutako erantzun immunea da jomuga. Gero eta estrategia berritzaileagoak ari dira agertzen, minbiziaren kontra antigorputz zein zelula zitotoxikoetan oinarritutako erantzun immuneak lortzeko. Ere mu honetan, nanopartikulek minbiziaren kontrako txertoen aukerak izugarri zabaltzen dituzte. Esaterako, nanopartikulak antigeno/adjubanteen garraiatzaile moduan erabiltzeak molekula hauen babesa ziurtatzen du *in vivo* administratzerakoan. Ez hori bakarrik, molekulen efektua bigarren mailako organo linfoideetara (hots, barera eta gongoil linfatikoetara) zuzendua izan daiteke, eta honela aktibazio sistemikoa ekidin eta albo-kalteak gutxitzea lortu. Gainera, nanopartikulen erabilerak beste onura bat du behin itu-organora heltzean: antigeno/adjubanteak hobeto identifikatzea, bertara erraztasun handiagoarekin sartu eta prozesatzen baitira, maila zelularri dagokionez nanopartikuletan erantsita baldin badoaz.

Azkenik, beren propietate fisiko-kimikoei esker, nanopartikulek kontraste-agente gisa joka dezakete. Hori dela eta, irudigintza-teknika ez-inbasiboetan erabil daitezke, erresonantzia magnetiko bidezko irudigintzan (ingelesez, *magnetic resonance imaging* (MRI)) edo irudigintza nuklearrean, esaterako. Aparteko ezaugarri honek farmako berrien aurkikuntza eta garapen-prozesua bizkortu lezake.

Tesi honetan burdin oxidozko nanopartikuletan oinarritutako nona-txertoak diseinatu, garatu eta frogatu dira. Nanopartikula hauek obalbumina (OVA) izeneko antigeno-eredu tumoralarekin eta CpG motiboak dituzten oligodeoxinukleotidoekin (CpG ODN; adjuvante bezala) funtzionalizatu dira. Nanotxerto hauen helburua melanoma-minbizi eredu baten aurkako erantzun immune espezifikoa lortzea da. Molekula immunoestimulatzaile libreekin alderatuz, burdin oxidozko nanopartikulazko nanotxertoak hiru abantaila nagusi ditu:

- 1) Tamaina txikiari (eskala nanometrikoan) esker, txerto hauek sistema linfatikotik bidaiatu dezakete, gongoil linfatikoetan metatuz eta injekzio-lekuan bahituta gelditu gabe.
- 2) Gongoiletara iristean, nanopartikulekin batera administratua izanez gero, antigenoaren aurkezpen gurutzatua areagotu daiteke, T azpimotako CD8 zelulen aktibazioa ahalbidetuz.
- 3) Ezaugarri magnetikoei esker, nanopartikula hauei hainbat ez-ohiko erabilpen ere eman dakizkieke: erresonantzia magnetikoaren kontraste-agente bezala; kanpoko eremu magnetiko bidez gidatuak izan; eta, hipertermia magnetikoaren efektuaren ondorioz, zelula tumoralen suntsitzea.

Cobaleda-Siles eta Gómez-Blanco doktoreek deskonposizio termiko deritzon metodoaren bidez sintetizatutako burdin oxidozko nanopartikulak (6-7 nm) erabili ziren ikerketan. Ekoitzitako produktu hau, guztiz karakterizatuta, izan da tesi honen abiapuntua. Lehenengo pausoa, beraz, nanopartikula hidrofobikoak gaineztatzea izan zen. Horretarako, polietilen glikol izeneko polimero polarra erabili zen. Polimero honi lotuta fosfolipidoak erabili ziren, molekula anfipatiko eta biobateragarria osatuz. Jokabide anfipatiko honek ahalbidetzen du estaldura polimerikoak nanopartikula hidrofobikoekin elkar eragitea, alde batetik, eta, bestetik, ingurune urtsuetan disolbatzea. Honela, burdin oxidozko nanopartikula-mizela beteak sortu ziren.

Estrategia ezberdinak erabili ziren antigenoa mizeletara lotzeko (OVA-mizelak). Batetik, amida-loturak gauzatu, geruza polimerikoaren funtzio taldeak (karboxilo taldea) eta antigenoaren amina taldeak erabiliz horretarako eta, bestetik adsortzio ez-espezifikoak. Adjubantearen kasuan (CpG-mizelak), interakzio elektrostatisak erabili ziren. Horretarako mizelen gainazalean DOTAP lipido kationikoa gehitu zen solubilizazio-prozesuan. Ondorioz, negatiboki kargatutako CpG ODNak burdin oxidozko nanopartikula-mizela beteekin lotzea lortu zen, hauek positiboak baitziren.

Bai antigenoaren eta baita adjubantearen presentzia ere, espektroskopia ultrabioleta-ikusgaiaren bidez frogatu zen. DLS eta TEM teknikek nanotxertoen tamaina 40 nm baino txikiagoa zela erakutsi zuten. Tamaina hau sistema linfatikotik bidaiatzeko ezin hobetzat hartzen da orokorrean, immunitate-sistemaren zelulen laguntzaren beharrik

gabe. Gainera, molekula biologiko hauek gehitu eta gero, mizelen gainazalek karga negatiboa azaldu zuten.

Irudigintza-teknika ezberdinak erabiltzea ezaugarri paregabetzat hartzen da gaur egungo farmakoen garapena sustatzeko. Burdin oxidozko nukleoak nanopartikulen biodistribuzioa MRIren bidez aztertzeke balio duen arren, hori ez zen tesi honetan aztertu. Ordea, beste irudigintza-modalitate batzuk ikertu nahi izan ziren. Helburu hori lortzeko, nanotxerto hauek bi modu ezberdinez markatu ziren. Lehendabizi, fosfolipido bati rhodamina B fluoroforoa gehitu zitzaion. Era honetan mizelen eta zelulen arteko interakzioa aztertu zen. Fluxu-zitometria erabiliz, nanotxerto hauen barneratzea ikusarazi zen makrofagoetan (J774A.1) eta hezur-muinetik hartutako zeluletan (ingelesez, *bone marrow derived cells* (BMDC)). Nanomizelek antigenoa eta adjuvantea zelulen konpartimentu espezifikotara bideratzea lortu zuten, fluoreszentzia mikroskopiak ziurtatu zuen bezala. Adjuvanteak, CpG ODNak alegia, nanomizeletara lotuta zegoen kasuetan euren errezeptorearekin batzea lortu zuen. Ez hori bakarrik, nanotxerto fluoreszente hauek *in vivo* administratzerakoan, barearen zeluletan hobeto barneratu ziren molekula libreekin alderatuta.

Irudigintza optikoa *in vitro* motako esperimenduak gauzatzeko eragingarri izan arren, irudigintza nuklearra *in vivo* motako biodistribuzioa aztertzeke egokiagoa da. Nanopartikulak markatzeko ⁶⁷Ga isotopoa erabili zen, haren ezaugarriak burdinaren antzekoak baitira. Antzekotasun horri esker, nanopartikulak zuzenean markatu ziren, mizelen gainazalean agente kelanteak gehitu behar izan gabe. Nanotxertoen biodistribuzioa aztertzeke fotoi bakarreko tomografia erabili zen. Lortutako irudiek erakutsi zuten nola mizelak gongoil linfatikoetan metatzen ziren. Seinale handiena injekzio-tokian aurkitu arren, gongoil linfatiko hurbil eta distalak argi ikus zitezkeen administratzeatik hiru orduetara ere. Organismoan zehar zirkulazioan dauden molekulak pasiboki metatu ohi dira tumoreetan, haiek duten handitutako erretentzio eta iragazkortasun efektuari esker. Hipotesi hori egiaztatzeke melanoma-minbizi zelulak arratoietan mentatu ziren. Nanotxerto erradioaktiboak injektatu eta gero metaketa pasibo txikia baina argia ikusi zen tumorean. Txertoen presentziak tumorean erantzun inflamatorio ez-espezifikoa aktiba ditzake, immunitate-sistemaren erantzuna areagotuz.

Nanotxertoen kokapena bai *in vitro* eta bai *in vivo* ere ikertu ondoren, nanotxertoen jarduera immunologikoa aztertu zen. Immunitate-sistemako zelulak (J774A.1 eta BMDCaK) CpG-mizelekin inkubatu eta gero, zitokina pro-inflamatorioen sekrezioa areagotu egin zen. Zelula dendritikoen heltzea ere aztertu zen. BMDCaKetik diferentziatutako zelula dendritikoak CpG-mizelekin inkubatzean, heltze-markatzaileen maila eta gongoil linfatikoetara migratzeko gaitasuna areagotu zela frogatu zen. Sortzetiko immunitatea aztertzerakoan aktibazio lokalizatua frogatu zen, hau da, bigarren mailako organo linfoideetako zelulen erantzuna ikustatu egin zen, jarduera sistemikorik aurkitu gabe. Jakina da CpG ODNek zitokina pro-inflamatorioak sistemikoki eragiten dituztela, albo-kalteak eraginez. Horregatik, adjuvantea mizelei lotzeak txertoari segurtasuna ematen dio.

CpG- eta OVA-mizelak arratoiei administratzerakoan IgG2ren produkzioa eragin zen, egungo txertoetan erabiltzen diren adjuvanteek egin ohi ez duten bezala. Antigorputz hau Th1 motako erantzunaren ondorioz ekoizten da, minbiziaren aurkako erantzun ezin hobe, alegia. Erantzun zelularri dagokionez, antigenoaren kontrako T CD8⁺ zelulen ehunekoak gora egin zuen arratoiak CpG- eta OVA-mizelekin immunizatzerakoan. Zelula hauen ahalmen zitotoxikoa areagotu egin zen antigenoa eta adjuvantea mizeletan garraiatzearen ondorioz. Ez hori bakarrik, efektore-fenotipoko T CD8⁺ zelulen ehunekoa ere gehiagotu zen, molekula libreekin konparatuz. Antigenoa aluminio-gatzekin batera erabiltzerakoan, emaitzak ez ziren hain onak izan: IgG2 antigorputzaren produkzioa eta T zelulen eragin zitotoxikoa ez ziren lortu.

Amaitzeko, nanotxerto hauen bidezko minbiziaren suntsipen-gaitasuna aztertu zen, bi esperimentu mota burutuz: profilaktikoa (tumorea garatu baino lehen) eta terapeutikoa (tumorea garatu eta gero). Aipatutako melanoma-zelulek OVA antigenoa espresatzen dutenez, diseinatutako nanotxertoak immunitate-sistema minbiziaren kontra aktibatzeke gai dira.

Ahalmen profilaktikoa aztertzeke, nanotxertoak bi astetik behin administratu ziren (bi injekzio) eta hogeita batgarren egunean minbizi-zelulak injektatu ziren. Nanotxertoekin immunizatutako arratoiek tumorearen haziera eragotzi zuten eta haien biziraupen-tasa handitu zen.

Bestalde, tumoreek tamaina egokia zutenean (zazpigarren egunean) nanotxertoak injektatu ziren hiru administraziotan (zazpi, hamar eta hamahirugarren egunetan). Nanotxertoek tumorearen haziera moteltzea lortu zuten, biziraupen-tasa altua mantenduz. Beste terapia talde guztiek nanotxertoen konbinazioarekin lortutakoak baino emaitza okerragoak erakutsi zituzten.

Laburbilduz, tesi honetan antigeno eta adjubanteen garraio-sistema berria aurkezten da. Garraio-sistema hau burdin oxidozko nanopartikuletan oinarritzen da, material hobeezina izanik minbiziaren aurkako txertoak garatzeko. Diseinatutako nanotxertoak material biobateragarriak erabiliz sintetizatuak izan dira, aplikazio klinikora gerturatuz. Kimika konplexuak erabili gabe, markaketa-protokoloek nanotxertoen jokaera aztertzea ahalbidetu zuten bai *in vitro* eta bai *in vivo*. Beraz, irudigintza optikoen bidez nanosistemek antigenoa eta adjubantea immunitate-sistemako zelulei eramateko duten eraginkortasuna frogatu zen. Bestalde, irudigintza nuklearra erabiliz nanotxertoen biodistribuzioa aztertzea posible izan zen, teknika ez-inbasiboak erabiliz eta gongoil linfatikoetan metatzen zirela frogatuz. Nanotxertoek eragindako erantzun immunea minbiziari aurre egiteko hobeezina azaldu zen, ohiko adjubante eta txertoen erantzuna hobetuz. Antigenoaren aurka gauzatutako erantzunek melanoma-minbizi ereduari aurre egiteko efektu espezifiko eta indartsua azaldu zuten, nanotxertoetan gehitu eta gero. Ondorioz, burdin oxidozko nanopartikula-mizela beteak diseinatuak eta frogatuak izan dira antigeno eta adjubante-molekulak sistema linfatikotik garraia ditzaten. Gongoil linfatikoetara helduz, minbizi-zelulen kontrako erantzun immune optimoa garatzea lortu dute nanotxerto hauek.

Summary

The complexity and heterogeneity of cancer makes the task of finding durable and efficient treatments an extremely difficult challenge. Conventional cancer therapies such as chemotherapy and radiotherapy can cause acute side effects, mainly due to their low selectivity between healthy and malignant cells. To overcome this drawback, many of the strategies have focused on developing drug carriers able to target cancer cells and improve the loaded drug selectivity and accumulation rate in tumours. However, to date this type of approach has not shown the promising results that the research community expected. Since immune cells can proliferate and expand upon receiving activation signals, potent anticancer immune responses can be achieved using low amounts of immunostimulatory drugs. Therefore, by using nanoparticles to target immune cells rather than tumour cells and for programming the immune system to attack the cancer cells it may improve the overall anticancer treatment.

Although immunotherapy is not necessarily a new weapon against cancer, it is only in the last decade when it has gained significant interest and shown clinical success. However, the immunosuppressive environment surrounding tumour tissue can avoid immune surveillance and decrease the efficacy of the immunotherapy. Loading immunostimulatory molecules (i.e.: antigens and/or adjuvants) into nanoparticles provides the opportunity to enhance the co-localisation, biodistribution and release kinetics, improving the efficacy of the therapy. Thus, by combining nanotechnology and immunotherapy in anticancer treatments more effective and durable outcomes may be achieved.

In this thesis, iron oxide nanoparticles (IONPs) are used as platform to display, deliver and track the developed vaccines. The model tumour antigen ovalbumin (OVA) and CpG oligodeoxynucleotide (ODNs), a Toll-like receptor 9 (TLR 9) agonist, were used as antigenic and adjuvant moieties, respectively. The general aim was to develop a modular vaccine platform that could have wide applicability, be easy to make and take advantage of multimodal imaging to visualize its delivery to the target.

Summary

Chapter I describes the functioning of the immune system and its close relation with cancer development. Challenges needed to overcome immunosuppression and the role that nanotechnology can play is also discussed.

In the chapter II, the assembly and characterisation of the developed nanovaccines is described. By using amphiphilic phospholipids linked to polyethylene glycol (PEG-PLs), water soluble and stable IONP-filled micelles were achieved by the ligand addition method. The biomolecules (CpG ODNs and OVA) were attached to the IONP-filled micelles in different ways. CpG ODNs carrying micelles exploited electrostatic interactions using the cationic lipid DOTAP to form a DOTAP/PEG-PLs-based coating that confers the micelles with a positive surface charge and allows the capture of the negatively charged CpG ODNs. The antigen-carrying nanosystems were developed using two different strategies: 1) adsorption to IONP-filled micelles taking advantage of unspecific interactions; and 2) covalent attachment between carboxylic acid groups present in the PEG-PL coating and amine groups of the protein antigen, forming an amide bond mediated by EDC/NHSS linkers. The functionalisation of the IONP-filled micelles with the immunostimulatory molecules was characterised by UV-visible, DLS, TEM and zeta potential studies. Both types of nanoconstructs, i.e., CpG- and OVA-IONP micelles, had small hydrodynamic diameters (<40 nm) and negative surface charges, which are considered optimal properties for draining from the skin directly to the lymph nodes (LNs).

IONPs have been widely used as contrast agents for magnetic resonance imaging (MRI). In this thesis, extra imaging capabilities were included to study the *in vitro* and *in vivo* behaviour of the IONP-filled micelles combining fluorescence studies and nuclear imaging, as described in chapter III. To study the intracellular fate of the IONP-filled micelles by fluorescence microscopy and flow cytometry, a phospholipid modified with rhodamine B was included in the micelle coating process. The studies showed good cellular uptake and co-localisation with the intracellular targets (endosomal compartments expressing TLR 9). Using fluorescently labelled OVA and CpG ODNs, it was possible to observe that IONP-filled micelles improved their uptake by cells of the immune system *in vivo*.

Nuclear imaging studies were carried out next to study the biodistribution of the IONP-filled micelles. ^{67}Ga was used for radiolabelling the nanovaccines and showed high affinity for the iron oxide core. Single-photon emission computed tomography (SPECT) studies demonstrated rapid trafficking of the IONP-filled micelles not only to LNs draining the site of injection but also to more distal LNs in both healthy and B16-F10-OVA tumour bearing mice. A modest tumour accumulation was observed for both CpG- and OVA-IONP micelles.

Finally, in chapter IV, the anticancer application of the developed nanosystems was tested and analysed. In terms of immunological activity, CpG-IONP micelles showed enhanced immunostimulatory activity compared to free CpG ODN molecules in the J774A.1 macrophage cell line and in bone marrow derived cells (BMDCs). Moreover, the maturation status of the dendritic cells (DCs) was enhanced by CpG ODNs carrying IONP micelles, both in terms of maturation marker expression and LN-homing marker levels. The innate immune response was also enhanced by directing the adjuvant to the LNs, inducing the activation of resident DCs and natural killer (NK) cells and avoiding the systemic release of cytokines and widespread immunostimulatory responses elicited by the free adjuvant.

The adaptive immune response was also analysed administering both the antigen- and the adjuvant-carrying nanosystems. The humoral response was enhanced by inducing an IgG subclass switch towards Th1-type responses and IgG2 antibodies. The cell-mediated response was significantly enhanced immunizing mice with CpG- and OVA-IONP micelles (e.g. increased percentage of antigen-specific CD8^+ T cells). Moreover, these T cells showed an effector phenotype and enhanced killing capabilities.

The antitumoural efficacy of the designed IONP-filled micelles was investigated in both the prophylactic and therapeutic vaccination setting in the melanoma tumour model. The prophylactic vaccination conferred protection against tumour growth and increased the survival of mice co-injected with CpG- and OVA-IONP micelles. Administration of the nanovaccines also slowed down the growth of established tumours and prolonged survival.

Summary

In summary, this thesis work has designed, developed and tested a novel IONP-based anticancer vaccine that exploits size-promoted trafficking to LNs to elicit efficient anticancer immunity. By chemistry free fluorescent-labelling and ^{67}Ga radiolabelling, these nanovaccines could be tracked by complementary imaging techniques allowing a better understanding of the designed nanoconstructs.

1

Introduction

1.1. Immune system as weapon against cancer

Cancer is not simply a single disease. It is many diseases with some common themes encompassing diverse types of disorders resulting from abnormal and uncontrolled growth of cells. This aberrant behaviour is an outcome of genetic instability over long periods. Cancer confers to cells changes that extend their lifespan in a non-controlled manner. The nature of these genetic aberrations is diverse (disruption of tumour suppressor genes, overexpression of proto-oncogenes, changes in the genome by insertion of oncogenic virus, etc.), and can be triggered by external substances and events (alcohol, tobacco, sunlight, obesity or the acquisition of chronic infections) or by inherent factors such as age and secretion of certain hormones.¹ This heterogeneity results in tumours having unique characteristics and self-identity, making cancer a disease difficult to classify, treat and defeat.

Although genetic mutations present in tumours are wide-ranging, there is, however, a consensus in classifying the vast catalogue of different genotypes into six main acquired changes that almost all cancer types have in common:²

1. Ability to be independent from external and controlled growth signals;
2. Insensitivity to growth-inhibitory signals coming from the extracellular environment or from intracellular control points;
3. Evasion of programmed cell death, the so-called antiapoptotic capacity;
4. Potential to replicate in an uncontrolled manner;
5. Capability to induce the formation of new blood vessels around the growing tissue, a process known as angiogenesis;
6. Ability to invade other tissues, i.e., to metastasise organs different from the one where malignant cells belong to.

Those are the main processes that a 'normal' or healthy cell must go through in order to achieve a transformed tumour phenotype. As described by Hanahan and Weinberg in 2000, during the progressive transition from healthy cells to malignant derivatives, cells must undergo a multistep process comparable to Darwinian evolution that will confer them alterations in multiple and diverse sites in the genome. This succession of genetic changes can lead to progressive conversion of normal cells into tumour cells

with one or more acquired growth advantages, resulting in more than 100 different types of cancer.^{3,4}

Given the wide genetic heterogeneity that this disease can show, it is not surprising that the development of malignant neoplasms is the second leading cause of death globally, only after cardiovascular diseases.⁵ The most recent data show that the new cases of cancer came to 14.1 million and that 8.2 million died from this disease in 2012 worldwide, and it has been estimated that by 2025 19.3 million people are expected to develop cancer each year.^{6,7} It is obvious that conventional therapies are not effective enough to control tumour growth and that new approaches are needed to explore, support and accelerate the fight against cancer.

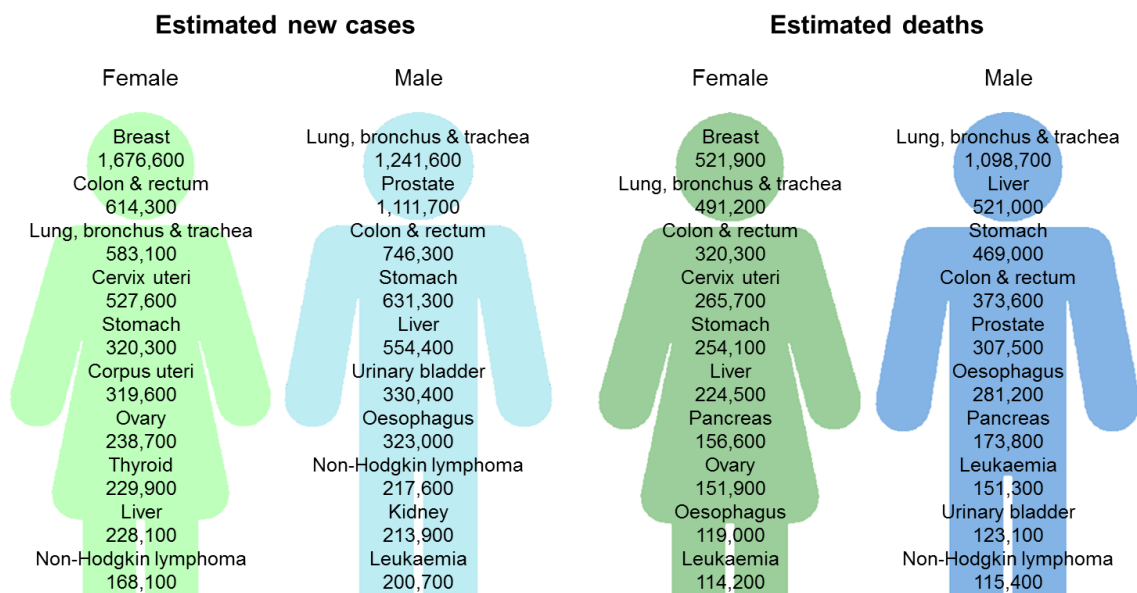


Figure 1.1. Estimated new cancer cases and deaths worldwide for leading cancer sites in 2012. Figure taken from American Cancer Society. *Global Cancer Facts and Figures 3rd edition*. Atlanta: American Cancer Society; 2015. Copyright 2015, American Cancer Society, Inc.

The most common anticancer treatments are surgery, chemotherapy and radiation therapy. Chemotherapy has been intensively used against cancer for decades.^{8,9} However, the conventional therapies rely on the rapid proliferation and uncontrolled growth of tumour cells. In other words, chemo- and radiotherapy take advantage of a natural characteristic such as cell division to attack tumour cells, assuming that the normally growing healthy tissue will be less susceptible to the attack. Still, severe side effects are typically associated with this class of therapies since certain cell types such

as leucocytes, hair follicles and mucosa maintain a high proliferation rate over their whole lifespan.

Another powerful tool in the arsenal of treatments against cancer is immunotherapy. Cancer immunotherapy attempts to harness both the power and specificity of the immune system to attack tumours. It was already used at the end of the 19th century when William B. Coley, the father of cancer immunotherapy, took advantage of the immune system of his patients to treat inoperable tumours.¹⁰ Coley realized that infections after surgery in cancer patients enhanced their antitumour treatment and theorized that the recovery was due to the action of immune system. However, major advances in the field of cancer immunotherapy did not arrive until the early 1980s when the first successful treatments involving the immune system came out. For instance, S. Rosenberg and co-workers demonstrated the existence of cytotoxic leukocytes able to kill autologous tumour cells and R. Levy and colleagues reported the first monoclonal antibody (mAb) for cancer treatment.^{11,12}

Today, there is much better knowledge about basic immunology and more and more information is available about the immune system's response against cancer. For the development of anticancer immunotherapies it is necessary to study and understand the functioning of the immune system (**Figure 1.2**).

A foreign object (e.g. bacteria, virus, etc.) or an abnormal cell contains certain signals that the immune system can detect. Firstly, common features present in microbes or aberrant expressions in cells can activate the early innate immune system in an unspecific manner, evoking a fast and immediate response in which phagocytes like macrophages and neutrophils are activated. On the other hand, professional antigen-presenting cells (APCs), such as the mentioned macrophages, dendritic cells (DCs) or the B lymphocytes are able to recognize and/or phagocyte the foreign object.^{13,14}

The most important APCs are DCs, which have the ability to evoke different immune responses depending on how the antigen is presented on their surfaces. On the one hand, when pathogens are taken up by APCs from the extracellular matrix, they are engulfed by the cell and incorporated into endosomal compartments where, after processing the particular peptides belonging to the pathogen, they will be

incorporated into the major histocompatibility complex (MHC) class II molecules. This class of antigen presenting molecules will specifically bind to the T cell receptors (TCR) present on the surface of $CD4^+$ lymphocytes.^{15,16}

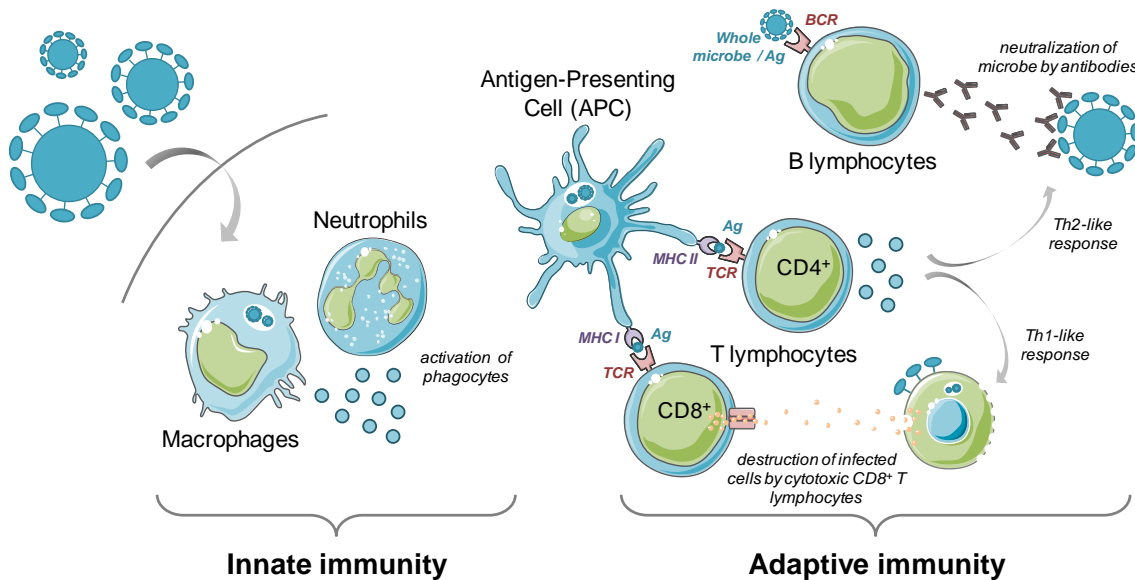


Figure 1.2. Immune response elicited by foreign pathogens. Firstly, cells from the innate system phagocyte the foreign object and produce cytokines in response. APCs are able to present the antigenic parts of the pathogen by two different ways: MHC class II molecules present in APCs specifically binds to the TCR of the $CD4^+$ T cells. Depending on the antigen type, these cells differentiate to Th2- or Th1-type response. The former one helps the B lymphocytes to produce humoral response against the external harm (antibodies) and the Th1-type pattern supports $CD8^+$ T cells. These $CD8^+$ cytotoxic lymphocytes recognise the antigen presented in APCs by MHC class I and, with the help of $CD4^+$ T cells, are able to specifically destroy infected cells.

Depending on the nature of the pathogen (bacteria, fungus, virus, parasite, etc.) and the expression of co-stimulatory molecules by the innate immune cells, these $CD4^+$ T cells can differentiate into two kinds of T helper lymphocytes, Th1- or Th2-type cells, each of which will support different types of immune responses.^{17–20} On the other hand, intracellular pathogens, such as viruses and some bacteria, are detected inside the APCs, processed until proteic fragments are achieved and incorporated into MHC class I molecules. The antigen loaded into the MHC class I is then presented in the cell membrane, allowing it to be recognized by the TCR of $CD8^+$ T cells.^{21–23} This other type of T lymphocytes, in contrast with the $CD4^+$ type, have a cytotoxic function; i.e., once they meet the antigen bound to the MHC class I molecules present in the APCs, $CD8^+$ T lymphocytes are able to specifically recognize and attack cells showing these antigenic moieties. Cells ‘marked’ with foreign antigens can be infected cells or, in the case of anticancer immunity, tumour cells expressing antigenic molecules. The

aforementioned Th1-type response mediated by CD4⁺ T cells supports and enhances this cell-killing activity of cytotoxic CD8⁺ T lymphocytes (CTLs).

Finally, B lymphocytes can also recognize the antigenic molecules present in the pathogens and, with the modulation by CD4⁺ T helper cells, they secrete antibodies specific against the processed antigen. These antibodies are able to neutralise, agglutinate into clumps and precipitate out the pathogenic moieties, pointing out the potentially harmful targets to the phagocytes. All together, the adaptive immunity with the help of the innate response, confer a specific protection that will last the whole lifespan of the individual. Thus, the immune system will remember the already processed microbe (or threat) and will respond much more efficiently to a second infection – in other words, the organism becomes immunized against the specific pathogen.

1.1.1. Immune system role in cancer suppression and promotion

Although a more complete understanding of the immune system and the mechanisms by which the immune system interacts with the tumour is still needed, it is clear that the immune system plays a role in cancer development. For instance, it has been reported that gene knockouts of certain subsets of immune cells, blockade of some cytokines (important molecules in the propagation of immune response, such as interferon gamma (IFN- γ)) and/or disruption of signalling pathways regulating immune responses decreases the chances of tumour rejection.^{24,25} In addition, it has been recently demonstrated that classical anticancer therapies such as chemotherapy and radiotherapy need an intact immune system to effectively induce remission of the tumour.^{26–28} These conventional therapies are thought to stimulate the host's innate and adaptive immunities and sometimes even trigger the activation of long-term T cell responses, which improves the overall efficacy of the treatment.^{29–31} In fact, the groups of G. Kroemer and L. Zitvogel demonstrated in 2007 that chemotherapy and radiotherapy treatment is not effective when administered to immunocompromised mice or when important cell receptors implicated in the immune response are

disrupted or blocked.³² This link between the immune system and conventional anticancer therapies was supported some years later by So and colleagues.³³

Research over the last decades provides confirmation that immune system recognises tumour cells and specifically attacks them.^{34,35} Moreover, there is a consensus about the type of immune response that is needed for cancer treatment. Although antibodies can draw attention to cancer cells and facilitate their elimination by phagocytes,^{36–38} the most efficient attack against tumours is the specific cytotoxic action of CTLs mediated by a robust Th1-type response.^{39–42}

An important question, however, is why the immune system by itself cannot always defeat cancer? Despite having acquired several transformations or mutations that allows them growing without control, tumour cells are still part of the self-tissue so the immune system cannot effectively target them as ‘foreign’ or ‘non-self’. This leads to tumour-tolerance in most of the cases, whereas in infectious diseases the immune system is more clearly alerted and instructed. Thus, some aspects of the tumour cells make them visible to the immune system, such as the mutations that they can gain, while other features can lead to cancer immune tolerance and escape.

The tumour cells are in continuous contact with the immune system during their development, meaning that in the transformation from normal cells to malignant ones the tumour tissue is able to modulate the immunity. This is a well-established theory known as immunoediting, which has been extensively described by Robert D. Schreiber and co-workers.^{43–46} Since the early 1900s when Paul Ehrlich postulated that the immune system is able to both recognise and protect against cancer,⁴⁷ the hypotheses of the immunosurveillance and the immunomodulation (encompassed both in the immunoediting theory) has been widely studied.

Firstly, in late 1950s, M. Burnet and L. Thomas started describing that tumour cells could accumulate antigenic properties able to induce an immunological response and also that cellular immunity was able to preserve tissue homeostasis, eliminating neoplastic cells.^{48,49} Later on, studies in mice showed that tumour cells can elicit anticancer immune responses by themselves and therefore, some molecules on the surface of these tumours must be detected as ‘foreign’ by the immune system. These

antigenic moieties were named tumour-associated antigens (TAAs).^{50,51} Thanks to all these findings, M. Burnet postulated the theory of immunosurveillance and defined it as an evolutionary necessity of the adaptive immune system to protect against cancer development.⁵²

Therefore, the malignant transformation of healthy cells is actually happening under this surveillance. In these circumstances, tumour cells can modulate the immune response and gain more genetic changes to evade this control. An evidence of this phenomenon is that tumour cells developed in mice lacking competent immunity are more immunogenic than tumours grown in immunocompetent animals.⁵³ In other words, the absence of immunosurveillance during tumour development results in malignant cells lacking 'defences' against the immune system's attack. Today, it is known that tumours are edited by their microenvironment, including the immune response against them, and acquire the ability to suppress the immunosurveillance. Under this surveillance of both innate and adaptive immune responses, tumour cells sculpt their immune 'identity' and can end in three possible scenarios, which are interlinked (**Figure 1.3**):

a) Elimination: It occurs when the immune system successfully eliminates the malignant tissue. For this, innate and adaptive immune responses have to be intact and act together towards complete tumour regression. In the first instance, innate immune cells such as phagocytes detect the malignant tissue and are activated, producing pro-inflammatory cytokines such interleukin 12 (IL-12), IL-6 and tumour necrosis factor (TNF- α). As in the case of an intracellular infection, professional APCs are able to take up and process dead tumour cells, fractions or debris, allowing the presentation of specific antigenic moieties of the malignant tissue to the cells regulating adaptive immunity in the draining lymph nodes (LNs). In this way, CD8⁺ T cells become tumour-specific by interacting with tumour antigens presented on MHC class I molecules.⁵⁴ With the help of Th1-type CD4⁺ T cells, cell-mediated immunity can specifically attack the tumour until its total remission.⁵⁵ To achieve complete tumour rejection, this process must be successfully carried out each time that a new antigenic part of the tumour arises. Therefore, due to the immunoediting process itself, tumour

cells can gain additional neoplastic transformations that avoid elimination and allow progressing to subsequent scenarios.

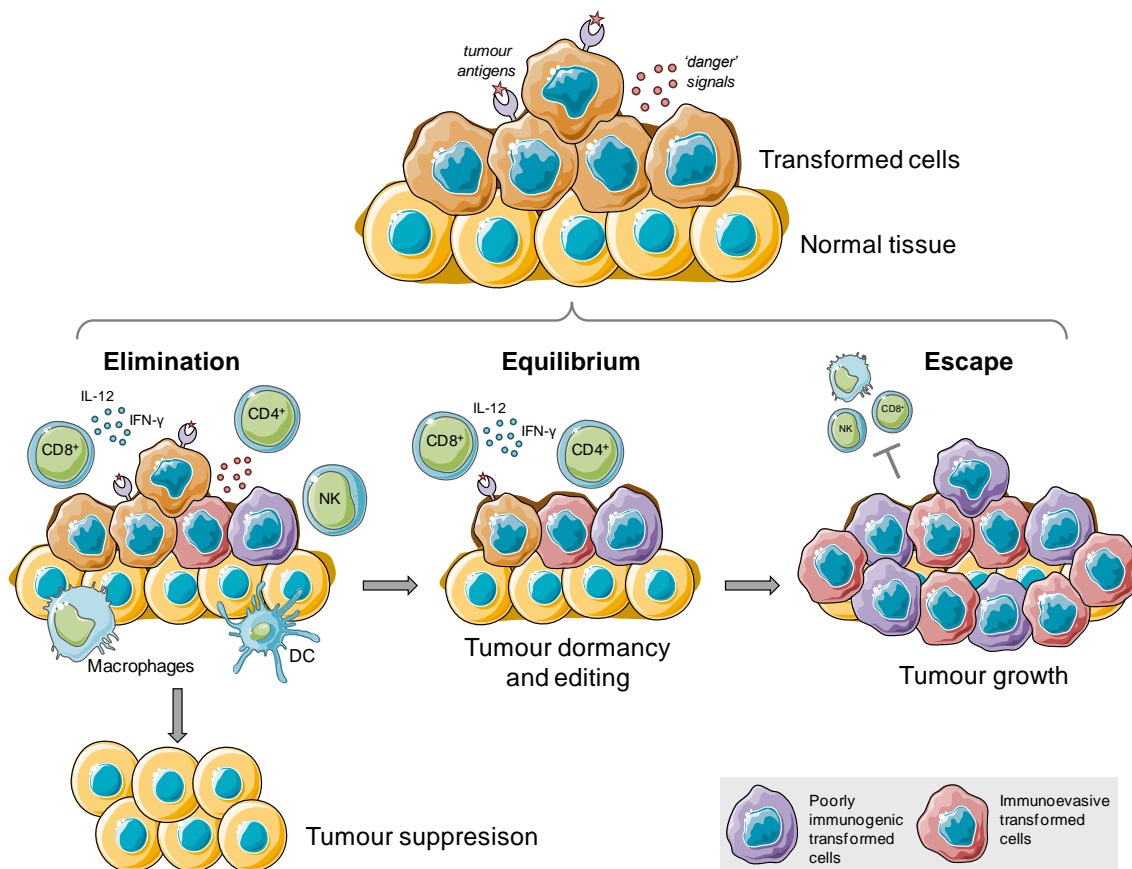


Figure 1.3. Schematic representation of the cancer immunoediting concept. During the transformation process from normal tissue to malignant cells, the immune system can lead to the total elimination of the tumour, which can either reach an equilibrium phase over years or be defeated by the immunosuppression strategies coming from the abnormal tissue. Figure adapted from *Science*, 2011, **331**, 1565.⁴⁵

b) **Equilibrium**: During the elimination phase, tumour cells are subjected to a huge selection force that may result in a malignant variant that has acquired abilities to overcome elimination by the immune system. Therefore, tumour cells that have survived can now start a dynamic equilibrium that will end up in one of the other two phases. In other words, some tumour cells can undergo a Darwinian selection process to finally mutate into variants that can escape from immunosurveillance. This new populations can again be defeated by the immune system, going back to the elimination phase or, in contrast, acquire sufficient mutations and/or enough reduction of immunogenicity to finally escape and grow without control. This latter process is slow, and can last many years until the tumour can finally escape and be clinically detectable.⁵⁶

c) Escape: Finally, when the tumour cells have been immunoedited over the long equilibrium phase, they can reduce their immunogenicity or become resistant to the attack and specific elimination by the immune system. In this final scenario, malignant tissue is able to grow and expand avoiding the assaults of the innate, the adaptive or both types of immunities. The molecular basis of tumour escape include production of immunosuppressive cytokines, activation of immunosuppressive T cells, decrease of tumour recognition by loss of antigen expression or MHC molecules, insensitivity to IFN- γ or evasion from cell-mediated cytotoxicity.⁵⁷⁻⁶² All these characteristics are the product of the wide and diverse interaction over long periods between tumour cells and the immune system.

1.1.2. Cancer immunotherapies

There has been a huge effort towards understanding the mechanisms by which tumour cells can progress through these immune phases and finally escape the immune system's attack. Editors of Science highlighted in 2013 the advances done in the field of immunotherapy as the 'Breakthrough of the Year'.⁶³ During the past 20 years, different approaches have been adopted to develop immunotherapy-based treatments. By using immunotherapy, the side effects of conventional anticancer treatments can be avoided or reduced due to the specificity of the immune system.

Since the mechanisms that cancer uses to evade the host immunity are so diverse and different in nature, there are also multiple possible immunotherapy approaches. The most general classification of cancer immunotherapies is the division between 'passive' and 'active' therapies. Passive immunotherapies are based on intrinsic antineoplastic effects,⁶⁴⁻⁶⁷ such as the tumour-targeting mAbs. Active therapies usually block/activate key processes or molecules harnessing the functioning of host immune system (e.g. anticancer vaccines).⁶⁸⁻⁷¹ As shown in **Figure 1.4**, there is a wide variety of immunotherapies that can be included into each of the two subdivisions:

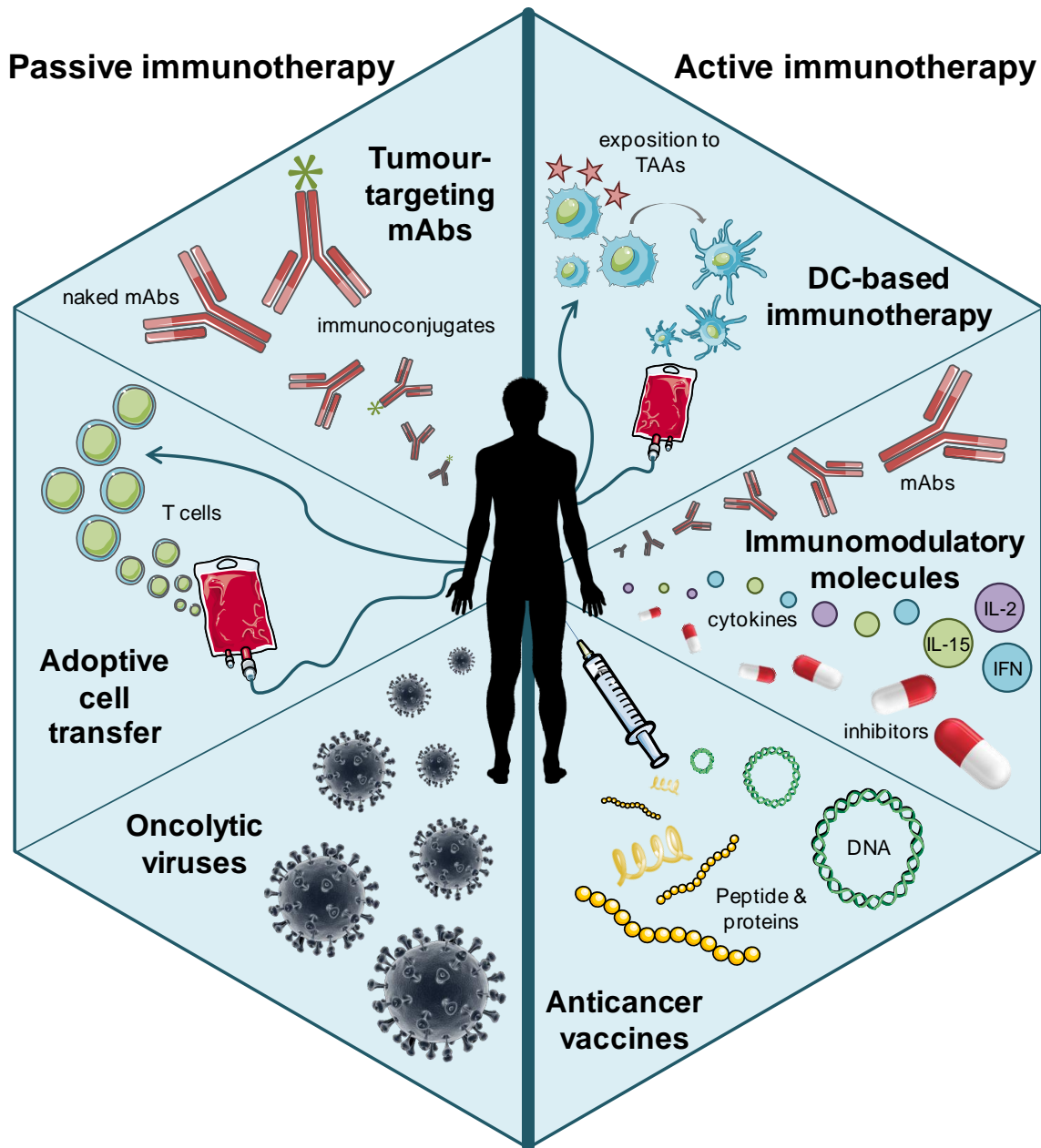


Figure 1.4. Current cancer immunotherapies. The different types of immunotherapeutics developed over the last decades can be divided into two main groups: passive immunotherapies, which include tumour-targeting mAbs, adoptive cell transfer and oncolytic viruses; and active immunotherapies, such as DC-based immunotherapy, immunomodulatory molecules and anticancer vaccines. Figure adapted from *Oncotarget*, 2014, 5, 12472.¹⁰¹

a) Passive immunotherapy:

✓ *Tumour-targeting mAbs:* With a relatively large number of molecules already in clinical use, mAbs are the most widely applied immunotherapy approach,^{72–74} either altering receptors present in tumour cells, neutralizing trophic/development signals or recognizing TAAs.^{75–78} There are at least 5 different types of tumour-targeting antibodies depending on their functionality or the nature of their targets: mAbs able to

block survival pathways in tumour cells;^{79,80} mAbs activators of lethal pathways in malignant cells;^{81,82} mAbs conjugated to toxic molecules able to specifically target tumour cells;^{83,84} mAbs with the ability to target tumour cells and then activate antibody-dependent cell-mediated cytotoxicity (ADCC) by host immunity;⁸⁵⁻⁸⁷ and the antibodies engineered to bind tumour antigens and a T cell-specific molecule, the so-called 'bispecific T cell engagers' (BiTEs).⁸⁸⁻⁹⁰

✓ *Adoptive cell transfer*: This type of therapy consists of transferring modified lymphocytes into a patient, either from autologous or allogenic origin (i.e. from the same patient or from a donor, respectively). The circulating or tumour-infiltrating lymphocytes are extracted, educated and selected *ex vivo* to specifically attack the tumour cells and administered to the patient, alone or in combination with immunostimulatory molecules.⁹¹⁻⁹³ The most successful approaches of this type are based on the transfer of genetically modified T cells endowed with diverse features which include enhanced antigen specificity, augmented proliferation, elevated cytokine secretion, increased tumour-infiltrating ability and more efficient cytotoxicity.^{94,95} It is worth highlighting that although there is no approved adoptive cell transfer procedure for cancer treatment, several clinical trials are currently ongoing.^{66,67}

✓ *Oncolytic viruses*: There have been several successful results employing non-pathogenic viruses with the ability to specifically infect tumour cells and induce their destruction.^{96,97} The mechanisms by which these kinds of viruses can be cytotoxic to tumour cells comprise intrinsic properties of the viral strain or genetic modifications that endow virus with the ability to produce cancer-cell killing compounds.⁹⁸⁻¹⁰⁰ However, so far no approved therapy using oncolytic viruses has been approved for cancer treatment (source <http://www.fda.gov>).

b) Active immunotherapy:

✓ *DC-based immunotherapies*: This kind of immunotherapy refers to the extraction of circulation monocytes from the patient or from a donor, differentiation towards mature DC phenotype and re-infusion to the patient. DCs are *ex vivo* exposed to diverse antigenic fractions of tumour-origin, such as TAA-derived peptides, genetic

material encoding TAAs or tumour cell lysates.¹⁰²⁻¹⁰⁵ Thanks to this exposure, DCs can process and load TAAs *ex vivo* and therefore prime adaptive immune cells once re-infused *in vivo*. Although it is a relatively safe therapy that has been extensively explored over the last two decades, the high cost of the treatment hampers widespread application.^{106,107}

✓ *Immunomodulatory mAbs, cytokines and small molecules:* These types of systems have been extensively applied with clinical useful results. Immunomodulatory mAbs can either 1) block immunosuppressive receptors present in immune cells;^{108,109} 2) inhibit the ligands of these receptors in the tumour cells;¹¹⁰ 3) activate co-stimulatory receptors of immune cells;^{111,112} or 4) neutralize immunosuppressive factors secreted by tumour or immune cells.¹¹³ Immunostimulatory cytokines are mostly employed in combination with other types of (immuno)therapies. For example, cytokines administered with tumour-targeting mAbs can boost their ADCC.¹¹⁴⁻¹¹⁷ Small-molecule inhibitors of the immunosuppressive metabolism can block certain steps of tumour escape pathways.^{118,119} All of these strategies help the host immunity to fight against the rise of malignant cells, alone or in combination with other therapies.¹²⁰⁻¹²⁶

✓ *Peptide- and DNA-based anticancer vaccines:* This type of therapy is based on the administration of TAAs encompassing both full-length proteins and short peptides or TAA-coding DNA constructs in combination with immunostimulatory molecules (the so-called adjuvants) in order to promote DC maturation once injected into the patient. Once administered, DCs take up these vaccines and present the TAA-derived epitopes to induce a potent tumour-specific T cell-based immune response.¹²⁷⁻¹³⁰ Adjuvants employed in combination with TAAs can include oil suspensions, aluminium salts, virosomes or agonist of pattern recognition receptors (PRRs). The administration of PRR agonists is considered as an immunotherapy by itself, as they can have *per se* antineoplastic effects.^{131,132} PRRs are receptors present in the innate immune system cells and are able to recognize a wide variety of 'danger' signals, including 'pathogen-associated molecular patterns' (PAMPs) and endogenous 'damage-associated molecular patterns' (DAMPs). Anticancer vaccines including TAAs and adjuvant moieties such as PAMPs/DAMPs are therefore designed to 'wake up' the

intrinsic host antitumour immunity.^{133,134} Although no TAAs-based vaccines are approved for human use, several PRR agonists are actually employed in anticancer therapy (sources <http://www.fda.gov> and <http://www.ema.europa.eu/ema/>).

This general classification of the possible immunotherapies shows the wide range of processes and pathways that can be targeted in cancer immunotherapy. All of these approaches have as common aim the need to drive tumours towards the elimination phase, helping the host immune system in one way or another. If the tumour has reached the equilibrium phase, the immunotherapy must unbalance again the response until achieving the elimination of cancer cells. In contrast, if tumour escapes from immunity and can be clinically detectable (the most common scenario) the immunotherapy should be able to re-activate the specific response against the escaping tumour towards the elimination phase. In this thesis an anticancer vaccine will be developed. TAAs and PAMP-based adjuvants will be employed as immunostimulatory molecules in order to induce antitumour immunity. Moreover, by tailoring conventional vaccine approaches, more complex and sophisticated immune tools will be designed.

1.2. Constructing anticancer vaccines

As described in the previous section, the immune system is highly prepared and specialised in protecting the host against external pathogenic microbes, where innate immunity provides a first line of defence and an adaptive immunity is able to target the harmful microorganisms in a much more specific and long-term manner. This role of the immune system has been understood since Edward Jenner noted that having contact with a virus specific for other species like the cowpox virus, conferred immune protection against human smallpox without causing severe symptoms.¹³⁵ With this simple observation, the science of the vaccination started in the late 18th century, although it was not until almost 100 years later when the studies of L. Pasteur and R. Koch identified microbes as responsible for causing the disease and its transmission between individuals. The technological advances in the following centuries allowed progressing in vaccination science. The result is that two infectious diseases have been eradicated (smallpox and rinderpest) and twenty-seven can now be successfully avoided by vaccination.

The canonical vaccines used can be broadly defined as a biological preparation able to specifically activate the immune system against a certain disease-causing agent. According to this definition, anticancer vaccines can be developed for inducing immune responses that protect against tumour cell growth. Vaccines can be classified in different groups depending on the type of biological preparation employed.^{136,137} Apart from the conventional vaccine strategies employed for most common infectious diseases (i.e., live attenuated vaccines^{138–141} and killed/inactivated vaccines^{142–145}), there are two main approaches that can be used for constructing anticancer vaccines:

a) Recombinant/DNA vaccines: Similar to the case of the anticancer vaccines, this type of technology refers to the administration of a protein (i.e. an antigen) coded as genetic material. Recombinant vaccines insert the genes encoding the protein or peptides into vectors (usually from viral origin, although also bacteria are used) able to deliver the antigenic parts to the cells of immune system.^{146–149} In contrast, DNA vaccines refer to antigen-coding naked DNA administration or attached to several types of carriers.^{150–153} It is worth noting that several types of recombinant and DNA

vaccines have been evaluated as anticancer vaccines, due to their great capacity to induce strong CTL responses against the expression of TAA encoded in the administered genetic material.^{154–158}

b) Subunit vaccines: This strategy of vaccination is based on the administration of isolated full-length antigens, peptides or antigenic fragments in combination with immunostimulatory moieties, generally carried together by delivery systems.¹⁵⁹ The induced immune response against subunit vaccines will depend not only on the nature of the chosen antigens and adjuvants, but also on the type of carrier. Over the last decades, the subunit vaccine approach has gained significantly in popularity and use, benefiting from the advances obtained in the field of reverse vaccinology (employment of bioinformatics for finding vaccine targets quickly and efficiently) and the improvement in protein production and manufacturing. Subunit vaccines have been employed successfully against several infectious diseases, such as hepatitis B and influenza,^{160,161} and are widely considered promising candidates for constructing anticancer vaccines.^{162–164}

The application of vaccinology to cancer treatment is not straightforward because of the low immunogenicity of tumour cells compared to pathogens. Nevertheless, of these two approaches, the subunit-like strategies allow playing with the different moieties needed for the construction of an optimal anticancer vaccine. By splitting the vaccine up into subunit fractions, it is possible to efficiently choose and optimize each part and even include other technologies such as nanotechnology and molecular imaging to facilitate the drug discovery and development (DDD) process.

In this thesis, an anticancer vaccine inspired in the subunit vaccine strategy will be designed. Hence, developing this anticancer vaccine includes three areas: choosing optimal antigen (or antigens) specific for targeting tumour cells; selecting and improving adjuvants for obtaining potent immune responses; and developing good carrier candidates, which can vary in nature, composition and function (**Figure 1.5**).

Designing the anticancer vaccine

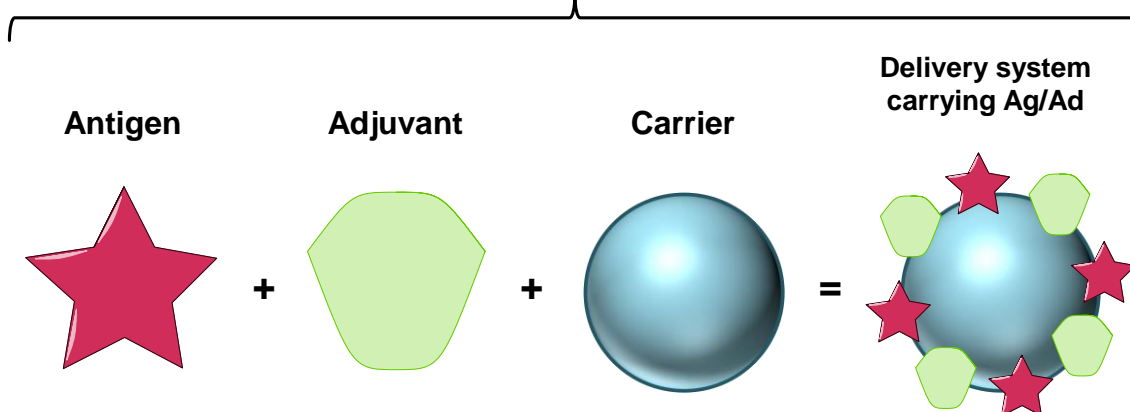


Figure 1.5. Schematic representation of the strategy followed for designing the anticancer vaccine. The anticancer vaccine designed in this thesis is based in the subunit strategy and must include three moieties to induce a potent immune response: antigen, adjuvant and a carrier.

1.2.1. Antigen

The selection of an appropriate antigen is a key aspect for the development of anticancer vaccines. Antigens used in cancer vaccines should preferably be molecules only present or overexpressed on tumour cells. It is known that protein antigens generate T cell-dependent responses, whereas antigenic polysaccharides induce mainly humoral (antibody-based) immunity.¹³⁷ Hence, proteins and peptides are the most common types of antigens in anticancer vaccines.^{165,166} Selection of the antigenic part from a tumour is not an easy task, because antigens presented in a vaccine must fulfil several characteristics, such as tumour-specificity, possibility to use for a wide range of cancer types and easy production and manipulation. Most of the employed TAAs are derived from self-antigens that are overexpressed in tumour cells and, therefore, they are not different enough in order to properly distinguish from healthy tissue. In contrast, tumour proteins harbouring mutations (the so-called neoantigens) have been studied and employed in subunit vaccines.¹⁶⁷⁻¹⁶⁹ Since resolving the problem of the election of optimal TAA is not the main objective of this thesis, the model antigen ovalbumin (OVA) was chosen for testing the efficacy of the developed vaccine. This full-length antigen is the main protein present in egg white and can act as a tumour neoantigen. Its commercial availability and low cost make OVA an ideal candidate for use as model antigenic molecule. Moreover, several OVA-expressing tumour models have been developed specifically to test the efficacy of different

immunotherapy strategies against cancer (based on the Web of Science search (<http://apps.webofknowledge.com>): OVA AND (cancer OR tumor) AND immunotherapy = 358 results for a search conducted on 30 march 2017).

1.2.2. Adjuvant

The immunostimulation elicited by antigens can be modest due to the lack of antigen nonspecific ‘danger’ signals.¹⁷⁰ Adjuvants are incorporated to vaccines in order to promote a more complete and potent immune response against the co-administered antigen.^{171,172} Adjuvants are defined as a wide range of excipients that do not provide immunity themselves, but stimulate the immune system to respond to a defined antigen.¹⁷³

This immunopotentiator effect can be achieved by different approaches including, for example, the presentation of the antigen to immune cells over longer periods, the so-called depot effect. Clear examples of depot effect-causing adjuvants are oil in water emulsions, such as the well-studied Freund’s adjuvant, which is considered the gold standard for adjuvants but is not approved for use in humans due to its side effects (sources <http://www.fda.gov> and <http://www.ema.europa.eu/ema/>). On the other hand, adjuvants such as aluminium salts act as irritants and are able to elicit immunological ‘danger’ signals that potentiate the antigen-derived adaptive immunity. For instance, aluminium hydroxide has been employed for over 70 years in vaccine preparations.^{174,175} Despite eliciting a good Th2-type response (i.e., antibody production-based response optimal for fighting extracellular pathogens), alum-based adjuvants are not able to induce potent cell-mediated immunity (Th1-type response), which is required for an anticancer vaccine.¹⁷⁶

Taking advantage of the nature of the immune system, PAMPs are adjuvants that come from or mimic the immunostimulatory fragments of pathogenic microbes. There is a wide range of PAMPs that differ in the type of immunity that can generate.¹⁷⁷ These molecules are recognized by PRRs present in the immune cells and can be used as agonists to activate the signalling pathways required to elicit optimal immune responses. Among the different types of PRRs, toll-like receptors (TLRs) play an

important role in activating the host defences and in triggering the production of cytokines, essential for the expansion of adaptive immune responses.¹⁷⁸ There are 10 different types of TLRs in humans, which can broadly be classified based on their cellular location, i.e., as cell surface receptors (TLR 1, 2, 4, 5, 6 and 10) or in endosomal-lysosomal compartments (TLR 3, 7/8 and 9).¹⁷⁹ Their location is directly related to the binding specificity. Among the cell surface TLRs, TLR 4 recognizes lipopolysaccharides (LPS) present in the outer membrane of some bacteria and flagellin is recognised by TLR 5. TLR 2 can detect lipoproteins and lipoteichoic acids in combination with TLR 1 and TLR 6, respectively. Since these TLRs are located in the surface of immune cells, they are specialised in recognising extracellular pathogens. On the other hand, intracellular TLR 3, TLR 7/8 and TLR 9 bind specifically to double-stranded RNA, single-stranded RNA and certain type of DNA oligonucleotides, respectively. The location of these last TLRs in the endolysosomes allows them to detect intracellular infections, since the presence of microbial genetic materials inside the cytoplasm is a clear 'danger' signal for innate immune cells. Finally, TLR 10 is involved in anti-inflammatory functions and has not known ligand.

The immunologic perception of tumour cells by host immunity is similar to a disease caused by extracellular pathogens rather than to an intracellular infection. However, the immune response needed to defeat cancer is closer to that induced after an intracellular hazard signal – i.e. the activation of CTLs and the consequent specific killing activity. This specific recognition of 'infected' or 'abnormal' cells is one of the most critical aspects for achieving an effective immune response against cancer and, therefore, adjuvants that activate intracellular PRRs have attracted increasing interest for constructing anticancer vaccines.

DNA sequences with high content in cytosine-phosphate-guanine nucleotides repetitions (CpG sites) are commonly methylated in mammals, but unmethylated in bacterial genomes or viral DNA. These unmethylated CpG motifs are recognized by TLR 9, which is located within the endolysosomal compartments. CpG oligodeoxynucleotides (ODNs) are synthetic short single-stranded DNA molecules mimicking the pathogenic DNA, and are able to specifically activate TLR 9 for promoting rapid and vigorous immune responses against an antigen (**Figure 1.6**).

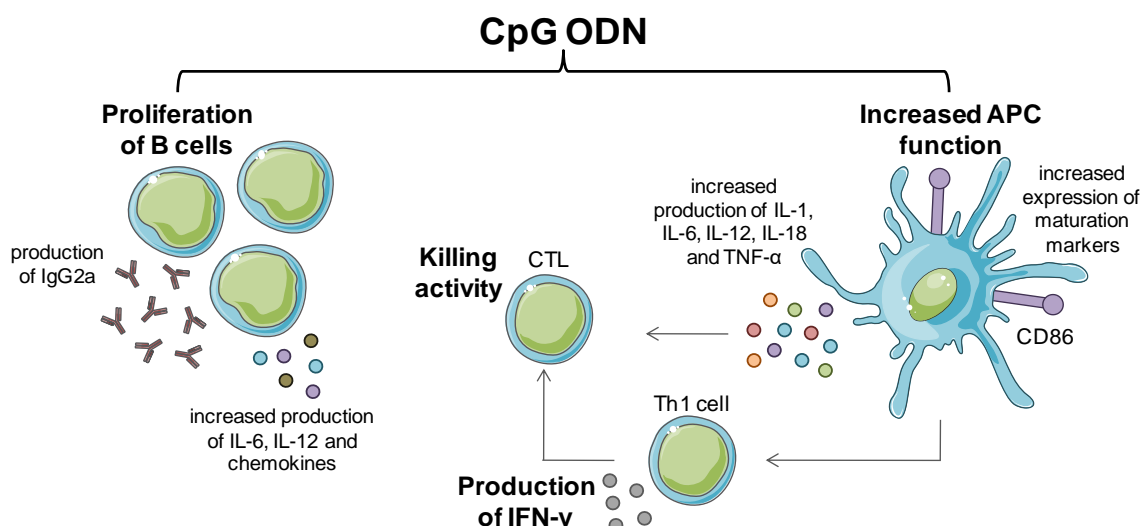


Figure 1.6. Action of CpG ODNs in immune system. CpG ODNs have a direct effect in B cells and in DCs, inducing pro-inflammatory and Th1-type cytokines. This kind of adjuvant enhances B cells proliferation and APC functions by inducing IgG2a isotype production and increased expression of maturation markers, respectively. The created cytokine milieu allows Th1-type cell expansion and CD8⁺ T cell differentiation towards CTLs with killing capacity. Figure adapted from *Nat. Rev. Immunol.*, 2004, **4**, 249.¹⁸⁰

These responses include activation of macrophages, B lymphocytes and DCs with production of Th1-type cytokines (IL-1, IL-6, IL-12, IL-18 and TNF- α) and chemokines. This cytokine pattern allows the differentiation of CD4⁺ naïve T cells towards a Th1-type profile. CpG ODNs are also able to promote activation of antigen-specific CTLs and proliferation of B cells.¹⁸⁰

In this thesis CpG ODNs will be used as adjuvants to induce potent Th1-type, humoral and cell-mediated immune responses, endowing the vaccine with the features to promote antitumour responses.

1.2.3. Carrier

The administration of antigen/adjuvant mixtures by themselves is not an ideal option. Small molecules are rapidly cleared from the circulation and have limited opportunity for targeting the same immune cell subsets. Thus, the use of delivery systems is almost always a necessity when employing antigen/adjuvant molecules. The carriers that have been used for developing vaccines include micro-size particles, virus-like particles (VLP), liposomes, immunostimulating complexes (ISCOMs), polymeric and inorganic nanoparticles (NPs) (Table 1.1).^{181–183}

Table 1.1. Summary and schematic representation of the different types of carriers for developing anticancer vaccines. Table adapted from *Front. Cell. Infect. Microbiol.*, 2013, 3, 13.¹⁸³

	Size range	Load examples (antigen/drug)	Schematic representation
VLPs [Ref. 184–188]	50-200 nm	Human papillomavirus (HPV) Human immunodeficiency virus (HIV) Influenza A virus (H1N1)	
Liposomes [Ref. 189–192]	50-500 nm	<i>Plasmodium falciparum</i> (Malaria) <i>Vibrio cholerae</i> (Cholera) <i>Helicobacter pylori</i> <i>Yersinia pestis</i> (Bubonic plague)	
ISCOMs [Ref. 193–196]	40 nm	Human immunodeficiency virus (HIV) Feline immunodeficiency virus (FIV)	
Polymeric NPs [Ref. 197–200]	100 nm - 5 μm	Docetaxel <i>Clostridium tetani</i> (Tetanus) Hepatitis B virus (HBV) <i>Mycobacterium tuberculosis</i> (Tuberculosis) <i>Corynebacterium diphtheriae</i> (Diphtheria)	
Inorganic NPs [Ref. 201–203]	2-400 nm	Influenza virus Hepatitis B virus (HBV)	

This thesis will use iron oxide nanoparticles (IONPs) as the core of the anticancer vaccine for targeted image-guided co-delivery of OVA and CpG ODNs as new approach to cancer nanomedicine. Hence, next it is briefly reviewed some traditional and emerging nanomedicine approaches in the fight against cancer.

1.3. Nanomedicine in anticancer therapy

The use and tuning of nanomaterials has revolutionized many different fields, among them medicine. Moreover, by taking advantage of the size similarity of nanomaterials to biological structures, nanotechnology can serve important new functions at the life science/human health interface providing new tools to better understand and manipulate the functioning of living organisms. Nanomedicine has become an exciting discipline, which promises to make a difference in diagnosing, treating and preventing diseases using either nanomaterials or nanoscale knowledge of organisms.^{204–208}

NP-based materials have been explored as systems to treat cancer employing diverse approaches (based on the Web of Science search (<http://apps.webofknowledge.com>): nanoparticles AND (cancer OR tumor) = 31 842 articles for a search conducted on 1 April 2017). Some of these nanoscale-sized (<1000 nm) platforms have gained importance as anticancer vaccines due to their stability, controlled load release features, greater uptake by APCs, improved tissue penetration and targeting properties. Therefore, NP-based systems are becoming established as potent new tools for cancer immunotherapy.²⁰⁹

Moreover, it is desirable to combine cancer therapy and diagnosis/imaging using a single agent. It is now widely accepted that to improve the efficiency of the overall DDD process it is also critically important to integrate molecular imaging approaches.^{210–212} Imaging not only streamlines DDD but also allows new opportunities in treatment management of targeted therapies by improving patient selection, predicting response to therapy and/or toxicity, optimization of the duration, dose and schedule of treatment, providing real time biological information and improving early disease detection, disease staging and personalised treatments.^{213–215}

NPs are excellent tools to accomplish the fusion of therapy and diagnosis, known as theranostics. The unique characteristics of certain NPs such as mechanical, magnetic, optical and quantum properties, allow them to be used simultaneously as carrier and as contrast agent in molecular imaging studies.^{216–220} Thus, together with advances in NP-design, synthesis and biofunctionalisation to precisely target and optimize a specific biological response, there is a growing need for incorporating imaging features

in NPs to gain better understanding and predict how they will respond and be processed *in vivo*.

1.3.1. Anticancer therapies using IONPs

IONPs are widely considered the most clinically translatable and versatile material for biomedicine.^{221–223} It has been shown that IONPs present long term *in vivo* biotransformation without inducing severe or even sub-acute toxicity due to the cellular iron metabolism.²²⁴ In fact, several IONP formulations have been approved for use as magnetic resonance imaging (MRI) contrast agents and for treatment of iron deficiency by the US food and drug administration (FDA) and European Medicines Agency (EMA).²²⁵

Besides for imaging, anticancer therapies have used IONPs in different ways (as reviewed by Gallo et al. and Lee et al.).^{226,227} The main use of IONPs in cancer is for improving chemotherapy, for which different approaches have been reported in order to achieve targeted, controlled and efficient drug release. On the one hand, the incorporation of specific ligands allows targeting tumour cells, as reported by Vyas et al., where hyaluronan-coated IONPs were employed to deliver doxorubicin to a human breast cancer cell line.²²⁸ Other studies have demonstrated for instance magnetically-mediated NP retention in tumours, harnessing the magnetic properties of the employed carrier.²²⁹ Different strategies have also been developed to control the release of chemotherapeutic drugs from IONPs.^{230–232} For instance, Lee et al. reported an IONP-based smart drug delivery system to treat pancreatic cancer. The incorporation of a specific ligand allowed targeting the IONPs to tumour and stromal cells. Moreover, this study also demonstrated drug controlled release by conjugating an anticancer drug (gemcitabine) via a lysosomally cleavable linker.²³³

IONPs have also been used in magnetic hyperthermia, where the ability to generate and localise heat in the tumour under an external magnetic field is used to kill cancer cells, which in general are more heat-sensitive. This type of therapy exploiting the intrinsic properties of IONPs has been already studied in preclinical and clinical

trials.^{234–236} Salunkhe et al. nicely reviewed the status of magnetic hyperthermia and described the advantages and challenges for its application *in vivo*.²³⁷

Gene delivery is another successful anticancer therapy that has been studied using IONPs.^{238–242} Due to the large surface-to-volume ratio and wide variety of surface ligands employed in coating IONPs, high amounts of genetic material can be loaded and delivered.^{243,244} For example, Chen et al. reported IONP-based delivery systems carrying radiolabelled small interfering RNA (siRNA) to block tumour growth. In this way, they were able to demonstrate tumour monitoring by MRI and simultaneous gene- and radio-therapy.²⁴⁵

1.3.2. State of the art anticancer nanovaccines

The delivery of a tumour antigen and adjuvant such as TLR agonist using NPs as carrier has been explored for over a decade. However, there are now a myriad of new nanotechnology-enabled possibilities to efficiently transport these types of molecules to enhance their efficacy and safety profiles. Strategies can include innovative ways to enhance delivery of antigen/adjuvant mixtures carried by conventional drug delivery systems (liposomes, polymeric NPs, nanoemulsions, etc.). For example, Kitaoka et al. reported enhanced administration of solid-in-oil (S/O) nanodispersions of OVA and CpG ODNs by transdermal immunization using skin patches.²⁴⁶ Bourquin et al., on the other hand, chose gelatin-based NPs to deliver CpG ODNs because of the gelatin high biocompatibility and stability during storage.²⁴⁷ In order to direct antigen to DCs, Lee et al. adsorbed IgG molecules into biodegradable poly(lactic-co-glycolic acid) (PLGA) NPs carrying OVA/CpG ODNs and demonstrated the induction of antigen-specific antitumour T cell response.^{248,249} Another new approach is to exploit the ability to form NPs by self-assembly of modified antigen/adjuvants. In this way, Rattanakit et al. proposed the self-assembly of cholesterol-modified CpG ODNs and the subsequent incorporation of OVA in order to induce efficient antigen-specific Th1-type immune responses.²⁵⁰

Strategies using polymeric NPs and liposomes as carriers have the advantage of being biodegradable and biocompatible delivery systems. Moreover, they can provide

protection from premature release of the loaded molecules in order to control antigen release and avoid systemic toxicity of adjuvants. Polymeric NPs and liposomes have been the main systems to develop anticancer vaccines in last few years. For instance, De Jong et al. demonstrated that CpG ODNs encapsulation into liposomes can direct the adjuvant activity to immune cells, avoid toxic effects of soluble adjuvant and reduce tumour growth when co-injected with antigen.²⁵¹ Co-administration of OVA/CpG ODNs into liposome-based NPs as antitumour therapeutic vaccines was reported by Wakita et al., demonstrating the generation of antitumour-specific CTLs that lead to slower tumour growth in mice.²⁵² On the other hand, a modular anticancer nanovaccine based on RNA-lipoplexes, which contained viral genetic material and TAAs encoded in the RNA molecules, was described in 2016 by Kranz et al. The main novelty of this formulation was in the ability to be broadly applied, since the genetic material administered could be designed specifically for each cancer type allowing a more personalized approach to cancer treatment.²⁵³

Polymeric NPs such as polyethylene glycol (PEG)- and PLGA-based NPs have also been employed as OVA/CpG ODNs carriers. For example, Jain et al. reported PEG-based hydrogels of about 500 nm to deliver OVA and CpG ODNs. The observed T cell activation was promising, although no experiments using animals were carried out.²⁵⁴ On the other hand, Ilyinskii et al. reported PEG/PLGA synthetic vaccine particles that were able to entrap OVA/CpG molecules and elicit a potent but safe immune response under microdosing conditions (5 µg/mice).²⁵⁵ Wilson et al., in contrast, proposed pH responsive endosomolytic polymer NPs (able to disrupt endosome membrane once internalised) in order to co-deliver antigen and CpG ODNs enhancing Th1-type responses *in vivo*.²⁵⁶ Moreover, pathogen mimetic PLGA-based NPs loading OVA antigen and modified with two TLR agonists (CpG ODNs and monophosphoryl lipid A (MPLA)) were described recently by Siefert et al. in order to enhance vaccine efficacy.²⁵⁷

The laboratories of M. Swartz and J. Hubbell have explored the new concept of targeted and direct delivery of antigen to secondary lymphoid organs (SLOs) (i.e., spleen and LNs) exploiting polymeric NPs. In research published by Hirosue et al. and Nembrini et al. solid-core polymeric NPs were employed in order to deliver OVA

antigen, demonstrating the effects that the way of anchoring antigen has in the cellular uptake. They reported antigen coupling by a labile disulfide link to a NP that is able to induce antigen presentation in MHC class I molecules and subsequent Th1-type immune response.^{258,259} In the work published by Eby et al. they found no differences between solid-core NPs (<50 nm) and small polymer micelles (35 nm) formed by self-assembly in terms of antigen-specific immune response.²⁶⁰ However, shortly after Stano et al. demonstrated differences between these solid-core polymeric NPs (30 nm) and similarly composed polymersomes (watery-core spheres; 125 nm). While smaller NPs were able to induce strong CD8⁺ T cells activation and Th1-type responses, polymersomes enhanced the frequencies of antigen-specific CD4⁺ T cells. This work highlighted the importance that the particle size and the mode of release have when delivering antigen. Antigen-specific CD8⁺ T cells activation was enhanced when antigen was surface-conjugated to small solid-core NPs.²⁶¹ Moreover, de Titta et al. employed these solid-core NPs to conjugate antigen OVA and CpG ODNs as adjuvants (co-delivered on separate NPs) in order to induce potent antitumour immunity.²⁶²

However, imaging features were not included in any of these delivery systems for their tracking *in vivo*. The use of inorganic NPs for the development of anticancer vaccines has the advantage of endowing the formulation with such imaging properties. For example, Sen et al. showed the ability of antigen-conjugated quantum dots (QDs) to induce potent T cells activation *in vivo* and the value of having an imageable core to study their biodistribution.²⁶³ More recently, europium-doped gadolinium-based NPs were reported by Li et al. for enhanced OVA/CpG ODNs delivery and dual-mode imaging. In this work, the fluorescent properties of europium were exploited to analyse cell uptake by microscopy and gadolinium to track the NPs by MRI *in vivo*.²⁶⁴ Very recently Duan et al. reported metal-organic frameworks (MOF) with europium in order to transport OVA/CpG ODNs and induce potent antitumour effect in a melanoma model.²⁶⁵ Upconverting nanoparticles (UCNPs) exhibit photon upconversion, allowing infrared absorption (optimal for biomedical applications) and consequent UV-visible emission for fluorescence imaging. Xiang et al. employed this technology to load OVA antigen and mature *ex vivo* DCs for development of anticancer DC-based vaccines.²⁶⁶ In contrast, gold-based nanoparticles (AuNPs), which also have imaging properties,

have been shown to elicit immunostimulatory effects by themselves. For instance, Almeida et al. reported potent prophylactic and therapeutic antitumour effect when employing OVA- and CpG-conjugated AuNP (co-administered in separate NPs) and demonstrated that the injection of OVA-AuNPs was sufficient to reduce tumour growth.²⁶⁷

Few anticancer vaccines have reported to use IONPs (based on the Web of Science search (<http://apps.webofknowledge.com>): nanoparticles AND (cancer OR tumor) AND vaccine AND iron oxide = 24 articles for a search conducted on 24 March 2017). Most of these results are related to DC-based anticancer vaccines, where naked or antigen/adjuvant-conjugated IONPs are employed to *ex vivo* stimulate DCs and subsequent injection of the IONP-loaded mature DCs for biodistribution analysis by MRI.²⁶⁸⁻²⁷⁷ Among the studies employing IONPs as vaccine delivering platforms,²⁷⁸⁻²⁸¹ the most relevant studies have been published over the last two years. In 2015, Sungsuwan et al. reported that lipopeptide-coated IONPs carrying tumour-associated glycopeptide antigen were able to generate strong antibody responses and complement-mediated cytotoxicity.²⁸² Moreover, Shen et al. demonstrated in 2016 the ability of trifunctional IONP-based vaccines (loaded with OVA, CpG ODNs and a DC-targeting moiety) to efficiently target DC *in vivo* and induce tumour growth arrest.²⁸³

1.4. Justification and objectives of this research

Over the last decade immunotherapy has achieved successful clinical results in the treatment of cancer. A clear example is the use of mAbs such as anti-PD-1 and anti-CTLA-4 antibodies to block certain immunosuppressive strategies that tumour cells can acquire.^{284,285} However, these strategies are still limited to only a subset of patients and diseases and are used in combination with conventional therapies. Various studies have shown the possibility of activating immunity against cancer by using ‘vaccine-like’ formulations. However, most of the nanovaccines that have shown efficient induction of anticancer immunity are difficult to make or lack in their ability to provide imaging characteristics in order to follow their biodistribution. As imaging plays a growing role in preclinical cancer drug discovery, it is widely recognised that including not only one, but various imaging capabilities accelerates the DDD process, allowing a better understanding and prediction of the therapy effect already in the early stages. From a synthetic point of view, self-assembly holds considerable potential as a low-cost, high-yield technique to develop nanomedicines, as demonstrated by liposomal drug delivery systems.

This thesis aims to unify these three main properties (wide applicability, ease of production and multimodal imaging tracking characteristics) in order to design, develop and test a novel approach for antigen/adjuvant delivery and multimodal NP labelling (Chapter II) that exploits specific size and surface properties of magnetite-based nanocarriers to promote effective delivery to endosomal TLRs in APCs and *in vivo* LN targeting (Chapter III). This targeted delivery is shown to enhance the antitumour effect of the administered nanovaccine by inducing potent antigen-specific humoral and cellular immunity (Chapter IV) (**Figure 1.7**).

The specific objectives of this thesis can be summarised as:

- The production of water soluble IONP-filled micelles coated with biocompatible polymers by a self-assembly process. This coating must provide antigen/adjuvant anchoring sites, without altering the micelle formation process;

- The attachment of widely used immunostimulatory molecules (i.e., antigens and adjuvants) by simple procedures using biocompatible solvents and materials. This anchoring sites have to be applicable to most of the commonly employed biomolecules;
- The incorporation of complementary imaging features in order to achieve a multimodal imaging tracking of the drug delivery platform, by different imaging techniques both *in vitro* and *in vivo*;
- The use of these IONP-based vaccines to deliver the antigen/adjuvant to target tissues key in the development of a potent anticancer immune response. Once in the correct tissue, these IONP-filled micelles have to interact with specific intracellular compartments/receptors in cells of the immune system;
- The study and analysis of the immune responses elicited by these nanovaccines;
- The proof-of-concept demonstration of the efficacy of these IONP-filled vaccines as anticancer prophylactic and therapeutic agents in a mouse tumour model.

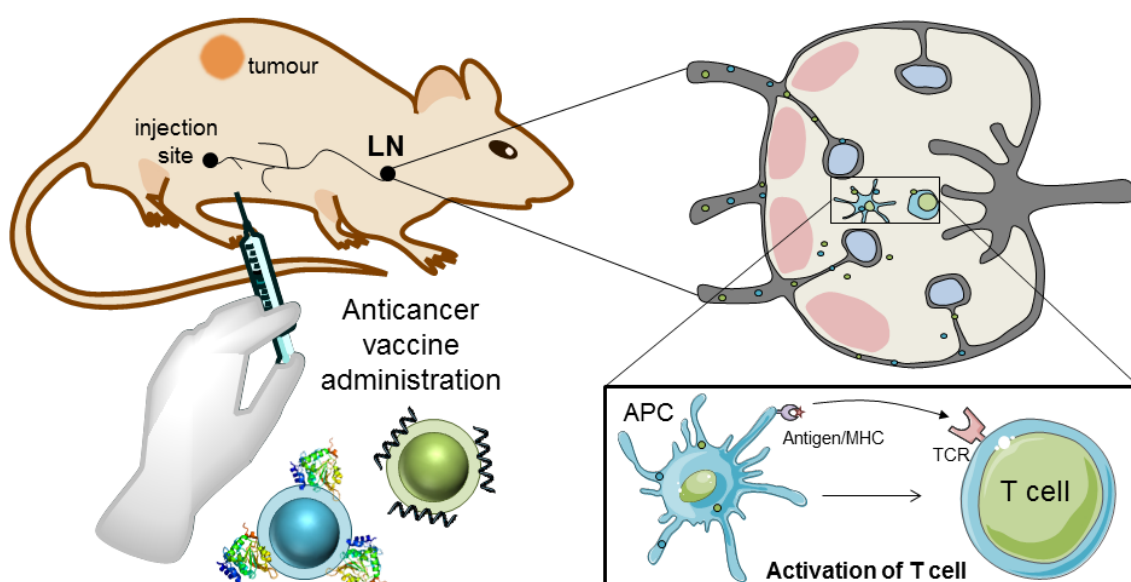


Figure 1.7. Application of designed anticancer vaccine. Proposed nanosystem is designed to provide effective lymphatic delivery of the vaccine components to SLOs such as LNs, where uptake by DCs facilitates the induction of potent humoral and cellular immunity.

References

1. National Cancer Institute. Risk Factors for Cancer. *National Cancer Institute* (2015). Available at: <https://www.cancer.gov/about-cancer/causes-prevention/risk>. (Accessed: 24th November 2016)
2. Hanahan, D. & Weinberg, R. A. The Hallmarks of Cancer. *Cell* **100**, 57–70 (2000).
3. Foulds, L. The experimental study of tumor progression: a review. *Cancer Res.* **14**, 327–39 (1954).
4. Nowell, P. C. The clonal evolution of tumor cell populations. *Science (80-)*. **194**, 23–8 (1976).
5. American Cancer Society. Global Cancer Facts & Figures 3rd Edition. *Am. Cancer Soc.* 1–61 (2015). doi:10.1002/ijc.27711
6. Torre, L. A. *et al.* Global Cancer Statistics, 2012. *CA Cancer J. Clin.* **65**, 87–108 (2015).
7. Cancer research UK. Cancer incidence statistics worldwide. (2016). Available at: <http://www.cancerresearchuk.org/health-professional/cancer-statistics/worldwide-cancer>.
8. Chabner, B. A. & Roberts, T. G. Chemotherapy and the war on cancer. *Nat. Rev. Cancer* **5**, 65–72 (2005).
9. DeVita, V. T. & Chu, E. A history of cancer chemotherapy. *Cancer Res.* **68**, 8643–8653 (2008).
10. Coley, W. The treatment of malignant tumors by repeated inoculations of erysipelas. With a report of ten original cases. *Am. J. Med. Sci.* **105**, 487–511 (1893).
11. Grimm, E. A., Mazumder, A., Zhang, H. Z. & Rosenberg, S. A. Lymphokine-activated killer cell phenomenon. Lysis of natural killer-resistant fresh solid tumor cells by interleukin 2-activated autologous human peripheral blood lymphocytes. *J. Exp. Med.* **155**, 1823–41 (1982).
12. Miller, R. A., Maloney, D. G., Warnke, R. & Levy, R. Treatment of B-Cell Lymphoma with Monoclonal Anti-Idiotypic Antibody. *N. Engl. J. Med.* **306**, 517–522 (1982).
13. O’Hagan, D. Recent advances in immunological adjuvants: the development of particulate antigen delivery systems. *Expert Opin. Investig. Drugs* **7**, 349–359 (1998).
14. Storni, T., Kündig, T. M., Senti, G. & Johansen, P. Immunity in response to particulate antigen-delivery systems. *Adv. Drug Deliv. Rev.* **57**, 333–355 (2005).
15. Vignali, D. a, Doyle, C., Kinch, M. S., Shin, J. & Strominger, J. L. Interactions of

- CD4 with MHC class II molecules, T cell receptors and p56lck. *Philos. Trans. R. Soc. London. B* **342**, 13–24 (1993).
16. Weenink, S. M. & Gautam, a M. Antigen presentation by MHC class II molecules. *Immunol. Cell Biol.* **75**, 69–81 (1997).
 17. Scott, P., Pearce, E., Cheever, a W., Coffman, R. L. & Sher, A. Role of cytokines and CD4+ T-cell subsets in the regulation of parasite immunity and disease. *Immunol. Rev.* **112**, 161–82 (1989).
 18. Romagnani, S. Type 1 T helper and type 2 T helper cells: functions, regulation and role in protection and disease. *Int. J. Clin. Lab. ...* **21**, 152–158 (1991).
 19. Golding, B. & Scott, D. E. Vaccine strategies: targeting helper T cell responses. *Ann. N. Y. Acad. Sci.* **754**, 126–37 (1995).
 20. Del Prete, G. The concept of type-1 and type-2 helper T cells and their cytokines in humans. *Int. Rev. Immunol.* **16**, 427–455 (1998).
 21. Braciale, T. J. *et al.* Antigen presentation pathways to class I and class II MHC-restricted T lymphocytes. *Immunol. Rev.* **98**, 95–114 (1987).
 22. Schubert, U. *et al.* Rapid degradation of a large fraction of newly synthesized proteins by proteasomes. *Nature* **404**, 770–774 (2000).
 23. Van Kaer, L. Major histocompatibility complex class I-restricted antigen processing and presentation. *Tissue Antigens* **60**, 1–9 (2002).
 24. Dighe, A. S., Richards, E., Old, L. J. & Schreiber, R. D. Enhanced in vivo growth and resistance to rejection of tumor cells expressing dominant negative IFN gamma receptors. *Immunity* **1**, 447–56 (1994).
 25. Ali, O. a. *et al.* Identification of immune factors regulating antitumor immunity using polymeric vaccines with multiple adjuvants. *Cancer Res.* **74**, 1670–1681 (2014).
 26. Ghiringhelli, F. *et al.* Activation of the NLRP3 inflammasome in dendritic cells induces IL-1 β -dependent adaptive immunity against tumors. *Nat. Med.* **15**, 1170–1178 (2009).
 27. Burnette, B. C. *et al.* The efficacy of radiotherapy relies upon induction of type I interferon-dependent innate and adaptive immunity. *Cancer Res.* **71**, 2488–96 (2011).
 28. Arce, F., Kochan, G., Breckpot, K., Stephenson, H. & Escors, D. Selective Activation of Intracellular Signalling Pathways In Dendritic Cells For Cancer Immunotherapy. *Anti-Cancer Agents Med. Chem.* **12**, 29–39 (2012).
 29. Apetoh, L., Mignot, G., Panaretakis, T., Kroemer, G. & Zitvogel, L. Immunogenicity of anthracyclines: moving towards more personalized medicine. *Trends Mol. Med.* **14**, 141–151 (2008).

30. Zitvogel, L., Apetoh, L., Ghiringhelli, F. & Kroemer, G. Immunological aspects of cancer chemotherapy. *Nat. Rev. Immunol.* **8**, 59–73 (2008).
31. Galluzzi, L., Senovilla, L., Zitvogel, L. & Kroemer, G. The secret ally: immunostimulation by anticancer drugs. *Nat. Rev. Drug Discov.* **11**, 215–233 (2012).
32. Apetoh, L. *et al.* Toll-like receptor 4–dependent contribution of the immune system to anticancer chemotherapy and radiotherapy. *Nat. Med.* **13**, 1050–9 (2007).
33. Oh, G.-S. *et al.* Activation of Lipopolysaccharide-TLR4 Signaling Accelerates the Ototoxic Potential of Cisplatin in Mice. *J. Immunol.* **186**, 1140–1150 (2011).
34. Janeway, C., Travers, P., Walport, M. & Shlomchik, M. in *Immunobiology: The Immune System in Health and Disease*. (New York: Garland Science, 2001).
35. Gajewski, T. F., Schreiber, H. & Fu, Y.-X. Innate and adaptive immune cells in the tumor microenvironment. *Nat. Immunol.* **14**, 1014–1022 (2013).
36. Iannello, A. & Ahmad, A. Role of antibody-dependent cell-mediated cytotoxicity in the efficacy of therapeutic anti-cancer monoclonal antibodies. *Cancer Metastasis Rev.* **24**, 487–499 (2005).
37. Ferris, R. L., Jaffee, E. M. & Ferrone, S. Tumor antigen-targeted, monoclonal antibody-based immunotherapy: Clinical response, cellular immunity, and immunoescape. *J. Clin. Oncol.* **28**, 4390–4399 (2010).
38. Rajasekaran, N., Chester, C., Yonezawa, A., Zhao, X. & Kohrt, H. E. Enhancement of antibody-dependent cell mediated cytotoxicity: a new era in cancer treatment. *ImmunoTargets Ther.* **4**, 91–100 (2015).
39. Hirshaut, Y. & Slovin, S. F. Harnessing T-Lymphocytes for Human Cancer Immunotherapy. *Cancer* **56**, 1366–1373 (1985).
40. Hariharan, K., Braslawsky, G., Black, A., Raychaudhuri, S. & Hanna, N. The Induction of Cytotoxic T Cells and Tumor Regression by Soluble Antigen Formulation. *Cancer Res.* **55**, 3486–3489 (1995).
41. Albert, M. L., Sauter, B. & Bhardwaj, N. Dendritic cells acquire antigen from apoptotic cells and induce class I-restricted CTLs. *Nature* **392**, 86–9 (1998).
42. Maher, J. & Davies, E. T. Targeting cytotoxic T lymphocytes for cancer immunotherapy. *Br. J. Cancer* **91**, 817–21 (2004).
43. Dunn, G. P., Bruce, A. T., Ikeda, H., Old, L. J. & Schreiber, R. D. Cancer immunoediting: from immunosurveillance to tumor escape. *Nat. Immunol.* **3**, 991–998 (2002).
44. Dunn, G. P., Old, L. J. & Schreiber, R. D. The Three Es of Cancer Immunoediting. *Annu. Rev. Immunol.* **22**, 329–360 (2004).

45. Schreiber, R. D., Old, L. J. & Smyth, M. J. Cancer immunoediting: integrating immunity's roles in cancer suppression and promotion. *Science (80-.)*. **331**, 1565–70 (2011).
46. Mittal, D., Gubin, M. M., Schreiber, R. D. & Smyth, M. J. New insights into cancer immunoediting and its three component phases – elimination, equilibrium and escape. *Curr. Opin. Immunol.* **27**, 16–25 (2014).
47. Ehrlich, P. Über den jetzigen Stand der Karzinomforschung. *Ned. Tijdschr. Geneesk.* **5**, 273–290 (1909).
48. Burnet, M. F. Cancer: a biological approach. *Br. Med. J.* **1**, 841–7 (1957).
49. Thomas, L. in *Cellular and Humoral Aspects of the Hypersensitive States* (ed. Lawrence, H. S.) 529–533 (Hoeber-Harper, 1959).
50. Old, L. J. & Boyse, E. A. Immunology of Experimental Tumors. *Annu. Rev. Med.* **15**, 167–186 (1964).
51. Klein, G. Tumor Antigens. *Annu. Rev. Microbiol.* **20**, 223–252 (1966).
52. Burnet, M. F. The concept of immunological surveillance. *Prog. Exp. Tumor Res.* **13**, 1–27 (1970).
53. Shankaran, V. *et al.* IFN γ and lymphocytes prevent primary tumour development and shape tumour immunogenicity. *Nature* **410**, 1107–11 (2001).
54. Huang, A. Y. C. *et al.* Role of bone marrow-derived cells in presenting MHC class I-restricted tumor antigens. *Science (80-.)*. **264**, 961–5 (1994).
55. Huang, H. *et al.* CD4⁺ Th1 cells promote CD8⁺ Tc1 cell survival, memory response, tumor localization and therapy by targeted delivery of interleukin 2 via acquired pMHC I complexes. *Immunology* **120**, 148–159 (2007).
56. Loeb, L. A., Loeb, K. R. & Anderson, J. P. Multiple mutations and cancer. *Proc. Natl. Acad. Sci.* **100**, 776–781 (2003).
57. García-Hernández, M. L., Hernández-Pando, R., Gariglio, P. & Berumen, J. Interleukin-10 promotes B16-melanoma growth by inhibition of macrophage functions and induction of tumour and vascular cell proliferation. *Immunology* **105**, 231–43 (2002).
58. Skinnider, B. F. The role of cytokines in classical Hodgkin lymphoma. *Blood* **99**, 4283–4297 (2002).
59. Curiel, T. J. *et al.* Specific recruitment of regulatory T cells in ovarian carcinoma fosters immune privilege and predicts reduced survival. *Nat. Med.* **10**, 942–949 (2004).
60. Marincola, F. M., Jaffee, E. M., Hicklin, D. J. & Ferrone, S. Escape of human solid tumors from T-cell recognition: molecular mechanisms and functional significance. *Adv. Immunol.* **74**, 181–273 (2000).

61. Kaplan, D. H. *et al.* Demonstration of an interferon gamma-dependent tumor surveillance system in immunocompetent mice. *Proc. Natl. Acad. Sci. U. S. A.* **95**, 7556–61 (1998).
62. Catlett-Falcone, R. *et al.* Constitutive activation of Stat3 signaling confers resistance to apoptosis in human U266 myeloma cells. *Immunity* **10**, 105–15 (1999).
63. Couzin-Frankel, J. Breakthrough of the year 2013. Cancer immunotherapy. *Science (80-.)*. **342**, 1432–3 (2013).
64. Weiner, L. M. Building better magic bullets--improving unconjugated monoclonal antibody therapy for cancer. *Nat. Rev. Cancer* **7**, 701–6 (2007).
65. Strebhardt, K. & Ullrich, A. Paul Ehrlich's magic bullet concept: 100 years of progress. *Nat. Rev. Cancer* **8**, 473–480 (2008).
66. Humphries, C. Adoptive cell therapy: Honing that killer instinct. *Nature* **504**, S13–S15 (2013).
67. Maus, M. V. *et al.* Adoptive Immunotherapy for Cancer or Viruses. *Annu. Rev. Immunol.* **32**, 189–225 (2014).
68. Melero, I., Hervas-Stubbs, S., Glennie, M., Pardoll, D. M. & Chen, L. Immunostimulatory monoclonal antibodies for cancer therapy. *Nat. Rev. Cancer* **7**, 95–106 (2007).
69. Rice, J., Ottensmeier, C. H. & Stevenson, F. K. DNA vaccines: precision tools for activating effective immunity against cancer. *Nat. Rev. Cancer* **8**, 108–120 (2008).
70. Melief, C. J. M. & van der Burg, S. H. Immunotherapy of established (pre)malignant disease by synthetic long peptide vaccines. *Nat. Rev. Cancer* **8**, 351–360 (2008).
71. Pardoll, D. M. The blockade of immune checkpoints in cancer immunotherapy. *Nat. Rev. Cancer* **12**, 252–264 (2012).
72. Alkan, S. S. Monoclonal antibodies: the story of a discovery that revolutionized science and medicine. *Nat. Rev. Immunol.* **4**, 153–156 (2004).
73. Weiner, L. M., Surana, R. & Wang, S. Monoclonal antibodies: versatile platforms for cancer immunotherapy. *Nat. Rev. Immunol.* **10**, 317–327 (2010).
74. Vacchelli, E. *et al.* Trial watch: Monoclonal antibodies in cancer therapy. *Oncoimmunology* **2**, e22789 (2013).
75. Cavallo, F., Calogero, R. A. & Forni, G. Are oncoantigens suitable targets for anti-tumour therapy? *Nat. Rev. Cancer* **7**, 707–713 (2007).
76. Michielsen, A. J., Ryan, E. J. & O'Sullivan, J. N. Dendritic cell inhibition correlates with survival of colorectal cancer patients on bevacizumab treatment.

- Oncoimmunology* **1**, 1445–1447 (2012).
77. Kute, T. *et al.* Understanding key assay parameters that affect measurements of trastuzumab-mediated ADCC against Her2 positive breast cancer cells. *Oncoimmunology* **1**, 810–821 (2012).
 78. Coulie, P. G., Van den Eynde, B. J., van der Bruggen, P. & Boon, T. Tumour antigens recognized by T lymphocytes: at the core of cancer immunotherapy. *Nat. Rev. Cancer* **14**, 135–146 (2014).
 79. de La Motte Rouge, T. *et al.* A novel epidermal growth factor receptor inhibitor promotes apoptosis in non-small cell lung cancer cells resistant to erlotinib. *Cancer Res.* **67**, 6253–62 (2007).
 80. Weiner, L. M. *et al.* Dose and Schedule Study of Panitumumab Monotherapy in Patients with Advanced Solid Malignancies. *Clin. Cancer Res.* **14**, 502–508 (2008).
 81. Kaplan-Lefko, P. J. *et al.* Conatumumab, a fully human agonist antibody to death receptor 5, induces apoptosis via caspase activation in multiple tumor types. *Cancer Biol. Ther.* **9**, 618–31 (2010).
 82. Forero-Torres, A. *et al.* Phase 2, multicenter, open-label study of tigatuzumab (CS-1008), a humanized monoclonal antibody targeting death receptor 5, in combination with gemcitabine in chemotherapy-naïve patients with unresectable or metastatic pancreatic cancer. *Cancer Med.* **2**, 925–932 (2013).
 83. Hughes, B. Antibody-drug conjugates for cancer: poised to deliver? *Nat. Rev. Drug Discov.* **9**, 665–7 (2010).
 84. Leal, M. *et al.* Antibody-drug conjugates: an emerging modality for the treatment of cancer. *Ann. N. Y. Acad. Sci.* **1321**, 41–54 (2014).
 85. Hubert, P. & Amigorena, S. Antibody-dependent cell cytotoxicity in monoclonal antibody-mediated tumor immunotherapy. *Oncoimmunology* **1**, 103–105 (2012).
 86. Houot, R., Kohrt, H. & Levy, R. Boosting antibody-dependant cellular cytotoxicity against tumor cells with a CD137 stimulatory antibody. *Oncoimmunology* **1**, 957–958 (2012).
 87. Winiarska, M., Glodkowska-Mrowka, E., Bil, J. & Golab, J. Molecular mechanisms of the antitumor effects of anti-CD20 antibodies. *Front. Biosci. (Landmark Ed.)* **16**, 277–306 (2011).
 88. Zugmaier, G. *et al.* Long-term survival and T-cell kinetics in relapsed/refractory ALL patients who achieved MRD response after blinatumomab treatment. *Blood* **126**, 2578–84 (2015).
 89. Choi, B. D., Pastan, I., Bigner, D. D. & Sampson, J. H. A novel bispecific antibody recruits T cells to eradicate tumors in the "immunologically

- privileged" central nervous system. *Oncoimmunology* **2**, e23639 (2013).
90. Walter, R. B. Biting back: BiTE antibodies as a promising therapy for acute myeloid leukemia. *Expert Rev. Hematol.* **7**, 317–319 (2014).
 91. Rosenberg, S. A. Cell transfer immunotherapy for metastatic solid cancer—what clinicians need to know. *Nat. Rev. Clin. Oncol.* **8**, 577–585 (2011).
 92. Restifo, N. P., Dudley, M. E. & Rosenberg, S. A. Adoptive immunotherapy for cancer: harnessing the T cell response. *Nat. Rev. Immunol.* **12**, 269–281 (2012).
 93. Aranda, F. *et al.* Trial Watch: Adoptive cell transfer for anticancer immunotherapy. *Oncoimmunology* **3**, e28344 (2014).
 94. Kershaw, M. H., Teng, M. W. L., Smyth, M. J. & Darcy, P. K. Supernatural T cells: genetic modification of T cells for cancer therapy. *Nat. Rev. Immunol.* **5**, 928–940 (2005).
 95. Merhavi-Shoham, E., Haga-Friedman, A. & Cohen, C. J. Genetically modulating T-cell function to target cancer. *Semin. Cancer Biol.* **22**, 14–22 (2012).
 96. Vähä-Koskela, M. J. V, Heikkilä, J. E. & Hinkkanen, A. E. Oncolytic viruses in cancer therapy. *Cancer Lett.* **254**, 178–216 (2007).
 97. Russell, S. J., Peng, K.-W. & Bell, J. C. Oncolytic virotherapy. *Nat. Biotechnol.* **30**, 658–70 (2012).
 98. Liu, Y. & Deisseroth, A. Oncolytic adenoviral vector carrying the cytosine deaminase gene for melanoma gene therapy. *Cancer Gene Ther.* **13**, 845–855 (2006).
 99. Russell, S. J. & Peng, K. W. Measles virus for cancer therapy. *Curr. Top. Microbiol. Immunol.* **330**, 213–41 (2009).
 100. Zhu, W. *et al.* Oncolytic adenovirus encoding tumor necrosis factor-related apoptosis inducing ligand (TRAIL) inhibits the growth and metastasis of triple-negative breast cancer. *Cancer Biol. Ther.* **14**, 1016–1023 (2013).
 101. Galluzzi, L. *et al.* Classification of current anticancer immunotherapies. *Oncotarget* **5**, 12472–508 (2014).
 102. Mayordomo, J. I. *et al.* Bone marrow-derived dendritic cells pulsed with synthetic tumour peptides elicit protective and therapeutic antitumour immunity. *Nat. Med.* **1**, 1297–302 (1995).
 103. Irvine, A. S. *et al.* Efficient nonviral transfection of dendritic cells and their use for in vivo immunization. *Nat. Biotechnol.* **18**, 1273–1278 (2000).
 104. Fields, R. C., Shimizu, K. & Mulé, J. J. Murine dendritic cells pulsed with whole tumor lysates mediate potent antitumor immune responses in vitro and in vivo. *Proc. Natl. Acad. Sci. U. S. A.* **95**, 9482–7 (1998).

105. Fučíková, J. *et al.* Poly I: C-activated dendritic cells that were generated in CellGro for use in cancer immunotherapy trials. *J. Transl. Med.* **9**, 223 (2011).
106. Kantoff, P. W. *et al.* Sipuleucel-T Immunotherapy for Castration-Resistant Prostate Cancer. *N. Engl. J. Med.* **363**, 411–422 (2010).
107. Higano, C. S. *et al.* Sipuleucel-T. *Nat. Rev. Drug Discov.* **9**, 513–514 (2010).
108. Fong, L. & Small, E. J. Anti-Cytotoxic T-Lymphocyte Antigen-4 Antibody: The First in an Emerging Class of Immunomodulatory Antibodies for Cancer Treatment. *J. Clin. Oncol.* **26**, 5275–5283 (2008).
109. Lipson, E. J. Re-orienting the immune system. Durable tumor regression and successful re-induction therapy using anti-PD1 antibodies. *Oncoimmunology* **2**, e23661 (2013).
110. Zou, W. & Chen, L. Inhibitory B7-family molecules in the tumour microenvironment. *Nat. Rev. Immunol.* **8**, 467–477 (2008).
111. Melero, I. *et al.* Monoclonal antibodies against the 4-1BB T-cell activation molecule eradicate established tumors. *Nat. Med.* **3**, 682–5 (1997).
112. Melero, I., Hirschhorn-Cymerman, D., Morales-Kastresana, A., Sanmamed, M. F. & Wolchok, J. D. Agonist Antibodies to TNFR Molecules That Costimulate T and NK Cells. *Clin. Cancer Res.* **19**, 1044–1053 (2013).
113. Schnurr, M. & Duewell, P. Breaking tumor-induced immunosuppression with 5'-triphosphate siRNA silencing TGF β and activating RIG-I. *Oncoimmunology* **2**, e24170 (2013).
114. Cheung, I. Y., Hsu, K. & Cheung, N.-K. V. Activation of Peripheral-Blood Granulocytes Is Strongly Correlated With Patient Outcome After Immunotherapy With Anti-GD2 Monoclonal Antibody and Granulocyte-Macrophage Colony-Stimulating Factor. *J. Clin. Oncol.* **30**, 426–432 (2012).
115. Robertson, M. J. *et al.* A Dose-Escalation Study of Recombinant Human Interleukin-18 in Combination With Rituximab in Patients With Non-Hodgkin Lymphoma. *J. Immunother.* **36**, 331–341 (2013).
116. Gorin, N.-C. *et al.* Administration of alemtuzumab and G-CSF to adults with relapsed or refractory acute lymphoblastic leukemia: results of a phase II study. *Eur. J. Haematol.* **91**, 315–21 (2013).
117. Tomov, B. *et al.* Therapeutic response of untreatable hepatocellular carcinoma after application of the immune modulators IL-2, BCG and melatonin. *Anticancer Res.* **33**, 4531–5 (2013).
118. Muller, A. J., DuHadaway, J. B., Donover, P. S., Sutanto-Ward, E. & Prendergast, G. C. Inhibition of indoleamine 2,3-dioxygenase, an immunoregulatory target of the cancer suppression gene Bin1, potentiates cancer chemotherapy. *Nat. Med.* **11**, 312–319 (2005).

119. Manuel, E. R. & Diamond, D. J. A road less traveled paved by IDO silencing: Harnessing the antitumor activity of neutrophils. *Oncoimmunology* **2**, e23322 (2013).
120. Hodj, F. S. *et al.* Improved survival with ipilimumab in patients with metastatic melanoma. *N. Engl. J. Med.* **363**, 711–23 (2010).
121. Deeks, E. D. Nivolumab: A Review of Its Use in Patients with Malignant Melanoma. *Drugs* **74**, 1233–1239 (2014).
122. Eggermont, A. M. *et al.* Isolated Limb Perfusion With High-Dose Tumor Necrosis Factor- α in Combination With Interferon- γ and Melphalan for Nonresectable Extremity Soft Tissue Sarcomas: A Multicenter Trial. *J. Clin. Oncol.* **14**, 2653–65 (1996).
123. van Horssen, R., Ten Hagen, T. L. M. & Eggermont, A. M. M. TNF- α in Cancer Treatment: Molecular Insights, Antitumor Effects, and Clinical Utility. *Oncologist* **11**, 397–408 (2006).
124. Deroose, J. P. *et al.* 20 Years Experience of TNF-Based Isolated Limb Perfusion for In-Transit Melanoma Metastases: TNF Dose Matters. *Ann. Surg. Oncol.* **19**, 627–635 (2012).
125. Gibney, G. T. *et al.* Preliminary results from a phase 1/2 study of INCB024360 combined with ipilimumab (ipi) in patients (pts) with melanoma. *J. Clin. Oncol.* **32**, (2014).
126. Young, A., Mittal, D., Stagg, J. & Smyth, M. J. Targeting Cancer-Derived Adenosine: New Therapeutic Approaches. *Cancer Discov.* **4**, 1–10 (2014).
127. Vacchelli, E. *et al.* Trial watch: Peptide vaccines in cancer therapy. *Oncoimmunology* **1**, 1557–1576 (2012).
128. Valmori, D. *et al.* Vaccination with NY-ESO-1 protein and CpG in Montanide induces integrated antibody/Th1 responses and CD8 T cells through cross-priming. *Proc. Natl. Acad. Sci. U. S. A.* **104**, 8947–52 (2007).
129. Aruga, A. Vaccination of biliary tract cancer patients with four peptides derived from cancer-testis antigens. *Oncoimmunology* **2**, e24882 (2013).
130. Senovilla, L. *et al.* Trial watch: DNA vaccines for cancer therapy. *Oncoimmunology* **2**, e23803 (2013).
131. Narayan, R. *et al.* Immunomodulation by Imiquimod in Patients with High-Risk Primary Melanoma. *J. Invest. Dermatol.* **132**, 163–169 (2012).
132. Demaria, S., Vanpouille-Box, C., Formenti, S. C. & Adams, S. The TLR7 agonist imiquimod as an adjuvant for radiotherapy-elicited in situ vaccination against breast cancer. *Oncoimmunology* **2**, e25997 (2013).
133. Stathopoulos, A. *et al.* Exploring the Therapeutic Efficacy of Glioma Vaccines Based on Allo- and Syngeneic Antigens and Distinct Immunological

- Costimulation Activators. *J. Clin. Cell. Immunol.* **1**, 4 (2012).
134. Hailemichael, Y. & Overwijk, W. W. Peptide-based anticancer vaccines: The making and unmaking of a T-cell graveyard. *Oncoimmunology* **2**, e24743 (2013).
 135. Jenner, E. An Inquiry into the Causes and Effects of Variolae Vaccinae, a Disease Discovered in Some Western Counties of England. *London: Sampson Low* (1798).
 136. Scott, C. Classifying Vaccines: From Cowpox to the Cutting Edge. *BioProcess International* 14–23 (2004).
 137. Baxter, D. Active and passive immunity, vaccine types, excipients and licensing. *Occup. Med. (Chic. Ill)*. **57**, 552–556 (2007).
 138. Minor, P. D. Live attenuated vaccines: Historical successes and current challenges. *Virology* **479–480**, 379–92 (2015).
 139. Chen, G. L. & Subbarao, K. in *Current topics in microbiology and immunology* **333**, 109–132 (2009).
 140. Locht, C. & Mielcarek, N. Live attenuated vaccines against pertussis. *Expert Rev. Vaccines* **13**, 1147–1158 (2014).
 141. Tennant, S. M. & Levine, M. M. Live attenuated vaccines for invasive Salmonella infections. *Vaccine* **33**, C36–C41 (2015).
 142. Cohen, J. I. Strategies for herpes zoster vaccination of immunocompromised patients. *J. Infect. Dis.* **197**, S237-41 (2008).
 143. Ljungman, P. Vaccination of immunocompromised patients. *Clin. Microbiol. Infect.* **18**, 93–99 (2012).
 144. Waldeland, H. & Frenkel, J. K. Live and killed vaccines against toxoplasmosis in mice. *J. Parasitol.* **69**, 60–5 (1983).
 145. Muotiala, A., Hovi, M. & Mäkelä, P. H. Protective immunity in mouse salmonellosis: comparison of smooth and rough live and killed vaccines. *Microb. Pathog.* **6**, 51–60 (1989).
 146. Hruby, D. E. Vaccinia virus vectors: new strategies for producing recombinant vaccines. *Clin. Microbiol. Rev.* **3**, 153–70 (1990).
 147. Arnon, A. & Levi, R. Synthetic recombinant vaccines against viral agents. *Int. Arch. Allergy Immunol.* **108**, 321–6 (1995).
 148. Henderson, D. A. & Moss, B. *Recombinant Vaccinia Virus Vaccines*. *Vaccines* (Saunders, 1999).
 149. Ohtsuka, J. *et al.* Vero/BC-F: an efficient packaging cell line stably expressing F protein to generate single round-infectious human parainfluenza virus type 2 vector. *Gene Ther.* **21**, 775–784 (2014).

150. Alarcon, J. B., Waive, G. W. & McManus, D. P. DNA vaccines: technology and application as anti-parasite and anti-microbial agents. *Adv. Parasitol.* **42**, 343–410 (1999).
151. Robinson, H. L. & Pertmer, T. M. DNA vaccines for viral infections: basic studies and applications. *Adv. Virus Res.* **55**, 1–74 (2000).
152. Liu, M. A. DNA vaccines: a review. *J. Intern. Med.* **253**, 402–10 (2003).
153. Ferraro, B. *et al.* Clinical applications of DNA vaccines: current progress. *Clin. Infect. Dis.* **53**, 296–302 (2011).
154. Harrop, R., John, J. & Carroll, M. W. Recombinant viral vectors: Cancer vaccines. *Adv. Drug Deliv. Rev.* **58**, 931–947 (2006).
155. Larocca, C. & Schlom, J. Viral Vector-Based Therapeutic Cancer Vaccines. *Cancer J.* **17**, 359–371 (2011).
156. Cawood, R. *et al.* Recombinant viral vaccines for cancer. *Trends Mol. Med.* **18**, 564–574 (2012).
157. Fioretti, D., Iurescia, S., Fazio, V. M. & Rinaldi, M. DNA vaccines: developing new strategies against cancer. *J. Biomed. Biotechnol.* **2010**, 174378 (2010).
158. Yang, B., Jeang, J., Yang, A., Wu, T. C. & Hung, C.-F. DNA vaccine for cancer immunotherapy. *Hum. Vaccin. Immunother.* **10**, 3153–64 (2015).
159. Moyle, P. M. & Toth, I. Modern Subunit Vaccines: Development, Components, and Research Opportunities. *ChemMedChem* **8**, 360–376 (2013).
160. Mulder, A. M. *et al.* Toolbox for Non-Intrusive Structural and Functional Analysis of Recombinant VLP Based Vaccines: A Case Study with Hepatitis B Vaccine. *PLoS One* **7**, e33235 (2012).
161. Del Giudice, G., Fracapane, E., Della Cioppa, G. & Rappuoli, R. Aflunov®: a vaccine tailored for pre-pandemic and pandemic approaches against influenza. *Expert Opin. Biol. Ther.* **13**, 121–135 (2013).
162. Schiller, J. T. & Lowy, D. R. Papillomavirus-like particle based vaccines: cervical cancer and beyond. *Expert Opin. Biol. Ther.* **1**, 571–581 (2001).
163. Buteau, C., Markovic, S. N. & Celis, E. Challenges in the development of effective peptide vaccines for cancer. *Mayo Clin. Proc.* **77**, 339–49 (2002).
164. Felnerova, D., Viret, J.-F., Glück, R. & Moser, C. Liposomes and virosomes as delivery systems for antigens, nucleic acids and drugs. *Curr. Opin. Biotechnol.* **15**, 518–529 (2004).
165. Schneble, E., Clifton, G. T., Hale, D. F. & Peoples, G. E. in *Methods in Molecular Biology* (ed. Thomas, S.) **1403**, 797–817 (Springer Science+Business Media, 2016).

166. Hirayama, M. & Nishimura, Y. The present status and future prospects of peptide-based cancer vaccines. *Int. Immunol.* **28**, 319–328 (2016).
167. Polyakova, A., Kuznetsova, K. & Moshkovskii, S. Proteogenomics meets cancer immunology: mass spectrometric discovery and analysis of neoantigens. *Expert Rev. Proteomics* **12**, 533–541 (2015).
168. Menez-Jamet, J., Gallou, C., Rougeot, A. & Kosmatopoulos, K. Optimized tumor cryptic peptides: the basis for universal neo-antigen-like tumor vaccines. *Ann. Transl. Med.* **4**, 266–266 (2016).
169. Sun, Z., Chen, F., Meng, F., Wei, J. & Liu, B. MHC class II restricted neoantigen: A promising target in tumor immunotherapy. *Cancer Lett.* **392**, 17–25 (2017).
170. Zepp, F. Principles of vaccine design—Lessons from nature. *Vaccine* **28**, C14-24 (2010).
171. Petrovsky, N. & Aguilar, J. C. Vaccine adjuvants: Current state and future trends. *Immunol. Cell Biol.* **82**, 488–496 (2004).
172. Dey, A. K. & Srivastava, I. K. Novel adjuvants and delivery systems for enhancing immune responses induced by immunogens. *Expert Rev. Vaccines* **10**, 227–251 (2011).
173. Guy, B. The perfect mix: recent progress in adjuvant research. *Nat. Rev. Microbiol.* **5**, 505–517 (2007).
174. Marrack, P., McKee, A. S. & Munks, M. W. Towards an understanding of the adjuvant action of aluminium. *Nat. Rev. Immunol.* **9**, 287–293 (2009).
175. Clapp, T., Siebert, P., Chen, D. & Jones Braun, L. Vaccines with Aluminum-containing Adjuvants: Optimizing Vaccine Efficacy and Thermal Stability. *J. Pharm. Sci.* **100**, 388–401 (2011).
176. Grun, J. L. & Maurer, P. H. Different T helper cell subsets elicited in mice utilizing two different adjuvant vehicles: the role of endogenous interleukin 1 in proliferative responses. *Cell. Immunol.* **121**, 134–45 (1989).
177. Demento, S. L., Siefert, A. L., Bandyopadhyay, A., Sharp, F. A. & Fahmy, T. M. Pathogen-associated molecular patterns on biomaterials: a paradigm for engineering new vaccines. *Trends Biotechnol.* **29**, 294–306 (2011).
178. Baxevanis, C. N., Voutsas, I. F. & Tsitsilonis, O. E. Toll-like receptor agonists: current status and future perspective on their utility as adjuvants in improving anticancer vaccination strategies. *Immunotherapy* **5**, 497–511 (2013).
179. Kawai, T. & Akira, S. The role of pattern-recognition receptors in innate immunity: update on Toll-like receptors. *Nat. Immunol.* **11**, 373–384 (2010).
180. Klinman, D. M. Immunotherapeutic uses of CpG oligodeoxynucleotides. *Nat. Rev. Immunol.* **4**, 249–258 (2004).

181. Krishnamachari, Y., Geary, S. M., Lemke, C. D. & Salem, A. K. Nanoparticle Delivery Systems in Cancer Vaccines. *Pharm. Res.* **28**, 215–236 (2011).
182. Park, Y.-M. *et al.* Nanoparticle-Based Vaccine Delivery for Cancer Immunotherapy. *Immune Netw.* **13**, 177–183 (2013).
183. Gregory, A. E., Titball, R. & Williamson, D. Vaccine delivery using nanoparticles. *Front. Cell. Infect. Microbiol.* **3**, 13 (2013).
184. Noad, R. & Roy, P. Virus-like particles as immunogens. *Trends Microbiol.* **11**, 438–444 (2003).
185. Grgacic, E. V. L. & Anderson, D. A. Virus-like particles: Passport to immune recognition. *Methods* **40**, 60–65 (2006).
186. Ludwig, C. & Wagner, R. Virus-like particles—universal molecular toolboxes. *Curr. Opin. Biotechnol.* **18**, 537–545 (2007).
187. Al-Barwani, F., Donaldson, B., Pelham, S. J., Young, S. L. & Ward, V. K. Antigen delivery by virus-like particles for immunotherapeutic vaccination. *Ther. Deliv.* **5**, 1223–1240 (2014).
188. Schiller, J. T. & Lowy, D. R. Raising expectations for subunit vaccine. *J. Infect. Dis.* **211**, 1373–1375 (2015).
189. Altin, J. G., van Broekhoven, C. L. & Parish, C. R. Targeting dendritic cells with antigen-containing liposomes: antitumour immunity. *Expert Opin. Biol. Ther.* **4**, 1735–1747 (2004).
190. Henriksen-Lacey, M., Korsholm, K. S., Andersen, P., Perrie, Y. & Christensen, D. Liposomal vaccine delivery systems. *Expert Opin. Drug Deliv.* **8**, 505–519 (2011).
191. Schwendener, R. A. Liposomes as vaccine delivery systems: a review of the recent advances. *Ther. Adv. Vaccines* **2**, 159–182 (2014).
192. Tandrup Schmidt, S., Foged, C., Smith Korsholm, K., Rades, T. & Christensen, D. Liposome-Based Adjuvants for Subunit Vaccines: Formulation Strategies for Subunit Antigens and Immunostimulators. *Pharmaceutics* **8**, 7 (2016).
193. Sjölander, A., Cox, J. C. & Barr, I. G. ISCOMs: an adjuvant with multiple functions. *J. Leukoc. Biol.* **64**, 713–23 (1998).
194. Pearse, M. J. & Drane, D. ISCOMATRIX adjuvant for antigen delivery. *Adv. Drug Deliv. Rev.* **57**, 465–474 (2005).
195. Sanders, M. T., Brown, L. E., Deliyannis, G. & Pearse, M. J. ISCOM-based vaccines: The second decade. *Immunol. Cell Biol.* **83**, 119–128 (2005).
196. Sun, H.-X., Xie, Y. & Ye, Y.-P. ISCOMs and ISCOMATRIXTM. *Vaccine* **27**, 4388–4401 (2009).
197. Leleux, J. & Roy, K. Micro and Nanoparticle-Based Delivery Systems for Vaccine

- Immunotherapy: An Immunological and Materials Perspective. *Adv. Healthc. Mater.* **2**, 72–94 (2013).
198. Sahdev, P., Ochyl, L. J. & Moon, J. J. Biomaterials for Nanoparticle Vaccine Delivery Systems. *Pharm. Res.* **31**, 2563–2582 (2014).
 199. Rahimian, S. *et al.* Particulate Systems Based on Poly(Lactic-co-Glycolic)Acid (pLGA) for Immunotherapy of Cancer. *Curr. Pharm. Des.* **21**, 4201–16 (2015).
 200. Gutjahr, A. *et al.* Biodegradable Polymeric Nanoparticles-Based Vaccine Adjuvants for Lymph Nodes Targeting. *Vaccines* **4**, 34 (2016).
 201. Zarschler, K. *et al.* Ultrasmall inorganic nanoparticles: State-of-the-art and perspectives for biomedical applications. *Nanomedicine Nanotechnology, Biol. Med.* **12**, 1663–1701 (2016).
 202. Wang, F., Li, C., Cheng, J. & Yuan, Z. Recent advances on inorganic nanoparticle-based cancer therapeutic agents. *Int. J. Environ. Res. Public Health* **13**, (2016).
 203. DeLong, R. K. & Curtis, C. B. Toward RNA nanoparticle vaccines: Synergizing RNA and inorganic nanoparticles to achieve immunopotential. *WIREs Nanomedicine and Nanobiotechnology* **9**, e1415 (2017).
 204. Morrow, K. J., Bawa, R. & Wei, C. Recent Advances in Basic and Clinical Nanomedicine. *Med. Clin. North Am.* **91**, 805–843 (2007).
 205. Liu, Y., Miyoshi, H. & Nakamura, M. Nanomedicine for drug delivery and imaging: A promising avenue for cancer therapy and diagnosis using targeted functional nanoparticles. *Int. J. Cancer* **120**, 2527–2537 (2007).
 206. Murday, J. S., Siegel, R. W., Stein, J. & Wright, J. F. Translational nanomedicine: status assessment and opportunities. *Nanomedicine Nanotechnology, Biol. Med.* **5**, 251–273 (2009).
 207. Riehemann, K. *et al.* Nanomedicine - Challenge and perspectives. *Angew. Chemie Int. Ed.* **48**, 872–897 (2009).
 208. Sweeney, A. E. Nanomedicine concepts in the general medical curriculum: initiating a discussion. *Int. J. Nanomedicine* **10**, 7319–31 (2015).
 209. Li, X. *et al.* Nanomaterials in the application of tumor vaccines: advantages and disadvantages. *Onco. Targets. Ther.* **6**, 629–34 (2013).
 210. Willmann, J. K., van Bruggen, N., Dinkelborg, L. M. & Gambhir, S. S. Molecular imaging in drug development. *Nat. Rev. Drug Discov.* **7**, 591–607 (2008).
 211. Rudin, M. & Weissleder, R. Molecular imaging in drug discovery and development. *Nat. Rev. Drug Discov.* **2**, 123–31 (2003).
 212. Cunha, L., Szigeti, K., Mathé, D. & Metello, L. F. The role of molecular imaging in modern drug development. *Drug Discov. Today* **19**, 936–48 (2014).

213. Kim, J., Piao, Y. & Hyeon, T. Multifunctional nanostructured materials for multimodal imaging, and simultaneous imaging and therapy. *Chem. Soc. Rev.* **38**, 372–90 (2009).
214. Park, K. *et al.* New generation of multifunctional nanoparticles for cancer imaging and therapy. *Adv. Funct. Mater.* **19**, 1553–1566 (2009).
215. Lee, D.-E. *et al.* Multifunctional nanoparticles for multimodal imaging and theragnosis. *Chem. Soc. Rev.* **41**, 2656–2672 (2012).
216. Zhou, Q. *et al.* Different-Sized Gold Nanoparticle Activator/Antigen Increases Dendritic Cells Accumulation in Liver-Draining Lymph Nodes and CD8+ T Cell Responses. *ACS Nano* **10**, 2678–2692 (2016).
217. Slowing, I. I., Trewyn, B. G., Giri, S. & Lin, V. S.-Y. Mesoporous Silica Nanoparticles for Drug Delivery and Biosensing Applications. *Adv. Funct. Mater.* **17**, 1225–1236 (2007).
218. Yu, J., Huang, D.-Y., Yousaf, M. Z., Hou, Y.-L. & Gao, S. Magnetic nanoparticle-based cancer therapy. *Chinese Phys. B* **22**, 27506 (2013).
219. Barr, T. a, Krembuszewski, M., Gupta, M., Gray, D. & Mareque-Rivas, J. C. Quantum dots decorated with pathogen associated molecular patterns as fluorescent synthetic pathogen models. *Mol. Biosyst.* **6**, 1572–1575 (2010).
220. Gottardi, R. & Douradinha, B. Carbon nanotubes as a novel tool for vaccination against infectious diseases and cancer. *J. Nanobiotechnology* **11**, 7 (2013).
221. Bourrinet, P. *et al.* Preclinical Safety and Pharmacokinetic Profile of Ferumoxtran-10, an Ultrasmall Superparamagnetic Iron Oxide Magnetic Resonance Contrast Agent. *Invest. Radiol.* **41**, 313–324 (2006).
222. Colombo, M. *et al.* Biological applications of magnetic nanoparticles. *Chem. Soc. Rev.* **41**, 4306–34 (2012).
223. Couto, D., Freitas, M., Carvalho, F. & Fernandes, E. Iron Oxide Nanoparticles: An Insight into their Biomedical Applications. *Curr. Med. Chem.* **22**, 1808–1828 (2015).
224. Levy, M. *et al.* Long term in vivo biotransformation of iron oxide nanoparticles. *Biomaterials* **32**, 3988–3999 (2011).
225. Soenen, S. J. H. & De Cuyper, M. Assessing iron oxide nanoparticle toxicity in vitro: current status and future prospects. *Nanomedicine* **5**, 1261–1275 (2010).
226. Gallo, J., Long, N. J. & Aboagye, E. O. Magnetic nanoparticles as contrast agents in the diagnosis and treatment of cancer. *Chem. Soc. Rev.* **42**, 7816–7833 (2013).
227. Lee, N. *et al.* Iron Oxide Based Nanoparticles for Multimodal Imaging and Magneto-responsive Therapy. *Chem. Rev.* **115**, 10637–89 (2015).
228. Vyas, D. *et al.* Doxorubicin-Hyaluronan Conjugated Super-Paramagnetic Iron

- Oxide Nanoparticles (DOX-HA-SPION) Enhanced Cytoplasmic Uptake of Doxorubicin and Modulated Apoptosis, IL-6 Release and NF-kappaB Activity in Human MDA-MB-231 Breast Cancer Cells. *J. Nanosci. Nanotechnol.* **15**, 6413–22 (2015).
229. Chertok, B., David, A. E. & Yang, V. C. Brain tumor targeting of magnetic nanoparticles for potential drug delivery: Effect of administration route and magnetic field topography. *J. Control. Release* **155**, 393–399 (2011).
230. Zou, P. *et al.* Superparamagnetic iron oxide nanotheranostics for targeted cancer cell imaging and pH-dependent intracellular drug release. *Mol. Pharm.* **7**, 1974–1984 (2010).
231. Niu, C. *et al.* Doxorubicin loaded superparamagnetic PLGA-iron oxide multifunctional microbubbles for dual-mode US/MR imaging and therapy of metastasis in lymph nodes. *Biomaterials* **34**, 2307–2317 (2013).
232. Javid, A. *et al.* Biocompatible APTES-PEG modified magnetite nanoparticles: Effective carriers of antineoplastic agents to ovarian cancer. *Appl. Biochem. Biotechnol.* **173**, 36–54 (2014).
233. Lee, G. Y. *et al.* Theranostic nanoparticles with controlled release of gemcitabine for targeted therapy and MRI of pancreatic cancer. *ACS Nano* **7**, 2078–2089 (2013).
234. Maier-Hauff, K. *et al.* Intracranial thermotherapy using magnetic nanoparticles combined with external beam radiotherapy: Results of a feasibility study on patients with glioblastoma multiforme. *J. Neurooncol.* **81**, 53–60 (2007).
235. Johannsen, M., Thiesen, B., Wust, P. & Jordan, A. Magnetic nanoparticle hyperthermia for prostate cancer. *Int. J. Hyperth.* **26**, 790–795 (2010).
236. Silva, A. C. *et al.* Application of hyperthermia induced by superparamagnetic iron oxide nanoparticles in glioma treatment. *Int. J. Nanomedicine* **6**, 591–603 (2011).
237. Salunkhe, A. B. B., Khot, V. M. M. & Pawar, S. H. H. Magnetic Hyperthermia with Magnetic Nanoparticles: A Status Review. *Curr. Top. Med. Chem.* **14**, 572–594 (2014).
238. Medarova, Z., Pham, W., Farrar, C., Petkova, V. & Moore, A. In vivo imaging of siRNA delivery and silencing in tumors. *Nat. Med.* **13**, 372–7 (2007).
239. Taratula, O. *et al.* Multifunctional nanomedicine platform for cancer specific delivery of siRNA by superparamagnetic iron oxide nanoparticles-dendrimer complexes. *Curr. Drug Deliv.* **8**, 59–69 (2011).
240. Wang, C. *et al.* Dual-purpose magnetic micelles for MRI and gene delivery. *J. Control. Release* **163**, 82–92 (2012).
241. Jiang, S., Eltoukhy, A., Love, K., Langer, R. & Anderson, D. Lipidoid-Coated Iron

- Oxide Nanoparticles for Efficient DNA and siRNA delivery. *Nano Lett.* 1–6 (2013). doi:doi: 10.1021/nl304287a
242. Hu, S. H. *et al.* Surfactant-free, lipo-polymersomes stabilized by iron oxide nanoparticles/polymer interlayer for synergistically targeted and magnetically guided gene delivery. *Adv. Healthc. Mater.* **3**, 273–282 (2014).
 243. Xie, J., Liu, G., Eden, H. S., Ai, H. & Chen, X. Surface engineered magnetic nanoparticle platforms for cancer imaging and therapy. *Acc. Chem. Res.* **XXX**, 883–892 (2011).
 244. Kievit, F. M. & Zhang, M. Surface engineering of iron oxide nanoparticles for targeted cancer therapy. *Acc. Chem. Res.* **44**, 853–862 (2011).
 245. Chen, J. *et al.* Superparamagnetic iron oxide nanoparticles mediated (131)I-hVEGF siRNA inhibits hepatocellular carcinoma tumor growth in nude mice. *BMC Cancer* **14**, 114 (2014).
 246. Kitaoka, M., Naritomi, A., Hirakawa, Y., Kamiya, N. & Goto, M. Transdermal Immunization using Solid-in-oil Nanodispersion with CpG Oligodeoxynucleotide Adjuvants. *Pharm. Res.* **32**, 1486–1492 (2015).
 247. Bourquin, C. *et al.* Targeting CpG Oligonucleotides to the Lymph Node by Nanoparticles Elicits Efficient Antitumoral Immunity. *J. Immunol.* **181**, 2990–8 (2008).
 248. Lee, Y.-R. *et al.* Biodegradable nanoparticles containing TLR3 or TLR9 agonists together with antigen enhance MHC-restricted presentation of the antigen. *Arch. Pharm. Res.* **33**, 1859–1866 (2010).
 249. Lee, Y.-R., Lee, Y.-H., Kim, K.-H., Im, S.-A. & Lee, C.-K. Induction of Potent Antigen-specific Cytotoxic T Cell Response by PLGA-nanoparticles Containing Antigen and TLR Agonist. *Immune Netw.* **13**, 30 (2013).
 250. Rattanakiat, S., Nishikawa, M. & Takakura, Y. Self-assembling CpG DNA nanoparticles for efficient antigen delivery and immunostimulation. *Eur. J. Pharm. Sci.* **47**, 352–358 (2012).
 251. de Jong, S. *et al.* Encapsulation in liposomal nanoparticles enhances the immunostimulatory, adjuvant and anti-tumor activity of subcutaneously administered CpG ODN. *Cancer Immunol. Immunother.* **56**, 1251–1264 (2007).
 252. Wakita, D. *et al.* An indispensable role of type-1 IFNs for inducing CTL-mediated complete eradication of established tumor tissue by CpG-liposome co-encapsulated with model tumor antigen. *Int. Immunol.* **18**, 425–434 (2006).
 253. Kranz, L. M. *et al.* Systemic RNA delivery to dendritic cells exploits antiviral defence for cancer immunotherapy. *Nature* **534**, 396–401 (2016).
 254. Jain, S., Yap, W. T. & Irvine, D. J. Synthesis of Protein-Loaded Hydrogel Particles in an Aqueous Two-Phase System for Coincident Antigen and CpG

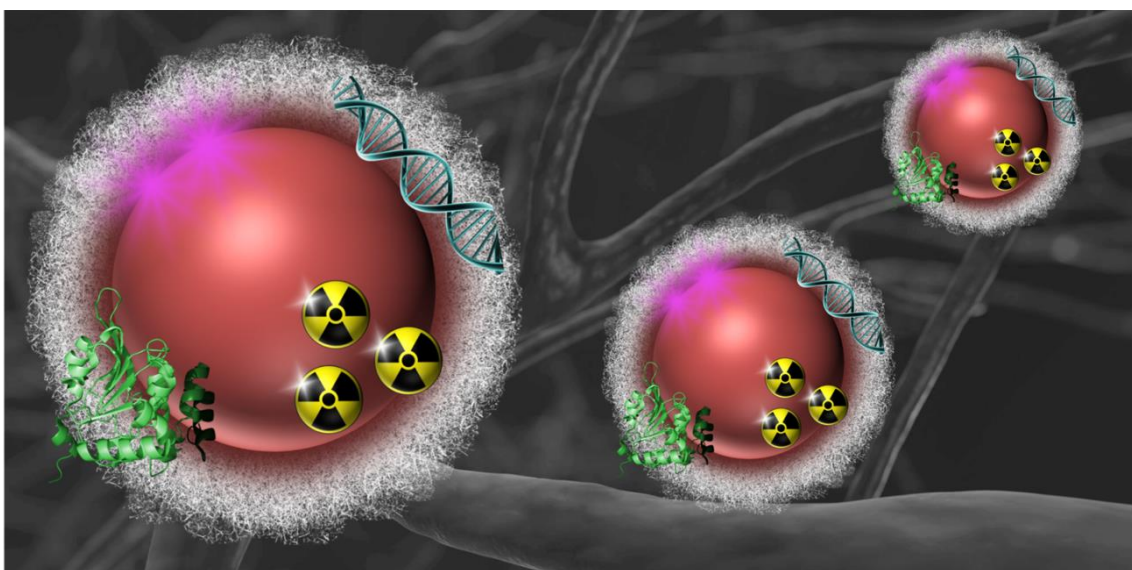
- Oligonucleotide Delivery to Antigen-Presenting Cells. *Biomacromolecules* **6**, 2590–2600 (2005).
255. Ilyinskii, P. O. *et al.* Adjuvant-carrying synthetic vaccine particles augment the immune response to encapsulated antigen and exhibit strong local immune activation without inducing systemic cytokine release. *Vaccine* **32**, 2882–95 (2014).
 256. Wilson, J. T. *et al.* pH-Responsive nanoparticle vaccines for dual-delivery of antigens and immunostimulatory oligonucleotides. *ACS Nano* **7**, 3912–25 (2013).
 257. Siefert, A. L., Caplan, M. J. & Fahmy, T. M. Artificial bacterial biomimetic nanoparticles synergize pathogen-associated molecular patterns for vaccine efficacy. *Biomaterials* **97**, 85–96 (2016).
 258. Hirosue, S., Kourtis, I. C., van der Vlies, A. J., Hubbell, J. A. & Swartz, M. A. Antigen delivery to dendritic cells by poly(propylene sulfide) nanoparticles with disulfide conjugated peptides: Cross-presentation and T cell activation. *Vaccine* **28**, 7897–7906 (2010).
 259. Nembrini, C. *et al.* Nanoparticle conjugation of antigen enhances cytotoxic T-cell responses in pulmonary vaccination. *Proc. Natl. Acad. Sci.* **108**, E989–E997 (2011).
 260. Eby, J. K. *et al.* Polymer micelles with pyridyl disulfide-coupled antigen travel through lymphatics and show enhanced cellular responses following immunization. *Acta Biomater.* **8**, 3210–3217 (2012).
 261. Stano, A., Scott, E. A., Dane, K. Y., Swartz, M. A. & Hubbell, J. A. Tunable T cell immunity towards a protein antigen using polymersomes vs. solid-core nanoparticles. *Biomaterials* **34**, 4339–4346 (2013).
 262. de Titta, A. *et al.* Nanoparticle conjugation of CpG enhances adjuvancy for cellular immunity and memory recall at low dose. *Proc. Natl. Acad. Sci. U. S. A.* **110**, 19902–7 (2013).
 263. Sen, D., Deerinck, T. J., Ellisman, M. H., Parker, I. & Cahalan, M. D. Quantum Dots for Tracking Dendritic Cells and Priming an Immune Response In Vitro and In Vivo. *PLoS One* **3**, e3290 (2008).
 264. Li, Z. *et al.* Combination Delivery of Antigens and CpG by Lanthanides-Based Core-Shell Nanoparticles for Enhanced Immune Response and Dual-Mode Imaging. *Adv. Healthc. Mater.* **2**, 1309–1313 (2013).
 265. Duan, F. *et al.* A simple and powerful co-delivery system based on pH-responsive metal-organic frameworks for enhanced cancer immunotherapy. *Biomaterials* **122**, 23–33 (2017).
 266. Xiang, J. *et al.* Antigen-Loaded Upconversion Nanoparticles for Dendritic Cell Stimulation, Tracking, and Vaccination in Dendritic Cell-Based Immunotherapy. *ACS Nano* **9**, 6401–6411 (2015).

267. Almeida, J. P. M., Lin, A. Y., Figueroa, E. R., Foster, A. E. & Drezek, R. A. In vivo Gold Nanoparticle Delivery of Peptide Vaccine Induces Anti-Tumor Immune Response in Prophylactic and Therapeutic Tumor Models. *Small* **11**, 1453–1459 (2015).
268. Dekaban, G. A. *et al.* Semiquantitation of Mouse Dendritic Cell Migration In Vivo Using Cellular MRI. *J. Immunother.* **32**, 240–251 (2009).
269. Mou, Y. *et al.* In vivo migration of dendritic cells labeled with synthetic superparamagnetic iron oxide. *Int. J. Nanomedicine* **6**, 2633–2640 (2011).
270. de Chickera, S. N. *et al.* Labelling dendritic cells with SPIO has implications for their subsequent in vivo migration as assessed with cellular MRI. *Contrast Media Mol. Imaging* **6**, 314–327 (2011).
271. Noh, Y.-W., Jang, Y.-S., Ahn, K.-J., Lim, Y. T. & Chung, B. H. Simultaneous in vivo tracking of dendritic cells and priming of an antigen-specific immune response. *Biomaterials* **32**, 6254–6263 (2011).
272. Zhang, X. *et al.* Cellular magnetic resonance imaging of monocyte-derived dendritic cell migration from healthy donors and cancer patients as assessed in a scid mouse model. *Cytotherapy* **13**, 1234–1248 (2011).
273. de Chickera, S. *et al.* Cellular MRI as a suitable, sensitive non-invasive modality for correlating in vivo migratory efficiencies of different dendritic cell populations with subsequent immunological outcomes. *Int. Immunol.* **24**, 29–41 (2012).
274. Martelli, C. *et al.* In Vivo Imaging of Lymph Node Migration of MNP- and ¹¹¹In-Labeled Dendritic Cells in a Transgenic Mouse Model of Breast Cancer (MMTV-Ras). *Mol. Imaging Biol.* **14**, 183–196 (2012).
275. Ferguson, P. M., Slocombe, A., Tilley, R. D., Hermans, I. F. & Clarke, M. Using Magnetic Resonance Imaging to Evaluate Dendritic Cell-Based Vaccination. *PLoS One* **8**, e65318 (2013).
276. Xu, Y. *et al.* Superparamagnetic MRI probes for in vivo tracking of dendritic cell migration with a clinical 3 T scanner. *Biomaterials* **58**, 63–71 (2015).
277. Jin, H. *et al.* Magnetic Enrichment of Dendritic Cell Vaccine in Lymph Node with Fluorescent-Magnetic Nanoparticles Enhanced Cancer Immunotherapy. *Theranostics* **6**, 2000–2014 (2016).
278. Cruz, L. J. *et al.* Multimodal Imaging of Nanovaccine Carriers Targeted to Human Dendritic Cells. *Mol. Pharm.* **8**, 520–531 (2011).
279. Kim, D. K., Chang, J. H. & Kang, Y. J. Efficient internalization of peptide-conjugated SPIONs in dendritic cells for tumor targeting. *J. Nanosci. Nanotechnol.* **12**, 5191–5198 (2012).
280. Lundquist, C. *et al.* Characterization of Free and Porous Silicon-Encapsulated

- Superparamagnetic Iron Oxide Nanoparticles as Platforms for the Development of Theranostic Vaccines. *Med. Sci.* **2**, 51–69 (2014).
281. Shevtsov, M. A. *et al.* 70-kDa heat shock protein coated magnetic nanocarriers as a nanovaccine for induction of anti-tumor immune response in experimental glioma. *J. Control. Release* **220**, 329–340 (2015).
 282. Sungsuwan, S., Yin, Z. & Huang, X. Lipopeptide-Coated Iron Oxide Nanoparticles as Potential Glycoconjugate-Based Synthetic Anticancer Vaccines. *ACS Appl. Mater. Interfaces* **7**, 17535–17544 (2015).
 283. Shen, L. *et al.* Vaccination with trifunctional nanoparticles that address CD8 + dendritic cells inhibits growth of established melanoma. *Nanomedicine* **11**, 2647–2662 (2016).
 284. Guo, L., Zhang, H. & Chen, B. Nivolumab as Programmed Death-1 (PD-1) Inhibitor for Targeted Immunotherapy in Tumor. *J. Cancer* **8**, 410–416 (2017).
 285. Camacho, L. H. CTLA-4 blockade with ipilimumab: biology, safety, efficacy, and future considerations. *Cancer Med.* **4**, 661–72 (2015).

2

Design, synthesis and characterisation of the PEGylated IONP-filled nanovaccines



2.1. Introduction

NPs composed of diverse types of materials have great potential for application in many different areas of biomedicine and raise new possibilities in the diagnosis and treatment of cancer. However, the properties of the NPs have to be carefully designed, modified and controlled according to the specific application, as these properties may significantly affect their function and performance. As a whole, the characteristics of NPs are finely tuned by choosing a suitable synthesis method, adding specific surface coatings, incorporating imaging probes and by functionalising with desired biomolecules (**Figure 2.1**). This chapter will describe the design and synthesis of the IONP-based anticancer vaccines developed during this thesis.

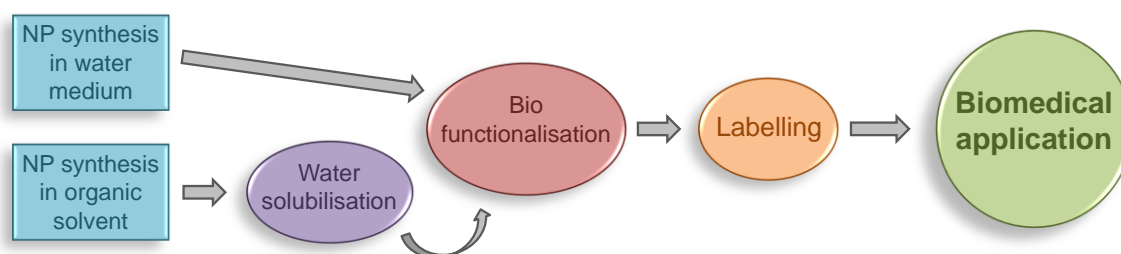


Figure 2.1. Flow diagram representing the synthetic pathways for the production of NPs for biomedical applications. Depending on the type of synthetic methodology adopted, nanomaterials must undergo a water solubilisation process in order to be suitable for *in vivo* applications. The selected biofunctionalisation and possible labelling procedures for their trafficking will depend on the final application. Figure adapted from *Nano Today*, 2010, 5, 213.¹

2.1.1. Physicochemical properties and synthesis of IONPs

IONPs present widespread applications in diverse areas, such as biotechnology, materials and environmental sciences, and engineering. IONPs are also promising materials for life sciences and human health applications, mainly due to the combination of good biocompatibility with excellent control of size, composition, shape and unique magnetic behaviour. For instance, materials that contain metals such as cobalt, nickel, gadolinium or the here employed iron present ferromagnetic properties at room temperature, which is an important characteristic for their biological and medical use. However, from a low toxicity point of view having iron makes the material much more suitable for *in vivo* applications.² When particles are small enough (10-20 nm), IONPs present superparamagnetic behaviour – i.e. they have

the ability to become magnetized after application of an external magnetic field and to rapidly lose magnetization once the external field is removed.^{3,4} The two main forms of IONPs, magnetite (Fe_3O_4) and its oxidized form maghemite ($\gamma\text{-Fe}_2\text{O}_3$), present excellent superparamagnetic properties at room temperature and physiological conditions. From the biomedical application point of view, these magnetic NPs provide the following capabilities:

1. IONPs can be used as drug carriers with the ability to be directed non-invasively by external magnetic fields to the target tissues. Moreover, since upon the removal of the magnetic field the 'active' behaviour of IONPs disappears, these NPs can be easily dispersed (without aggregating) and processed by cellular components, avoiding toxicity;⁵
2. IONPs can act as contrast agents for MRI;⁶
3. IONPs can directly treat tumours by magnetic hyperthermia;⁷
4. Apart from magnetic properties, IONPs can also be excellent drug delivery systems. Diameters below 100 nm allow NPs to have high surface areas for molecule/drug loading, longer circulation lifetimes, lower sedimentation rates and enhanced tissue penetration.² The loading of drugs into IONPs avoids rapid renal clearance and, therefore, enhances the treatment effect.

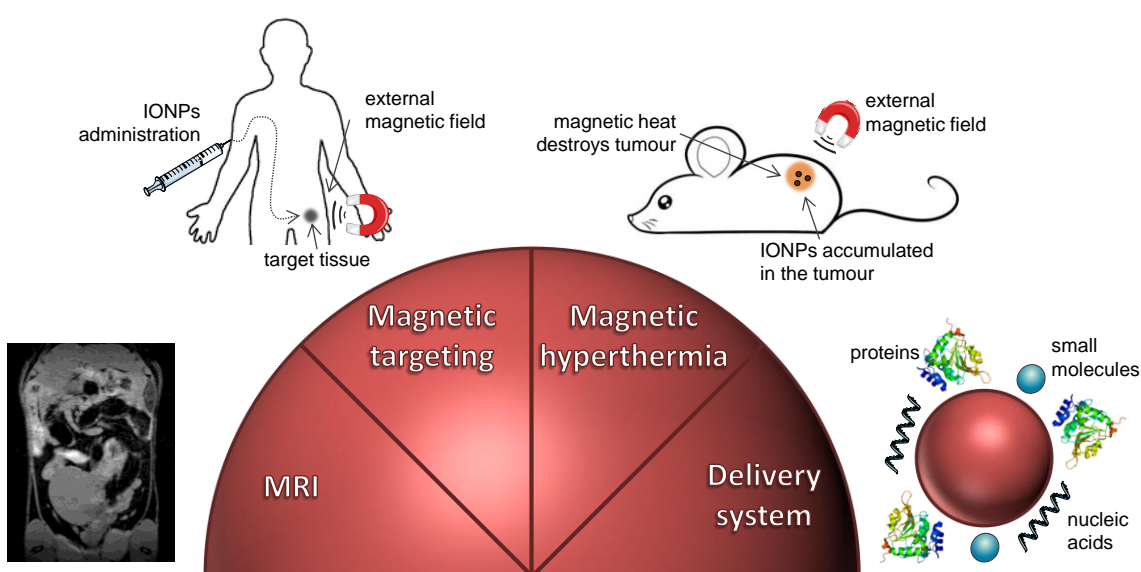


Figure 2.2. Schematic representation of biomedical applications of IONPs. These applications include: contrast agents for MRI; magnetically driven targeting of NPs to desired tissues by non-invasive external field; tumour cells destruction by magnetic hyperthermia; and delivery systems for bioactive molecules.

Hence, IONPs-based systems are considered promising biocompatible and versatile platforms for biomedical applications (**Figure 2.2**).

The synthesis method used for the preparation of IONPs will affect the particle size, shape and surface chemistry and the extent to which it is possible to obtain a narrow size distribution. All these characteristics, which need to be accurately controlled during the synthesis, determine the final magnetic properties and the desired behaviour *in vitro* and *in vivo*.⁸ The most common methods to prepare IONPs are: coprecipitation, microemulsion, hydrothermal synthesis, sonochemical synthesis and thermal decomposition.⁹⁻¹⁴

Among them, the thermal decomposition method is ideal for the preparation of highly crystalline and monodisperse IONPs with narrow size distributions. In this method iron precursors are dissolved in organic solvents and then heated until achieving a controlled thermolysis.^{13,15} As reported in 2004 by Sun et al., nontoxic and commercially available iron precursors such as iron chloride or tris(acetylacetonato) iron(III) ($\text{Fe}(\text{acac})_3$) can be used for the preparation of IONPs by this method.¹⁶ Several organic compounds, such as oleic acid and oleylamine, can also be added to the reaction in order to enhance the monodispersity and the formation of small NPs. By controlling the temperature, time of reaction and solvent type among other parameters, this method allows getting NPs of different sizes and shapes with high reproducibility between batches. Hence, thermal decomposition was chosen as the synthetic method for the IONPs developed in this thesis work.

2.1.2. Water solubilisation of IONPs

Despite having many advantages, the thermal decomposition method produces IONPs coated with hydrophobic molecules. In this way, the resulting NPs are only soluble in non-polar solvents, which is a drawback for biomedical applications. However, this disadvantage can be easily overcome by ligand exchange or addition processes that provide the desired water solubility and stability in biological environments.

a) **Ligand exchange:** This method involves replacing undesired surface molecules (e.g. hydrophobic) by hydrophilic molecules with groups that have higher affinity for the NP. Although widely employed for water solubilisation, the ligand exchange method can involve complicated reactions and often presents problems with controlling the ligand exchange amount and rate.^{17–19}

b) **Ligand addition:** As alternative to ligand exchange, NPs can be encapsulated within hydrophilic coatings without altering the pre-existing layer. In this way, amphiphilic molecules can be exploited to bind or encapsulate the hydrophobic NPs providing aqueous solubility with the hydrophilic part. There are several types of amphiphilic compounds that can be employed, such as phospholipids, saccharides, acrylic acid polymers, etc.^{20–22}

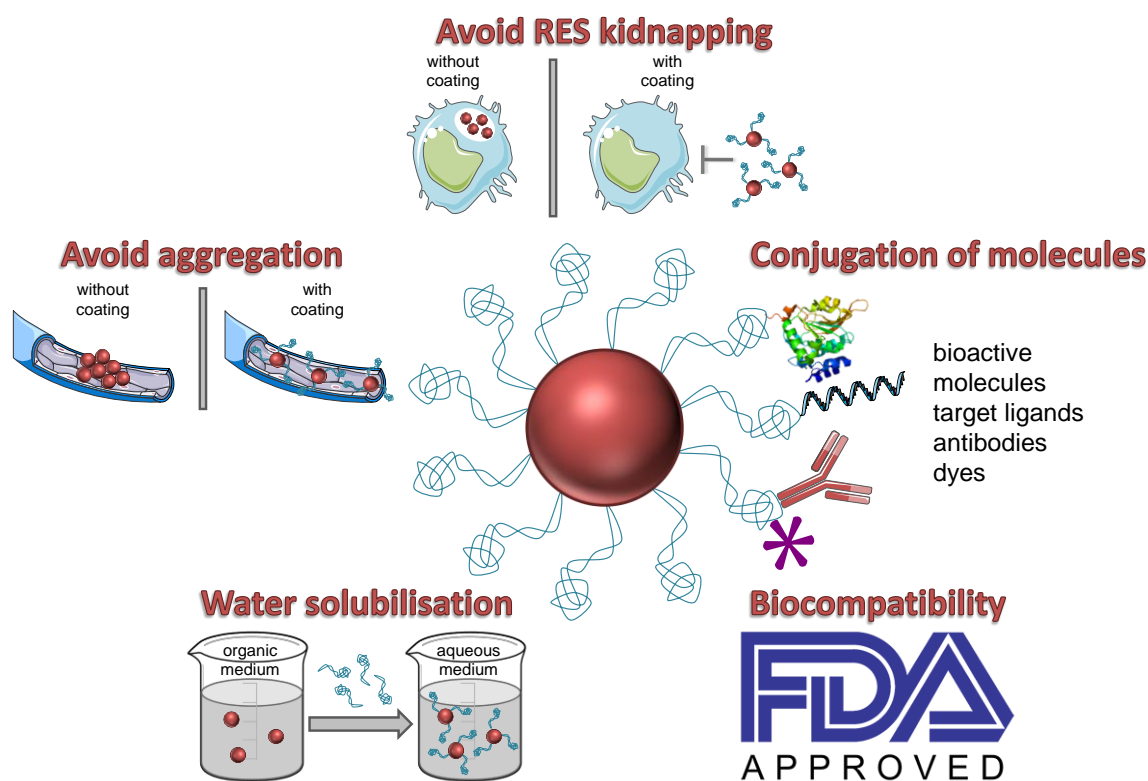


Figure 2.3. Advantages of using PEG-based coatings for NPs. Biocompatible PEG-based molecules are able to solubilise hydrophobic particles, avoid aggregation of NPs in physiological conditions, reduce the uptake of NPs by RES and allow attachment of biomolecules.

The incorporated hydrophilic coating must be selected according to the desired application. Among the biocompatible polymers, PEG-based coatings are widely used for *in vivo* biomedical applications.²³ PEGylation confers the NPs with useful properties (Figure 2.3), such as: 1) solubility in aqueous medium; 2) enhanced stability over a

wide range of pH values; 3) longer *in vivo* circulation lifetime by avoiding the premature uptake by the reticuloendothelial system (RES); 4) functional groups for bioconjugation; and 5) a biocompatible coating approved for its use in humans (source <http://www.fda.gov>).²⁴⁻²⁹

Phospholipids linked to PEG (PEG-PLs) with different molecular weights are commercially available. In this way, in this thesis the ligand addition method was adopted to encapsulate hydrophobic IONPs in PEGylated phospholipid micelles. Since the PEG-PLs can have a variety of end groups, the resulting IONP-filled micelles can be successfully produced with suitable surface chemical properties for further biofunctionalisation.

2.1.3. Biofunctionalisation of IONP-filled micelles

Attachment of molecules to the surface of NPs can be achieved through different binding strategies: conjugation chemistry, encapsulation during NP synthesis, adsorption based on charge or hydrophobic interactions and affinity-based systems (Figure 2.4).^{30,31}

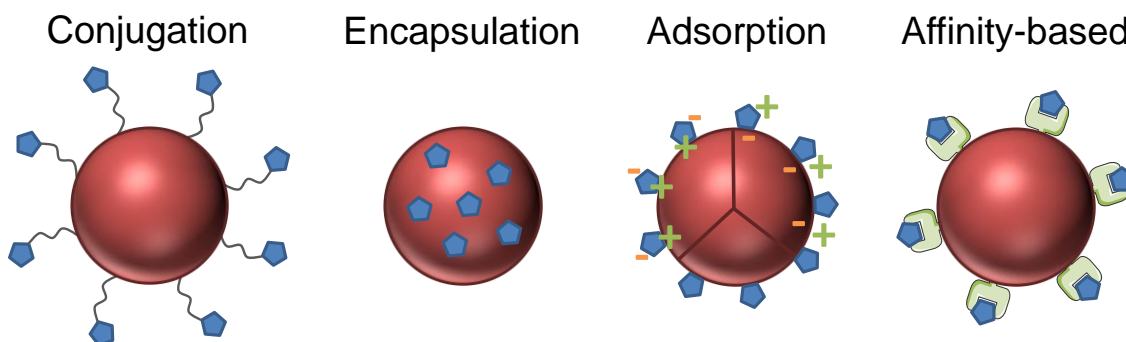


Figure 2.4. Different binding ways between NP and molecules. Biofunctionalisation NPs can be carried out through different strategies, such as covalent binding by conjugation chemistry, encapsulation, adsorption and affinity-based interactions. Figure adapted from *Vaccine*, 2014, **32**, 327.³¹

a) Conjugation chemistry: Covalent attachment of (bio)molecules can be achieved exploiting the functional groups present on the surface of the NPs and the (bio)molecules. The covalent bond formed allows strong attachment but can also provide controlled release if it is cleavable under certain conditions (pH, temperature, in the presence of enzymes, etc.).

b) Encapsulation: Biomolecules can be encapsulated during the NP production, unifying the synthesis and biofunctionalisation steps. However, these types of NPs typically have to be degraded in order to release the cargo, which can be a drawback for instance for efficiently and quickly delivering antigens to target cells.

c) Adsorption: Hydrophobic or electrostatic interactions are also exploited to form conjugates by the adsorption of (bio)molecules directly onto the NP surfaces. This binding type provides relatively weak attachment and rapid release *in vivo*.

d) Affinity-based systems: It is based on receptor-ligand molecular recognition. NPs have to be modified with the receptor and the cargo must be conjugated with the ligand, or *vice versa*. Therefore, affinity-based functionalisation involves previous covalent attachment or chemical modification of both the NP and drug load/(bio)molecule.

In the case of vaccines, the loaded antigen/adjuvant must interact with immune cells to elicit the desired immune response. In this thesis, both adsorption and conjugation chemistry were used to find the best interaction between immunostimulatory molecules and their specific receptors once internalized by immune cells.

2.1.4. Labelling of IONP-filled micelles

One of the advantages of incorporating a magnetic core into the vaccine is the capacity to track the administered formulation, a very desirable property for the DDD process, where traceable vehicles can help to identify more quickly the optimal candidates.^{32,33} Besides this intrinsic characteristic that allows IONPs to be tracked by MRI, additional imaging properties can be incorporated in this type of drug carriers systems through different types of labelling (**Figure 2.5**).

Fluorescent probes, widely used in biomedicine for a variety of purposes, can be used to visualise the cellular fate of NPs and their cargos. Among these probes are natural or synthetic proteins with fluorescent properties, such as the green fluorescent protein.³⁴ However, the incorporation of these proteins as imaging probes decreases

the available sites/space on the surface of NPs for loading other desired molecules. On the other hand, small synthetic dyes can be conjugated to several types of inorganic molecules much as they are conjugated to proteins, nucleic acids and lipids, making them a more versatile option for labelling drugs and drug delivery systems. Fluorophores such as rhodamine, fluorescein isothiocyanate (FITC) and cyanine can be attached to polymers and phospholipids coating the NPs, without affecting their other imaging properties.³⁵

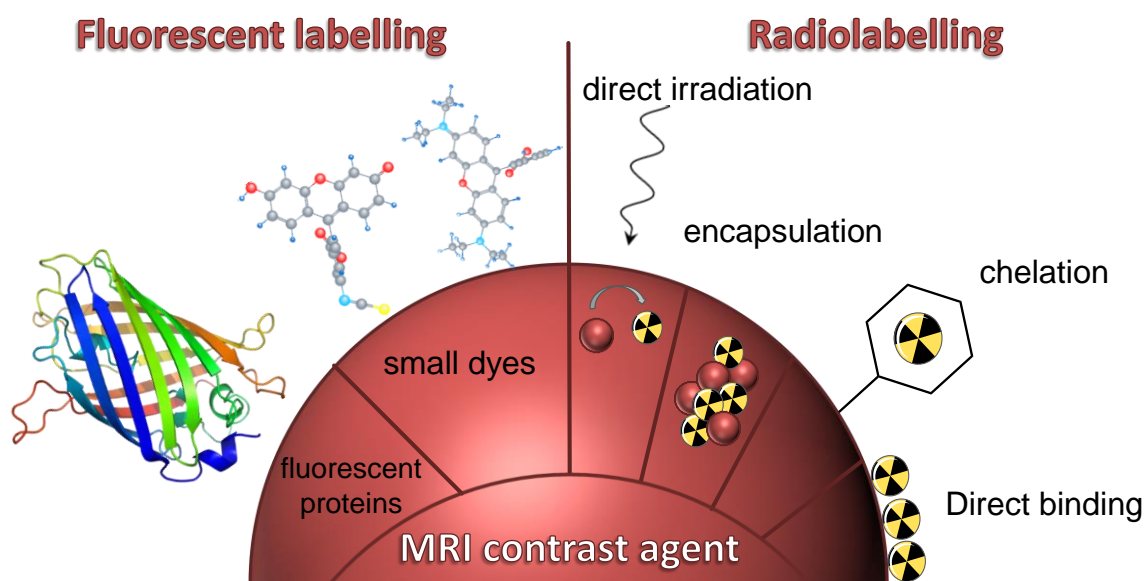


Figure 2.5. Schematic representation of the different labelling strategies that can be adopted to provide trimodal (MRI/fluorescence/nuclear) imaging IONPs. Apart from the intrinsic magnetic properties of the IONPs, NPs can be labelled with fluorescent proteins or small dyes and radiolabelled through different methods, such as direct beam irradiation, radionuclide encapsulation, radioisotope chelation or direct attachment of radioactive atoms to the NP core.

Although fluorescence microscopy and related imaging techniques are ideal for *in vitro* applications, optical imaging suffers from limited depth penetration through soft tissue and still needs major technology advances for clinical translation. On the other hand, nuclear imaging is the most sensitive clinical imaging technique.³⁶ Hence, there has been growing interest in incorporating radioactive probes into NP-based formulations for biodistribution and pharmacokinetic studies. The strategies used to date can be classified in four general groups:

- a) Direct beam irradiation: This methodology is based on the direct bombardment of the nanomaterials with protons/neutrons in order to produce radionuclides at the core of NPs.³⁷ The main disadvantage of direct radiolabelling is the need of a cyclotron

and the fact that the starting material is radioactive from the moment that it is synthesised, which complicates its subsequent manipulation.

b) Radionuclide encapsulation: As in the case of (bio)molecules, radionuclides can be encapsulated during the NPs synthesis process.³⁸ However, the consequent manipulation of the NPs must be performed in radiation controlled facilities as in the previous case.

c) Radionuclide chelation: So far most studies have required radiolabelling of NPs, including IONPs, using organic chemistry-based protocols.^{39–46} This type of approach relies on attaching chelating compounds to the NP surface, which are then able to efficiently entrap radionuclides. However, these types of reactions involve multistep synthesis and low reaction yields. A further caveat is that high loading of organic chelators on the surface of the NP can alter the pharmacological and/or pharmacokinetic properties of the NP leading to suboptimal targeting and biodistribution. Moreover, the addition of chelating groups can interfere with the biofunctionalisation process.

d) Direct radiolabelling: To overcome the aforementioned limitations a few chelate-free approaches suitable for radiolabelling NPs after their full functionalisation have been recently reported.^{47–50} This radiolabelling approach takes advantage of the surface properties of NPs to promote direct attachment of radioisotopes without altering the properties of the final delivery system.⁵¹

Combining fluorescent labelling and radiolabelling, with the intrinsic characteristics of the IONPs, it was possible to develop vaccine delivery systems that can be tracked both *in vitro* and *in vivo* using a synergistic multimodal imaging approach.

2.2. Results and discussion

2.2.1. Synthesis of IONP-based micelles

The synthesis and characterisation of the hydrophobic IONPs was conducted by Dr. Cobaleda-Siles and Dr. Gómez-Blanco, as reported elsewhere.^{52,53} The hydrophobic oleic acid-coated magnetite NPs were the starting building block of this thesis project.

The first step was to get a hydrophilic system using PEG-PLs by the ligand addition technique. This was done using the thin film hydration method. In this method the PEG-PLs self-assemble around the IONPs and encapsulate the hydrophobic core forming IONP-filled micelles (**Figure 2.6**).⁵⁴

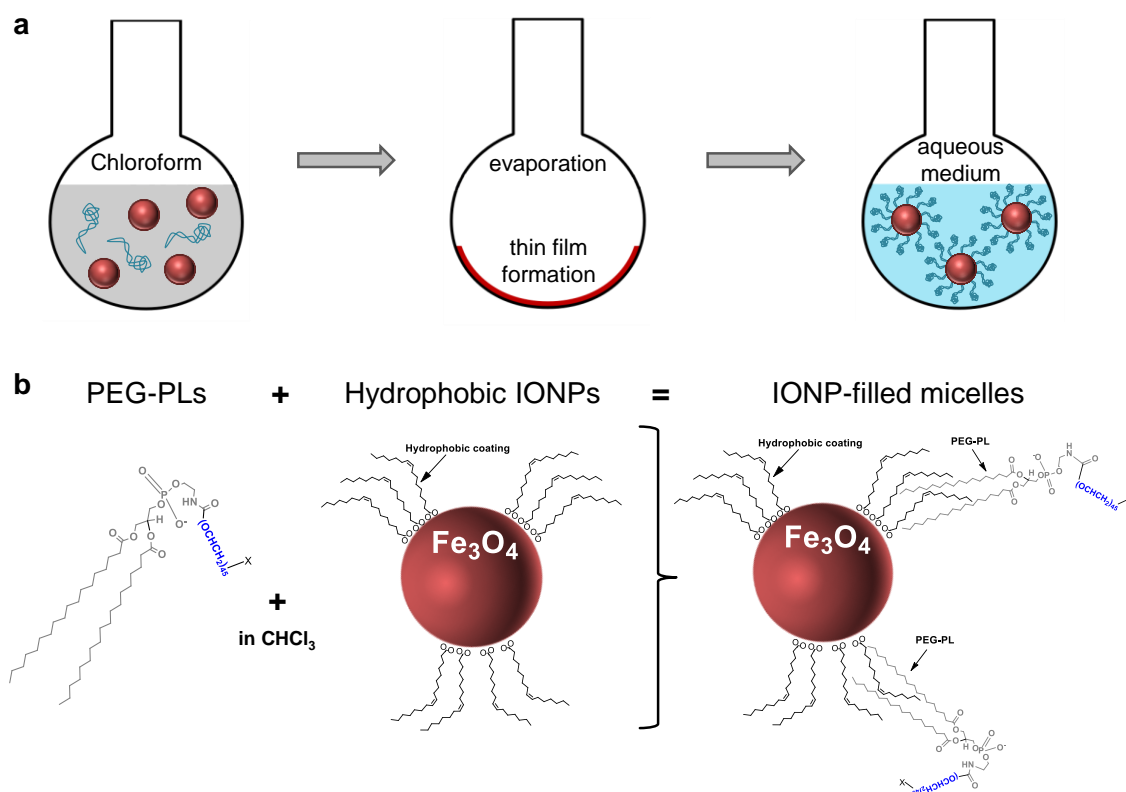


Figure 2.6. Schematic representation of the water solubilisation method used to develop IONP-filled micelles. (a) Scheme of the thin film hydration method where the amphiphilic molecules are used in order to solubilise hydrophobic NPs and (b) representation of the IONP-filled micelles by self-assembly of PEG-PLs around the metallic cores.

The best results were obtained when hydrophobic NPs and PEG-PLs were mixed in a mass ratio of 1:2 (IONP:PEG-PLs) in chloroform and allowed to evaporate overnight. After complete evaporation of the solvent, the resulting sample was heated to favour micelle formation and hydrated by adding aqueous solutions. First, large aggregates

and the IONPs that were not encapsulated inside PEG-PLs were separated and discarded by centrifugation (9700g, 5 min), and the resulting supernatant was filtered through a 0.45 μm low protein binding membrane filter. Next, empty (IONP free) micelles were removed by several cycles of washing and centrifugation (369 000g, 40 min), and the final pellets containing the small IONP-filled micelles were resuspended in aqueous solution.

The iron content in the IONP-filled micelles was determined by inductively coupled plasma-atomic emission spectrometry (ICP-AES). Once the Fe content was determined and assuming that the IONPs are perfect spheres with a diameter of 6.6 nm (Supporting Information, Figure S2.1) and composed of magnetite (Fe_3O_4), the concentration of IONP and number of iron atoms per IONP could be determined as follows:

$$\text{Volume (IONP)} = 4/3 \cdot \pi \cdot r^3 = 4/3 \cdot \pi \cdot (3.322 \times 10^{-7})^3 = 1.5356 \times 10^{-19} \text{ cm}^3$$

$$\rho (\text{Fe}_3\text{O}_4) = 5.17 \text{ g}\cdot\text{cm}^{-3}$$

$$m = \rho (\text{Fe}_3\text{O}_4) \cdot V (\text{IONP}) = 5.17 \cdot 1.5356 \times 10^{-19} = 7.9392 \times 10^{-19} \text{ g}$$

$$\text{moles of Fe}_3\text{O}_4 = m / \text{MW} (\text{Fe}_3\text{O}_4) = 7.9392 \times 10^{-19} / 231.533 = 3.4290 \times 10^{-21} \text{ moles}$$

$$\text{moles of Fe} = 3 \cdot \text{moles of Fe}_3\text{O}_4 = 3 \cdot 3.4290 \times 10^{-21} = 1.0287 \times 10^{-20} \text{ moles}$$

$$\text{atoms of Fe per IONP} = \text{mole Fe in IONP} \cdot N_A = 1.0287 \times 10^{-20} \cdot 6.022 \times 10^{23} = 6195$$

The above synthetic protocol could be reproduced to obtain PEGylated water soluble IONPs, containing *ca.* 10-20 mM of Fe (2-3 μM of IONP).

2.2.2. Attachment strategy of CpG ODNs

The strategy for CpG ODNs adjuvant attachment was based on electrostatic interactions between the IONP-filled micelles containing positively charged lipids and the negatively charged nucleic acids.

Synthetic CpG ODNs are being developed as vaccine adjuvants and have had promising results in human use, entering phase III clinical trials against several types of cancer,

including melanoma, lymphoma and non-small cell lung cancer, either alone or in combination with chemotherapy.⁵⁵ However, the main disadvantage of these types of molecules is that the natural phosphodiester (PO) link between nucleotides is unstable and a target for cleavage by nucleases. To overcome this drawback, CpG ODNs have been modified to have a phosphorothioate (PS) backbone, which is more stable and less sensitive to nucleases than the PO ODNs (**Figure 2.7**).⁵⁶ Thus, in this thesis CpG ODNs (19 bases; sequence: 5'-TCCATGACGTTCTGATGC-3') with PS backbone were used. Nevertheless, both types of CpG ODNs have negative charge conferred by the backbone, which makes possible exploiting electrostatic interactions between nucleic acids and IONP surface.

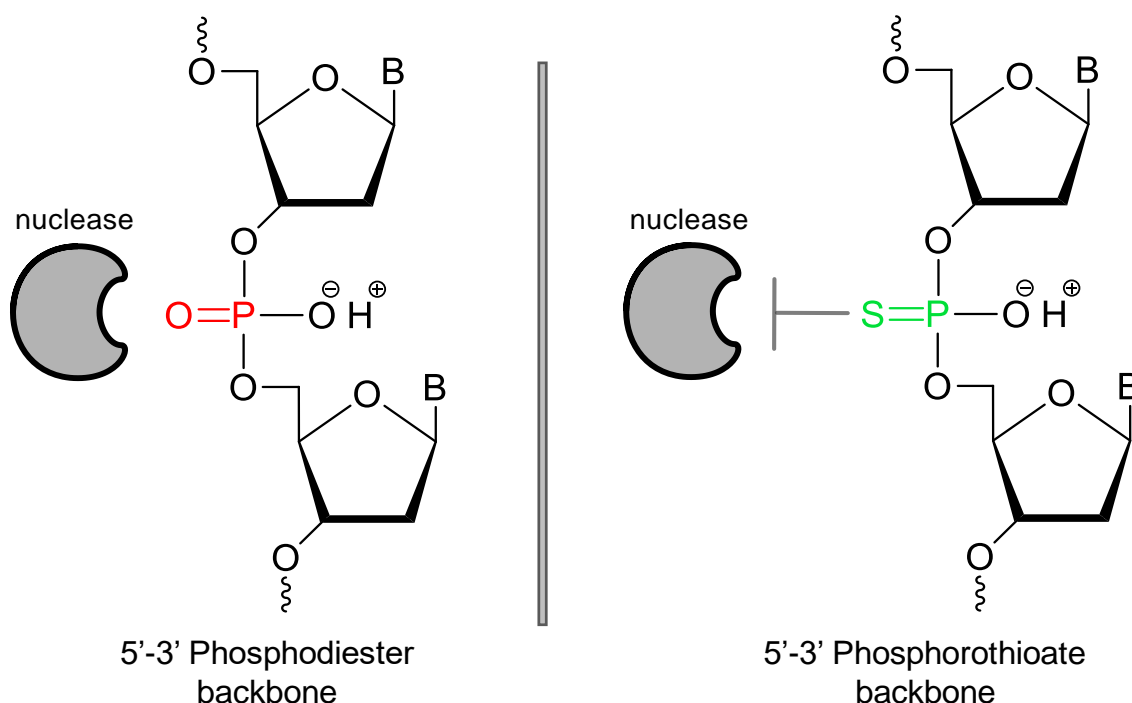


Figure 2.7. Chemical structure of the CpG ODNs backbone. PO linkage is sensitive to nucleases cleavage, while PS backbone can avoid processing by these types of enzymes.

The attachment of the CpG ODNs required the identification of the most appropriate combination of lipids to provide a suitable size, stability and CpG ODN attachment. Three different combinations of PEG-PLs were tested, with:

1. DPPE-mPEG(2000): PEG-PLs with methoxy end groups (OMe) were employed to coat IONPs as non-positively charged control;

2. DSPE-aPEG(2000): PEG-PLs with amine (NH_2) end groups were used to confer a positive surface charge at acidic pHs and, hence, facilitate the binding of the short ODNs;
3. DPPE-mPEG(2000) & DOTAP: Incorporation of the cationic lipid DOTAP was tested, which has a single quaternary amine that is fully charged at all pHs.

Following the micelle preparation/purification method described before, the size of the resulting micelles was determined by dynamic light scattering (DLS). The three different combinations allowed obtaining micelles with approximately the same size, with a mean hydrodynamic diameter between 30 and 50 nm (**Figure 2.8a, b**). The addition of DOTAP increased the polydispersity index (PDI), meaning that this type of micelle had broader size distribution in comparison to samples formed only with PEG-PLs.

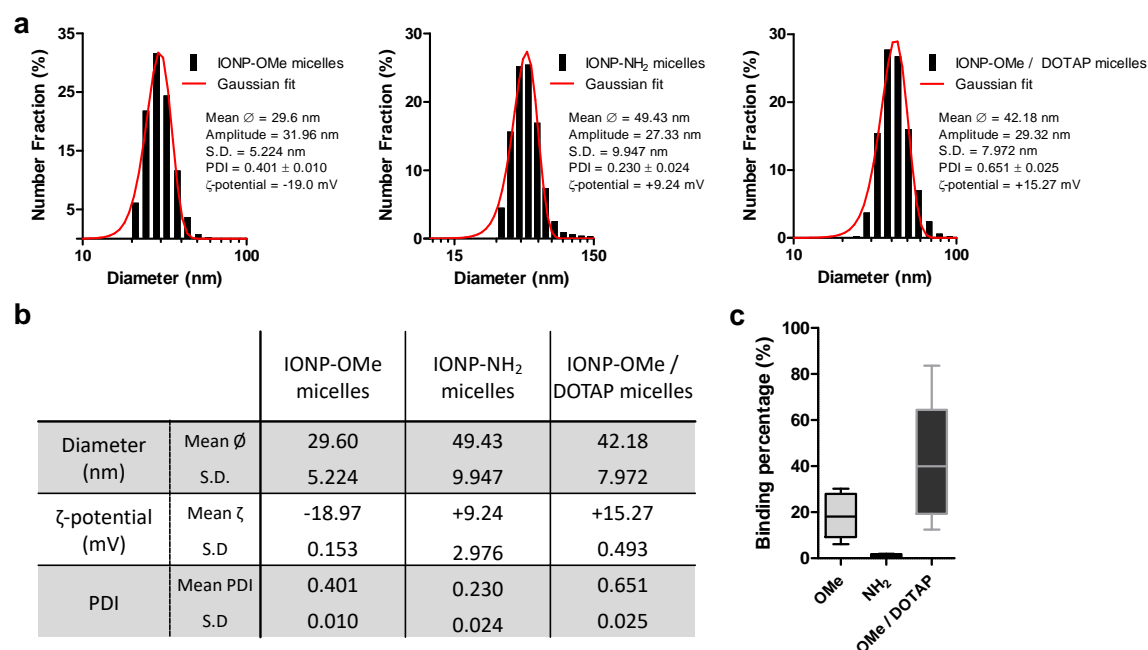


Figure 2.8. Characterisation of the different IONP-filled micelles explored to attach CpG ODNs. (a) DLS size measurements of OMe, NH_2 and OMe/DOTAP PEG-PL coated micelles. (b) Comparison of hydrodynamic sizes, zeta potential and PDI of the tested three different PEG-PL options. (c) CpG ODN binding percentage depending on the type of coating.

For binding the CpG ODNs to IONP-filled micelles, specific amounts of micelle solution were mixed with the nucleic acid solution in nanopure water and incubated overnight under continuous stirring. The unbound molecules were removed by ultrafiltration and centrifugation and the pellet resuspended in aqueous solution. To quantify the amount

of attached CpG ODNs, an aliquot of the sample was hydrolysed in basic solution (NaOH). The UV absorption of the hydrolysed CpG ODNs was measured and converted to concentration by comparison with a standard curve.

The PEGylated micelles containing methoxy end groups were negatively charged and showed poor ability to bind the CpG ODNs, having *ca.* 20 % of binding. The substitution of methoxy end groups by amine end groups resulted in slightly positive micelles, but surprisingly they did not bind CpG ODNs on their surfaces. Incorporation of the cationic lipid DOTAP in combination with DPPE-mPEG(2000) mixed in a mass ratio of 2:1 (PEG-PL:DOTAP), provided the best CpG ODN binding ability without affecting the hydrodynamic size of the micelles (Figure 2.8b, c). Therefore, this was the adopted strategy for generating the adjuvant carrying IONP-filled micelles.

Next, further characterisation of the selected formulation was carried out. UV absorption of these micelles showed the characteristic adsorption peak at 260 nm for CpG ODNs after subtraction of the IONP-DOTAP contribution (Figure 2.9a).

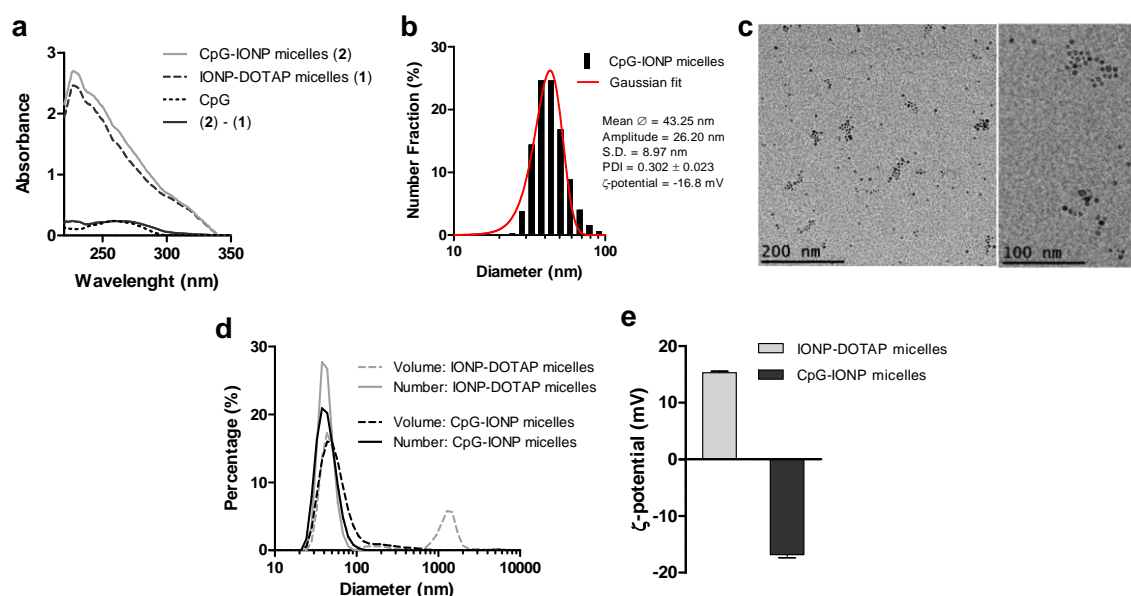


Figure 2.9. Characterisation of the CpG-IONP micelles. (a) UV absorbance spectra of CpG-IONP micelles, IONP-DOTAP micelles, CpG ODNs, and CpG-IONP micelles after removing the contribution of the IONP-DOTAP micelles. (b) Size distribution obtained by DLS and zeta potential of CpG-IONP micelles. (c) Representative TEM images of CpG-IONP micelles. Comparison of (d) DLS size and (e) zeta potential between IONP-DOTAP micelles before and after biofunctionalisation with CpG ODNs.

The size of the CpG-IONP micelles was determined by DLS and transmission electron microscopy (TEM) (Figure 2.9b, c). Both techniques showed that the diameter of the

CpG-IONP micelles remained stable (*ca.* 40 nm) for at least 2 weeks after their formation, with a mean diameter of 43.25 ± 8.97 nm. DLS experiments showed that the addition of CpG ODNs did not change significantly the diameter of the IONP-DOTAP micelles (Figure 2.9d).

It was determined that on average the CpG-IONP micelles contained 10 CpG ODN molecules per each IONP. Analysis of the surface charge further demonstrated the presence of the CpG ODNs on the micelle surface. The zeta potential of the parent DOTAP-containing IONP micelles was positive whereas CpG-IONP micelles showed a zeta potential of -16.8 mV (Figure 2.9e).

2.2.3. Attachment strategy of model antigen OVA

In this thesis OVA is used as the model antigen. Commercially available OVA is often contaminated with endotoxins, which can affect the *in vitro* and *in vivo* immunological studies.⁵⁷

First, it was tested if the purchased OVA was endotoxin-free by incubation with J774A.1 macrophages cell line and measurement of produced IL-6 cytokine by enzyme-linked immunosorbent assay (ELISA). The high levels of IL-6 induced were consistent with endotoxin contamination (Figure 2.10a).

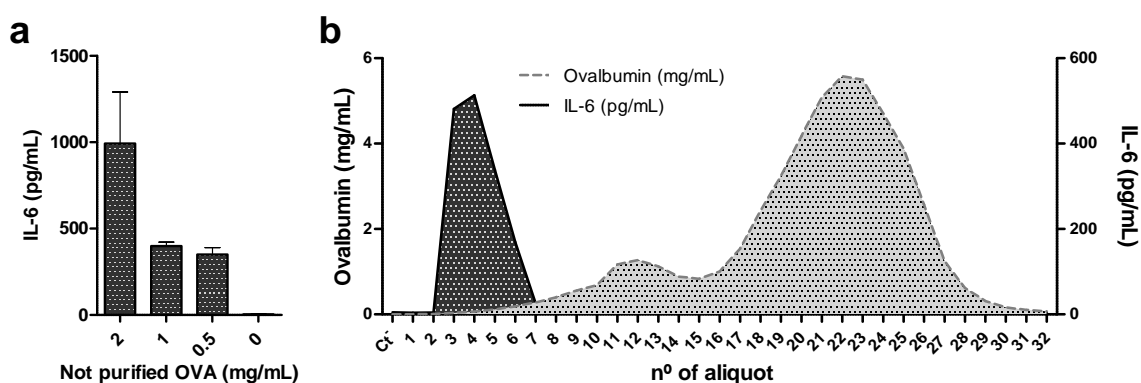


Figure 2.10. Purification of OVA protein from endotoxin fraction present in the commercial product. (a) J774A.1 macrophages IL-6 production after stimulation with non-purified OVA. (b) Analysis of fractionated OVA sample passed through an ÄKTA purifier chromatography: OVA content (grey dotted line) represented in the left axis in mg/mL and IL-6 production (black line) after incubation of the sample in J774A.1 macrophages for 24 h showed in the right axis (pg/mL).

Therefore, the first step was to obtain endotoxin-free antigen. The contaminated OVA was purified through an ÄKTA purifier chromatography system and fractionated into aliquots to separate the protein antigen from the LPS molecules. All the fractions were analysed for protein content by bicinchoninic acid (BCA) assay and IL-6 production after incubation of each aliquot with J774A.1 macrophages (Figure 2.10b). The results of the purification process showed that endotoxin was present in the first 7 aliquots as shown by the ability to induce IL-6 release in the J774A.1 macrophages. Notably, there were two protein fractions with different sizes. Fractions 17-27 were collected to obtain a solution with *ca.* 3 mg/mL of pure OVA antigen, ready for attachment to IONP-filled micelles.

Two different strategies were explored to attach OVA to the IONP micelles: 1) covalent conjugation between amine groups present in OVA and carboxylic end groups of the PEG-PLs; and 2) simple adsorption of the protein to the micelle surface by unspecific hydrophobic and electrostatic interactions.

a) Covalent conjugation:

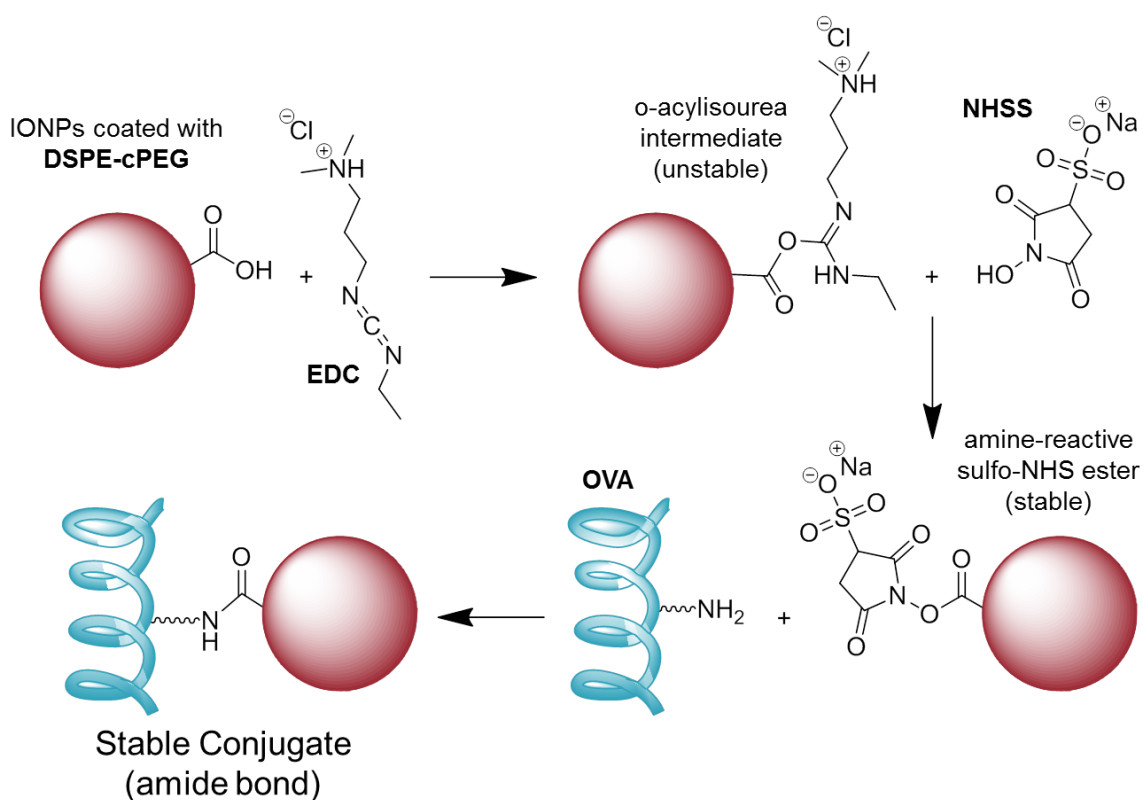


Figure 2.11. Scheme of the carbodiimide crosslinker chemistry employed for the attachment of the OVA model antigen to the IONP-filled micelles. Primary amines present in the OVA protein react with

the carboxylic groups of the PEG-PLs coating the IONPs, mediated by EDC/NHSS linkers. Only one carboxylic/amine group per IONP/OVA are represented for clarity purposes.

To covalently conjugate the OVA protein, the IONPs were encapsulated in micelles containing PEG-PLs with carboxylic end groups (DSPE-cPEG(2000)) in combination with DPPE-mPEG(2000). 1-Ethyl-3-[-3-dimethylaminopropyl]carbodiimide hydrochloride (EDC) in combination with N-hydroxysulfosuccinimide (sodium salt) (NHSS) were used for crosslinking the micelle carboxylic acids to primary amines of OVA forming amide bonds (**Figure 2.11**).

Carboxylic groups of the PEG-PLs were activated by adding EDC/NHSS to the IONP-COOH micelles solution and stirring for 2 h. After the elimination of the linker excess by ultrafiltration, the activated micelles were mixed with the purified OVA and stirred overnight. The unbound protein molecules were eliminated by ultrafiltration and the final concentration of the bound OVA was determined by BCA assay.

The combination of PEG-PLs used (DPPE-mPEG(2000) and DSPE-cPEG(2000); mass ratio of 1:1) resulted in IONP-filled micelles with an average size of 29.04 ± 5.57 nm (**Figure 2.12a**).

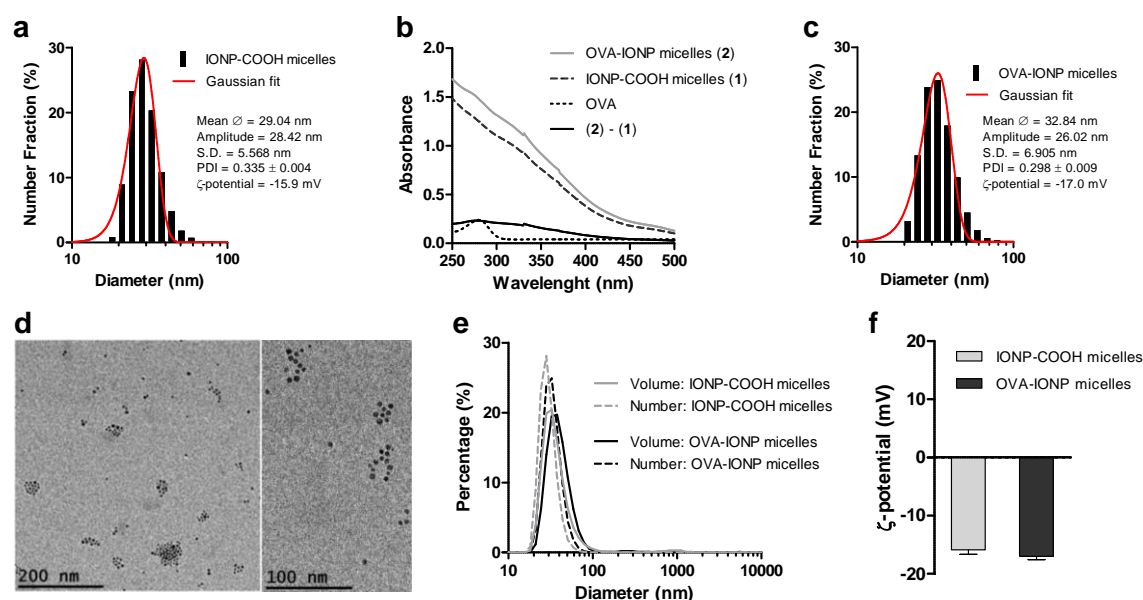


Figure 2.12. Characterisation of the IONP-COOH and OVA-IONP micelles (covalent conjugation). (a) Size distribution obtained by DLS of IONP-COOH micelles. (b) UV-visible absorbance spectra of OVA-IONP micelles, IONP-COOH micelles, OVA and OVA-IONP micelles after removing the contribution of the IONP-COOH micelles. (c) Size distribution measured by DLS of OVA-IONP micelles. (d) Representative TEM images of OVA-IONP micelles. Comparison of (e) size and (f) zeta potential between IONP-COOH micelles before and after biofunctionalisation with OVA.

The UV-visible absorption spectra of these micelles showed after removing the contribution of IONP-COOH micelles the characteristic peak of the OVA at 280 nm with absorption also at 350 nm characteristic of protein aggregation (Figure 2.12b). The characterisation by DLS and TEM techniques of the OVA-IONP micelles showed an average diameter of 32.84 ± 6.90 nm over a two week period after their preparation (Figure 2.12c, d). As in the case of the adjuvant carrying system, the addition of OVA molecules to the IONP-COOH micelles did not modify significantly the mean size or size distribution (PDI index) (Figure 2.12a, c and e). These synthesis afforded IONP-filled micelles with 2-4 OVA molecules per IONP. Both the parent IONP-COOH micelles and the OVA-IONP micelles had a negative zeta potential (Figure 2.12f), which was consistent with the presence of carboxylic groups and negatively charged OVA proteins (pI 4.63).

b) Binding by adsorption:

To explore whether OVA protein can be adsorbed in IONP-filled micelles, the same protocol described above was followed without adding EDC/NHSS linkers.

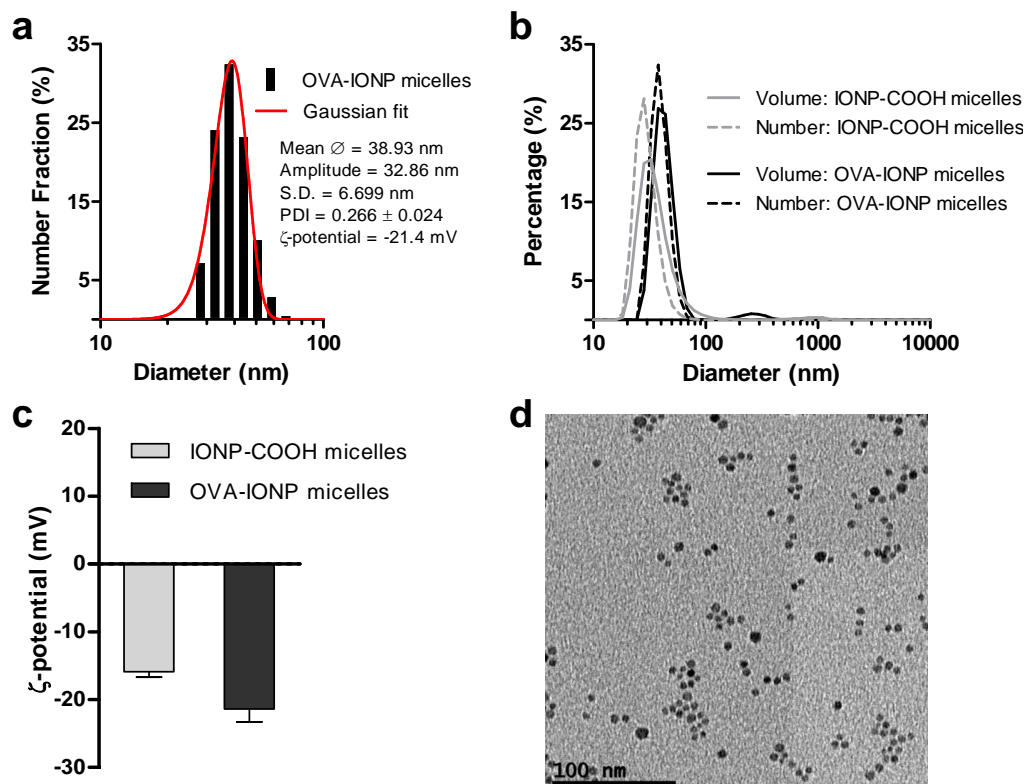


Figure 2.13. Characterisation of the OVA-IONP micelles (adsorption). (a) Size distribution obtained by DLS of OVA-IONP micelles. Comparison of (b) size and (c) zeta potential between IONP-COOH micelles before and after biofunctionalisation with OVA. (d) Representative TEM images of OVA-IONP micelles.

OVA-IONP micelles conjugated by adsorption presented similar size compared to the samples synthesised by the previous binding method, as demonstrated by DLS and TEM techniques (Figure 2.13a, b and d). These OVA-IONP micelles also had a negative zeta potential (Figure 2.13c) and contained *ca.* 2 OVA molecules per each IONP.

2.2.4. Development of the multimodal imaging contrast agent

To track the designed systems *in vitro*, both the parent (IONP-DOTAP and IONP-COOH) and biofunctionalised (CpG-IONP and OVA-IONP) micelles were fluorescently labelled by addition of commercially available rhodamine B-modified DPPE phospholipid (DPPE-Rho) during the process of dissolving in chloroform and formation of a thin layer of dry lipid film by gentle evaporation. The protocol to micelle formation was conducted in this case in darkness to prevent any potential fluorescent dye bleaching.

By adding a 5% molar lipid ratio of DPPE-Rho, it was possible to obtain strongly fluorescent IONP-filled micelles without affecting the size and the subsequent attachment of CpG ODNs or OVA (Figure 2.14).

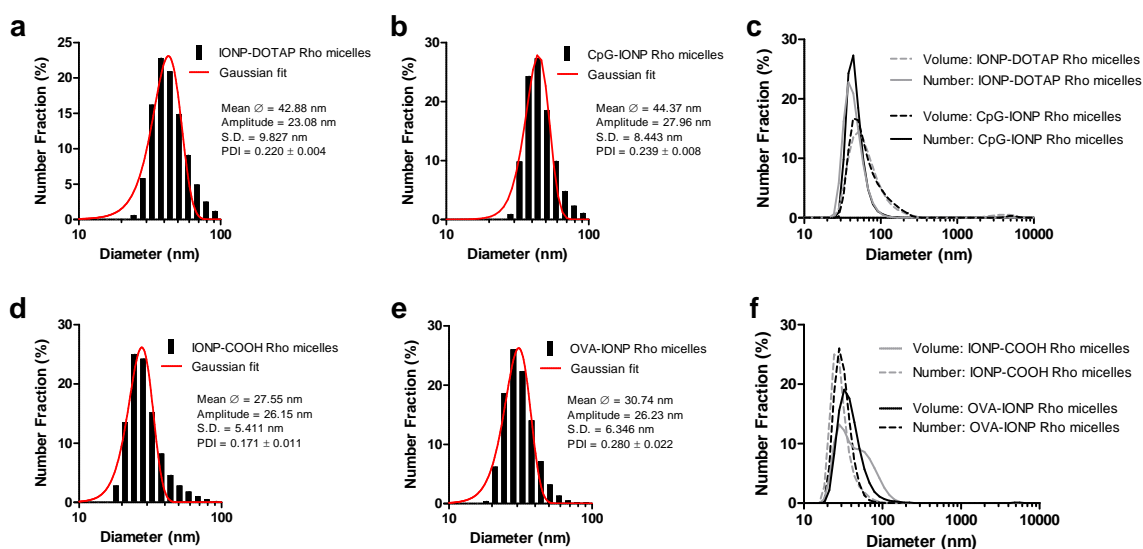


Figure 2.14. Characterisation of the CpG-IONP and OVA-IONP micelles fluorescently labelled with 5% DPPE-Rho. Size distribution obtained by DLS of fluorescently labelled (a) parent IONP-DOTAP micelles, (b) CpG-IONP micelles and (c) size comparison of both samples. Size distribution of (d) IONP-COOH micelles and (e) OVA-IONP micelles with DPPE-Rho. (f) Comparison between both hydrodynamic sizes.

The UV-visible spectra of these micelles showed the characteristic peak of the rhodamine B around 560 nm (Figure 2.15a, c) and the fluorescence emission at *ca.* 580

nm confirmed the presence of the fluorophore in both systems (Figure 2.15b, d). The amount of incorporated DPPE-Rho per NP varied somewhat depending on the micelle type with more molecules of rhodamine B per IONP in the CpG-IONP micelles (*ca.* 130) than in the case of OVA-IONP micelles (*ca.* 15).

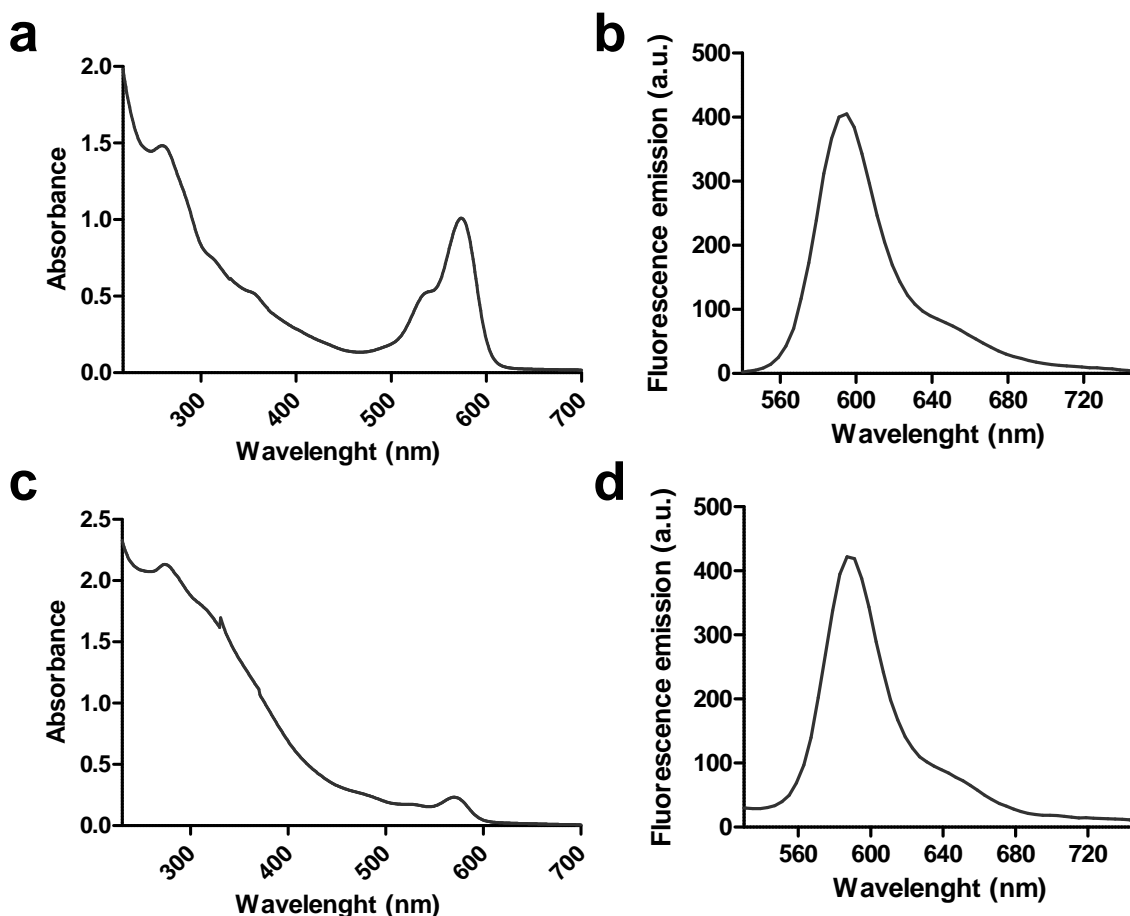


Figure 2.15. Spectroscopy characterisation of the fluorescently labelled CpG-IONP and OVA-IONP micelles with DPPE-Rho. UV-visible spectra of labelled (a) CpG- and (c) OVA-IONP micelles. Fluorescence spectra of (b) CpG- and (d) OVA-IONP micelles with DPPE-Rho.

The incorporation of the fluorescence probe allowed analysing the uptake and cellular fate of these nanoconstructs in cells of the immune system by fluorescence microscopy and flow cytometry (Chapter III).

To employ these nanovaccines in nuclear imaging studies, the direct surface recognition (direct radiolabelling) of ^{67}Ga by the magnetite core was explored. Despite the growing interest in radiolabelling NPs, few inorganic NPs have been successfully radiolabelled with gallium even using organic chelate-based approaches.^{58–60} Among all the available radioisotopes, gallium seemed a suitable choice for direct IONP core

binding. It has been extensively used in biological studies as a redox-inactive iron substitute due to the similarity of Ga^{3+} and Fe^{3+} in charge, size (Fe^{3+} 0.65 Å; Ga^{3+} 0.62 Å)⁶¹ and binding properties,^{62,63} and studies have shown that many biological systems cannot distinguish between these two hard Lewis acids.⁶⁴

Micelles with the different PEG-PL coatings (DPPE-mPEG(2000) and DSPE-cPEG(2000)) were mixed with ^{67}Ga citrate radioactive solution under acidic conditions and elevated temperature (70 °C), in order to favour the direct binding. ^{67}Ga excess was then removed by ultrafiltration and the radiolabelling efficiency percentage determined as the radioactive fraction retained in the IONP-containing sample out of the total added radioactivity.

To demonstrate the specific attachment of the radioisotope to the iron oxide core, other types of NPs were used as comparison. Micelles filled with CdSe/ZnS core/shell QDs with similar core size and PEG-PLs were also prepared as previously reported by Maldonado et al.⁶⁵ The magnetite-filled micelles showed excellent ^{67}Ga capture even at subnanomolar NP concentrations without significant differences between the different PEG-PLs forming the outer surface of the micelle, while identically coated QDs were not able to incorporate ^{67}Ga at so low concentrations. In fact, QD-filled micelles needed 100 fold increase of NP concentration to reach 50 % of radiolabelling yield, compared to IONP-filled micelles (Figure 2.16a).

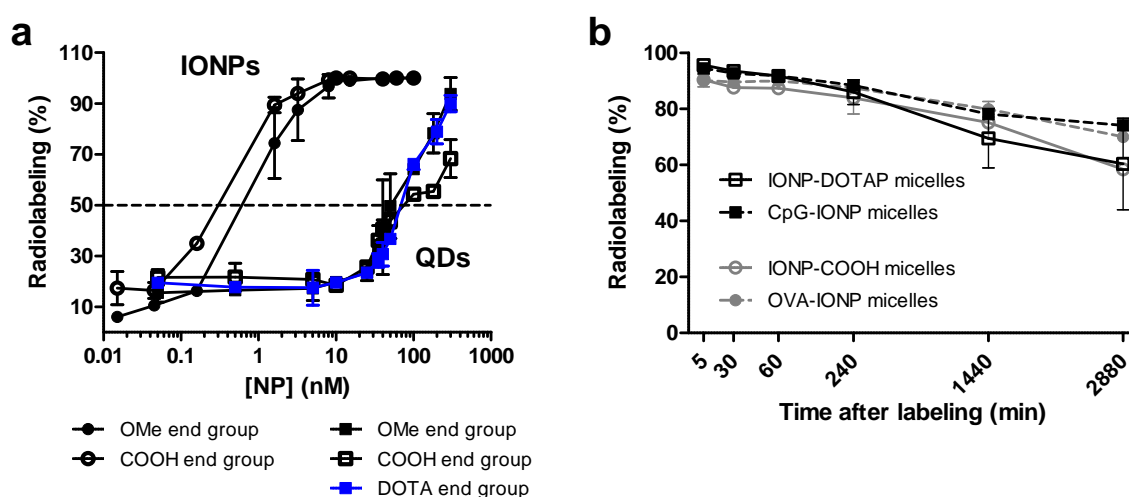


Figure 2.16. Characterisation of the radiolabelled IONP-filled micelles. (a) ^{67}Ga incorporation efficiency at different NP concentrations for CdSe/ZnS QD- and IONP-filled micelles with OMe, COOH and DOTA end groups (pH 3.8 ± 0.1 , 30 min, 70 °C). (b) Stability of the radiolabelled IONP micelles used in this thesis. ^{67}Ga labelled IONP-filled micelles were incubated with 10^6 -fold molar excess of the macrocyclic chelator DOTA. Data are presented as mean \pm SEM of two separate experiments.

In order to improve the direct labelling efficiency of the QD-based systems, the radionuclide chelator DOTA (1,4,7,10-tetraazacyclododecane-1,4,7,10-tetraacetic acid) was incorporated into QD-filled micelles by amide bond formation with the PEG-PLs. The ^{67}Ga capture by the QD-filled micelles functionalised with DOTA was still much lower than for the DOTA-free IONP micelles (Figure 2.16a).

These results suggest that binding to the IONP inorganic nanocrystal appears to be much more favourable than binding to this archetypical Ga^{3+} chelator. Although chemical conjugation of organic chelators to inorganic NPs is the most widely used method for radiolabelling NPs, a few recent studies are beginning to show that resorting to organic chemistry may not be necessary for some inorganic NPs.⁶⁶ Consistent with previously reported results with $^{99\text{m}}\text{Tc}$ labelling of IONPs and QDs,^{52,65} the surface of inorganic NPs appears to be a very useful site for binding the radionuclides in a surface-specific manner. In the case of Ga^{3+} binding, a recent study shows that to achieve a high radiolabelling yield even the best chelators have to be used in micromolar concentrations, as was clearly shown in the Figure 2.16a.⁶⁷ Thus, a high loading of DOTA would be required to see its effect in the overall ^{67}Ga capture capacity of the inorganic NP. Such high loading of DOTA is difficult to achieve in some cases. Even if achieved, the presence of DOTA on the NP surface may affect other properties of the NP. For instance, in the here described inorganic NP-filled micelles the NP:PEG-PL ratio is *ca.* 1:100.⁵⁴ Thus, at low NP concentrations, even in the case of using exclusively the DOTA modified PEG-PLs to form the QD-filled micelles, it is not possible to reach sufficiently high chelator concentrations to match the strong binding promoted by the magnetite core.

Apart from the radiolabelling efficiency, another parameter to take into account is the radiochemical integrity, i.e., the stability of the radiolabelled IONPs. This parameter is very important for biomedical applications, since the bound radionuclides can be released from the NP upon *in vivo* injection. In fact, once in the body, Ga^{3+} atoms can bind to transferrin as Fe^{3+} does. Therefore, the radiolabelled parent IONP-DOTAP and IONP-COOH micelles and the biofunctionalised CpG-IONP and OVA-IONP micelles were incubated over 48 h in the presence of a large excess of DOTA as competing ligand (10^6 moles of DOTA per mol of IONP), simulating the presence of chelating agents *in vivo*.

Chapter II

After 24 h of incubation, 70 % of the radioactivity was still found attached to the IONPs and even 48 h after still 60 % of the added radioactivity remained in the IONP core, confirming the formation of strong Ga^{3+} -iron oxide interactions (Figure 2.16b).

Taken together, these results show that this organic chemistry-free radiolabelling with $^{67}\text{Ga}^{3+}$ is efficient and specific for the IONP-filled micelles even without macrocyclic chelators. In this way, the reactive groups present in the PEG-PLs can be used to covalently or non-covalently attach antigen and/or adjuvants, conferring to these nanoconstructs a wide versatility and modular role for binding different types of molecules for immunomodulation and immunotherapy applications.

2.3. Conclusions

Two delivery systems capable of carrying antigen/adjuvant molecules were successfully designed, developed and characterised. Firstly, a water solubilisation step was carried out in order to confer solubility and protection to the IONPs. Using a method and materials similar to those used for development of liposome formulations, the hydrophobic IONPs were coated with several types of PEG-PLs, resulting in magnetic nanocarriers with different surface chemistry. All the formulation types had a mean diameter of 30-40 nm, demonstrated by consistent results.

A synthetic CpG ODN adjuvant with PS backbone was coupled to the PEGylated IONP-filled micelles by electrostatic interactions. The best micelle coating strategy included the presence of the cationic lipid DOTAP, which increased the surface charge of the micelle and induced electrostatic binding with the negatively charged CpG ODN molecules, with a binding percentage of *ca.* 40 % and a final loading ratio of 10 CpG ODN molecules per each IONP. A model antigen (OVA) was bound to the IONP-filled micelles by direct adsorption and covalent conjugation. In both cases, the OVA:IONP ratio was 2-4 OVA molecules per NP. The mean hydrodynamic diameter of the developed nanosystems once functionalised was <50 nm (**Table 2.1**), which is considered an optimal size range for targeted *in vivo* vaccine delivery via the lymphatic system to reach lymphoid organs (Chapters III and IV).

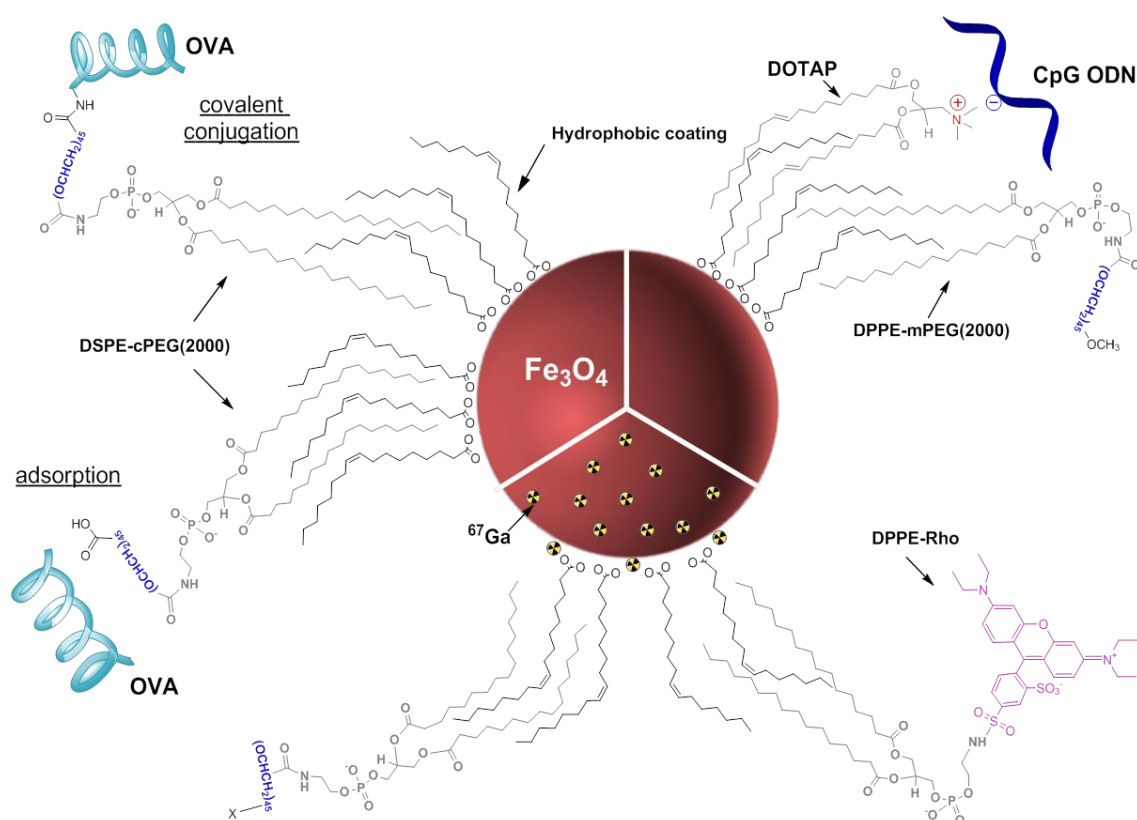
Table 2.1. Comparison of hydrodynamic sizes, with its PDI, measured by DLS and zeta potential of all developed parent and biofunctionalised IONP-filled micelles. The table includes also de size distribution measured by TEM of the hydrophobic magnetite core.

		Oleic acid coated IONP	IONP-DOTAP micelles	CpG-IONP micelles (DOTAP)	IONP-COOH micelles	OVA-IONP micelles (conjugation)	OVA-IONP micelles (adsorption)
Diameter (nm)	Mean ϕ	6.644	42.18	43.25	29.04	32.84	38.93
	S.D.	0.990	7.972	8.970	5.568	6.905	6.699
ζ -potential (mV)	Mean ζ	----	+15.27	-16.84	-15.88	-17.0	-21.4
	S.D	----	0.493	1.384	1.953	2.046	3.803
PDI	Mean PDI	----	0.651	0.302	0.335	0.298	0.266
	S.D	----	0.025	0.023	0.004	0.009	0.024

The incorporation of a fluorescent probe was also achieved without affecting the size and bioconjugation capabilities of the IONP-filled micelles. This thesis work shows that

the magnetite core of these nanoconstructs has high affinity for $^{67}\text{Ga}^{3+}$. Moreover, it demonstrates that radiolabelling with $^{67}\text{Ga}^{3+}$ is very efficient for IONP-filled micelles even without macrocyclic chelators, but not for identical micelles filled with CdSe/ZnS QDs.

Hence, IONP-filled micelles are ideal and readily adaptable for creating effective antigen/adjuvant delivery systems by combining simple self-assembly processes with standard conjugation chemistry. Moreover, the here described nanovaccines could be easily coated with a fluorescent dye or/and a radionuclide without affecting the size, leading to a multimodal and versatile platform for development of anticancer vaccines (Scheme 2.1).



Scheme 2.1. Schematic representation of the strategies used for the preparation of OVA-IONP and CpG-IONP micelles and for organic chemistry-free ^{67}Ga and rhodamine labelling.

2.4. Supporting Information of Chapter II

TEM characterisation confirmed the size of the hydrophobic IONP synthesised by thermal decomposition method.

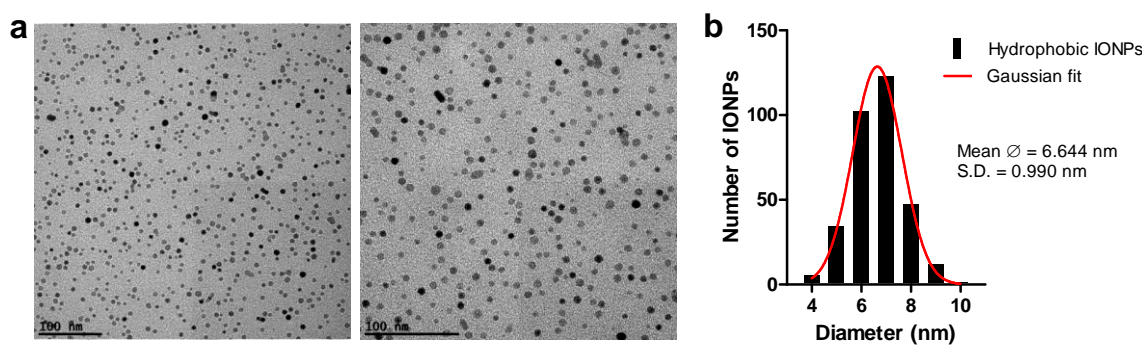


Figure S2.1. Size characterisation of the magnetite NPs employed in this thesis. (a) Representative TEM image of the hydrophobic IONPs and (b) the size distribution of more than 200 NPs.

References

1. Thanh, N. T. K. & Green, L. A. W. Functionalisation of nanoparticles for biomedical applications. *Nano Today* **5**, 213–230 (2010).
2. Akbarzadeh, A., Samiei, M. & Davaran, S. Magnetic nanoparticles: preparation, physical properties, and applications in biomedicine. *Nanoscale Res. Lett.* **7**, 144 (2012).
3. Wahajuddin & Arora, S. Superparamagnetic iron oxide nanoparticles: magnetic nanoplatforms as drug carriers. *Int. J. Nanomedicine* **7**, 3445–3471 (2012).
4. Kodama, R. . Magnetic nanoparticles. *J. Magn. Magn. Mater.* **200**, 359–372 (1999).
5. Polyak, B. & Friedman, G. Magnetic targeting for site-specific drug delivery: applications and clinical potential. *Expert Opin. Drug Deliv.* **6**, 53–70 (2009).
6. Wáng, Y. X. J. & Idée, J.-M. A comprehensive literatures update of clinical researches of superparamagnetic resonance iron oxide nanoparticles for magnetic resonance imaging. *Quant. Imaging Med. Surg.* **7**, 88–122 (2017).
7. Salunkhe, A. B. B., Khot, V. M. M. & Pawar, S. H. H. Magnetic Hyperthermia with Magnetic Nanoparticles: A Status Review. *Curr. Top. Med. Chem.* **14**, 572–594 (2014).
8. Guardia, P., Labarta, A. & Batlle, X. Tuning the Size, the Shape, and the Magnetic Properties of Iron Oxide Nanoparticles. *J. Phys. Chem. C* **115**, 390–396 (2011).
9. Wu, W., He, Q. & Jiang, C. Magnetic iron oxide nanoparticles: Synthesis and surface functionalization strategies. *Nanoscale Res. Lett.* **3**, 397–415 (2008).
10. Wu, W., Wu, Z., Yu, T., Jiang, C. & Kim, W.-S. Recent progress on magnetic iron oxide nanoparticles: synthesis, surface functional strategies and biomedical applications. *Sci. Technol. Adv. Mater.* **16**, 23501 (2015).
11. Patsula, V. *et al.* Superparamagnetic Fe₃O₄ Nanoparticles: Synthesis by Thermal Decomposition of Iron(III) Glucuronate and Application in Magnetic Resonance Imaging. *ACS Appl. Mater. Interfaces* **8**, 7238–7247 (2016).
12. He, X., Zhong, W., Au, C.-T. & Du, Y. Size dependence of the magnetic properties of Ni nanoparticles prepared by thermal decomposition method. *Nanoscale Res. Lett.* **8**, 446 (2013).
13. Wang, D., Ma, Q. & Yang, P. Synthesis of Fe₃O₄ nanoparticles with tunable and uniform size through simple thermal decomposition. *J. Nanosci. Nanotechnol.* **12**, 6432–8 (2012).
14. Navaladian, S., Viswanathan, B., Viswanath, R. P. & Varadarajan, T. K. Thermal decomposition as route for silver nanoparticles. *Nanoscale Res. Lett.* **2**, 44–48 (2007).

15. Asuha, S., Zhao, S., Wu, H. Y., Song, L. & Tegus, O. One step synthesis of maghemite nanoparticles by direct thermal decomposition of Fe-urea complex and their properties. *J. Alloys Compd.* **472**, L23–L25 (2009).
16. Sun, S. *et al.* Monodisperse MFe₂O₄ (M = Fe, Co, Mn) nanoparticles. *J. Am. Chem. Soc.* **126**, 273–279 (2004).
17. Lattuada, M. & Hatton, T. A. Functionalization of Monodisperse Magnetic Nanoparticles Functionalization of Monodisperse Magnetic Nanoparticles. **23**, 2158–2168 (2007).
18. Chen, Z. P. *et al.* Preparation and characterization of water-soluble monodisperse magnetic iron oxide nanoparticles via surface double-exchange with DMSA. *Colloids Surfaces A Physicochem. Eng. Asp.* **316**, 210–216 (2008).
19. Smolensky, E. D., Park, H.-Y. E., Berquó, T. S. & Pierre, V. C. Surface functionalization of magnetic iron oxide nanoparticles for MRI applications - effect of anchoring group and ligand exchange protocol. *Contrast Media Mol. Imaging* **6**, 189–99 (2011).
20. Dubertret, B. In Vivo Imaging of Quantum Dots Encapsulated in Phospholipid Micelles. *Science (80-.)*. **298**, 1759–1762 (2002).
21. Pellegrino, T. *et al.* Hydrophobic nanocrystals coated with an amphiphilic polymer shell: A general route to water soluble nanocrystals. *Nano Lett.* **4**, 703–707 (2004).
22. Geissbuehler, I. *et al.* Lipid-coated nanocrystals as multifunctionalized luminescent scaffolds for supramolecular biological assemblies. *Angew. Chemie Int. Ed.* **44**, 1388–1392 (2005).
23. Jokerst, J. V, Lobovkina, T., Zare, R. N. & Gambhir, S. S. Nanoparticle PEGylation for imaging and therapy. *Nanomedicine* **6**, 715–28 (2011).
24. Alconcel, S. N. S., Baas, A. S. & Maynard, H. D. FDA-approved poly(ethylene glycol)–protein conjugate drugs. *Polym. Chem.* **2**, 1442 (2011).
25. Stolnik, S. *et al.* Surface modification of poly(lactide-co-glycolide) nanospheres by biodegradable poly(lactide)-poly(ethylene glycol) copolymers. *Pharm. Res.* **11**, 1800–8 (1994).
26. Lukyanov, A. N. & Torchilin, V. P. Micelles from lipid derivatives of water-soluble polymers as delivery systems for poorly soluble drugs. *Adv. Drug Deliv. Rev.* **56**, 1273–89 (2004).
27. Lankveld, D. P. *et al.* Blood clearance and tissue distribution of PEGylated and non-PEGylated gold nanorods after intravenous administration in rats. *Nanomedicine* **6**, 339–349 (2011).
28. Perrault, S. D. & Shih, W. M. Virus-inspired membrane encapsulation of DNA nanostructures to achieve in vivo stability. *ACS Nano* **8**, 5132–5140 (2014).

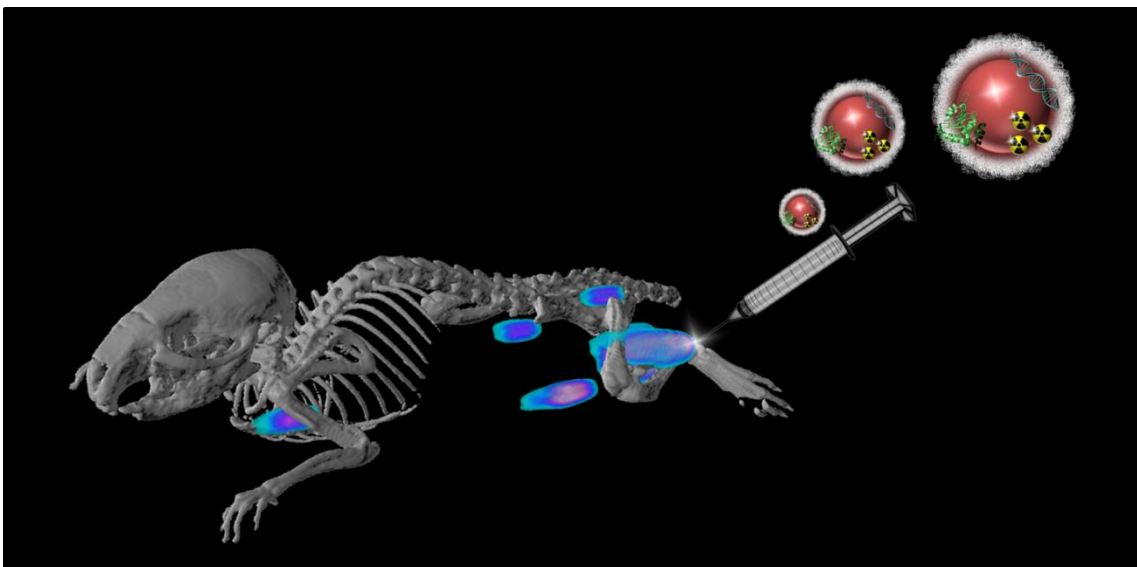
29. Yang, Q., Moulder K, R., Cohen, M. S., Cai, S. & Forrest, L. M. Cabozantinib Loaded DSPE-PEG2000 Micelles as Delivery System: Formulation, Characterization and Cytotoxicity Evaluation. *BAOJ Pharm. Sci.* **1**, 1–20 (2015).
30. Sperling, R. A. & Parak, W. J. Surface modification, functionalization and bioconjugation of colloidal inorganic nanoparticles. *Philos. Trans. R. Soc. London A* **368**, 1333–1383 (2010).
31. Zhao, L. *et al.* Nanoparticle vaccines. *Vaccine* **32**, 327–337 (2014).
32. Willmann, J. K., van Bruggen, N., Dinkelborg, L. M. & Gambhir, S. S. Molecular imaging in drug development. *Nat. Rev. Drug Discov.* **7**, 591–607 (2008).
33. Rudin, M. & Weissleder, R. Molecular imaging in drug discovery and development. *Nat. Rev. Drug Discov.* **2**, 123–31 (2003).
34. Lee, I. H. *et al.* Imageable antigen-presenting gold nanoparticle vaccines for effective cancer immunotherapy in vivo. *Angew. Chemie Int. Ed.* **51**, 8800–8805 (2012).
35. Huang, H.-C. *et al.* Formulation of novel lipid-coated magnetic nanoparticles as the probe for in vivo imaging. *J. Biomed. Sci.* **16**, 86 (2009).
36. Pysz, M. A., Gambhir, S. S. & Willmann, Jürgen K., M. D. Molecular Imaging: Current Status and Emerging Strategies. *Clin. Radiol.* **65**, 500–516 (2010).
37. Gibson, N. *et al.* Radiolabelling of engineered nanoparticles for in vitro and in vivo tracing applications using cyclotron accelerators. *Arch. Toxicol.* **85**, 751–773 (2011).
38. Cydzik, I. *et al.* A novel method for synthesis of ⁵⁶Co-radiolabelled silica nanoparticles. *J. Nanoparticle Res.* **14**, 1185–1193 (2012).
39. Torres Martin de Rosales, R. *et al.* Synthesis of ⁶⁴Cu(II)-bis(dithiocarbamatebisphosphonate) and its conjugation with superparamagnetic iron oxide nanoparticles: in vivo evaluation as dual-modality PET-MRI agent. *Angew. Chemie Int. Ed.* **50**, 5509–13 (2011).
40. Ogawa, K., Mukai, T., Inoue, Y., Ono, M. & Saji, H. Development of a novel ^{99m}Tc-chelate-conjugated bisphosphonate with high affinity for bone as a bone scintigraphic agent. *J. Nucl. Med.* **47**, 2042–7 (2006).
41. Torres Martin de Rosales, R. *et al.* (^{99m}Tc)-bisphosphonate-iron oxide nanoparticle conjugates for dual-modality biomedical imaging. *Bioconjug. Chem.* **22**, 455–65 (2011).
42. Lewin, M. *et al.* Tat peptide-derivatized magnetic nanoparticles allow in vivo tracking and recovery of progenitor cells. *Nat. Biotechnol.* **18**, 410–4 (2000).
43. Jarrett, B. R., Gustafsson, B., Kukis, D. L. & Louie, A. Y. Synthesis of ⁶⁴Cu-labeled magnetic nanoparticles for multimodal imaging. *Bioconjug. Chem.* **19**, 1496–504 (2008).

44. Lee, H.-Y. *et al.* PET/MRI dual-modality tumor imaging using arginine-glycine-aspartic (RGD)-conjugated radiolabeled iron oxide nanoparticles. *J. Nucl. Med.* **49**, 1371–9 (2008).
45. Glaus, C., Rossin, R., Welch, M. J. & Bao, G. In vivo evaluation of (64)Cu-labeled magnetic nanoparticles as a dual-modality PET/MR imaging agent. *Bioconjug. Chem.* **21**, 715–22 (2010).
46. Patel, D. *et al.* The cell labeling efficacy, cytotoxicity and relaxivity of copper-activated MRI/PET imaging contrast agents. *Biomaterials* **32**, 1167–76 (2011).
47. Boros, E., Bowen, A. M., Josephson, L., Vasdev, N. & Holland, J. P. Chelate-free metal ion binding and heat-induced radiolabeling of iron oxide nanoparticles. *Chem. Sci.* **6**, 225–236 (2014).
48. Chen, F. *et al.* Chelator-free synthesis of a dual-modality PET/MRI agent. *Angew. Chemie Int. Ed.* **52**, 13319–23 (2013).
49. Goel, S., Chen, F., Ehlerding, E. B. & Cai, W. Intrinsically radiolabeled nanoparticles: an emerging paradigm. *Small* **10**, 3825–30 (2014).
50. Chakravarty, R. *et al.* Intrinsically germanium-69-labeled iron oxide nanoparticles: synthesis and in-vivo dual-modality PET/MR imaging. *Adv. Mater.* **26**, 5119–23 (2014).
51. Jauregui-osoro, M. *et al.* Biocompatible inorganic nanoparticles for [18F]-fluoride binding with applications in PET imaging. *Dalt. Trans.* **40**, 6196–6205 (2011).
52. Gomez Blanco, N. *et al.* Iron oxide-filled micelles as ligands for fac-[M(CO)₃]⁺ (M = (99m)Tc, Re). *Chem. Commun.* **48**, 4211–3 (2012).
53. Cobaleda-siles, M. *et al.* An Iron Oxide Nanocarrier for dsRNA to Target Lymph Nodes and Strongly Activate Cells of the Immune System. *Small* **10**, 5054–5067 (2014).
54. Carion, O., Mahler, B., Pons, T. & Dubertret, B. Synthesis, encapsulation, purification and coupling of single quantum dots in phospholipid micelles for their use in cellular and in vivo imaging. *Nat. Protoc.* **2**, 2383–2390 (2007).
55. Krieg, A. M. CpG still rocks! Update on an accidental drug. *Nucleic Acid Ther.* **22**, 77–89 (2012).
56. Meng, W., Yamazaki, T., Nishida, Y. & Hanagata, N. Nuclease-resistant immunostimulatory phosphodiester CpG oligodeoxynucleotides as human Toll-like receptor 9 agonists. *BMC Biotechnol.* **11**, 88 (2011).
57. Watanabe, J., Miyazaki, Y., Zimmerman, G. a., Albertine, K. H. & McIntyre, T. M. Endotoxin Contamination of Ovalbumin Suppresses Murine Immunologic Responses and Development of Airway Hyper-reactivity. *J. Biol. Chem.* **278**, 42361–8 (2003).

58. Hwang, D. W. *et al.* A nucleolin-targeted multimodal nanoparticle imaging probe for tracking cancer cells using an aptamer. *J. Nucl. Med.* **51**, 98–105 (2010).
59. Zambre, A. *et al.* Evaluation of tumor targeting efficacy of ⁶⁷Ga-labeled bombesin peptide functionalized gold nanoparticle in mice model. *J. Nucl. Med.* **55**, 1386– (2014).
60. Xing, Y., Zhao, J., Conti, P. S. & Chen, K. Radiolabeled nanoparticles for multimodality tumor imaging. *Theranostics* **4**, 290–306 (2014).
61. Shannon, R. D. Revised effective ionic radii and systematic studies of interatomic distances in halides and chalcogenides. *Acta Crystallogr. Sect. A* **32**, 751–767 (1976).
62. Bernstein, L. R. Mechanisms of therapeutic activity for gallium. *Pharmacol. Rev.* **50**, 665–82 (1998).
63. Sun, H., Li, H. & Sadler, P. J. Transferrin as a Metal Ion Mediator. *Chem. Rev.* **99**, 2817–2842 (1999).
64. Kaneko, Y., Thoendel, M., Olakanmi, O., Britigan, B. E. & Singh, P. K. The transition metal gallium disrupts *Pseudomonas aeruginosa* iron metabolism and has antimicrobial and antibiofilm activity. *J. Clin. Invest.* **117**, 877–88 (2007).
65. Maldonado, C. R. *et al.* QD-filled micelles which combine SPECT and optical imaging with light-induced activation of a platinum(IV) prodrug for anticancer applications. *Chem. Commun.* **49**, 3985–7 (2013).
66. Hu, H. *et al.* PET and NIR optical imaging using self-illuminating (⁶⁴Cu)-doped chelator-free gold nanoclusters. *Biomaterials* **35**, 9868–76 (2014).
67. Berry, D. J. *et al.* Efficient bifunctional gallium-68 chelators for positron emission tomography: tris(hydroxypyridinone) ligands. *Chem. Commun.* **47**, 7068–70 (2011).

3

In vitro and in vivo trafficking and biodistribution of the constructed nanovaccines



3.1. Introduction

3.1.1. Multimodal imaging

The application of molecular imaging will increasingly become a highly desired, if not essential part of the DDD process. Molecular imaging is expected to reduce the high attrition rates in DDD and allow early identification of the best drug candidates. The rapid rise of the field of nanotechnology applied to medical diagnosis has been partly due to the powerful and unique characteristics of NPs as imaging agents. The combination of different imaging modalities (multimodal imaging) promises to improve the quantification and localisation of biological processes, provide new insights of known diseases and help in better characterising newly discovered imaging probes and drugs.¹⁻³ Since each imaging modality has intrinsic limitations, probes such as NPs that can amalgamate two or more of these techniques are highly desirable.

There are different types of imaging techniques available for medical diagnosis and each one is able to detect specific signal types (**Figure 3.1**). The most relevant imaging modalities for this thesis are described next.

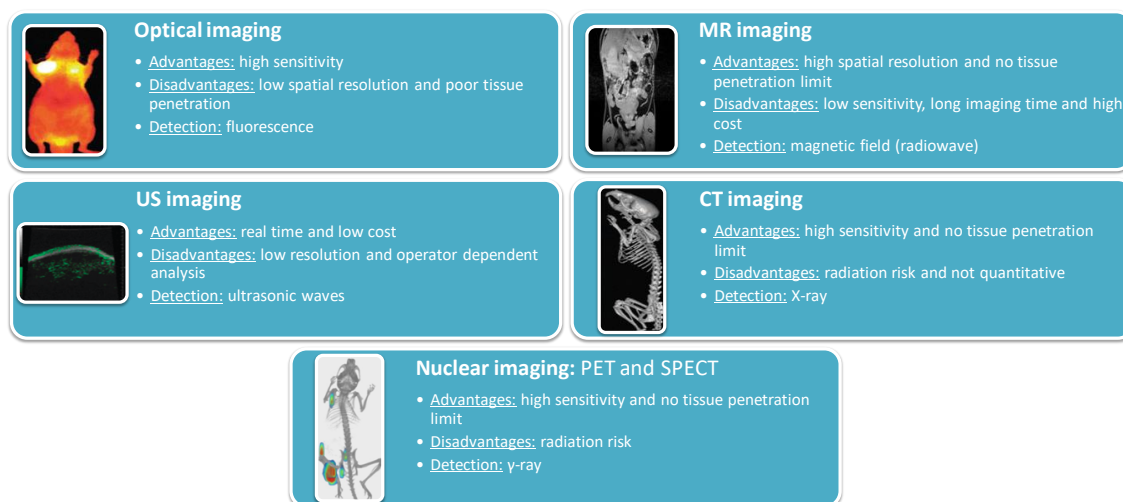


Figure 3.1. Advantages and disadvantages of some of the imaging techniques available for biomedical applications. Figure adapted from *Chem. Soc. Rev.*, 2012, **41**, 2656.⁴

MRI presents two main advantages as imaging modality for clinical applications: high spatial resolution (25-100 μm) and no tissue penetration limit, which allow obtaining excellent morphological information.^{5,6} IONPs have been widely explored as contrast agent for MRI due to their intrinsic magnetic properties and their safety for use in

humans.⁷⁻⁹ The principal drawback of MRI, however, is the relatively low sensitivity and the long scan and processing time needed to get an image. Moreover, contrast agents used have to be administered in large quantities (in the order of micrograms to milligrams), which can be a big problem for many applications.

On the other hand, optical imaging is an important tool to characterise and understand the molecular biology of cancer (and diseases in general).^{10,11} Due to the limited tissue penetration (<1 cm), which arises from the adsorption and scattering characteristics of tissue components,¹² optical imaging is mainly used for *in vitro* or *ex vivo* assays. However, recently new technologies have emerged with promising results that could be suitable for clinical applications.¹³⁻¹⁵ Moreover, even *in vitro/ex vivo* optical imaging studies can speed up cancer diagnosis by improving biopsy procedures in terms of time and resolution.¹⁶

Finally, nuclear imaging has excellent potential for translational research from animal models to clinical applications.¹⁷⁻²¹ Although this imaging modality has relatively low spatial resolution (1-2 mm), nuclear imaging has no limit on tissue penetration depth and has higher sensitivity compared with MRI, which allows administering probes even at the nanogram range. There are two main nuclear imaging techniques: positron emission tomography (PET) and single-photon emission computed tomography (SPECT).^{22,23} Currently, PET is considered the most advanced nuclear imaging technique. Among all PET radionuclides, ¹⁸F and ⁶⁸Ga are the most widely used in clinical settings. Compared to ¹⁸F ($t_{1/2} = 110$ min), ⁶⁸Ga ($t_{1/2} = 68$ min) offers the advantage that it can be obtained from an in-house generator, turning ⁶⁸Ga into a more affordable and readily available choice for PET imaging (i.e., its use does not require a nearby cyclotron).²⁴ Moreover, since ⁶⁷Ga is a gamma emitting radionuclide ($t_{1/2} = 3.3$ days), Ga³⁺ chemistry can also be applied using cheaper and more readily available SPECT systems over longer periods of time. Thus, by using gallium as labelling probe, both PET and SPECT can be used for achieving images with high sensitivity.

The application of multimodal imaging allows investigating the intracellular fate of the developed IONP-based nanovaccines by optical techniques and the *in vivo* biodistribution by SPECT imaging.

3.1.2. Intracellular fate of NPs

In contrast to small molecule drugs, which mainly enter cells by passive diffusion or active transport through the cell membrane, NPs are mainly taken up via endocytosis. This process is described as an active transport by engulfment of a foreign body and its incorporation to the intracellular space still surrounded by the cell membrane. Once inside, the cell will process the entrapped material.

There are several types of endocytosis.^{25,26} Phagocytosis, for example, is mainly performed by phagocytes such as macrophages, monocytes and DCs. Particles, in contrast to nutrients suspended in the extracellular fluid, are more likely to be internalised by this type of pathway, where the cell membrane is extended to engulf the foreign body. Once the phagosome (or vesicle), is formed it will be processed depending on the ligand types present on the NP's surface. On the other hand, pinocytosis is a process in which the cell incorporates the nearby environment by invaginating a vesicle containing the extracellular fluid. This pathway is diverse in terms of receptors and molecules that are involved in the process. Overall, endocytosis of NPs can be mediated and controlled by many factors including exposed ligands, NP composition, size, shape or charge.²⁷⁻³³

NPs designed for acting as carriers of antigen and adjuvants must meet cells of the immune system. Fortunately, immune cells such as phagocytes are experts in the internalization of foreign bodies and particles by phagocytosis, in processing immunogenic molecules that they encounter and in activating immunological signals in response to these encounters. However, depending on how the immunostimulatory molecules are presented inside the cells, the immune response induced will be different.

In the case of the antigen the internalization via the endocytic pathway is necessary to trigger the proper response. In this way, NPs can direct the antigen to the phagocytic cells and allow the internalization into the endosomes, where it can be presented to other immune cells via specific receptors. In contrast, adjuvants can be very diverse in nature and, therefore, their final target receptor too. In this thesis, a TLR 9 ligand (CpG ODN) is used as adjuvant for stimulating immune cells. The target receptor TLR 9 is

expressed intracellularly within the endosomal compartments. Hence, NPs carrying this type of immunomodulatory ligand must allow endocytic internalization to permit the encounter between the CpG ODN cargo and TLR 9 in order to induce the adequate signalling pathway and immune response (**Figure 3.2**).

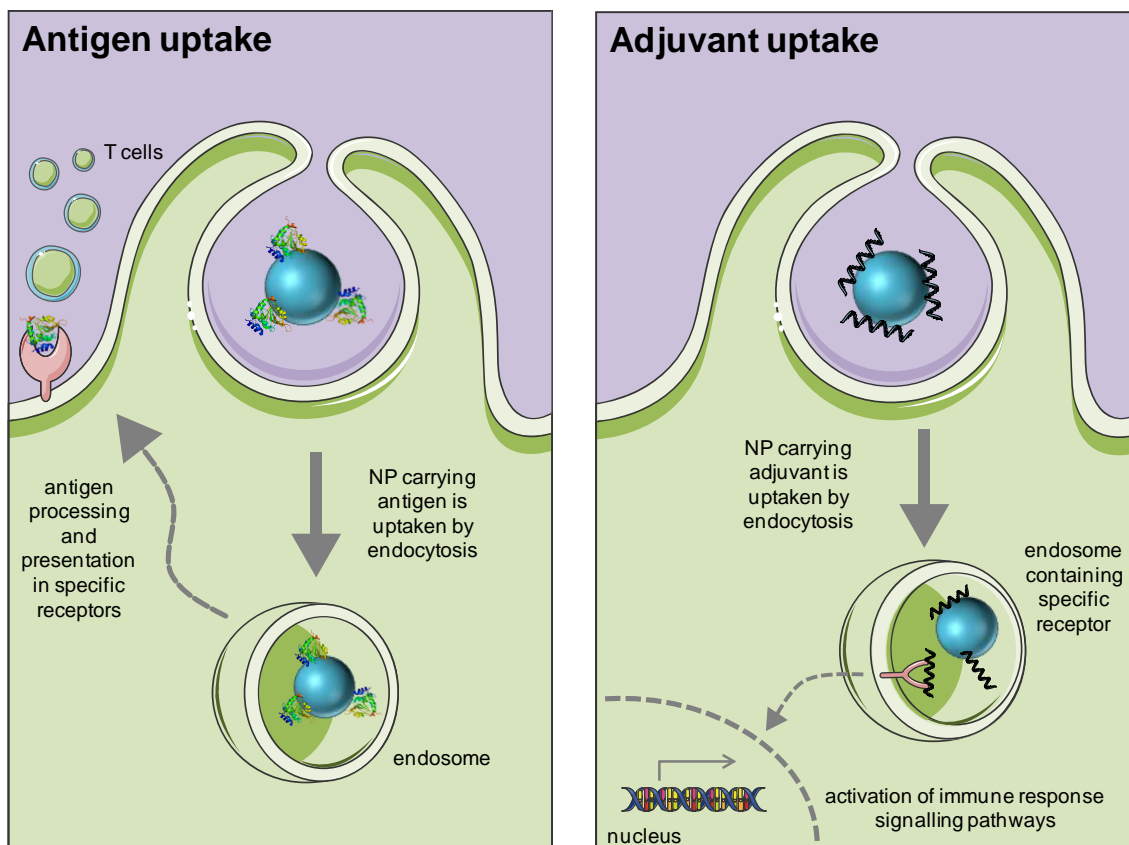


Figure 3.2. Uptake of antigen/adjuvant carrying NPs by phagocytic cells. Antigen loaded into NPs enters via endocytic pathway allowing its processing and the presentation to other immune cells. In contrast, adjuvants such as CpG ODNs have their specific receptor located inside the endosomes; NPs can allow adjuvant internalization via endocytic pathway, where the interaction between the specific receptor TLR 9 and its ligand occurs, and activate immune response signalling pathways.

3.1.3. *In vivo* biodistribution of NPs

As in the case of the intracellular fate, the *in vivo* biodistribution of NPs depends on several factors and can vary from one type of NPs to another. Focussing on the NP type chosen for this thesis, the biodistribution of IONPs has been extensively studied due to their wide-ranging applications in biomedical science.^{34–36} Already in the late 1980s, the pharmacokinetics and toxicity of intravenously injected ‘naked’ IONPs of about 80 nm was studied by Weissleder and co-workers. In this early biodistribution studies it was discovered that IONPs were mainly accumulated in RES organs, i.e., spleen and

liver. These 'naked' IONPs were found to have a slow systemic clearance, with a circulation half-life of 44.9 days, and led to incorporation into natural iron metabolic pathways.³⁷

However, when IONPs are optimized by tuning their size, adding coatings and or specific ligands, the *in vivo* biodistribution can be tailored. As in the case of other types of NPs, the size of IONPs can in part define their *in vivo* fate. The large IONPs studied by Weissleder et al. are rapidly accumulated in the liver and spleen, whereas smaller NPs can reach the draining LNs. Bourrinet et al. compared 30 nm dextran-coated IONP with the previously reported 80 nm NPs and showed enhanced LN-targeting when the smaller NPs were administered compared to the larger ones.³⁸ The presence of a coating can also influence the biodistribution of IONPs and has been mainly exploited to increase the circulation half-life and allow the delivery to other tissues rather than RES organs, as reviewed by Almeida et al.³⁹ Regarding the surface charge, it has been reported by several groups that a net negative charge can increase the retention in SLOs such as LNs.⁴⁰

For anticancer applications tumour targeting is desired to increase the efficacy of therapy and reduce side effects. In the case of anticancer vaccines, although LNs are the main desired destination, the accumulation in malignant tissue can also enhance the antitumour immune response by inducing inflammatory responses *in situ*.

Despite huge efforts for actively targeting drugs to the tumour environment modifying the NP surface with different tumour affinity ligands, passive approaches can also be used to achieve NP accumulation in the tumour. These passive approaches rely on the preferential accumulation of NPs at the target sites due to the inherent biophysicochemical properties of the NP (size, shape, charge, flexibility, etc.) and biological barriers they encounter. For instance, passive tumour targeting is based on the so-called enhanced permeability and retention (EPR) effect in tumour tissue, where the vascular permeability is abnormally increased.^{42,43} Due to the EPR effect very large particles cannot enter the tumour vasculature, whereas very small NPs or single molecules can easily enter through the leaky capillary barrier but can also be rapidly pushed out from malignant tissue, leading to poor tumour retention.

Therefore, NPs of an optimal size show enhanced tumour uptake and are retained longer (**Figure 3.3**).

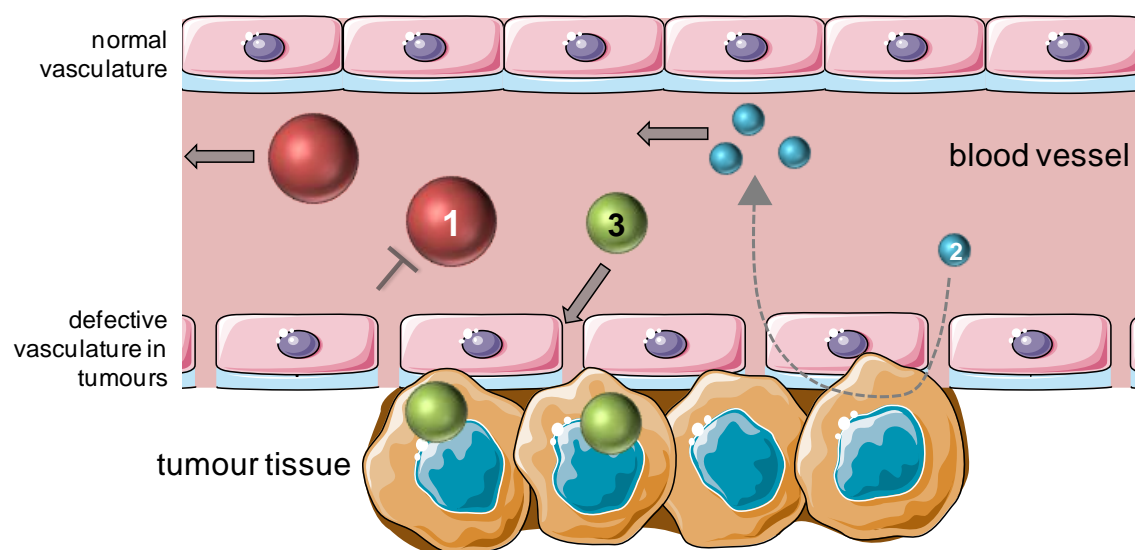


Figure 3.3. Effect of the NP size on tumour accumulation. EPR effect allows NPs uptake into tumour tissue, where the vasculature permeability is increased in comparison to normal tissue. 1) Particles larger than the cutoff size of the endothelium cannot flow through the barrier. 2) Very small NPs can be easily taken up but also expelled from tumour tissue. 3) NPs of optimal size are able to passively enter and accumulate into the tumour. Figure adapted from *Mol. Pharm.*, 2008, 5, 496.⁴¹

Next we report the results of applying the multimodal imaging properties of the designed anticancer vaccines to study both their intracellular trafficking in APCs and *in vivo* biodistribution in healthy and tumour-bearing mice.

3.2. Results and discussion

3.2.1. *In vitro* and *in vivo* trafficking of the micelles by optical imaging

The IONP-filled micelles were fluorescently labelled simply by addition of a commercially available rhodamine B-modified DPPE phospholipid during the solubilisation of the hydrophobic IONP by micelle formation (Chapter II). Since the target of these nanovaccines are cells of the innate immune system, the internalization and trafficking of CpG- and OVA-IONP micelles were investigated in a murine J774A.1 macrophage cell line and DCs from bone marrow derived cells (BMDCs), by flow cytometry and fluorescence microscopy.

Firstly, the uptake of the micelles was analysed by flow cytometry, in order to know if the chosen APCs, the DCs and macrophages, were able to bind these fluorescently labelled nanoconstructs. For this purpose, the rhodamine-labelled functionalised micelles were incubated for 3 h with the J774A.1 cells or overnight with the BMDCs. The cellular uptake of CpG- and OVA-modified particles analysed by flow cytometry showed efficient micelle uptake by both cell types (**Figure 3.4a-d**; gating strategy shown in Supporting Information, Figure S3.1).

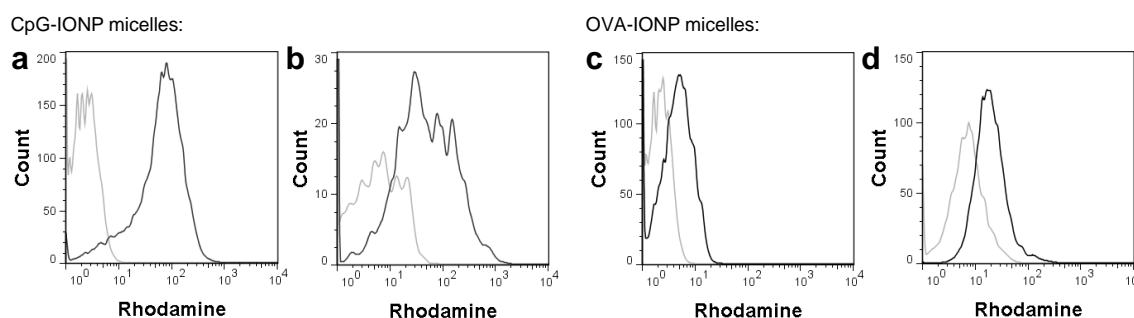


Figure 3.4. Uptake analysis of the fluorescently labelled (a, b) CpG- and (c, d) OVA-IONP micelles in immune system cells by flow cytometry. IONP micelles carrying the immunostimulatory molecules were taken up by both (a, c) J774A.1 macrophages and DCs (b, d). Samples fluorescence intensity in the cells was represented with a dark line, whereas the non-stained control was showed with a light line.

However, flow cytometry technique does not confirm the internalization of the NPs, neither the localisation inside the cells. To gain further information about the intracellular fate of the nanovaccines, they were analysed by fluorescence microscopy. As previously commented, the CpG ODNs must reach endosomal TLR 9 receptor.

Hence, first the internalization via endocytic pathway of the rhodamine-labelled CpG-IONP micelles was analysed in APCs. The results confirmed the good uptake and showed that the CpG-IONP micelles co-localised with late endosomes/lysosomes (stained with LysoTracker green dye), in both APCs types (**Figure 3.5**).

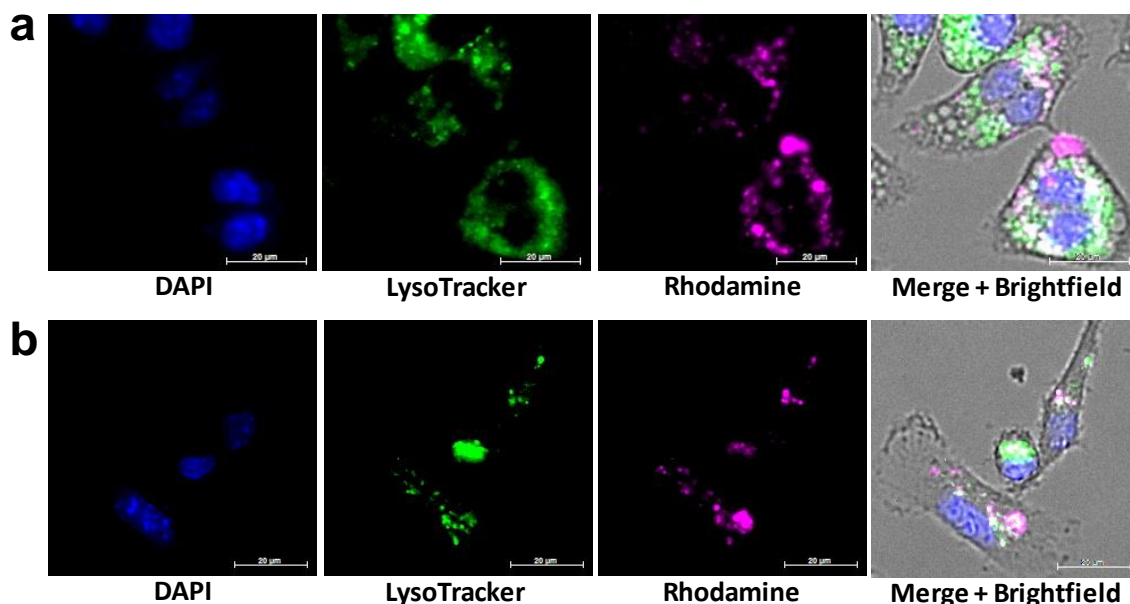


Figure 3.5. Trafficking of the fluorescently labelled CpG-IONP micelles in (a) J774A.1 macrophages and (b) BMDCs. After 3 h of incubation with the NPs, fluorescence microscopy showed the cellular uptake and co-localisation with endosomes/lysosomes. Nuclei were stained with DAPI (blue), endosomes/lysosomes were visualized with LysoTracker (green) and CpG-IONP micelles were labelled with DPPE-Rho (pink).

Next, the TLR 9 expression in J774A.1 macrophages and DCs was confirmed by flow cytometry, by labelling the TLR 9 with a specific fluorescent antibody and analysing its presence in the previously defined populations (**Figure 3.6a, c**). It was possible to demonstrate by fluorescence microscopy that the CpG-IONP micelles were capable of delivering the CpG ODN cargo to TLR 9 in both J774A.1 macrophages and BMDCs (**Figure 3.6b, d**).

Since antigens entering the endocytic pathway of APCs is critical for the generation of effective adaptive immune responses (MHC class II molecules acquire their peptides in endosomes), the intracellular location of the rhodamine labelled OVA-IONP micelles was investigated in the same way. The co-localisation with endosomes/lysosomes by fluorescent microscopy confirmed the endocytic delivery of OVA in both types of APCs (**Figure 3.7**).

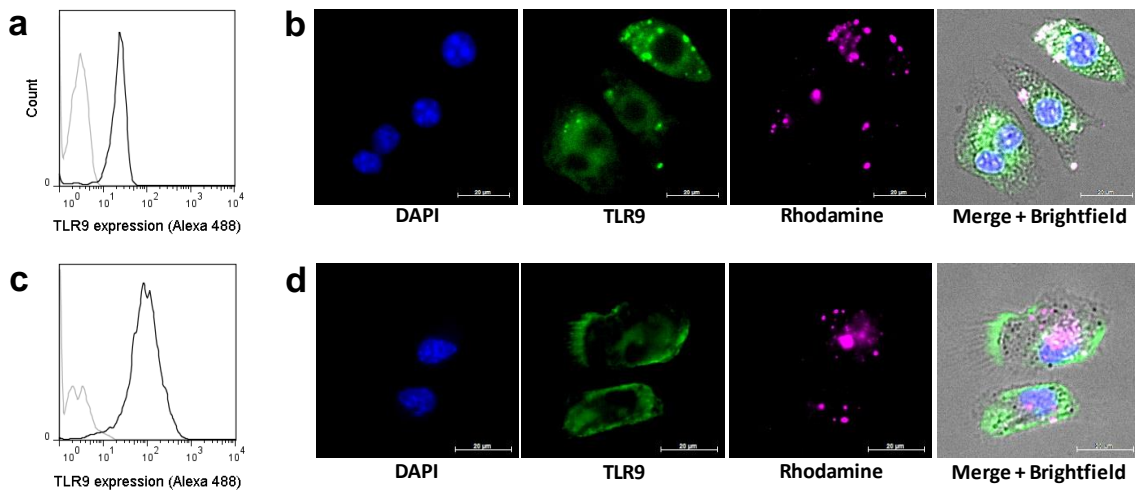


Figure 3.6. Trafficking of the fluorescently labelled CpG-IONP micelles in (a, b) J774A.1 macrophages and (c, d) BMDCs. (a, c) TLR 9 expression was analysed by flow cytometry: non-stained control cells (light line) and the cells immunolabelled with anti-TLR 9 antibody (dark line) are shown. (b, d) After 3 h of incubation with the NPs, fluorescence microscopy showed the cellular uptake and co-localisation with TLR 9. Nuclei were stained with DAPI (blue), TLR 9 was visualized with Alexa488 (green) secondary antibody and CpG-IONP micelles were labelled with DPPE-Rho (pink).

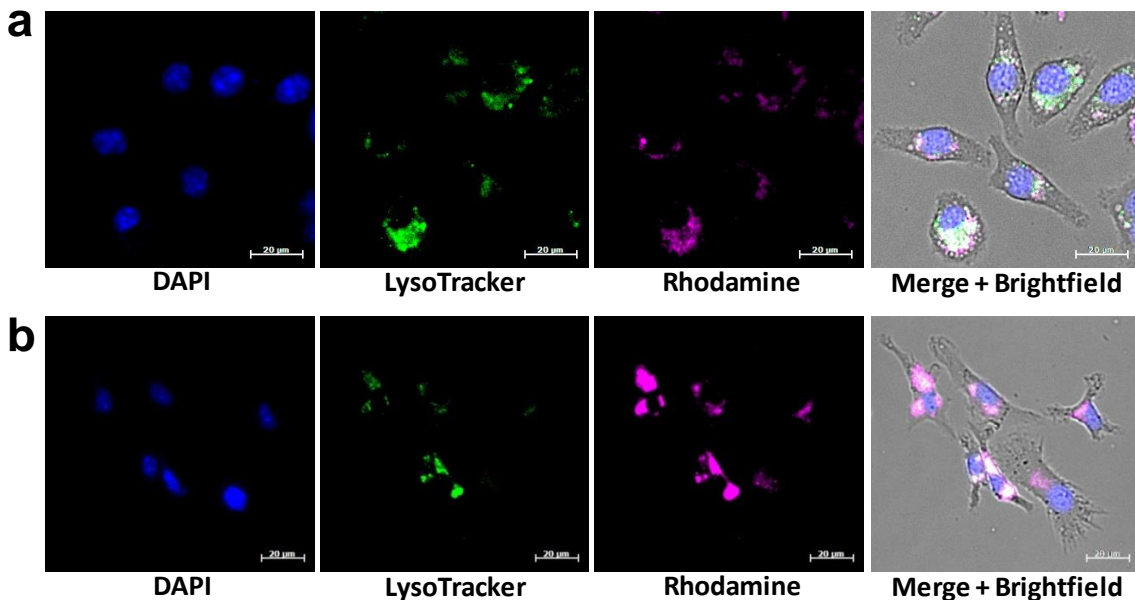


Figure 3.7. Trafficking of the fluorescently labelled OVA-IONP micelles in (a) J774A.1 macrophages and (b) BMDCs. After 3 h of incubation with the NPs, fluorescence microscopy showed the cellular uptake and co-localisation with endosomes/lysosomes. Nuclei were stained with DAPI (blue), endosomes/lysosomes were visualized with LysoTracker (green) and OVA-IONP micelles were labelled with DPPE-Rho (pink).

Although direct visualization of the fluorescently labelled NPs was not explored, flow cytometry was applied to study the *in vivo* cellular fate of the nanovaccines in different population of cells of the immune system. Commercially available fluorescent-labelled CpG ODNs and OVA antigen were prepared as previously described (Chapter II).

These fluorescent formulations were administered to mice by subcutaneous injection and 6 h after injection, spleens were harvested in order to study the NPs uptake in DCs (CD11c⁺ population), B cells (CD19⁺ population) and macrophages (F4/80⁺ population) (Supporting Information, Figure S3.2). When carried by IONP-filled micelles, CpG ODNs were efficiently targeted to the three types of immune cells and adjuvant accumulation was equal or even higher than with NP-free CpG ODNs (**Figure 3.8a-c**). In the same way, OVA antigen uptake was increased when loaded into IONP-filled micelles (Figure 3.8d-f).

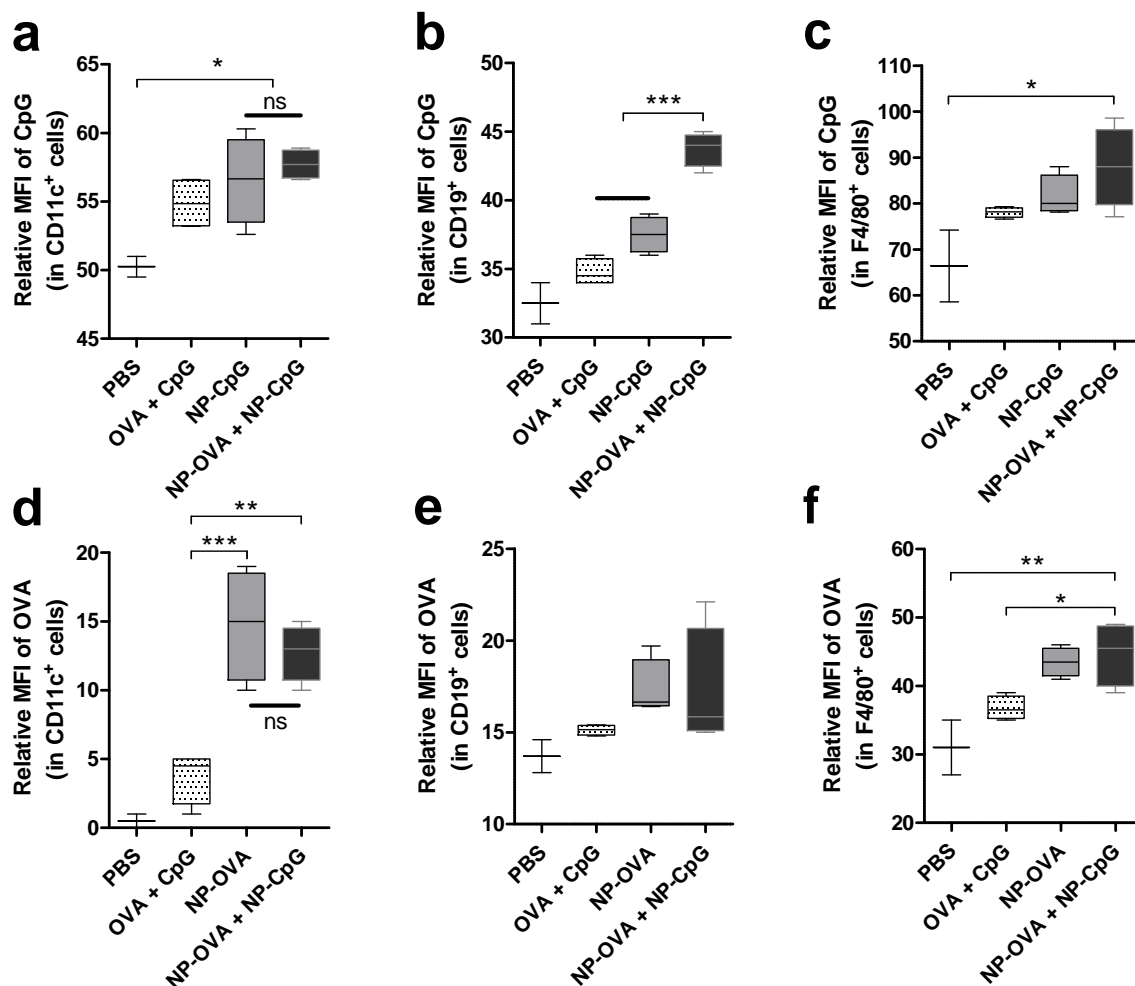


Figure 3.8. Cargos loaded into IONP-filled micelles reach more efficiently cell of immune system. C57BL/6 mice were administered with 5 μ g of Alexa647-labelled OVA and FITC-labelled CpG free or in conjugation with IONP micelles (*ca.* 31 μ g of magnetite) by subcutaneous injection in the right flank of the animals. 6 h after injection, mice were sacrificed and the fluorescence present in the harvested spleens in different immune system cell subtypes was analysed: (a, d) DCs; (b, e) B cells; and (c, f) macrophages. Relative mean fluorescence intensity (MFI) of (a-c) CpG ODNs and (d-f) OVA. Data are presented as mean \pm SEM of 4 mice per group. * $P < 0.05$, ** $P < 0.01$, *** $P < 0.001$, ns = non-significant by one-way ANOVA followed by Tukey's test.

3.2.2. *In vivo* biodistribution of the micelles by nuclear imaging

a) Healthy mice:

The *in vivo* biodistribution of the ⁶⁷Ga-labelled micelle vaccines was analysed by SPECT/CT. An important current target in cancer therapy and immunotherapy is efficient delivery of drugs and immunotherapeutics through the lymphatic system^{44–46} to target the draining LNs as key immunological command centres. The micelle vaccines were radiolabelled (Chapter II) and injected subcutaneously at different anatomical regions in mice. In this way, the possible site-dependent migration to draining LNs and how this might affect or be used to predict/explain the *in vivo* efficacy of the systems in immunization studies was investigated.

Firstly, the ‘nude’ IONP-COOH (**Figure 3.9**) and functionalised OVA-IONP micelles (**Figure 3.10**) were tracked 3 h and 24 h after subcutaneous injection in the left forearms, ventral flanks and hocks of healthy mice using SPECT/CT. The lymphatic drainage pattern was virtually identical for both types of IONP micelles, which is consistent with the notion that size is the main determinant of the NP’s lymphatic trafficking. SPECT/CT studies showed that 3 h after subcutaneous injection in the forearm, both ‘nude’ IONP-COOH and antigen loaded OVA-IONP micelles already reach the draining left axillary LN (Figure 3.9a, 3.10a). When the subcutaneous injection was performed in the flank in the ventral part of the animal, the intense signal at the site of injection prevented the detection of the IONP micelles in the draining inguinal LNs (Figure 3.9b, e and 3.10b, e).

Despite being the most extensively used immunization administration route in rodents, footpad injection is not the best choice from a humane point of view, due to the inflammation, swelling and consequent lameness that can cause in the animal limb. To avoid these unwanted side effects, the tarsal region just above the ankle (hock) was chosen as alternative to the footpad injection. It has been already reported that hock administration maintains the immunological response of the footpad injection as a result of very similar drainage patterns.^{47–49} It was found that after subcutaneous injection of IONP-COOH and OVA-IONP micelles in the left hind hock, both vehicles had migrated to the left inguinal and popliteal LNs at $t = 3$ h. A clear

signal was also detected in the axillary and iliac LNs (Figure 3.9c and 3.10c), which are directly connected via lymphatic vessels with the inguinal LNs and popliteal LNs, respectively.⁵⁰

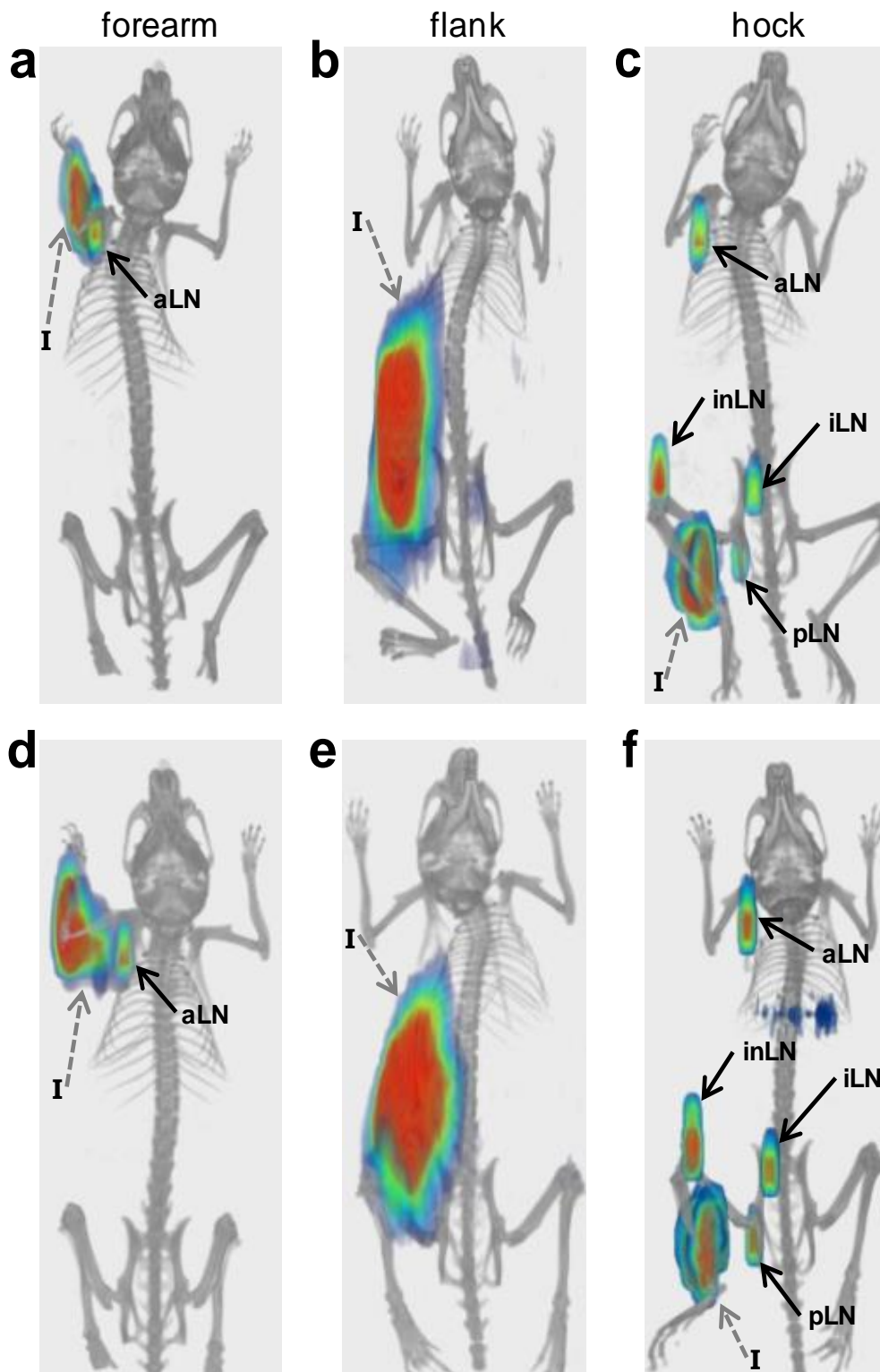


Figure 3.9. SPECT/CT images of mice injected with ^{67}Ga labelled IONP-COOH micelles (8 μg of magnetite) (a-c) 3 h and (d-f) 24 h post-injection in the left: (a, d) forearm (37.7 MBq), (b, e) flank (6.4 MBq) and (c, f) hind hock (7.3 MBq). aLN, axillary LN; inLN, inguinal LN; iLN, iliac LN; pLN, popliteal LN; injection site (I).

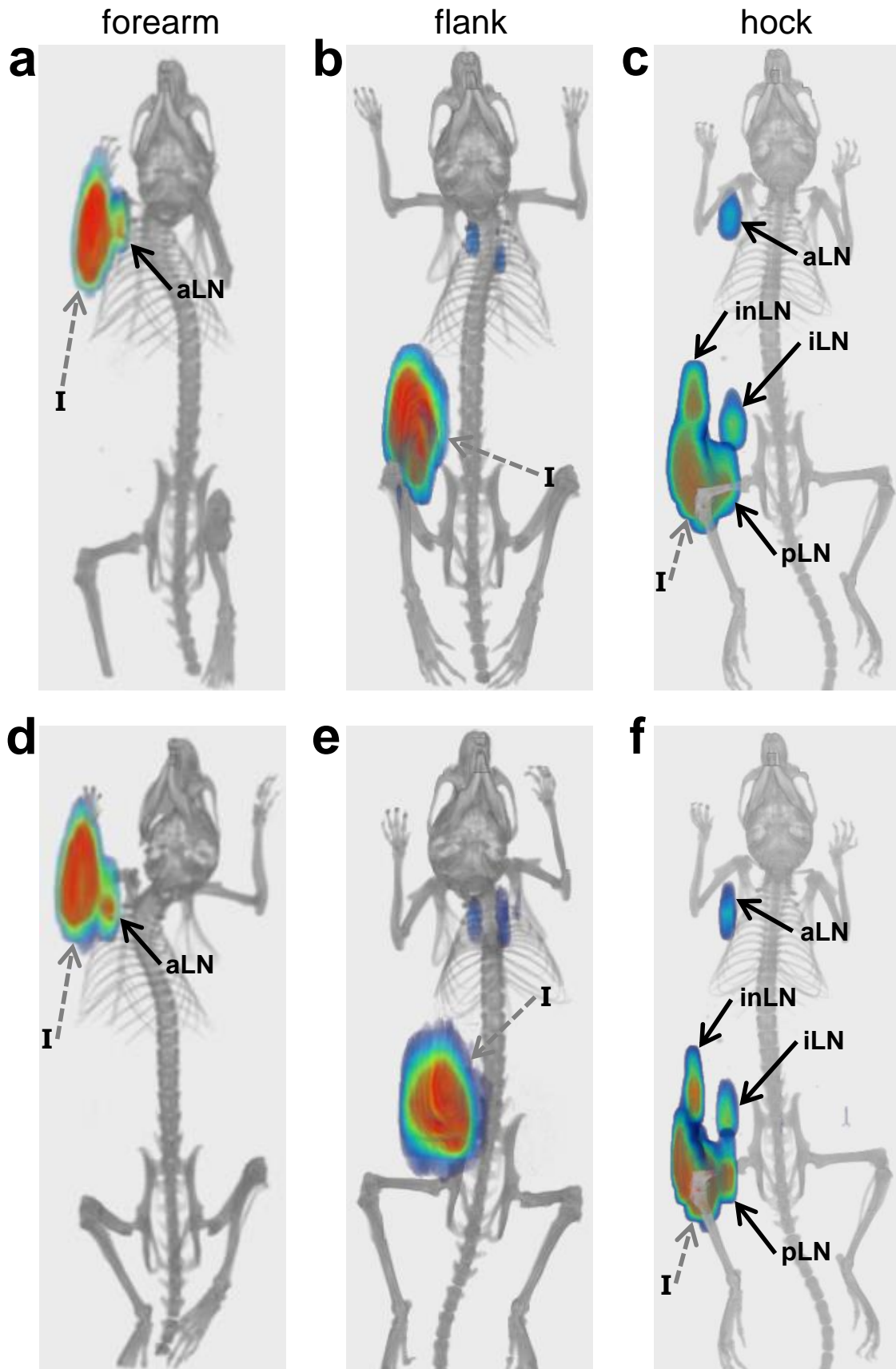


Figure 3.10. SPECT/CT images of mice injected with ^{67}Ga labelled OVA-IONP micelles (9 μg of magnetite) (a-c) 3 h and (d-f) 24 h post-injection in the left: (a, d) forearm (22 MBq), (b, e) flank (34.4 MBq) and (c, f) hind hock (12.2 MBq). aLN, axillary LN; inLN, inguinal LN; iLN, iliac LN; pLN, popliteal LN; injection site (I).

The *ex vivo* analysis of the harvested organs and further organ by organ gamma emission quantification was used to corroborate the results from the *in vivo* images with a more quantitative analysis. **Figure 3.11** shows the post mortem analysis both by *ex vivo* SPECT/CT imaging and Gamma Counter of IONP-COOH or OVA-IONP micelles 24 h after injection in the left forearms and flanks of mice. When the injection was done in the left forearm, a clear signal in the left axillary LN was found, corroborating the *in vivo* image at 3 h after injection. Furthermore, a weaker signal in the left brachial LN was also observable in the *ex vivo* SPECT/CT images and confirmed by the Gamma Counter analysis when injecting mice in the forearm (Figure 3.11b, f and 3.11d, h).^{51,52} Since the injection into the flank does not allow the observation of the inguinal LN, *ex vivo* analysis was the only way to demonstrate LN targeting using this administration route. Both the *ex vivo* SPECT/CT images and the Gamma Counter values showed a main accumulation in the inguinal LN (Figure 3.11c, g and 3.11e, i).

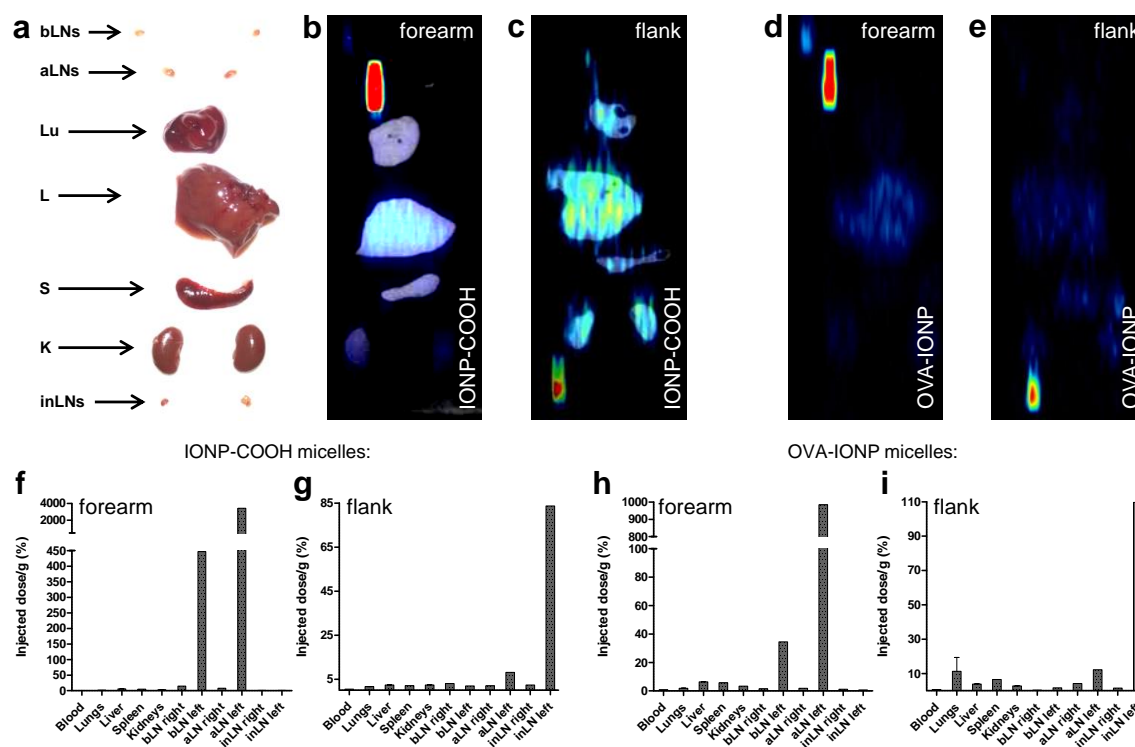


Figure 3.11. *Ex vivo* analysis of the OVA-IONP and the 'nude' COOH-IONP micelles biodistribution 24 h after forearm and flank injections. (a) Photograph of selected harvested organs, (b-e) SPECT/CT images of the extracted organs and (f-i) biodistribution expressed as injected dose percentage per gram of tissue. Mice were injected with (b, c, f, g) IONP-COOH and (d, e, h, i) OVA-IONP micelles by two different routes: (b, d, f, h) forearm and (c, e, g, i) flank. bLN, brachial LN; aLN, axillary LN; Lu, lungs; L, liver; S, spleen; K, kidneys; inLN, inguinal LN.

To complete the biodistribution analysis of antigen carrying micelles in healthy mice, the *ex vivo* studies of the hock administration route were performed 24 h after of injection. Since the *in vivo* images showed drainage to proximal and distal LNs, different SLOs were harvested for their further analysis *ex vivo*. Both SPECT/CT images and gamma counter analysis corroborated the drainage to the inguinal LN and therefore to the distal axillary LN. A clear accumulation was observed in the popliteal LN for both formulations. However, slight signal in the iliac and sciatic LNs was measured only by Gamma Counter (Figure 3.12).

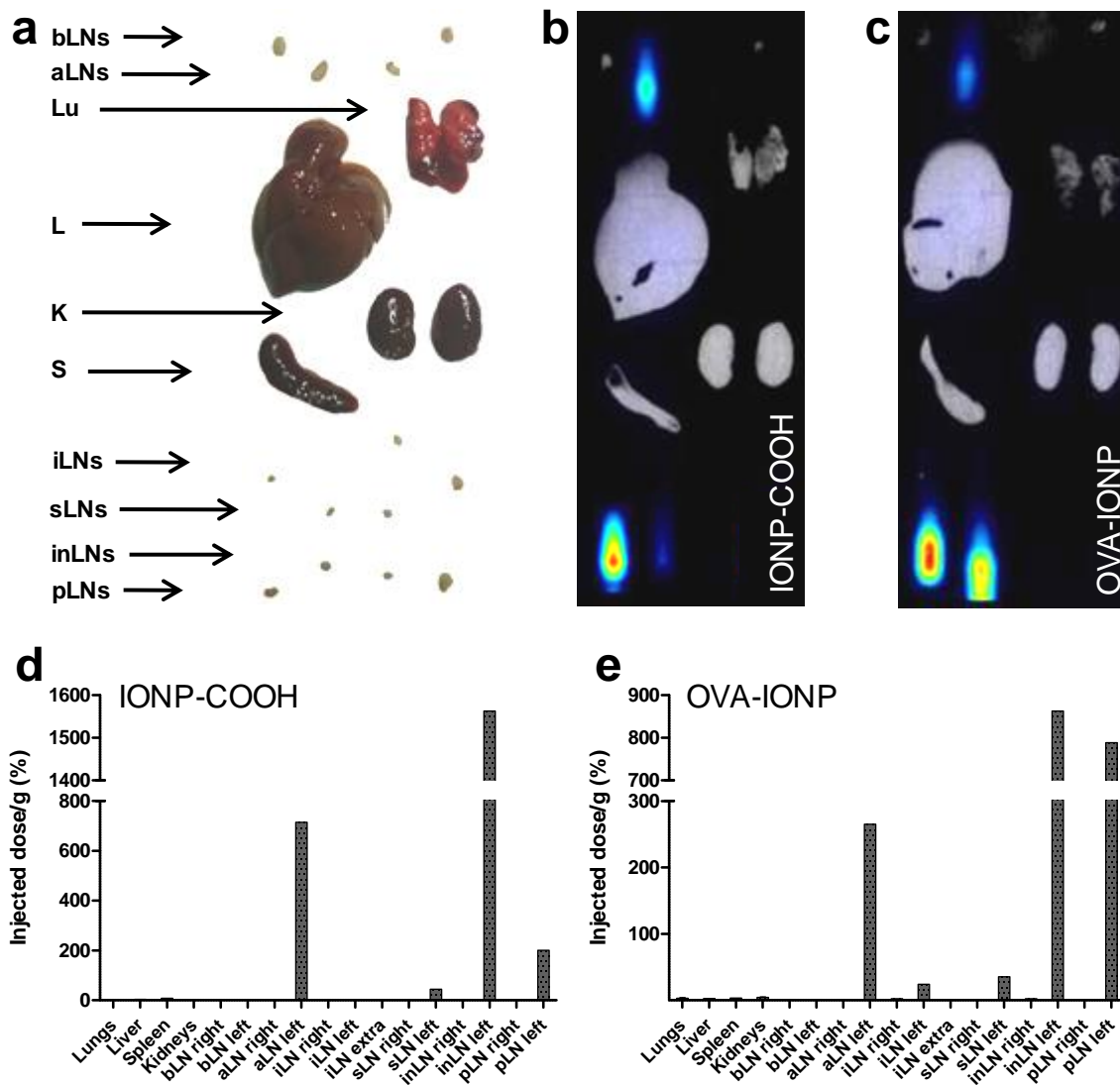


Figure 3.12. *Ex vivo* analysis of the ‘nude’ and OVA-IONP micelles biodistribution 24 h after hock injection. (a) Photograph of selected harvested organs, (b, c) SPECT/CT images of the extracted organs and (d, e) biodistribution expressed as injected dose percentage per gram of tissue. Mice were injected with (b, d) IONP-COOH (10.7 MBq) and (c, e,) OVA-IONP micelles (12.2 MBq). bLN, brachial LN; aLN, axillary LN; Lu, lungs; L, Liver; S, spleen; K, kidneys; iLN, iliac LN; sLN, sciatic LN; inLN, inguinal LN; pLN, popliteal LN.

b) Tumour-bearing mice:

Next, biodistribution experiments were carried out employing tumour bearing mice, both for antigen and adjuvant carrying micelles. In this thesis B16-F10 mouse melanoma model was used, which is highly aggressive, notoriously difficult to treat and known to metastasize from a primary subcutaneous site to other sites of the body.⁵³ A B16-F10 subline engineered to express the full-length OVA antigen (B16-F10-OVA cells) was used as tumour model. Flank and hock administrations routes were explored as these were the routes used in the immunization and cancer immunotherapy studies (Chapter IV). For this purpose, C57BL/6 mice were subcutaneously injected with the tumour cell line in the right back of the animals. When tumours were about 6-7 mm (*ca.* 100 mm³), mice were administered with radiolabelled CpG- or OVA-IONP micelles.

As in the case of healthy mice, LNs draining the site of injection showed a high signal already 3 h after administration, which was maintained and in some cases increased over two days (**Figures 3.13–3.16**). When the injection was done into the right ventral flank, both types of nanovehicles were accumulated in the axillary, iliac and inguinal LNs (Figure 3.13 and 3.14). In the case of the hock injection, the draining inguinal and popliteal LNs showed high accumulation of the micelle vaccines (Figure 3.15 and 3.16).

When analysing the accumulation of the micelles in the tumour by this two administration routes, SPECT/CT images showed modest accumulation. The strong signals coming from the LNs and the site of injection made it difficult to localise the tumour from the SPECT images. However, in all studies a signal in the tumour area could be detected 24-48 h after vaccine administration (Figure 3.13–3.16). The *ex vivo* analysis at 48 h clearly showed the presence of NPs in the tumour by comparing the gamma emission of the tumour tissue with that of other tissue including muscle and RES organs (liver and spleen) (Figure 3.13–3.16h). The biodistribution pattern of CpG- and OVA-IONP micelles was very similar, indicating that the NPs are able to self-drain to the lymphatic system and even to the tumour, without the need of extra targeting (Supporting Information, Figure S3.3).

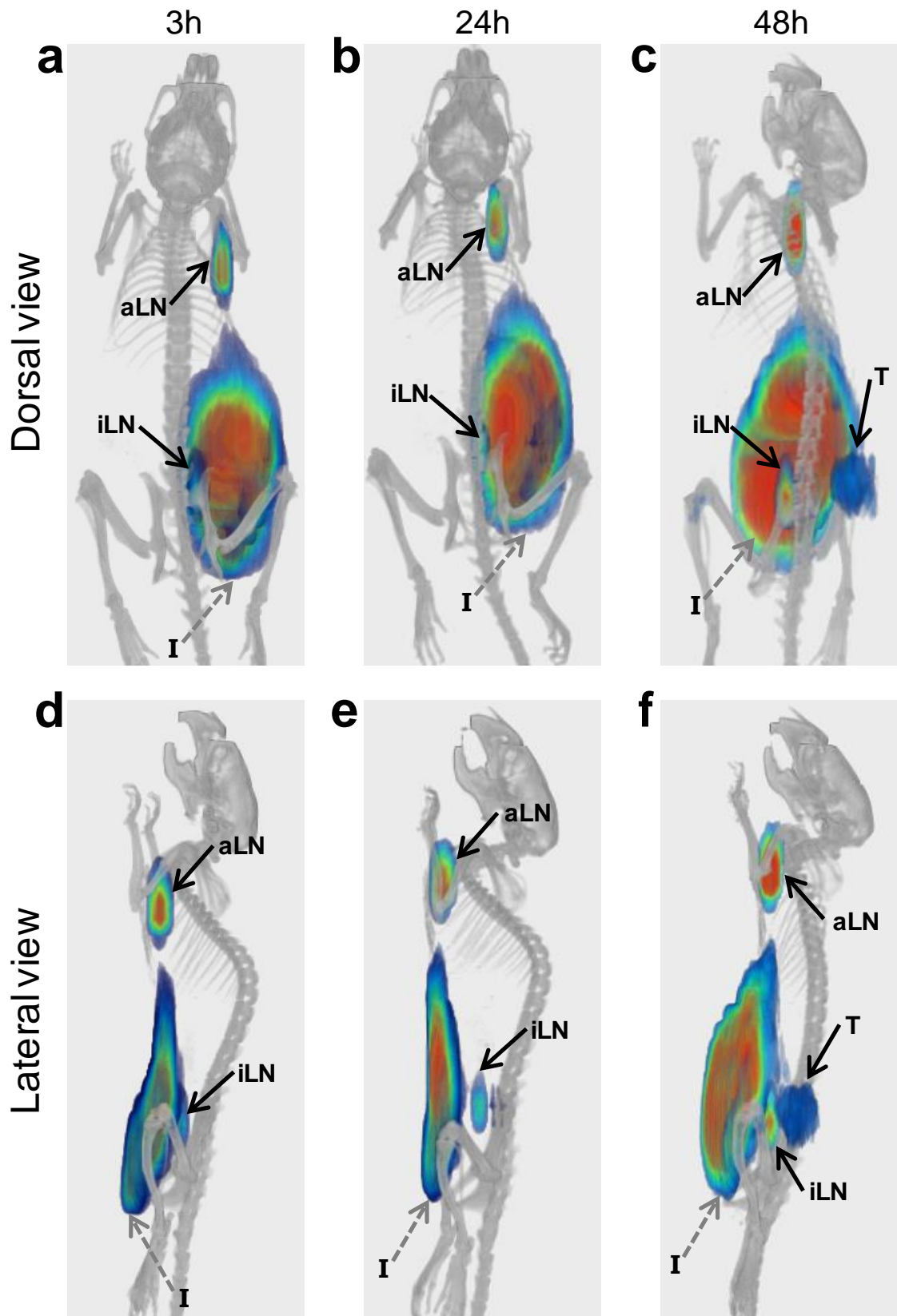


Figure 3.13. SPECT/CT images of melanoma tumour bearing mice injected in the flank with ^{67}Ga labelled OVA-IONP micelles (20.7 μg of magnetite, 41.0 MBq) (a, d) 3 h, (b, e) 24 h and (c, f) 48 h post-injection. (a-c) dorsal and (d-f) lateral views of *in vivo* images at different time points are shown. *Ex vivo* analysis by (g) SPECT/CT and (h) gamma counter 48 h after injection. T, tumour; bLN, brachial LN; aLN, axillary LN; Lu, lungs; L, liver; S, spleen; K, kidneys; iLN, iliac LN; sLN, sciatic LN; inLN, inguinal LN; pLN, popliteal LN; injection site (I).

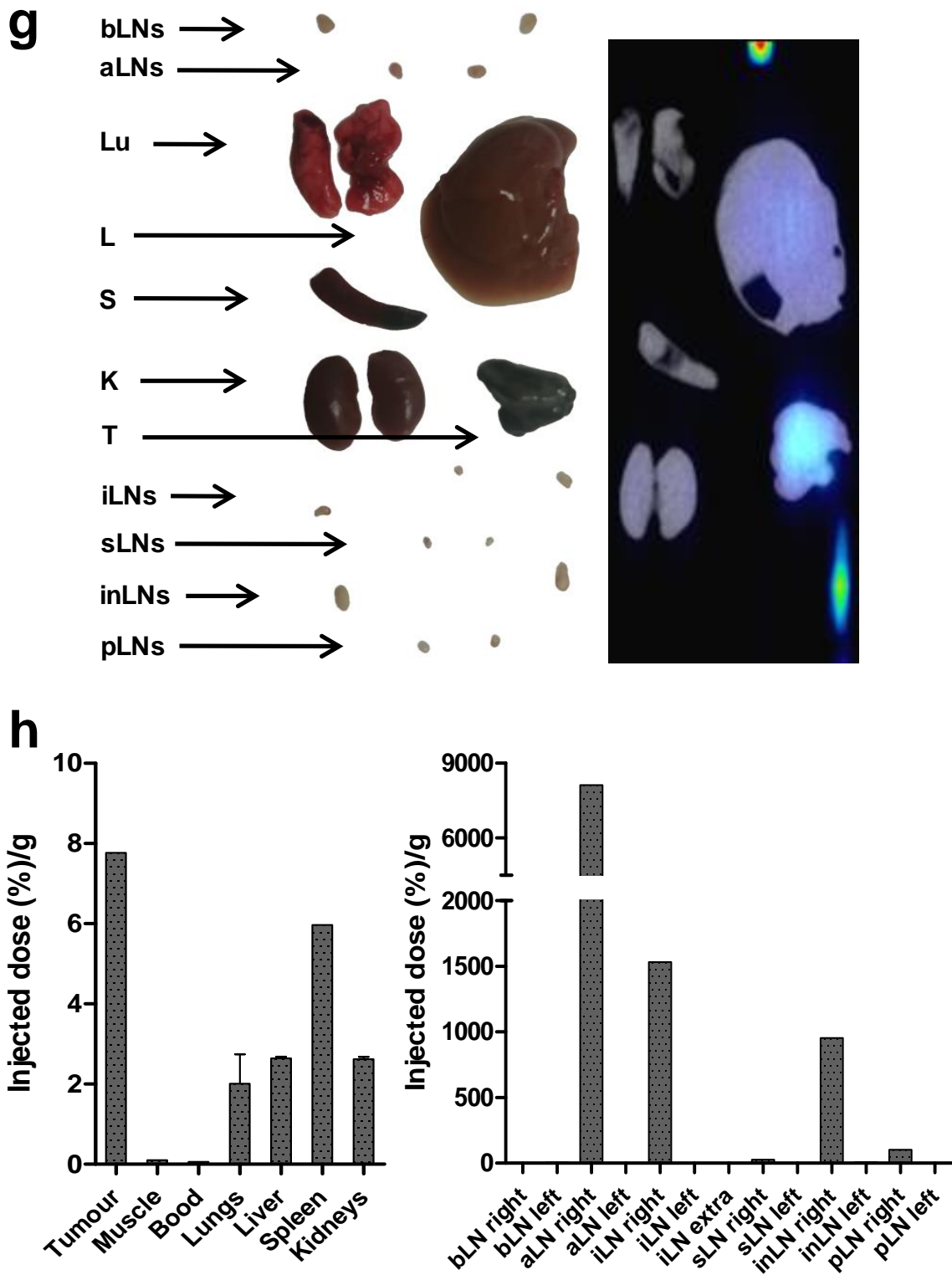


Figure 3.13 (Continued). SPECT/CT images of melanoma tumour bearing mice injected in the flank with ^{67}Ga labelled OVA-IONP micelles (20.7 μg of magnetite, 41.0 MBq) (a, d) 3 h, (b, e) 24 h and (c, f) 48 h post-injection. (a-c) dorsal and (d-f) lateral views of *in vivo* images at different time points are shown. *Ex vivo* analysis by (g) SPECT/CT and (h) gamma counter 48 h after injection. T, tumour; bLN, brachial LN; aLN, axillary LN; Lu, lungs; L, liver; S, spleen; K, kidneys; iLN, iliac LN; sLN, sciatic LN; inLN, inguinal LN; pLN, popliteal LN; injection site (I).

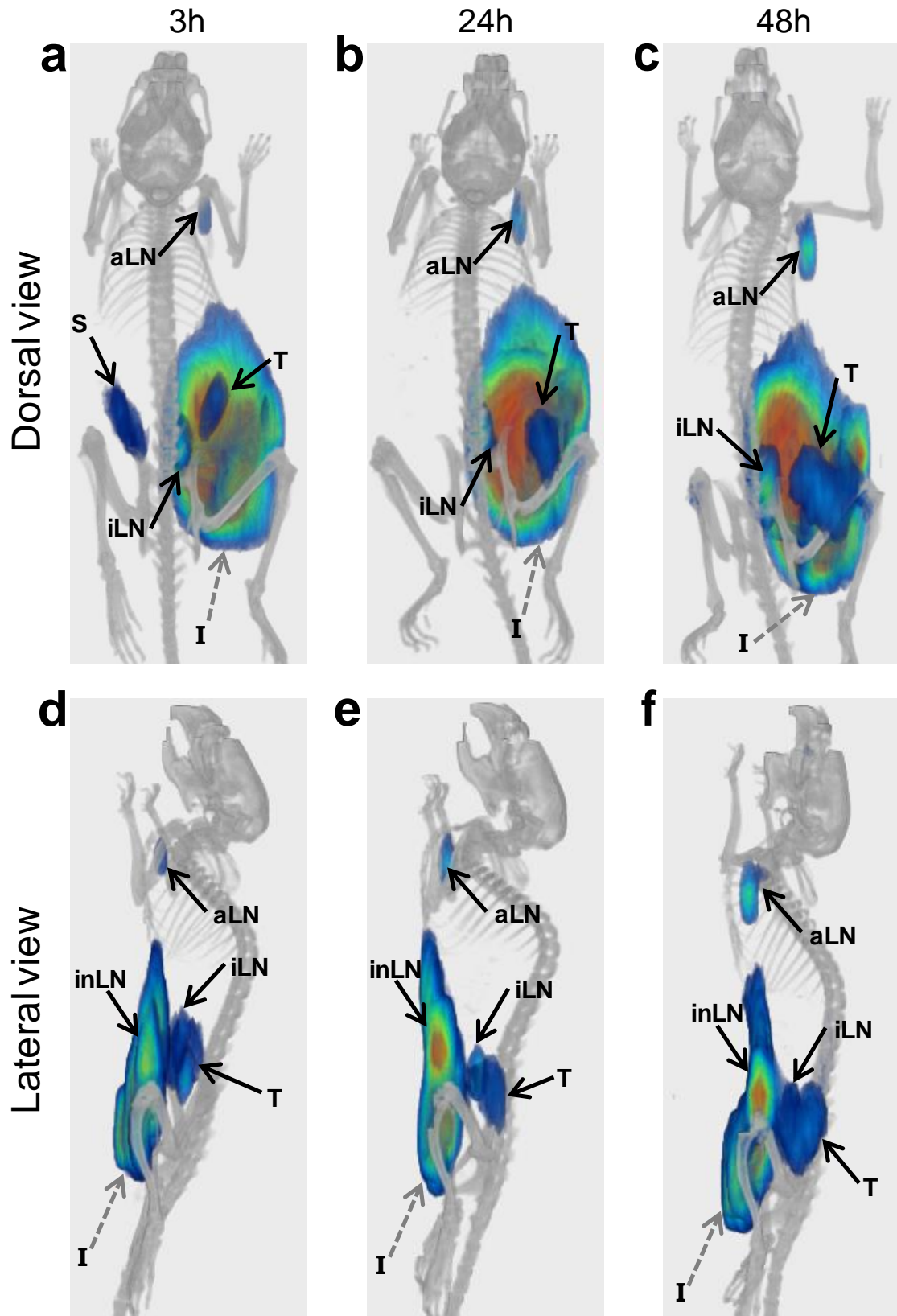


Figure 3.14. SPECT/CT images of melanoma tumour bearing mice injected in the flank with ^{67}Ga labelled CpG-IONP micelles (23.2 μg of magnetite, 42.2 MBq) (a, d) 3 h, (b, e) 24 h and (c, f) 48 h post-injection. (a-c) dorsal and (d-f) lateral views of *in vivo* images at different time points are shown. *Ex vivo* analysis by (g) SPECT/CT and (h) gamma counter 48 h after injection. T, tumour; bLN, brachial LN; aLN, axillary LN; Lu, lungs; L, liver; S, spleen; K, kidneys; iLN, iliac LN; sLN, sciatic LN; inLN, inguinal LN; pLN, popliteal LN; injection site (I).

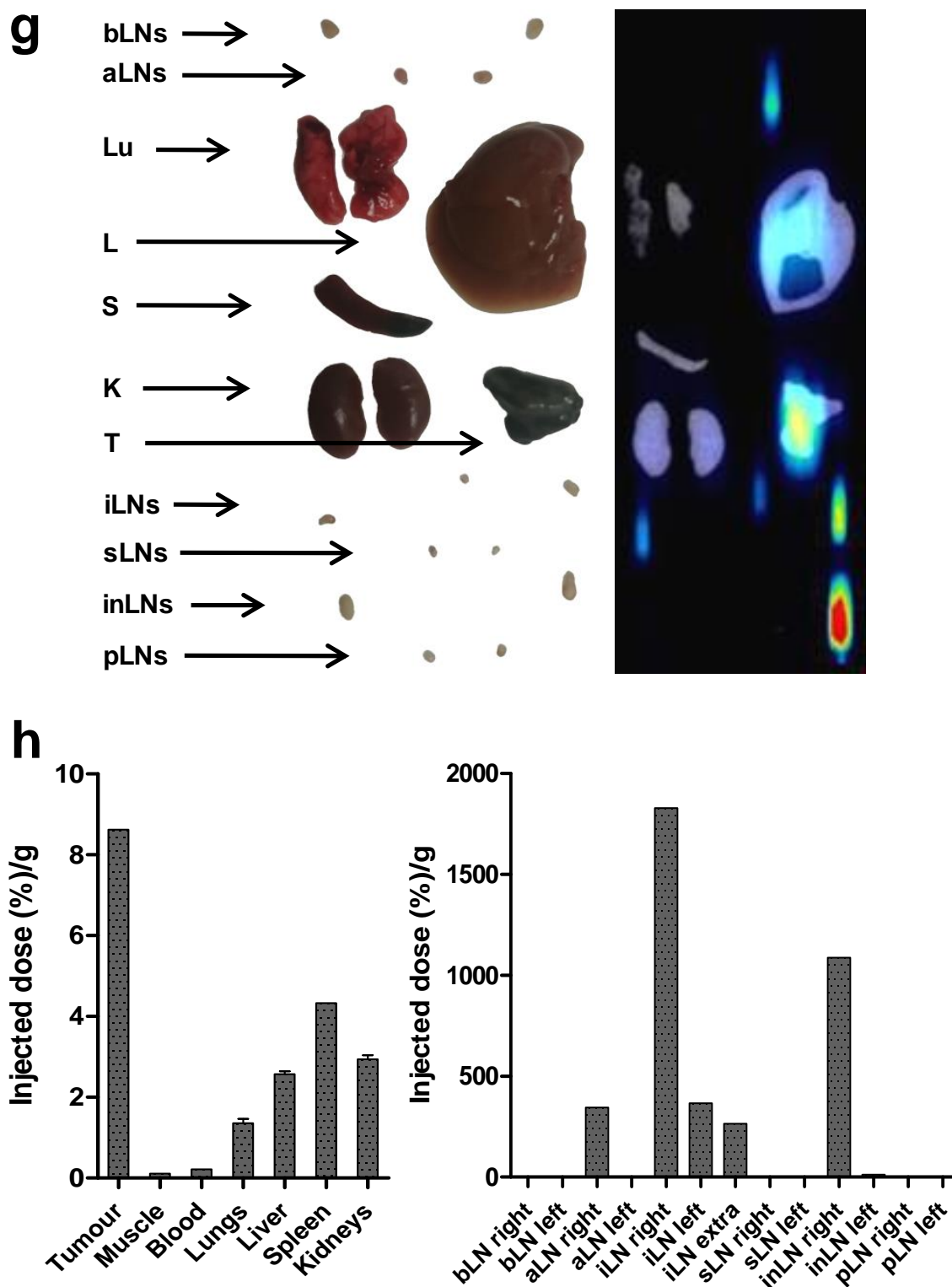


Figure 3.14 (Continued). SPECT/CT images of melanoma tumour bearing mice injected in the flank with ^{67}Ga labelled CpG-IONP micelles (23.2 μg of magnetite, 42.2 MBq) (a, d) 3 h, (b, e) 24 h and (c, f) 48 h post-injection. (a-c) dorsal and (d-f) lateral views of *in vivo* images at different time points are shown. *Ex vivo* analysis by (g) SPECT/CT and (h) gamma counter 48 h after injection. T, tumour; bLN, brachial LN; aLN, axillary LN; Lu, lungs; L, liver; S, spleen; K, kidneys; iLN, iliac LN; sLN, sciatic LN; inLN, inguinal LN; pLN, popliteal LN; injection site (I).

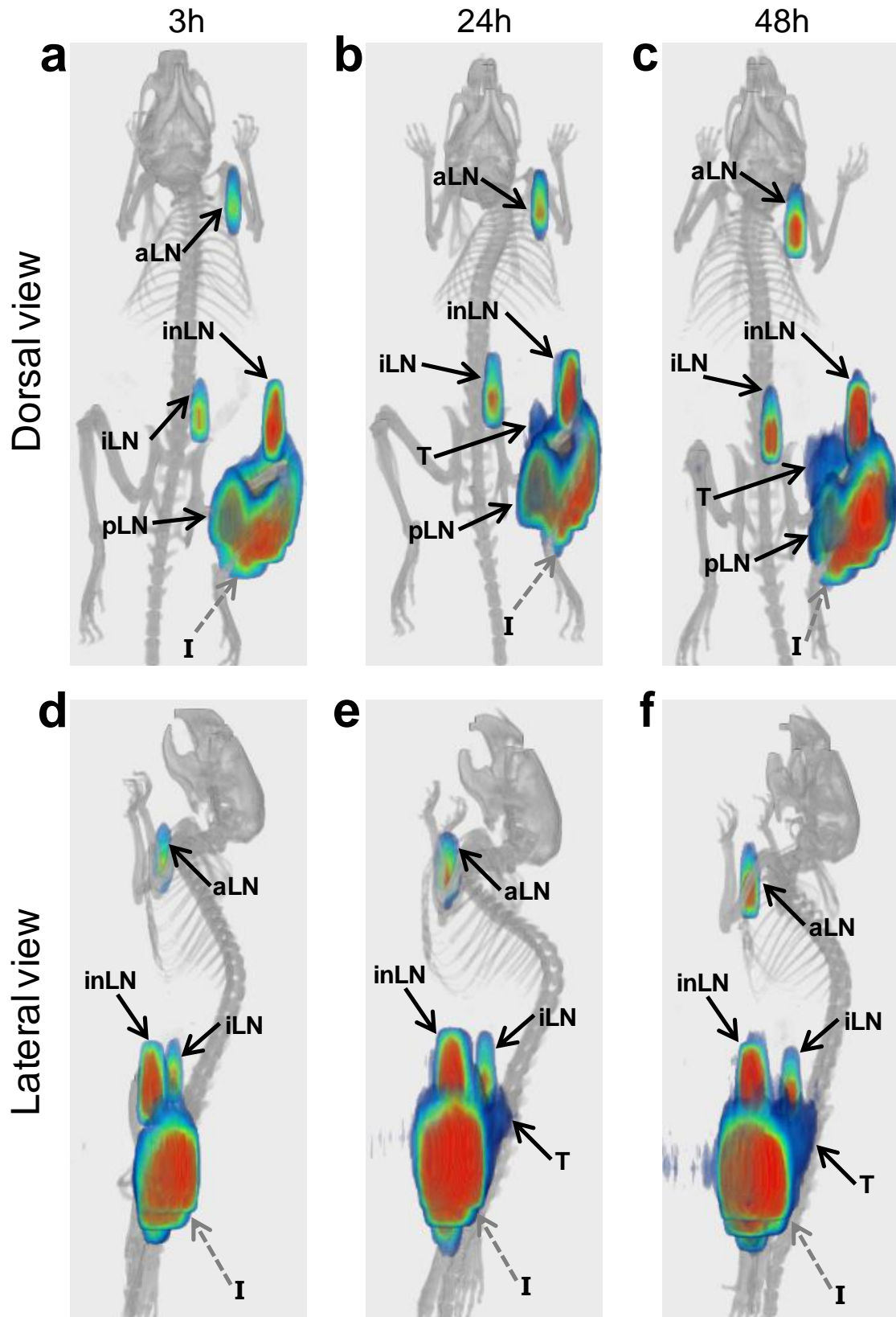


Figure 3.15. SPECT/CT images of melanoma tumour bearing mice injected in the hock with ^{67}Ga labelled OVA-IONP micelles (20.7 μg of magnetite, 40.7 MBq) (a, d) 3 h, (b, e) 24 h and (c, f) 48 h post-injection. (a-c) dorsal and (d-f) lateral views of *in vivo* images at different time points are shown. *Ex vivo* analysis by (g) SPECT/CT and (h) gamma counter 48 h after injection. T, tumour; bLN, brachial LN; aLN, axillary LN; Lu, lungs; L, liver; S, spleen; K, kidneys; iLN, iliac LN; sLN, sciatic LN; inLN, inguinal LN; pLN, popliteal LN; injection site (I).

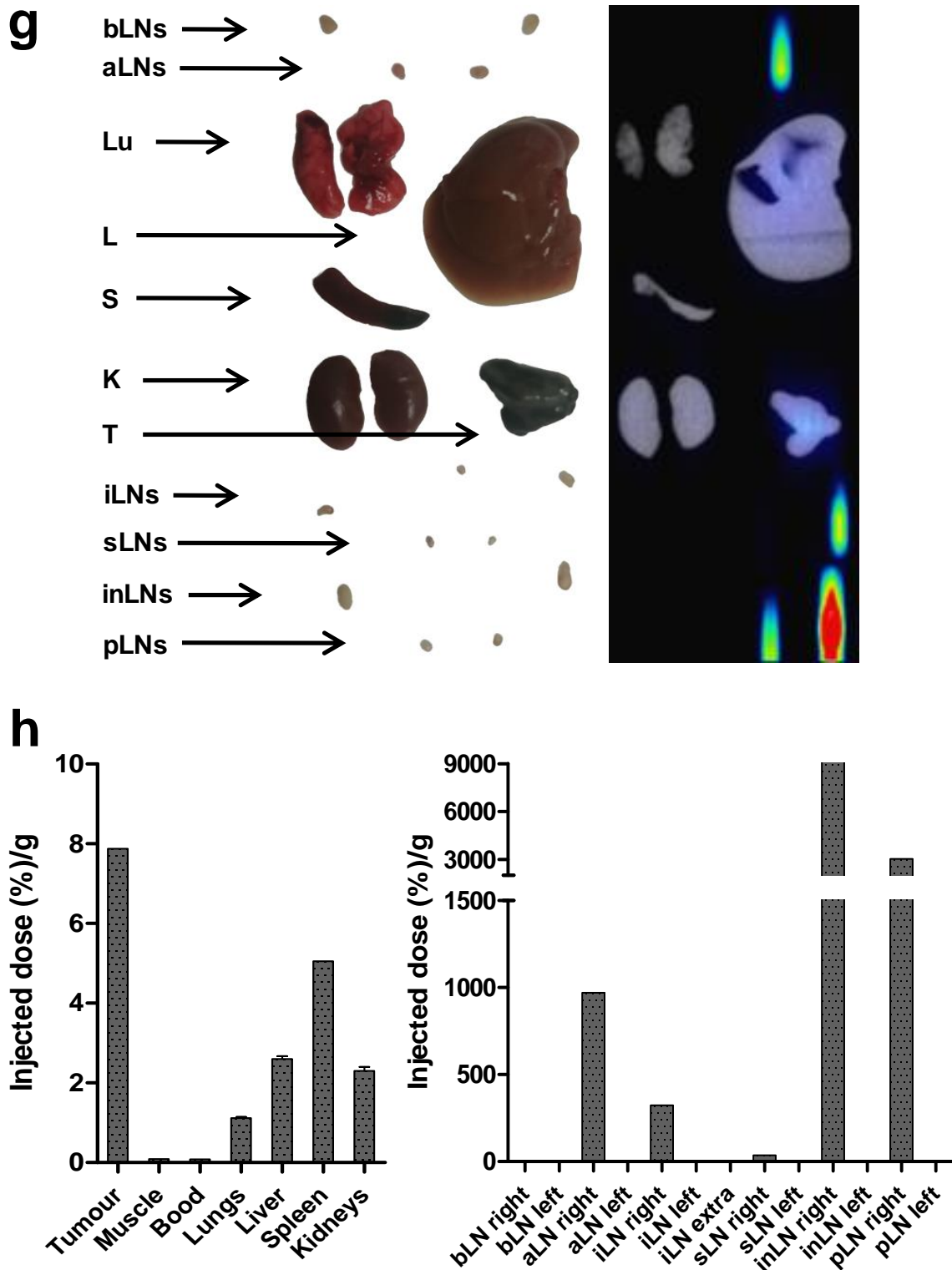


Figure 3.15 (Continued). SPECT/CT images of melanoma tumour bearing mice injected in the hock with ^{67}Ga labelled OVA-IONP micelles (20.7 μg of magnetite, 40.7 MBq) (a, d) 3 h, (b, e) 24 h and (c, f) 48 h post-injection. (a-c) dorsal and (d-f) lateral views of *in vivo* images at different time points are shown. *Ex vivo* analysis by (g) SPECT/CT and (h) gamma counter 48 h after injection. T, tumour; bLN, brachial LN; aLN, axillary LN; Lu, lungs; L, liver; S, spleen; K, kidneys; iLN, iliac LN; sLN, sciatic LN; inLN, inguinal LN; pLN, popliteal LN; injection site (I).

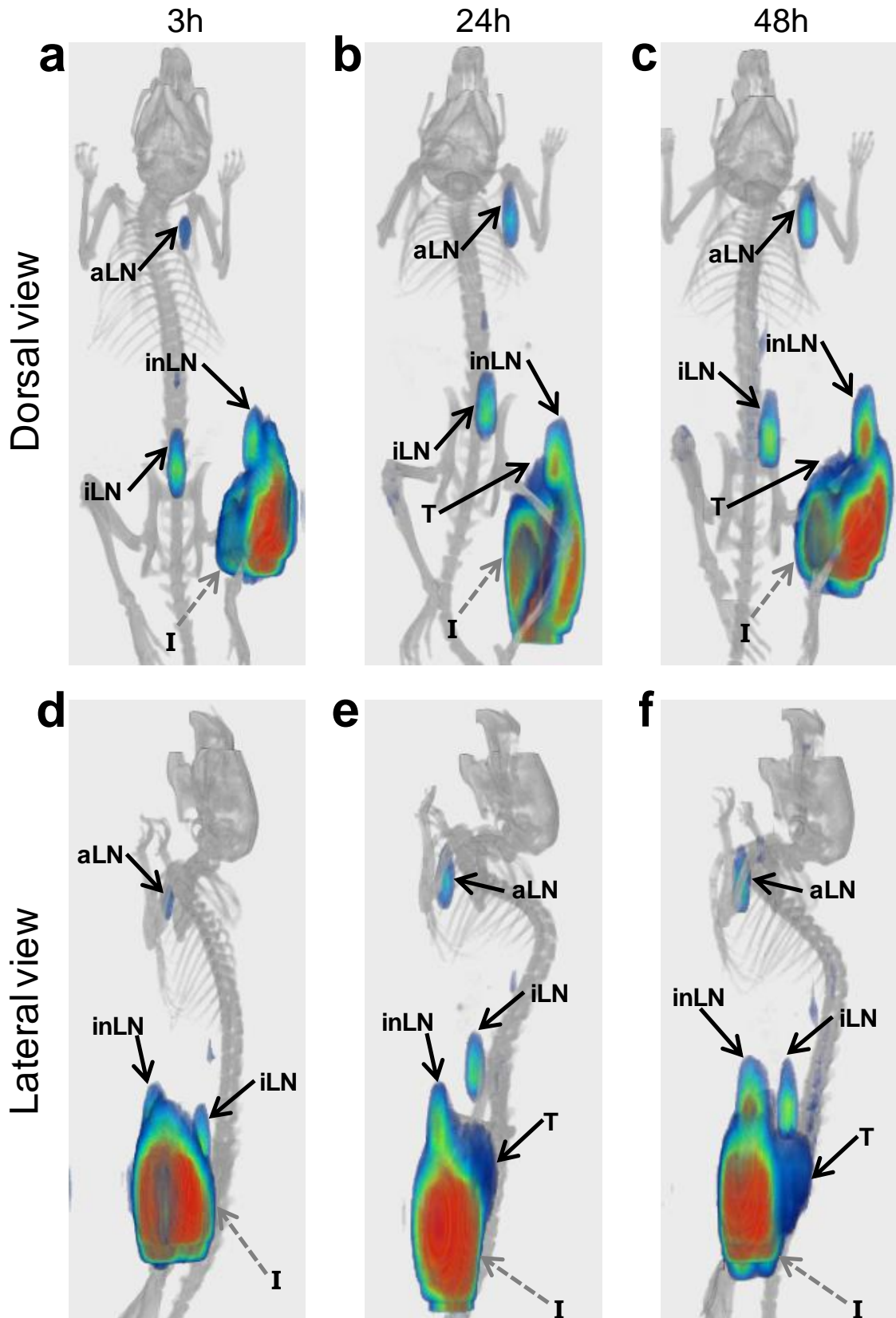


Figure 3.16. SPECT/CT images of melanoma tumour bearing mice injected in the hock with ^{67}Ga labelled CpG-IONP micelles (23.2 μg of magnetite, 43.4 MBq) (a, d) 3 h, (b, e) 24 h and (c, f) 48 h post-injection. (a-c) dorsal and (d-f) lateral views of *in vivo* images at different time points are shown. *Ex vivo* analysis by (g) SPECT/CT and (h) gamma counter 48 h after injection. T, tumour; bLN, brachial LN; aLN, axillary LN; Lu, lungs; L, liver; S, spleen; K, kidneys; iLN, iliac LN; sLN, sciatic LN; inLN, inguinal LN; pLN, popliteal LN; injection site (I).

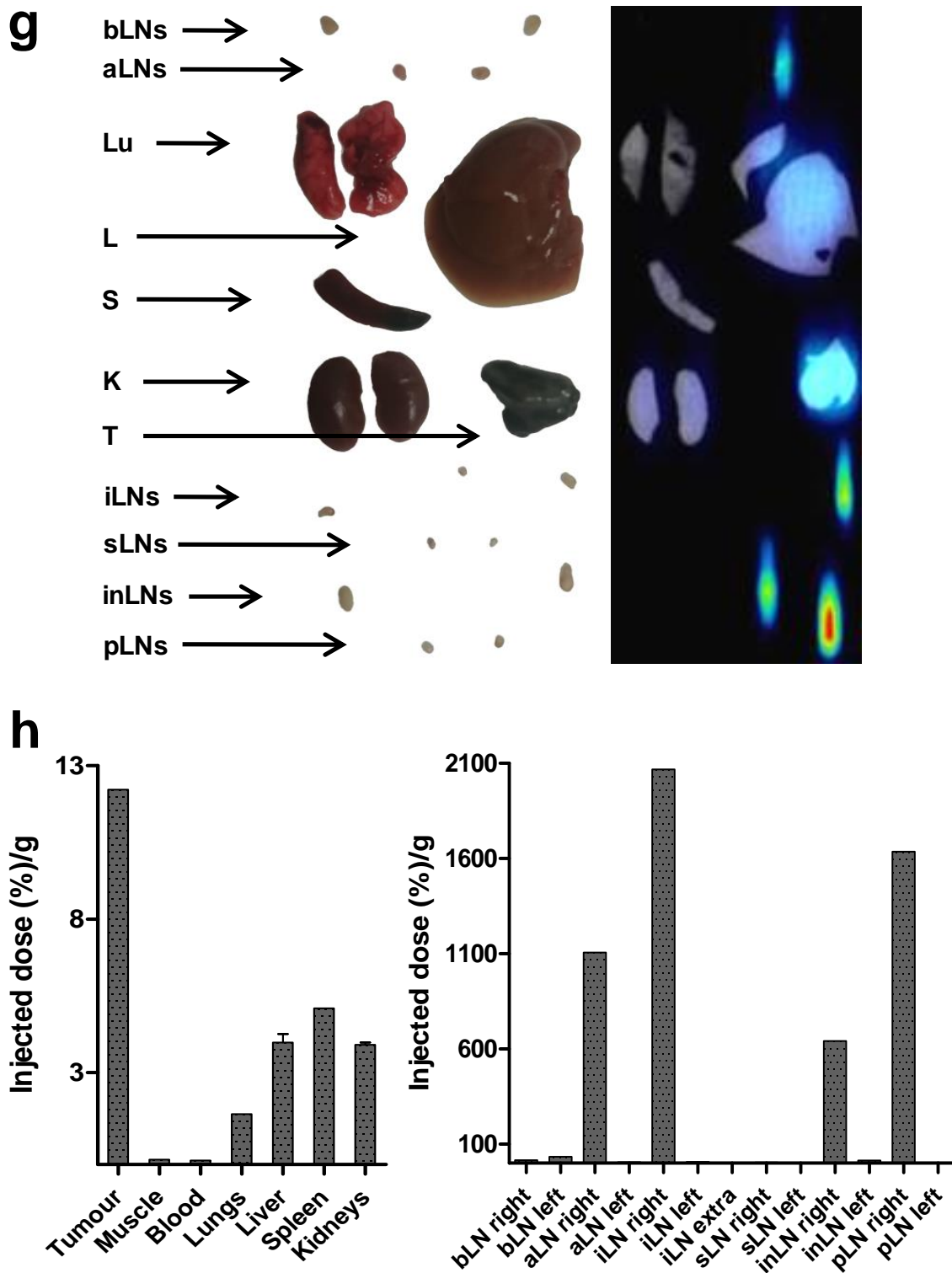


Figure 3.16 (Continued). SPECT/CT images of melanoma tumour bearing mice injected in the hock with ^{67}Ga labelled CpG-IONP micelles (23.2 μg of magnetite, 43.4 MBq) (a, d) 3 h, (b, e) 24 h and (c, f) 48 h post-injection. (a-c) dorsal and (d-f) lateral views of *in vivo* images at different time points are shown. *Ex vivo* analysis by (g) SPECT/CT and (h) gamma counter 48 h after injection. T, tumour; bLN, brachial LN; aLN, axillary LN; Lu, lungs; L, liver; S, spleen; K, kidneys; iLN, iliac LN; sLN, sciatic LN; inLN, inguinal LN; pLN, popliteal LN; injection site (I).

3.3. Conclusions

The easy incorporation of a fluorescent probe during the micelle formation process allowed investigating and demonstrating that these antigen/adjuvant loaded constructs are well-internalized by APCs via the endocytic pathway and that reach their cell compartments and receptors (endosomal TLR 9). *Ex vivo* analysis of the subcutaneously administered CpG- and OVA-IONP micelles showed efficient accumulation of both cargos into DCs, B cells and macrophages.

By a chemistry-free radiolabelling process the micelles incorporated ^{67}Ga , acting as nuclear imaging contrast agents which could be used to study their biodistribution by non-invasive SPECT imaging. These studies showed that the OVA- and CpG ODN-functionalised micelles (and parent 'nude' nanoconstructs) reach the LNs draining the site of injection as well as more distal LNs from different anatomical regions in healthy and tumour bearing mice. Moreover, nanovaccines showed also some accumulation in the B16 melanoma tumour when injected into the ventral flank and into the hock. There was no accumulation of NPs in the liver or in the spleen, which is the main location for most NPs administered intravenously. The found properties of the micelles to target the tumour draining LNs make these platforms promising contrast agents for cancer metastasis studies.

Overall, through multimodal imaging it was possible to study and confirm the ability of these size-selected IONP micelles to provide effective endosomal receptor targeting and excellent lymphatic trafficking of vaccine components to the LNs and tumour, as one of the recently postulated requirements for inducing potent cellular and humoral immune responses.

3.4. Supporting Information of Chapter III

Gating strategy for the *in vitro* uptake analysis of the fluorescently labelled CpG- and OVA-IONP micelles in J774A.1 macrophages and DCs from BMDCs.

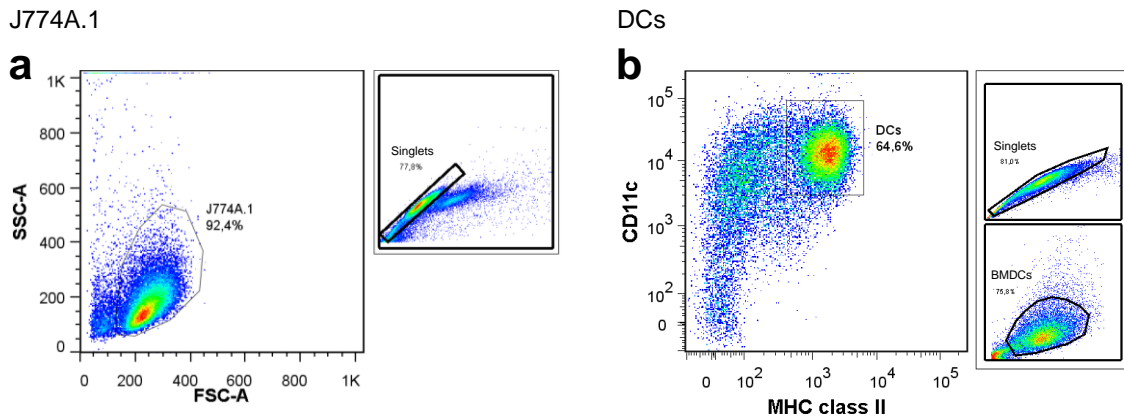


Figure S3.1. Cell gating strategies for the *in vitro* uptake analysis of the fluorescently labelled nanovaccines in immune system cells by flow cytometry. a) J774A.1 macrophages cell line and b) DC gating into BMDCs pool as double positive for CD11c and MHC class II markers.

Gating strategy for the *ex vivo* uptake analysis of the fluorescently labelled CpG- and OVA-IONP micelles in harvested spleens 6 h after injection. CpG and OVA fluorescent signal was analysed in DCs, B cells and macrophages.

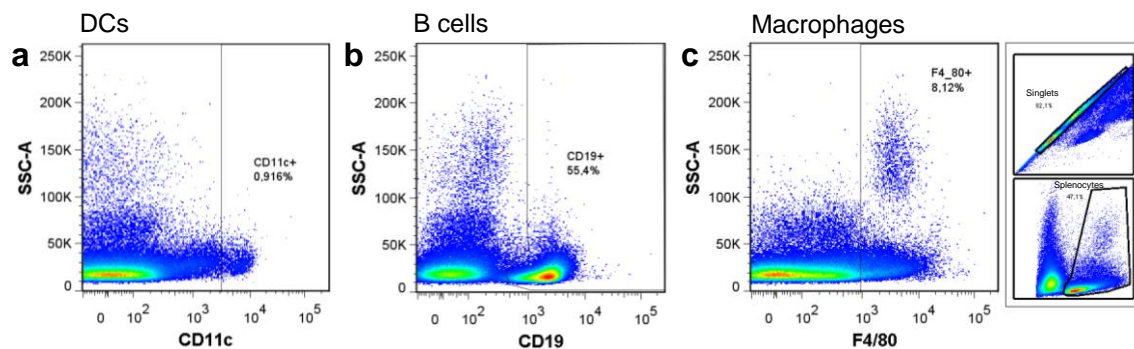


Figure S3.2. Cell gating strategies for the *ex vivo* uptake analysis of the fluorescently labelled nanovaccines in immune system cells by flow cytometry. Alexa647-labelled OVA and FITC-labelled CpG where analysed in a) DC (CD11c⁺), b) B cells (CD19⁺) and c) macrophages (F4/80⁺) present in harvested splenocytes.

Functionalised IONP micelles had very similar biodistribution pattern in tumour bearing mice independently of the loaded cargo.

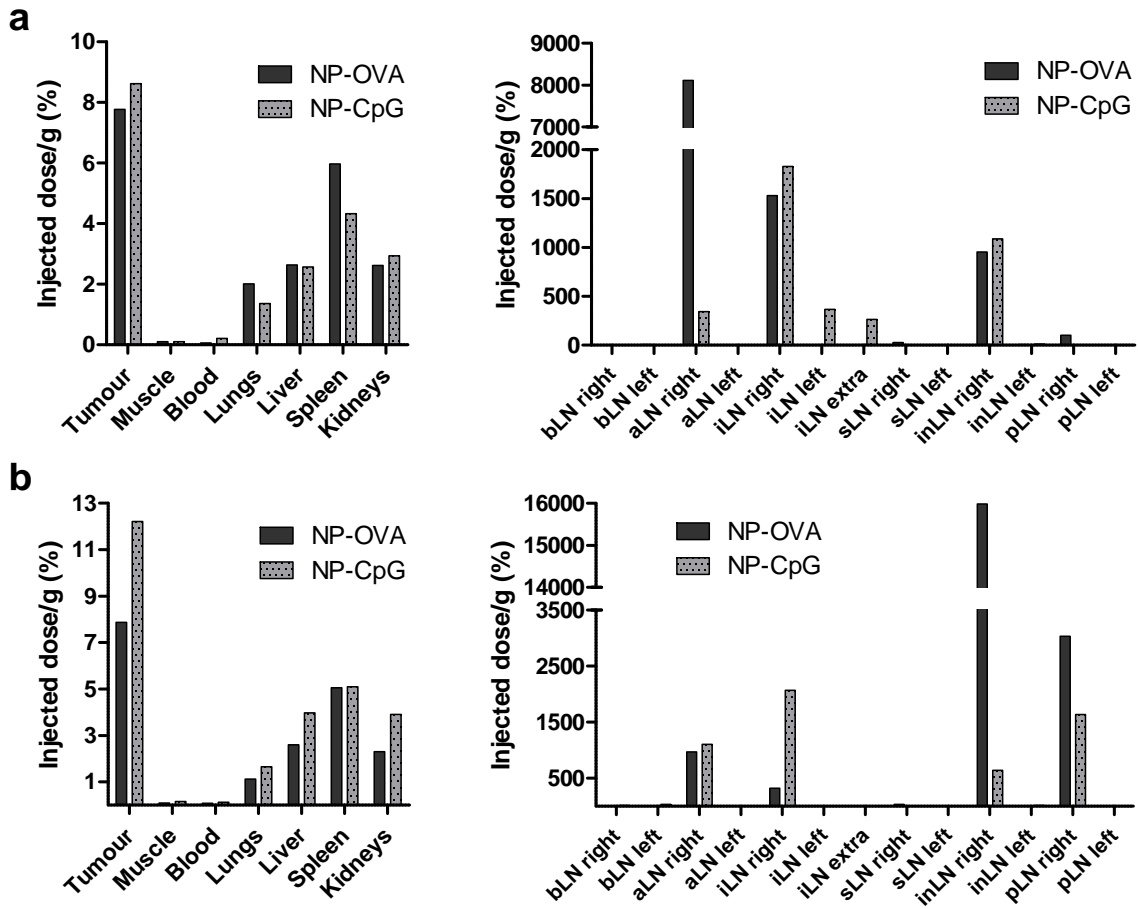


Figure S3.3. Ex vivo analysis by gamma counter 48 h after injection in the (a) flank or (b) hock of melanoma tumour bearing mice. bLN, brachial LN; aLN, axillary LN; iLN, iliac LN; sLN, sciatic LN; inLN, inguinal LN; pLN, popliteal LN.

References

1. Josephson, L., Kircher, M. F., Mahmood, U., Tang, Y. & Weissleder, R. Near-Infrared Fluorescent Nanoparticles as Combined MR/Optical Imaging Probes. *Bioconjug. Chem.* **13**, 554–560 (2002).
2. Kim, T. J., Chae, K. S., Chang, Y. & Lee, G. H. Gadolinium oxide nanoparticles as potential multimodal imaging and therapeutic agents. *Curr. Top. Med. Chem.* **13**, 422–33 (2013).
3. Fay, F. *et al.* Investigating the cellular specificity in tumors of a surface converting nanoparticle by multimodal imaging. *Bioconjug. Chem.* 7b00086 (2017). doi:10.1021/acs.bioconjchem.7b00086
4. Lee, D.-E. *et al.* Multifunctional nanoparticles for multimodal imaging and theragnosis. *Chem. Soc. Rev.* **41**, 2656–2672 (2012).
5. Julian, T. B. MRI: a role in clinical trials. *J. Magn. Reson. Imaging* **13**, 837–841 (2001).
6. Whitwell, J. L. Biomarkers in Randomized Clinical Trials: Magnetic Resonance Imaging. *Front. Neurol. Neurosci.* **39**, 101–108 (2016).
7. Schweiger, C., Gil, P., Parak, W. & Kissel, T. MRI contrast enhancement potential of different superparamagnetic iron oxide nanoparticle (SPION) formulations. *J. Control. Release* **148**, E67–E68 (2010).
8. Lee, J.-H. *et al.* Artificially engineered magnetic nanoparticles for ultra-sensitive molecular imaging. *Nat. Med.* **13**, 95–99 (2006).
9. Xiao, Y.-D. *et al.* MRI contrast agents: Classification and application (Review). *Int. J. Mol. Med.* **38**, 1319–1326 (2016).
10. Contag, C. H. In vivo pathology: seeing with molecular specificity and cellular resolution in the living body. *Annu. Rev. Pathol.* **2**, 277–305 (2007).
11. Chen, D., Monteiro-Riviere, N. A. & Zhang, L. W. Intracellular imaging of quantum dots, gold, and iron oxide nanoparticles with associated endocytic pathways. *Wiley Interdiscip. Rev. Nanomedicine Nanobiotechnology* **9**, (2017).
12. Massoud, T. F. & Gambhir, S. S. Molecular imaging in living subjects: seeing fundamental biological processes in a new light. *Genes Dev.* **17**, 545–580 (2003).
13. Figueiredo, J. L., Alencar, H., Weissleder, R. & Mahmood, U. Near infrared thoracoscopy of tumoral protease activity for improved detection of peripheral lung cancer. *Int. J. Cancer* **118**, 2672–2677 (2006).
14. Alencar, H. *et al.* Colonic adenocarcinomas: near-infrared microcatheter imaging of smart probes for early detection--study in mice. *Radiology* **244**, 232–8 (2007).
15. Jaffer, F. A. *et al.* Real-time catheter molecular sensing of inflammation in

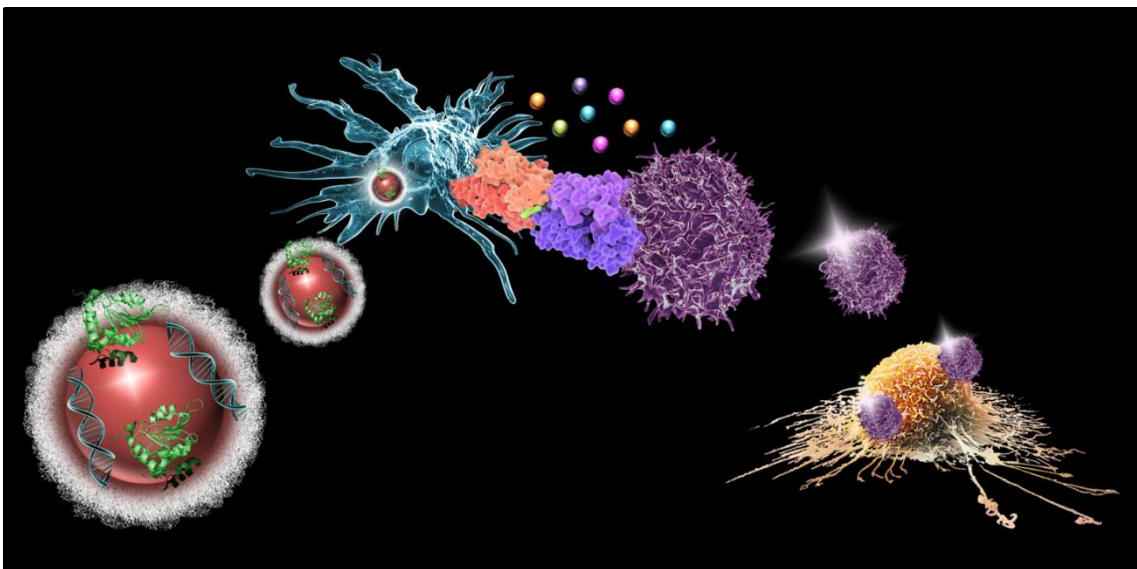
- proteolytically active atherosclerosis. *Circulation* **118**, 1802–1809 (2008).
16. Pierce, M. C., Javier, D. J. & Richards-Kortum, R. Optical contrast agents and imaging systems for detection and diagnosis of cancer. *Int. J. Cancer* **123**, 1979–1990 (2008).
 17. Strauss, L. G. & Conti, P. S. The Applications of PET in Clinical Oncology. *J. Nucl. Med.* **32**, 623–648 (1991).
 18. Cherry, S. R. & Gambhir, S. S. Use of positron emission tomography in animal research. *ILAR J.* **42**, 219–32 (2001).
 19. Luker, G. D. & Piwnica-Worms, D. Molecular Imaging in Vivo with PET and SPECT. *Acad. Radiol.* **8**, 4–14 (2001).
 20. Price, P. PET as a potential tool for imaging molecular mechanisms of oncology in man. *Trends Mol. Med.* **7**, 442–446 (2001).
 21. Chatziioannou, A. F. Molecular imaging of small animals with dedicated PET tomographs. *Eur. J. Nucl. Med.* **29**, 98–114 (2002).
 22. Hawkins, R. A. & Phelps, M. E. PET in clinical oncology. *Cancer Metastasis Rev.* **7**, 119–142 (1988).
 23. Rosenthal, M. S. *et al.* Quantitative SPECT imaging: a review and recommendations by the Focus Committee of the Society of Nuclear Medicine Computer and Instrumentation Council. *J. Nucl. Med.* **36**, 1489–1513 (1995).
 24. Velikyan, I. Prospective of ⁶⁸Ga-radiopharmaceutical development. *Theranostics* **4**, 47–80 (2013).
 25. Conner, S. D. & Schmid, S. L. Regulated portals of entry into the cell. *Nature* **422**, 37–44 (2003).
 26. Kumari, S., Mg, S. & Mayor, S. Endocytosis unplugged: multiple ways to enter the cell. *Cell Res.* **20**, 256–275 (2010).
 27. Jiang, W., Kim, B. Y. S., Rutka, J. T. & Chan, W. C. W. Nanoparticle-mediated cellular response is size-dependent. *Nat. Nanotechnol.* **3**, 145–50 (2008).
 28. Zhang, S., Li, J., Lykotrafitis, G., Bao, G. & Suresh, S. Size-dependent endocytosis of nanoparticles. *Adv. Mater.* **21**, 419–424 (2009).
 29. Champion, J. A. & Mitragotri, S. Role of target geometry in phagocytosis. *Proc. Natl. Acad. Sci. U. S. A.* **103**, 4930–4 (2006).
 30. Gratton, S. E. A. *et al.* The effect of particle design on cellular internalization pathways. *Proc. Natl. Acad. Sci. U. S. A.* **105**, 11613–11618 (2008).
 31. Chou, L. Y. T. *et al.* Strategies for the intracellular delivery of nanoparticles. *Chem. Soc. Rev.* **40**, 233–245 (2011).
 32. Albanese, A., Tang, P. S. & Chan, W. C. W. The effect of nanoparticle size, shape,

- and surface chemistry on biological systems. *Annu. Rev. Biomed. Eng.* **14**, 1–16 (2012).
33. Kou, L., Sun, J., Zhai, Y. & He, Z. The endocytosis and intracellular fate of nanomedicines: Implication for rational design. *Asian J. Pharm. Sci.* **8**, 1–10 (2013).
 34. Gupta, A. K. & Gupta, M. Synthesis and surface engineering of iron oxide nanoparticles for biomedical applications. *Biomaterials* **26**, 3995–4021 (2005).
 35. Gupta, A. K., Naregalkar, R. R., Vaidya, V. D. & Gupta, M. Recent advances on surface engineering of magnetic iron oxide nanoparticles and their biomedical applications. *Nanomedicine* **2**, 23–39 (2007).
 36. Laurent, S. *et al.* Magnetic Iron Oxide Nanoparticles: Synthesis, Stabilization, Vectorization, Physicochemical Characterizations, and Biological Applications. *Chem. Rev.* **108**, 2064–2110 (2008).
 37. Weissleder, R. *et al.* Superparamagnetic iron oxide: pharmacokinetics and toxicity. *Am. J. Roentgenol.* **152**, 167–173 (1989).
 38. Bourrinet, P. *et al.* Preclinical Safety and Pharmacokinetic Profile of Ferumoxtran-10, an Ultrasmall Superparamagnetic Iron Oxide Magnetic Resonance Contrast Agent. *Invest. Radiol.* **41**, 313–324 (2006).
 39. Almeida, J. P. M., Chen, A. L., Foster, A. & Drezek, R. In vivo biodistribution of nanoparticles. *Nanomedicine* **6**, 815–835 (2011).
 40. Rao, D. A., Forrest, L. M., Alani, A. W. G., Know, G. S. & Robinson, J. R. Biodegradable PLGA Based Nanoparticles for Sustained Regional Lymphatic Drug Delivery. *J. Pharm. Sci.* **99**, 2018–2031 (2010).
 41. Li, S.-D. & Huang, L. Pharmacokinetics and Biodistribution of Nanoparticles. *Mol. Pharm.* **5**, 496–504 (2008).
 42. Greish, K. in *Methods in Molecular Biology* **624**, 25–37 (2010).
 43. Maeda, H. Macromolecular therapeutics in cancer treatment: The EPR effect and beyond. *J. Control. Release* **164**, 138–44 (2012).
 44. Reddy, S. T. *et al.* Exploiting lymphatic transport and complement activation in nanoparticle vaccines. *Nat. Biotechnol.* **25**, 1159–64 (2007).
 45. Jewell, C. M., López, S. C. B. & Irvine, D. J. In situ engineering of the lymph node microenvironment via intranodal injection of adjuvant-releasing polymer particles. *Proc. Natl. Acad. Sci. U. S. A.* **108**, 15745–50 (2011).
 46. Xie, Y., Bagby, T. R., Cohen, M. S. & Forrest, M. L. Drug delivery to the lymphatic system: importance in future cancer diagnosis and therapies. *Expert Opin. Drug Deliv.* **6**, 785–92 (2009).
 47. Kerlin, R. & Watson, D. Effect of dextran sulphate on IgG subclass of antibody in

- efferent popliteal lymph of sheep. *Immunol. Cell Biol.* **65**, 411–417 (1987).
48. Kerlin, R. L. & Watson, D. L. The secondary immune response to *Staphylococcus aureus* vaccines in efferent popliteal lymph of sheep. *Immunology* **60**, 295–301 (1987).
 49. Kamala, T. Hock immunization: A humane alternative to mouse footpad injections. *J. Immunol. Methods* **328**, 204–214 (2007).
 50. Harrell, M. I., Iritani, B. M. & Ruddell, A. Lymph Node Mapping in the Mouse. *J. Immunol. Methods* **332**, 170–174 (2008).
 51. Tilney, N. L. Patterns of lymphatic drainage in the adult laboratory rat. *J. Anat.* **109**, 369–383 (1971).
 52. Thomas, S. N., Vokali, E., Lund, A. W., Hubbell, J. a. & Swartz, M. a. Targeting the tumor-draining lymph node with adjuvanted nanoparticles reshapes the anti-tumor immune response. *Biomaterials* **35**, 814–824 (2014).
 53. Overwijk, W. W. & Restifo, N. P. in *Current Protocols in Immunology* 1–33 (John Wiley and Sons: Hoboken, NJ, 2001). doi:10.1002/0471142735.im2001s39.B16

4

Application of the designed IONP-filled micelles as anticancer nanovaccine



4.1. Introduction

4.1.1. Anticancer immunity

Cancer and the immune system have a close relationship since the very beginning of tumour formation. Although the immune system can sometimes spontaneously win the battle, in cases the immunosuppression induced by tumour cells and/or its microenvironment leads to immune system evasion and uncontrolled growth of the abnormal cells. Understanding anticancer immunity is therefore essential in order to design and develop effective cancer immunotherapies by immunoengineering (**Figure 4.1**).

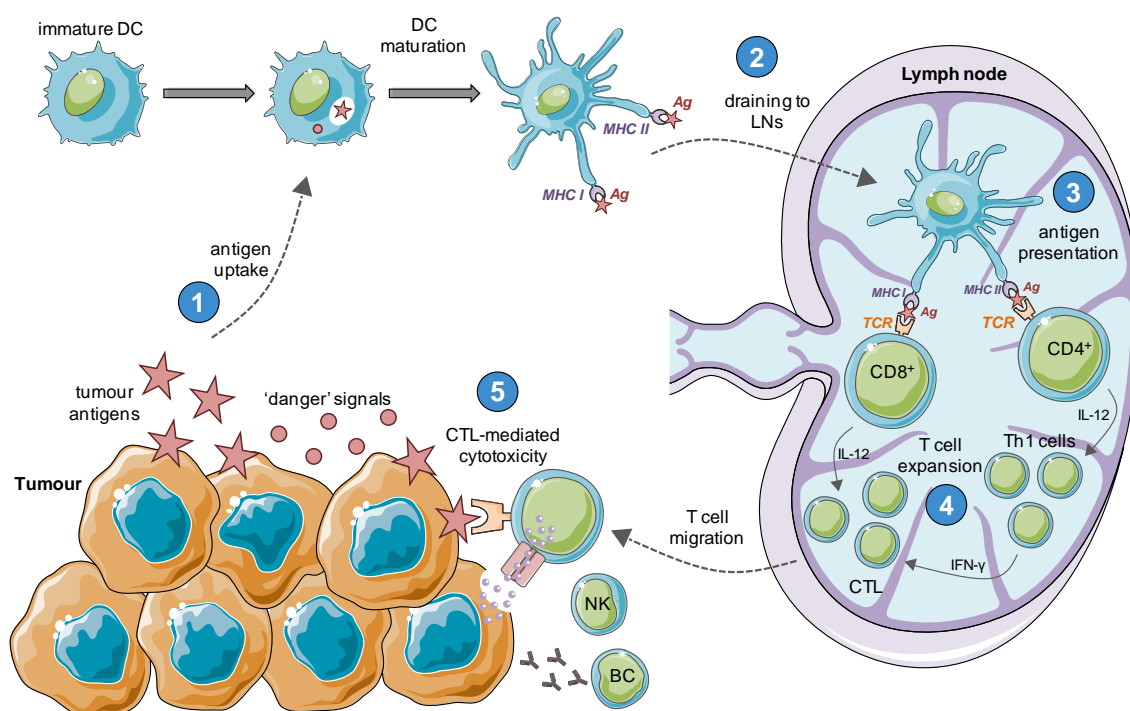


Figure 4.1. Representation of immune responses against tumour. Different steps are required for inducing an optimal anticancer immunity. Firstly, DCs must mature by taking up tumour antigens in combination with immunostimulatory 'danger' signals (1). Effective draining to LNs (2) is crucial in order to present tumour antigens to T cells (3). After interacting with tumour antigen with TCR, T cells must expand and differentiate towards Th1-type CD4⁺ cells and CD8⁺ CTLs (4). Finally, CTL are in charge of migrating and infiltrating into tumour tissue and mediate specific cytotoxicity (5). NKs and B lymphocytes will also play a role in the overall tumour killing process. Figure adapted from *Nat. Rev. Clin. Oncol.*, 2014, **11**, 509.¹

As in the case of an infection, antigens derived from tumour cells are taken up by APCs such as DCs and processed either in MHC class I or class II receptors. To achieve proper activation, i.e., maturation of DCs, additional 'danger' signals must reach the same cell

subset that has 'seen' the tumour antigen. Naturally, this can occur due to the inflammation niche that malignant tissue can induce, where diverse types of activation signals can be found.^{2,3}

APCs will encounter naive T cells within the LN and, through TCR-MHC class I/II interaction, T cells will be able to mature and proliferate into tumour antigen-specific cells. The CD8⁺ T cell subset will be in charge of developing cytotoxic capacity, abandoning the LN and specifically recognising and killing tumour cells. The differentiation of CD4⁺ T cells towards the Th1-type phenotype will be necessary in order to support the activity of CTLs. Moreover, mature DCs may also induce the natural killer (NK) cell responses. These cells of the innate immune system have the ability to 'naturally' react against tumour cells presenting TAAs or neoantigens on their surfaces.

Although the main required immune response against tumour cells is based on CTLs, an antibody response to the target tumour antigen can also have an important role in the overall antitumour immune response. CD4⁺ T helper cells can modulate the type of antibodies that are produced by B lymphocytes. Among the IgG antibody isotype, Th1-type cells enhance the production of the IgG2a type, whereas a Th2-type response is dominated by IgG1 antibodies.

Overall, inducing, modulating and enhancing antitumour immunity is a multistep challenge and has no straightforward solution. These benefits and contributions that NPs can provide in some anticancer immunotherapy approaches are briefly reviewed in next section.

4.1.2. Challenges for enhancing antitumour immunity using NPs

The knowledge about antitumour immunity that has been compiled over the last few decades allows now a more rational design of NP formulations aimed at enhancing antitumour immunity. Several key points of tumour immunity can be tailored and optimised using NPs.

a) Antigen uptake and processing:

Apart from virus-induced cancers that can be more immunoreactive, tumour cells are poorly immunogenic and therefore, APCs exposed to their antigens are not able to fully mature and prime T cells. The situation is worse in the absence of an extra activation signal. NPs have shown great success in this key aspect. By loading full-length TAAs or small peptides, NPs can direct their cargo to APCs and enhance the uptake of the antigen.⁴⁻⁶ For instance, liposomes can induce a depot effect prolonging the presence of the antigen in the injection site, favouring the gradual release of the antigenic moiety and the extended exposure of the antigen to the immune cells (reviewed by Henriksen-Lacey et al).⁷ In contrast, other types of NPs can directly interact with DCs and deliver the antigen via the endocytic pathway.^{8,9}

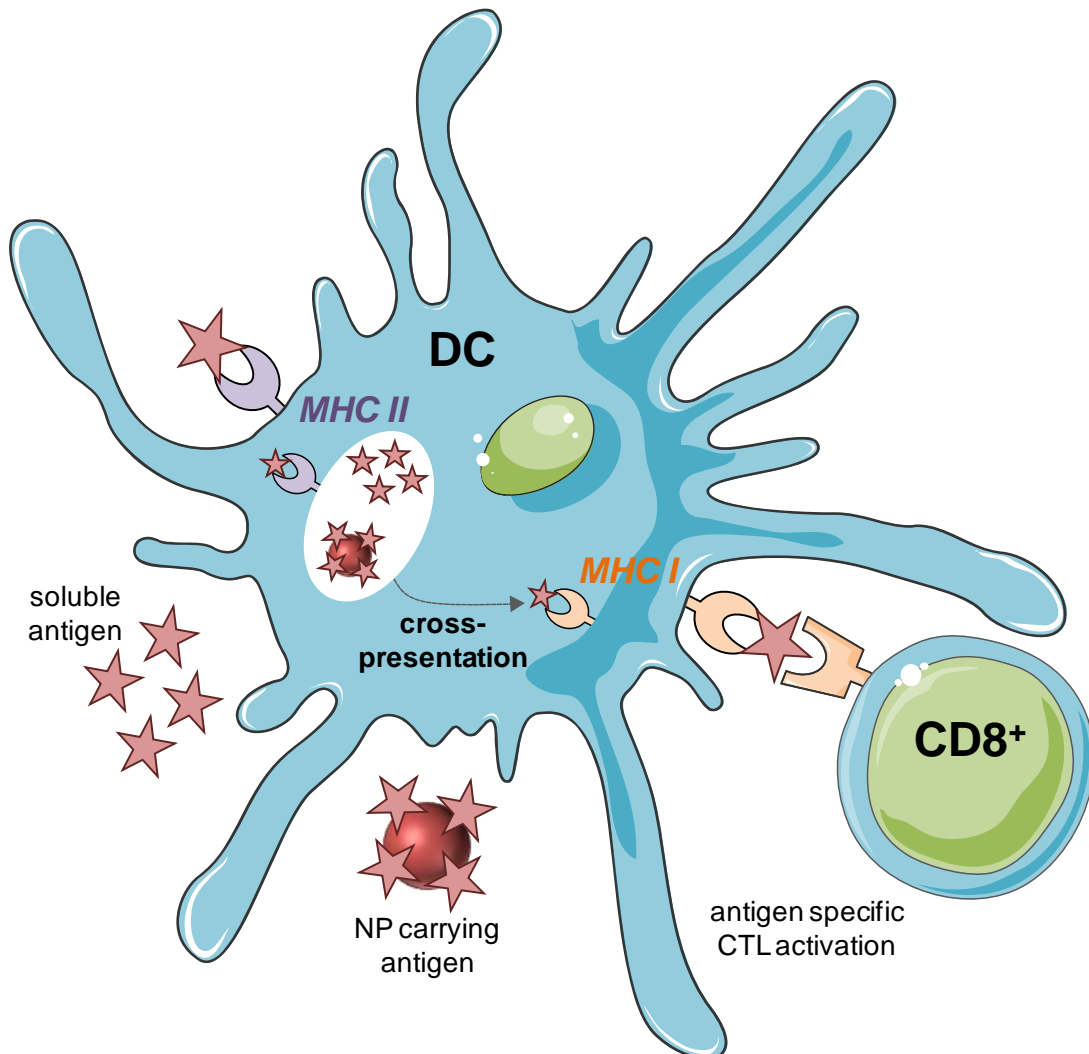


Figure 4.2. Antigen presentation by DCs can be enhanced loading the antigen into NPs. NPs can increase the antigen cross-presentation rate by promoting endosomal escape and MHC class I presentation towards CD8⁺ T cells.

One of the most important processes in generating a potent antitumour response is related to the way by which the antigen is presented to T cells by DCs. To achieve a potent cell-mediated immune response, tumour antigens must undergo a process called cross-presentation, where extracellularly taken up antigens are translocated from the endocytic pathway (presentation by MHC class II) to the intracellular antigen pathway (presentation by MHC class I). Unfortunately, most canonical vaccines have succeeded in promoting the presentation of the antigen by MHC class II molecules, inducing a Th2-type immunity and antibody production. Moreover, the injection of soluble antigens alone does not induce potent tumour cell killing activity. It has been reported that loading the antigen into NPs enhances the phagocytosis and the cross-presentation from MHC class II towards class I receptor, which will allow the activation of antigen-specific CD8⁺ T cells (**Figure 4.2**).¹⁰⁻¹²

Apart from the cellular immune response, B lymphocytes proliferation and the subsequent antibody production can be also enhanced by loading the antigenic molecules into NPs. It has been shown that NPs can increase the total levels of IgG2 against the loaded antigen. This enhanced production may be mediated by direct activation of B cells or by the indirect action of CTLs and CD4⁺ Th1-type cells. Both types of T lymphocytes can produce IFN- γ , which is a cytokine known to direct class switching to IgG2 (IgG2a, IgG2b and IgG2c).^{13,14}

b) Delivery of activation signal:

NPs themselves can act as adjuvant moieties depending on their composition. Liposomes are one of the best examples, since their lipid membranes can mimic cell envelopes of pathogens.¹⁵ NPs can also be loaded with adjuvant molecules. Antigen/adjuvant administration in the same NPs seems an ideal option, since the presentation of antigen in DCs that have not received a 'danger' signal by an adjuvant induces the activation of regulatory T cells that promote immunosuppressive function.¹⁶⁻¹⁸ However, co-loading of antigen/adjuvant in the same NP may not be necessary to achieve co-delivery to the same cell if other targeting strategies are adopted, which is a considerable formulation advantage. One strategy is to exploit NPs

of the same size for controlling the co-delivery of both types of immunostimulatory molecules in separate formulations.¹⁹

The adjuvant action needed for an optimal antitumour effect must include the maturation of DCs with a cytokine pattern able to induce Th1-type cells, such as the production of IL-12 or TNF- α cytokines. The loading of adjuvants into NPs can potentially enhance the pattern and magnitude of cytokine production by DCs, leading to a more potent antitumour response. The overall adjuvant action enhancement can also be facilitated by NP-mediated delivery to LNs, protection against rapid clearance and/or avoiding the fast degradation of the adjuvant molecules before reaching the target receptors.²⁰⁻²³

c) Lymphatic draining:

Even if the successful maturation of DCs in the tumour microenvironment or around the injection site is achieved, an antitumour response will be only induced if they reach SLOs to encounter T cells. Many vaccine strategies have failed in delivering antigen/adjuvant with the desired tissue specificity. This is because most canonical vaccines, such as those based in liposomes or microparticles, are focused on interacting with APC at the injection site, where antigen is transported to LNs once processed and presented by DCs.²⁴⁻²⁶ A problem of such an approach is that at the injection site DCs are at lower concentrations compared to other types of phagocytic cells (e.g. macrophages), making less probable antigen uptake by DCs (i.e. the need for adding DC specific targeting ligands to ensure the delivery).²⁷⁻²⁹ In contrast, LNs resident DCs are much more abundant and, therefore, antigen-loaded NPs that can reach LNs have increased chance to encounter and be processed by DCs. Apart from the DCs availability, another issue to take into account is the premature presentation of antigen. When antigen is delivered to peripheral DCs, it is *in situ* processed and presented in MHC receptors before reaching LNs, which can lead to antigen tolerance.³⁰⁻³³ Hence, it is crucial to design vaccine formulations taking into account the different cell phenotypes and concentrations that is mostly dependent on DCs location.³⁴⁻³⁷

Several strategies have been decisive to ensure antigen delivery directly to LN-resident DCs, such as active targeting of NPs to LN homing receptors. However, the simplest way is designing formulations that are able to self-drain to lymphatic vessels after subcutaneous administration.^{39,40} Thus, some studies have shown that large particles (>200 nm) are retained at the injection site and small NPs (*ca.* 40 nm) are more efficient for lymphatic uptake and retention in draining LNs (**Figure 4.3**).^{41–45}

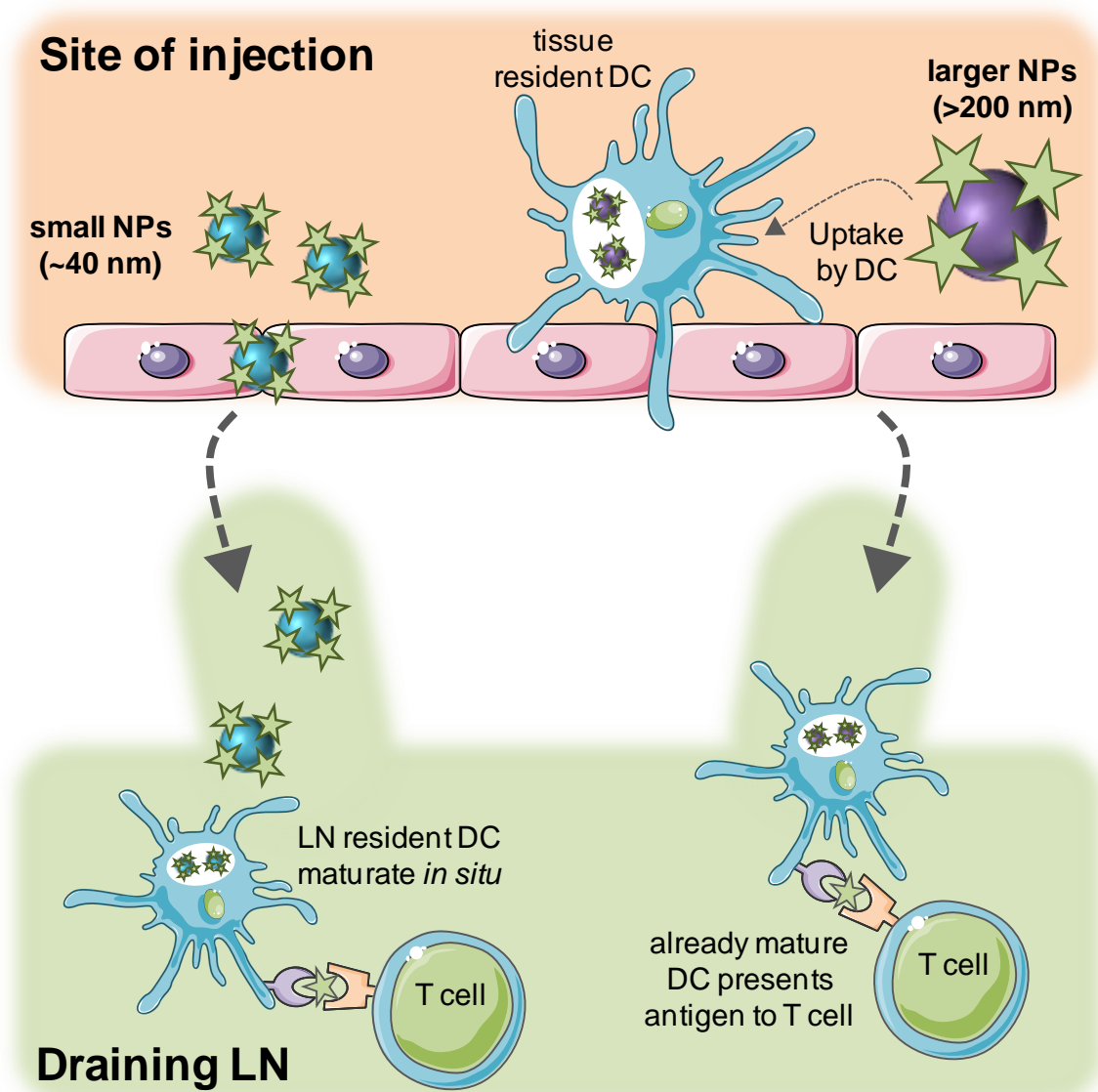


Figure 4.3. Antigen uptake by tissue resident- or LN resident-DC. Large NPs (>200 nm) deliver the antigen to peripheral DC, inducing the DC maturation in the site of injection. In contrast, small NPs (*ca.* 40 nm) can self-drain to SLOs and target LN resident DCs, avoiding antigen tolerance. Adapted from *Trends Immunol.*, 2006, **27**, 573.³⁸

4.2. Results and discussion

The designed nanoconstructs have been successfully characterised and their cellular fate and biodistribution investigated both *in vitro* and *in vivo* by diverse imaging techniques. Here, the ability of both CpG- and OVA-IONP micelles to induce a potent antitumour immune response is studied. This chapter has been divided into three main parts: 1) the study of the immune response using the CpG-IONP micelles acting as adjuvant and compared to free CpG ODNs molecules, both *in vitro* and *in vivo*; 2) the analysis of the immune response in mice (including humoral and cellular responses) when combining CpG- and OVA-functionalised IONP micelles; and 3) the application of both nanoconstructs as anticancer vaccine in an *in vivo* model of melanoma.

4.2.1. *In vitro* and *in vivo* immunostimulatory activity of the CpG-IONP micelles

First, the immunostimulatory activity and cytotoxicity of CpG-IONP micelles was tested *in vitro*. J774A.1 macrophage cell line and BMDCs were incubated for 24 h with the adjuvant carrying IONP micelles and selected pro-inflammatory cytokines secretion and cytotoxicity were analysed. As seen in **Figure 4.4**, the CpG-IONP micelles produced dose dependent activation of these cells. It was clearly noticeable that IL-6 and TNF- α production in J774A.1 macrophages treated with the CpG-IONP micelles was much higher than in cells treated with free CpG without NP-induced cytotoxic effects (Figure 4.4a, b and e). Similarly, CpG-IONP micelles provide significantly enhanced production of IL-6, TNF- α and IL-12 in BMDCs without any noticeable cytotoxicity due to the IONP micelle delivery vehicle (Figure 4.4c, d, f and Supporting Information, Figure S4.1). In both cases, commercial J774A.1 macrophage cell line and the primary culture of BMDCs, the maximum CpG ODN amount tested (12 $\mu\text{g}/\text{mL}$) was not able to match the cytokine secretion levels observed when loading small quantities of this adjuvant into the IONP micelles (Figure 4.4a-d and Supporting Information, Figures S4.1 and S4.2). Since the vehicle alone (IONP-DOTAP micelles) did not induce cytokine production, it is possible to assume that the seen increased effect is specifically due to the loaded

adjuvant, presumably because of the enhanced delivery to intracellular specific receptor TLR 9 when loading into IONP micelles.

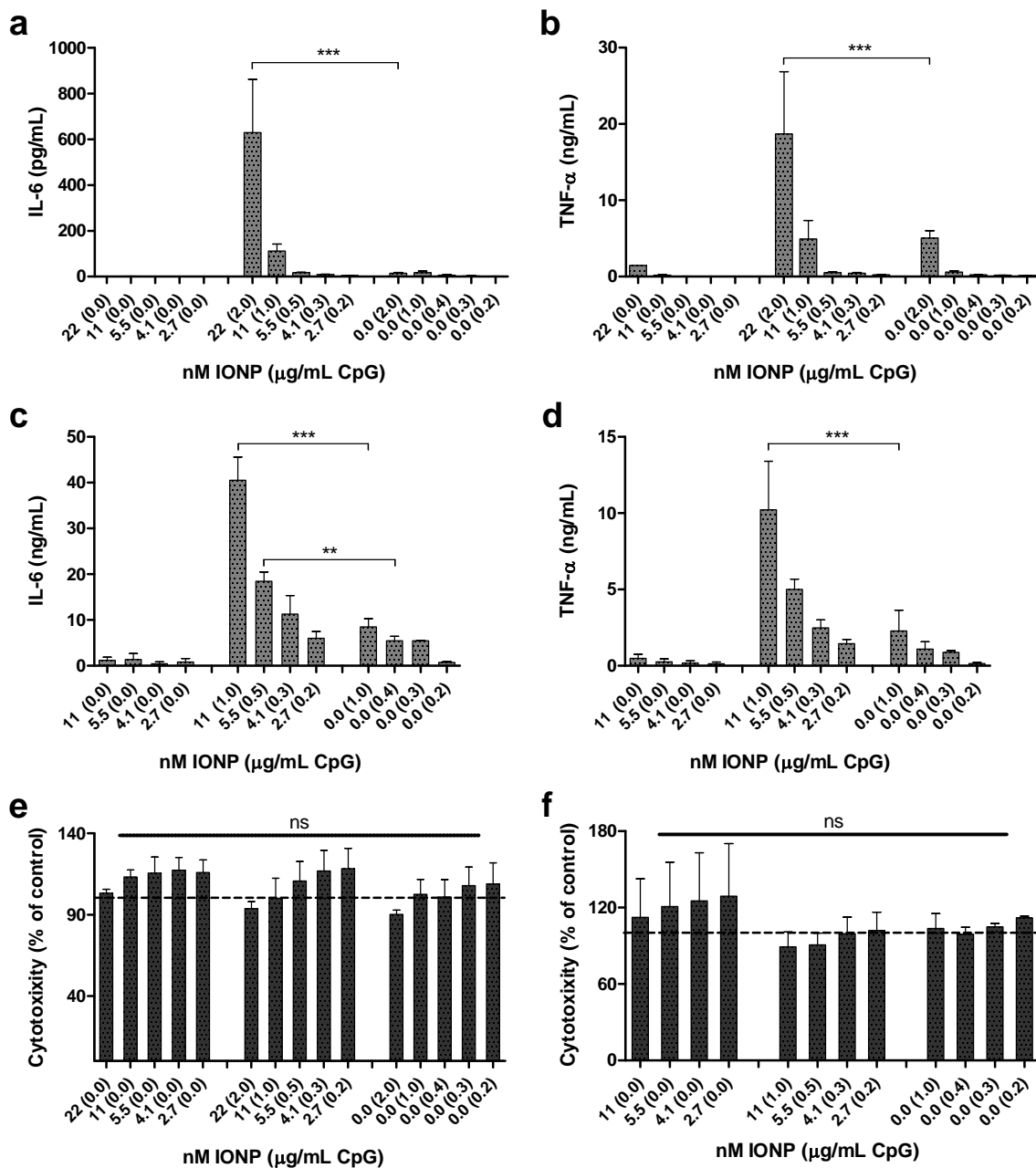


Figure 4.4. Immunostimulatory activity of CpG-IONP micelles *in vitro*. (a) IL-6 and (b) TNF- α production in J774A.1 macrophages and (c) IL-6 and (d) TNF- α cytokine production in BMDCs incubated for 24 h with IONP-filled micelles, CpG-IONP micelles or free CpG ODN. Cytotoxicity analysis of different concentrations of IONP-filled micelles, CpG-IONP micelles or free CpG ODN in (e) J774A.1 macrophages and (f) BMDCs, after 24 h incubation. Data are presented as mean \pm SEM of at least three independent experiments. **P < 0.01, ***P < 0.001, ns = non-significant by two-way ANOVA followed by Bonferroni's test.

In the specific case of DCs apart from cytokine production several other features, including their maturation status and migratory potential, have been shown to be

important for induction of effective immune responses against bacteria, viruses and malignant cells.^{46,47} The maturation status of CD11c⁺ DCs after incubation of BMDCs with the adjuvant carrying formulation, as assessed by increased surface expression of CD80 and CD86, was determined by flow cytometry. Results showed some increased expression of both activation markers on BMDCs after 24 h incubation with free CpG ODN. However, the expression of CD80 and CD86 was clearly enhanced in the presence of the CpG-IONP micelles (**Figure 4.5a, b**). In contrast, the levels remained the same as for the unstimulated control when the BMDCs were incubated with the CpG ODN-free IONP micelles. For effective induction of antitumour CTL-based responses, mature DCs must gain mobility and LN homing ability, which correlates with an increased expression of the chemokine receptor CCR7.⁴⁸ Flow cytometry studies showed significantly enhanced expression of CCR7 in BMDCs incubated with CpG-IONP micelles compared to free adjuvant (Figure 4.5c). CpG ODNs are also known to up-regulate MHC class II molecules in the surface of DCs *in vitro*.⁴⁹ However, the MHC class II molecules expression on the cell surface was slightly increased but not significantly changed after stimulation with both CpG-IONP micelles and free CpG ODNs (Figure 4.5d). The ratio between the percentage of mature DCs (CD11c⁺, MHC class II^{high}) and immature DCs (CD11c⁺, MHC class II^{low-intermediate}), which can be also affected by TLR agonists, did not significantly change (Supporting Information, Figure S4.3).

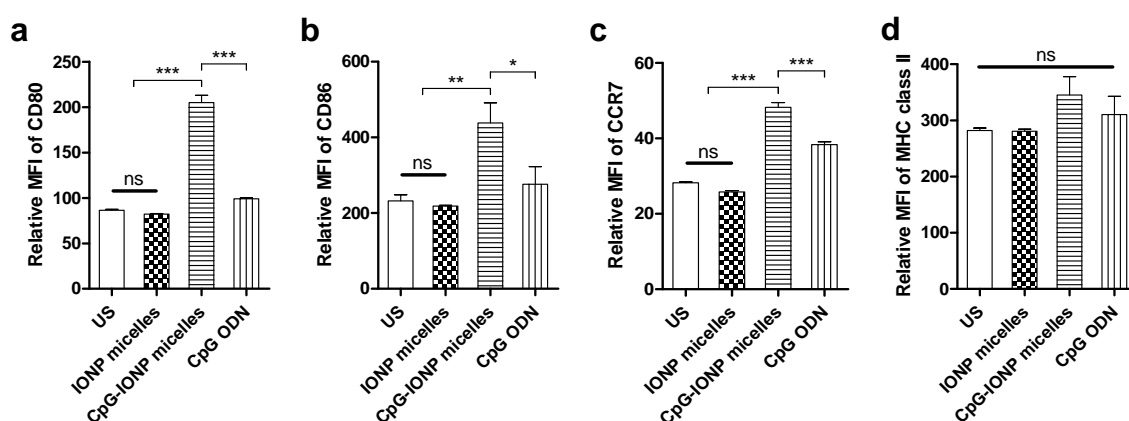


Figure 4.5. Immunologic maturation of DCs derived from BMDCs after incubation with CpG-IONP micelles *in vitro*. (a) CD80, (b) CD86, (c) CCR7 and (d) MHC class II MFI of CD11c⁺ unstimulated BMDCs and BMDCs incubated for 24 h with control IONP micelles, CpG-IONP micelles and CpG ODN; 2.7 nM of IONP micelles and 0.2 µg/mL of CpG ODN. Data are presented as mean ± SEM of at least three independent experiments. *P < 0.05, **P < 0.01, ***P < 0.001, ns = non-significant by one-way ANOVA followed by Tukey's test.

Systemic application of viral nucleic acids leads to an unspecific, generalized activation of the immune system that may be deleterious. One of the potential advantages of using NPs as delivery vehicle is to abolish systemic release of pro-inflammatory cytokines while providing strong immunostimulatory capacity at target organs such as the spleen and LNs. To examine the extent to which the systemic inflammatory response to CpG ODNs can be modulated by NP delivery, mice were subcutaneously injected in the forearm with 3 μg of CpG ODNs free and complexed to the IONP-DOTAP micelles (containing 38 μg of magnetite) and with PBS as control. Then, IL-6 levels were measured in blood serum of the injected mice at different time intervals. As expected, free CpG strongly increased serum levels of IL-6 already at 4 h post-injection. Notably, no increase in serum IL-6 levels was observed in mice injected with the CpG-IONP micelles compared to mice treated with PBS (Figure 4.6a).

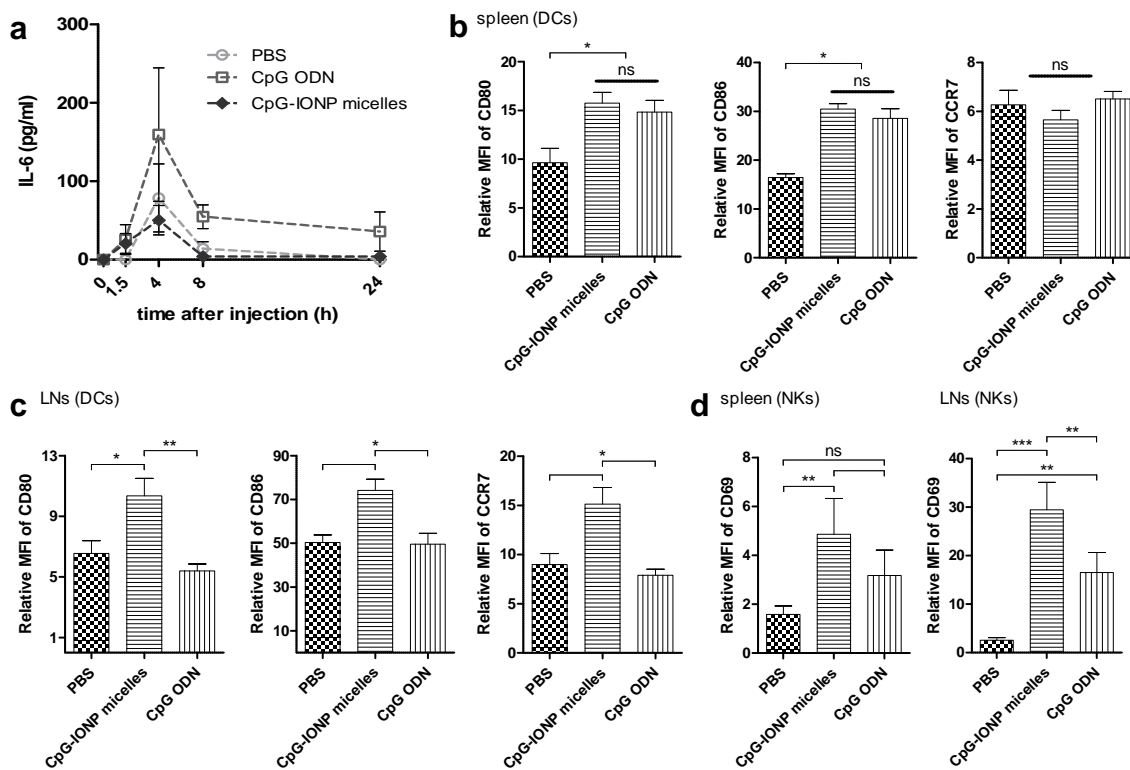


Figure 4.6. Comparison of the innate immune responses to CpG ODN and CpG-IONP micelles. C57BL/6 mice were subcutaneously injected in the forearm with 3 μg of CpG ODNs, free or in conjugation with the IONP-DOTAP micelles (containing 38 μg of magnetite). (a) Pro-inflammatory IL-6 cytokine production in blood serum, pre-injection and at several post-injection time points. (b–d) Representative CD80, CD86 and CCR7 MFI of CD11c⁺ positive DCs and of CD69 in NK cells (CD3⁻CD335⁺) extracted from spleen and from axillary LNs of mice 24 h after they were injected in the forearm with PBS, CpG-IONP micelles and CpG ODN. Data are presented as mean \pm SEM of 5 mice per group. *P < 0.05, **P < 0.01, ***P < 0.001, ns = non-significant by one-way ANOVA followed by Tukey's test.

To investigate the targeted effects in the spleen and LNs, the axillary LNs draining the injection site and spleen were harvested and the maturation status of the extracted cells (CD11c⁺ positive DCs and CD3⁻ CD335⁺ NKs) was analysed by flow cytometry comparing the expression levels of CD80, CD86 and CCR7 in DCs and of CD69 in NK cells. The results showed that the CpG-IONP micelles are as effective or more than free CpG ODNs at promoting maturation of these immune cells in the target SLOs (Figure 4.6b-d). In particular, it was observed a clear enhancement in the activation and maturation of immune cells present in the LNs, greater than in the spleen. This result can be explained by the preferential accumulation of IONP micelles in the draining LNs, as seen in the SPECT/CT nuclear imaging experiments (Chapter III). This enhanced local activation of DCs present in the LNs makes these vehicles optimal to act as vaccines, since it is known that the DC population in LNs is more complex than that in spleen and includes a subset that express DEC-205, a cell surface receptor for CpG ODNs that enhances antigen cross-presentation.^{28,50,51} Moreover, activated NKs are known to be recruited to LNs by DCs⁵² and play a role in the interaction between DCs and T lymphocytes inside the LNs.^{53,54}

Taken together, these results clearly demonstrate the efficacy of these IONP-based nanovehicles to successfully transport the adjuvant to the target receptor and tissue and therefore, the enhancement of the immunostimulatory activity of the CpG ODNs both *in vitro* and *in vivo*.

4.2.2. *In vivo* immunization studies with CpG- and OVA-IONP micelles

Once the innate immune response was studied using the CpG-IONP micelles, the next step was to analyse the ability of IONP micelles to carry and protect a protein antigen such as OVA and therefore, to induce antigen-specific adaptive immune responses. For this, BALB/c mice were immunized twice (2 weeks between both injections) with 5 µg of OVA free or as OVA-IONP micelles (containing *ca.* 53 µg of magnetite) by subcutaneous injection and antibody production against the injected protein was analysed in blood serum.

As mentioned, in response to antigens CD4⁺ Th lymphocytes can differentiate towards two main functional patterns: the Th1 subset, which participate in cell-mediated immune responses; and Th2 subset, which induces B cells to secrete antibodies. In the absence of 'danger' signal immunization with free antigens is known to induce a Th2-type response.⁵⁵ Hence, BALB/c mice were chosen for this first experiment, as it is the prototypical Th2-type mouse strain. Two of the subcutaneous routes explored by SPECT-CT imaging were employed in this antibody production analysis experiment: injection in the abdominal region, the so-called flank, or in the inner side of the front forearms of the animals. During 52 days after the first immunization with OVA free or in conjugation with the IONP micelles, blood samples were taken every 2 weeks and analysed for different IgG antibody isotypes. Induction of high IgG1 titers is associated with Th2-type response, while increased IgG2a titers is considered indicative of a Th1-type immune response.^{56–58}

Results in **Figure 4.7** show that the OVA-specific antibody responses obtained with OVA alone were as expected dominated by IgG1 isotype, and the animals did not produce IgG2a antibodies irrespective of the site of injection. The cytokine pattern induced by Th2-type cells preferentially induces switching to IgG1 subclass, which is mainly induced in the presence of soluble protein antigens.⁵⁹ IgG1 isotype plays an important role in several immune-protective functions, for instance in the complement system.⁶⁰

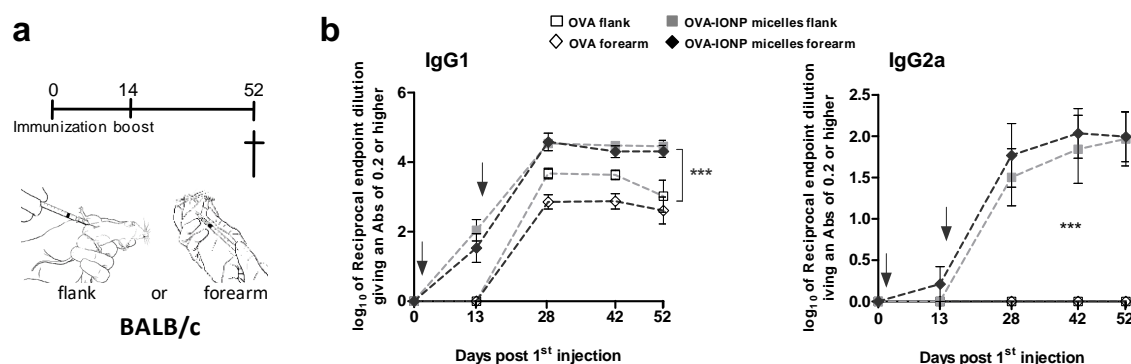


Figure 4.7. Conjugation of OVA to IONP-filled micelles enhanced OVA-specific antibody responses. (a) Immunization schedule. Five μg OVA free or in conjugation with the IONP micelles (*ca.* 53 μg of magnetite) were injected in BALB/c mice on day 0 and 14, subcutaneously in the flanks or in the forearms. Mice were sacrificed on day 52 and (b) anti-OVA IgG1 and IgG2a production was analysed in blood serum at different time points after first injection. Arrows represent the two immunizations. Data are presented as mean \pm SEM of 9 mice per group. *** $P < 0.001$ by two-way ANOVA followed by Bonferroni's test.

However, a more balanced Th1/Th2 response is wanted in order to induce a complete immunity protection, where other types of immune responses will be predominant, such as cellular cytotoxicity. It is described that the production of IgG2a antibody isotype is induced by and can protect against polysaccharide encapsulated pathogens.⁶¹ Moreover, IgG2a is considered to be more protective because of its greater capacity to fix complement than IgG1, and to induce ADCC by macrophages and NKs.^{62,63} Thus, a desired characteristic for a vaccine able to promote Th1-type response is the induction of IgG2a subclass.

Immunization with the OVA-IONP micelles resulted in significantly enhanced IgG1 and IgG2a OVA-specific antibody responses, greatly enhancing the Th1-type response in comparison to OVA antigen free, which was not able of inducing IgG2a subclass antibodies (Figure 4.7b).

IgG2a antibody secretion is known to be stimulated by Th1-type cytokines such as IFN- γ .^{64,65} Hence, 52 days after the first immunization, we explored the capability of cells derived from harvested spleens to produce IFN- γ , after their *ex vivo* restimulation with OVA free or in combination with the IONP-filled micelles (**Figure 4.8a**).

The immunizations and *ex vivo* restimulation of immune cells with free antigen are known to be very ineffective⁶⁶ and for accomplishing complete immune-protection a co-administration of a carrier or an adjuvant is needed.^{67,68} In agreement with that, it was observed an enhanced IFN- γ production by splenocytes in mice previously immunized with the OVA-IONP micelles compared with free OVA (Figure 4.8b). Next, the ability of IONP micelles to *ex vivo* present the antigen in an enhanced manner to splenocytes derived from already immunized mice was analysed. As shown in Figure 4.8c, OVA-IONP micelles were much more efficient in *ex vivo* restimulating splenocytes compared to OVA free antigen. The increased secretion of Th1-type cytokine IFN- γ was found to be OVA specific, since the parent IONP-COOH micelles did not show unspecific IFN- γ production in the absence of bound antigen (Supporting Information, Figure S4.5). Therefore, the IONP micelles seem to either *ex vivo* present and direct the antigen in a more efficient way or allow reaching greater amount of antigen to the cells, or promoting both processes at the same time.

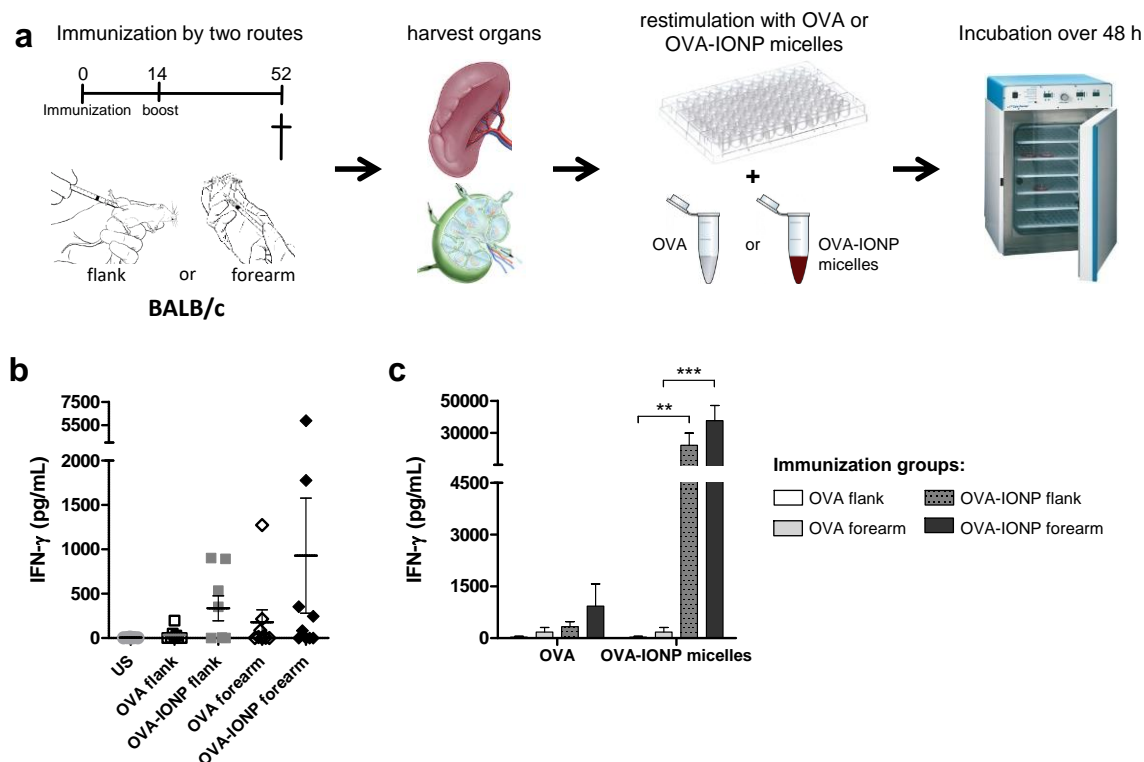


Figure 4.8. (a) Immunization schedule and scheme of *ex vivo* stimulation. Five μg OVA free or in conjugation with the IONP micelles (*ca.* 53 μg of magnetite) were injected in BALB/c mice on day 0 and 14, subcutaneously in the forearms or in the flanks. Mice were sacrificed on day 52 and splenocytes were harvested for further analysis. (b) INF- γ production of unstimulated (US) splenocytes or after stimulation in the presence of 10 $\mu\text{g}/\text{mL}$ OVA protein over two days. (c) Comparison between stimulating cells with free OVA or in conjugation with IONP micelles (10 $\mu\text{g}/\text{mL}$ OVA) over 48 h. Data are presented as mean \pm SEM of 9 mice per group. ** $P < 0.01$, *** $P < 0.001$ by two-way ANOVA followed by Bonferroni's test.

Taken together these results confirmed the good capacity of the IONP micelles for improving adaptive immune responses against the antigen they are carrying. So far, IONP micelles showed promising *in vivo* application as adjuvant/antigen delivery systems. The next step was to combine both types of NPs and analyse their capacity to act as a complete anticancer vaccine.

Adjuvants accepted for human use such as alum lack the capacity to generate cell-mediated Th1-type immune responses. However, there are a number of diseases, such as cancer and those caused by intracellular pathogens (e.g., HIV and malaria), for which there are no effective prophylactic or therapeutic vaccines and require vaccine formulations that promote a more Th1-type response as opposed to only Th2-type responses. Therefore, experiments were conducted to explore whether these new nanovaccines are strong inducers of Th1-type responses.

Adaptive immune responses were evaluated by comparing administration of OVA + CpG ODNs *versus* OVA-IONP + CpG-IONP micelles. For comparison, mice were also immunized with OVA adsorbed to alum, which is the most commonly used adjuvant in both human and veterinary vaccines. In contrast to the previous experiments, C57BL/6 mice were chosen for these experiments, as this is the prototypical Th1-type mouse strain. Thus, five μg of OVA free or as OVA-IONP micelles alone or combined with only 5 μg of free CpG ODNs or delivered by IONP micelles were administered twice (2 weeks between immunizations) by subcutaneous injection in the flanks (with total amount of injected magnetite carrier *ca.* 7 μg) and an extensive analysis of the adaptive immune response was conducted.

First, anti-OVA antibody production in blood serum was analysed 35 days after the first immunization (Figure 4.9a).

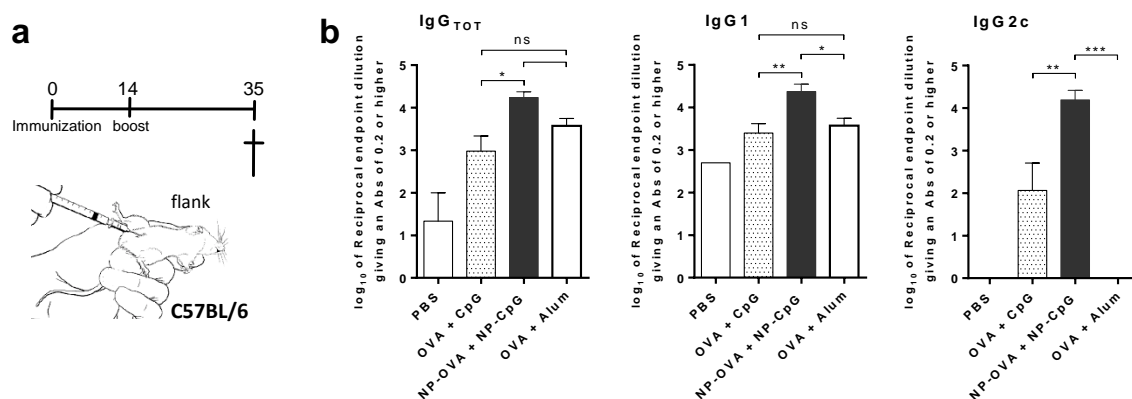


Figure 4.9. Combination of OVA and CpG ODNs to IONP-filled micelles enhanced OVA-specific antibody responses. (a) Immunization schedule. Five μg OVA and CpG ODN free or in conjugation with the IONP micelles (*ca.* 7 μg of magnetite) were injected in C57BL/6 mice on day 0 and 14, subcutaneously in the flanks. OVA-Alum mixture was included for comparison. (b) Mice were sacrificed on day 35 and total anti-OVA, anti-OVA IgG1 and IgG2c antibody production was analysed. Data are presented as mean \pm SEM of 5 mice per group. * $P < 0.05$, ** $P < 0.01$, *** $P < 0.001$, ns = non-significant by one-way ANOVA followed by Tukey's test.

As Figure 4.9b shows, mice immunized with OVA-IONP micelles co-administered with CpG-IONP micelles showed the best total IgG, IgG1 and IgG2c OVA-specific antibody responses. As expected, free OVA and CpG administration, but not OVA adsorbed to alum, induced IgG2c isotype, as well as high levels of IgG1 observed for both cases.^{69–71} The incorporation of adjuvant and antigen into IONP micelles increased not only IgG1 production, but also anti-OVA IgG2c isotype secretion. The co-administration of CpG-IONP micelles as complementary adjuvant to OVA-IONP micelles resulted in doubled

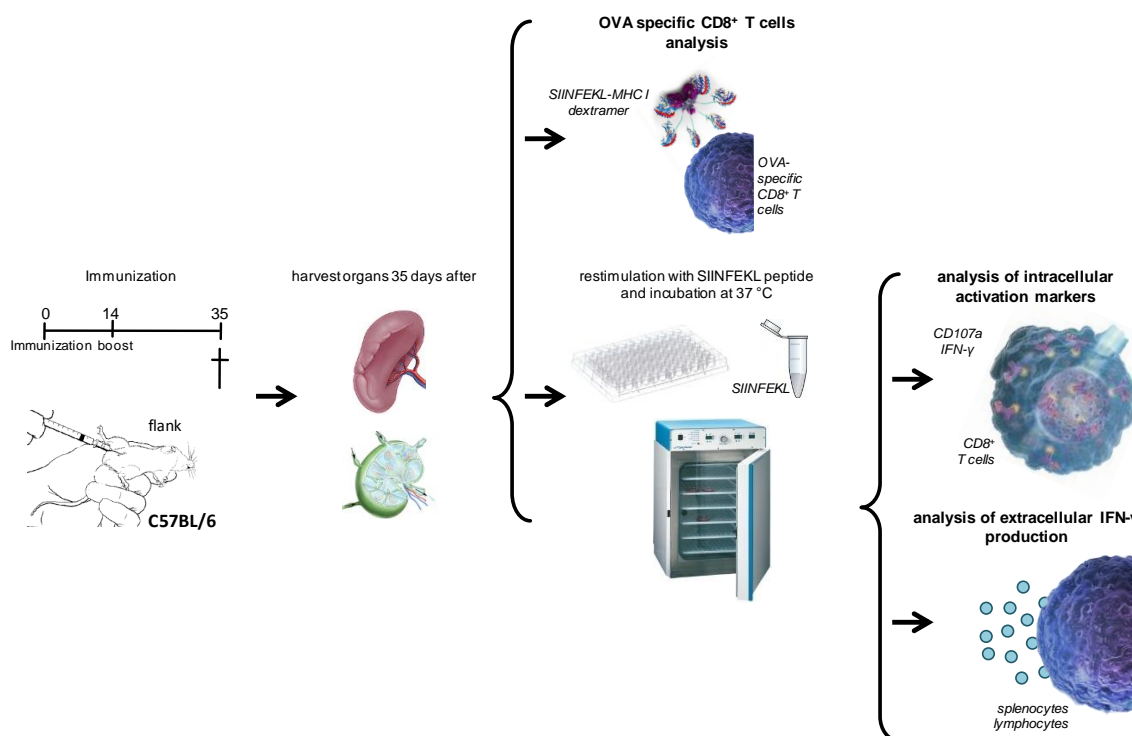
production of IgG2c subclass compared to the antigen carrying IONP micelles administered alone (Figure 4.9b and *vide supra* Figure 4.7b).

The cell mediated immune response was studied next. CD8⁺ T cells are the subclass of T cells capable of recognizing and killing virally infected cells, and are also critical in cancer immunotherapy for their ability to kill autologous cancer cells.⁷² The unique ability of CD8⁺ T cells to kill targets expressing antigens associated with MHC class I underpins the need of achieving the presentation of tumour antigens by APCs into this type of MHC molecule. In the case of OVA, the peptide SIINFEKL (OVA₂₅₇₋₂₆₄) is the MHC class I CD8⁺ T cell epitope. Once CD8⁺ T cells have seen the processed antigen and the necessary co-stimulation signals, they undergo several activation processes, such as production of cytokines and cytolytic molecules, which will increase their killing potential of targeted cells.

To analyse these cell mediated immune responses, 35 days after first immunization, mice were sacrificed and spleen and draining LNs harvested for further analysis. Two different analyses were performed to study the antigen-specific CD8⁺ T cell responses (**Scheme 4.1**):

1. Analysis of antigen-specific CD8⁺ T cell percentages: CD8⁺ T cells that have seen the OVA antigen processed by APCs *in vivo* will bind SIINFEKL epitope loaded into MHC class I. By staining the cells with SIINFEKL-MHC-I dextramer (fluorescently labelled MHC class I multimers loading the OVA epitope SIINFEKL), it was possible to measure the proportion of antigen-specific CD8⁺ T cells generated *in vivo*.⁷³

2. Analysis of CD8⁺ T cells functional ability: upon activation by APCs, CD8⁺ T cells produce diverse molecules to gain cell killing potential. Among others, IFN- γ is an important cytokine required for effective viral clearance produced by activated CTLs. CD107a is a marker of degranulation, a process that releases cytotoxic molecules from secretory vesicles of activated CD8⁺ T cells. After *ex vivo* SIINFEKL restimulation of harvested splenocytes, cells were stained with fluorescently labelled anti-IFN- γ and anti-CD107a and double positive cells representing functional antigen-specific CTLs were analysed.⁷⁴ Moreover, IFN- γ production was measured in cells derived from the harvested spleens, following SIINFEKL *ex vivo* restimulation over 48 hours.



Scheme 4.1. Immunization schedule and scheme of *ex vivo* analysis. Five μg OVA and CpG ODNs free or in conjugation with IONP micelles (*ca.* 7 μg of magnetite) were injected in C57BL/6 mice subcutaneously in the flank on day 0 and 14. Mice were sacrificed on day 35 and primary splenocytes and lymphocytes cultures were established for further analysis. SIINFEKL dextramer-positive CD8⁺ T cells percentage was analysed and, after *ex vivo* restimulation with SIINFEKL peptide, degranulation marker CD107a accumulation inside the cells and intracellular and extracellular IFN- γ production was determined.

Throughout the immunization period, the antigen-specific CD8⁺ T cells in blood serum were analysed first by staining cells derived from peripheral blood and spleen with fluorescently labelled SIINFEKL-MHC-I dextramer.

It was possible to observe how already after the initial injection (on day 14) the OVA-IONP micelles alone, in combination with CpG-IONP micelles or OVA-alum mixture were able to induce higher levels of SIINFEKL-specific T cells compared to the administration of free OVA and CpG ODNs (**Figure 4.10a**). However, four weeks after vaccination, only CpG-IONP micelles and alum immunized mice presented sustained SIINFEKL-specific T cells levels in peripheral blood (**Figure 4.10b**). At the end of the experiment (five weeks after the first injection), mice administered with OVA- and CpG-IONP micelles and OVA absorbed to alum had increased levels of SIINFEKL-specific T cells both in peripheral blood and the spleen (**Figure 4.10c, d**).

MHC class II molecules preferentially load epitopes derived from endocytosed exogenous antigens, whereas MHC class I molecules typically bind peptides coming

from endogenous proteins.⁷⁵ As confirmed by the observed results, soluble OVA protein is not able to elicit antigen-specific CD8⁺ T cells, i.e., cannot be presented by MHC class I molecules present in APCs (Figure 4.10). This fact is in concordance with previously reported results where soluble and no-conjugated exogenous antigens are generally processed and presented in MHC class II molecules.⁷⁶

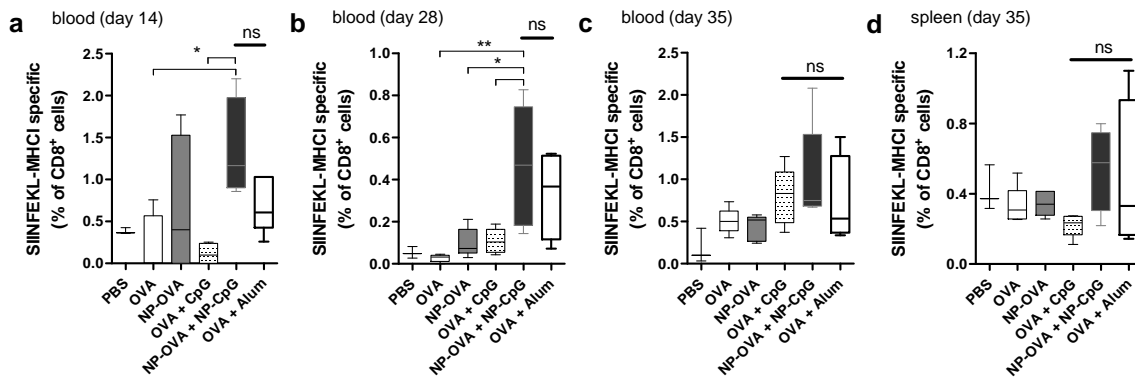


Figure 4.10. Co-administration of OVA-IONP micelles and CpG-IONP micelles increased OVA specific CD8⁺ T cell percentage *in vivo*. Five μ g OVA and CpG ODNs free or in conjugation with IONP micelles were injected in C57BL/6 mice subcutaneously in the flank on day 0 and 14; OVA-Alum mixture was included for comparison. SIINFEKL dextramer-positive CD8⁺ T cell percentage was analysed in peripheral blood cells on (a) day 14 and (b) 28 (two weeks after first and second injection, respectively) in order to monitor the immunization. Mice were sacrificed on day 35 and a final blood sample and splenocytes were harvested. SIINFEKL dextramer-positive CD8⁺ T cell percentage was measured in (c) blood and (d) spleen. Data are presented as mean \pm SEM of 5 mice per group. *P < 0.05, **P < 0.01, ns = non-significant by one-way ANOVA followed by Tukey's test.

Different adjuvants (such as CpG ODNs) and particulate structures can promote the cross-presentation of exogenous soluble antigens such as OVA from MHC class II to class I molecules, promoting the engulfment of antigen by the so-called phagocytosis process.^{77,78} Generation of SIINFEKL-specific CD8⁺ T cells after subcutaneous immunization of mice with the IONP-filled micelles as OVA delivery system (Figure 4.10), indirectly confirms that cross-presentation occurs.

Moreover, mice immunized with OVA-IONP micelles alone (without CpG ODNs-based adjuvancy) were able to induce slightly increased levels of CD8⁺ T cells specific for the antigen, compared to OVA alone. Cross-presentation of antigen and subsequent presentation by MHC class I molecules allows inducing cell-mediated immune response necessary to protect against intracellular infections and cancer.⁷⁹

The functional ability of the induced CTLs was analysed next. 35 days after the first immunization, the harvested splenocytes were restimulated *ex vivo* with SIINFEKL

peptide and intracellular IFN- γ production and CD107a degranulation marker accumulation were studied. Although antigen-specific CTLs were found both in mice immunized with antigen/adjuvant carrying IONP-filled micelles and in OVA mixed with alum (*vide supra* Figure 4.10), mice immunized with the combination of OVA and CpG-IONP micelles, but not free antigen/adjuvant or antigen absorbed to alum, were observed to have higher levels of IFN- γ producing CD8⁺ T cells (Figure 4.11a).

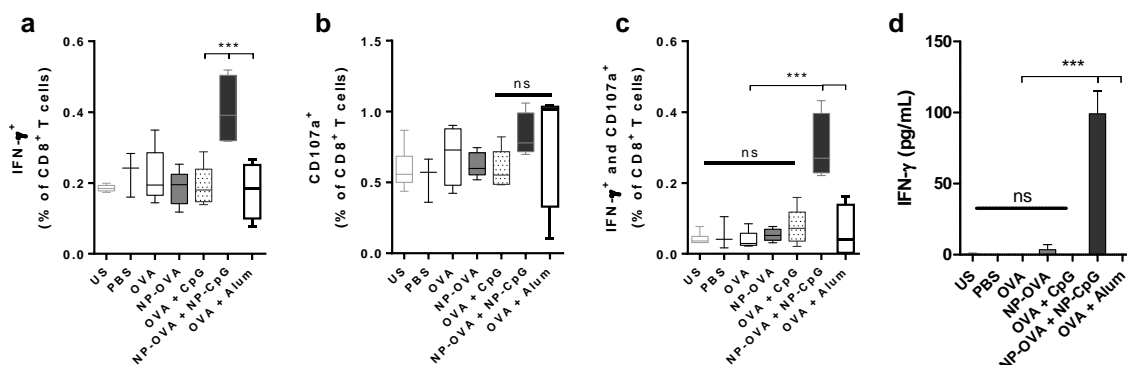


Figure 4.11. Co-administration of OVA-IONP micelles and CpG-IONP micelles enhanced cell killing potential of CD8⁺ T cell *in vivo*. Five μg OVA and CpG ODNs free or in conjugation with IONP micelles were injected in C57BL/6 mice subcutaneously in the flank on day 0 and 14; OVA-Alum mixture was included for comparison. Mice were sacrificed on day 35 and splenocytes were *ex vivo* restimulated with 10 $\mu\text{g}/\text{mL}$ SIINFEKL peptide over (a-c) 5 h or (d) 48 h. (a) Intracellular IFN- γ production and (b) degranulation marker CD107a were analysed by flow cytometry. (c) Functional cytotoxic CD8⁺ T cells were represented as IFN- γ and CD107a double positive cells. (d) Extracellular IFN- γ production. Data are presented as mean \pm SEM of 5 mice per group. *** $P < 0.001$, ns = non-significant by one-way ANOVA followed by Tukey's test.

This increased IFN- γ production by CD8⁺ T cells correlates with enhanced ability to defeat viral infections, intracellular pathogens and to control tumour development.^{80,81}

Upon encountering antigen, activated CD8⁺ T cells express the lysosomal-associated membrane protein CD107a on the cell surface due to degranulation process and have been shown to mediate cytolytic activity in an antigen-specific manner.⁸² Both CpG-IONP micelles and alum-immunized mice showed slight increase of this marker compared to PBS control (Figure 4.11b).

Moreover, when the cell killing potential of functional antigen-specific cytotoxic CD8⁺ T cells was analysed by detection of double positive CTLs producing both intracellular IFN- γ and the degranulation marker CD107a, only those mice that had been treated with the CpG-IONP micelles gave double positive cells. This could not be observed in

mice that were treated with alum, which confirms the incapacity of alum to induce Th1-type responses (Figure 4.11c).

Further demonstration of the enhanced *in vivo* responses obtained from vaccinated mice that concurrently received CpG-IONP micelles is that spleen cells collected from them produced significantly more IFN- γ following *ex vivo* restimulation with SIINFEKL than those vaccinated with OVA alone, free OVA-CpG mixture and OVA-IONP micelles alone. Alum did not induce IFN- γ production after *ex vivo* restimulation, corroborating previous results (Figure 4.11d). The higher the intensity of IFN- γ production the higher capacity of CTLs to secrete effector cytokines directed against the target cells.⁸³ Moreover, IFN- γ has been described to act as a protective cytokine against tumour development involved in direct anti-proliferative and anti-metabolic effects and even playing a role in avoiding angiogenesis within the tumour.⁸⁴

It is known that the induction of a stable long-term T cell immunity is desired in order to get complete protection. Memory T cells are more abundant than naive cells, they are maintained for longer periods and they have the ability to rapidly answer to an interaction with a seen antigen.^{85,86} Several types of memory CD8⁺ T cells have been described depending on the expression of activation and homing markers. CD44 adhesion molecule is a canonical memory cell marker and it is known to mediate migration, proliferation and T cell activation.⁸⁷⁻⁹⁰ L-selectin (CD62L) on the other hand, is a LN homing receptor and can modulate the functional properties of T cells depending on its expression levels.⁹¹ Based on these markers, two types of memory subsets can be defined: central memory T cells (T_{CM}), which present CD44^{high}CD62L^{high} phenotype; and effector memory T cells (T_{EM}) with CD44^{high}CD62L^{low} expression.^{92,93} This T_{EM} cell subset is mostly present in the spleen and non-lymphoid tissues and is used as the main mechanism for specifically eliminating the antigen during the initial phase and the subsequent encounters.⁹⁴

Thus, it was explored whether the incorporation of the antigen and the adjuvant into the IONP micelles could increase antigen-specific T_{EM}, described as CD44^{high}CD62L^{low}. As showed in the **Figure 4.12**, only the co-administration of OVA- and CpG-IONP

micelles induced significantly higher levels of T_{EM} specific for SIINFEKL, both in peripheral blood and the spleen (Figure 4.12a, b).

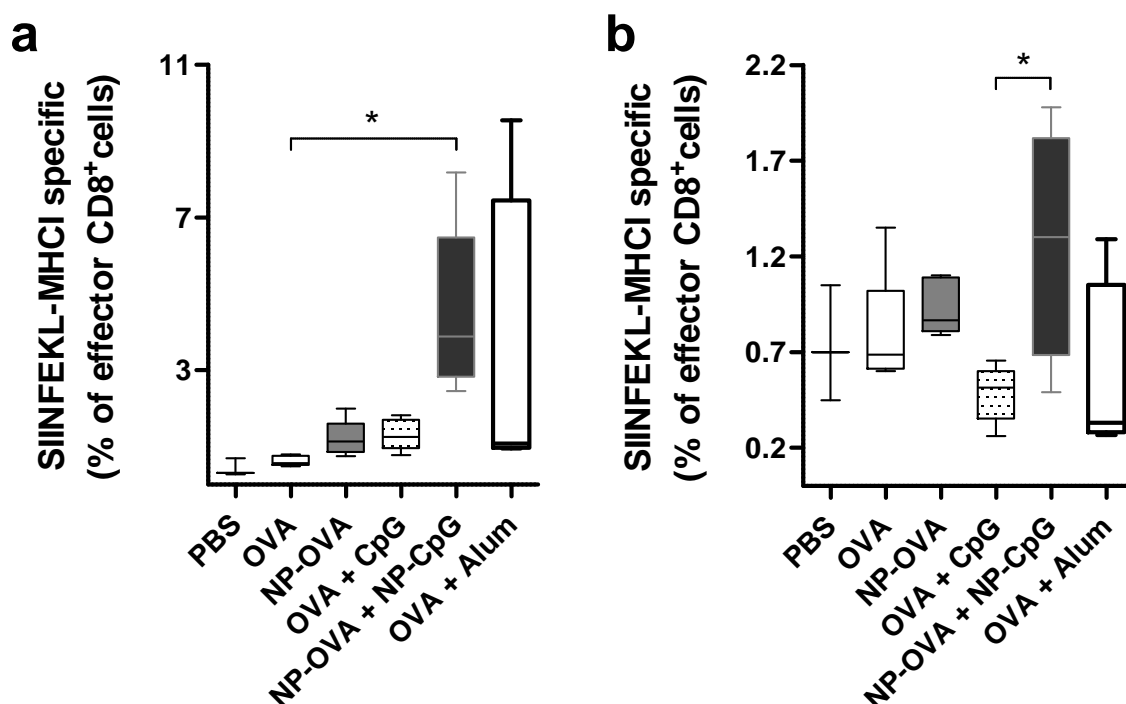


Figure 4.12. Co-administration of OVA-IONP micelles and CpG-IONP micelles increased OVA specific CD8⁺ T_{EM} cell percentage *in vivo*. Five μ g OVA and CpG ODNs free or in conjugation with IONP micelles were injected in C57BL/6 mice subcutaneously in the flank on day 0 and 14; OVA-Alum mixture was included for comparison. Mice were sacrificed on day 35 and CD44^{high}CD62L^{lo} (T_{EM}) CD8⁺ T cells that were SIINFEKL-specific were analysed in (a) blood serum and (b) spleen. Data are presented as mean \pm SEM of 5 mice per group. *P < 0.05 by one-way ANOVA followed by Tukey's test.

Taken together, these *in vivo* immunization results demonstrate enhanced humoral and cell mediated immune response when immunizing mice with the CpG ODNs and OVA antigen loaded into IONP micelles. IONP micelles were able to increase the anti-OVA antibody production in blood serum, as well as the percentage of OVA-specific CD8⁺ T cells, inducing enhanced effector functions, such as cytotoxic response (increased CD107a expression) and INF- γ production.

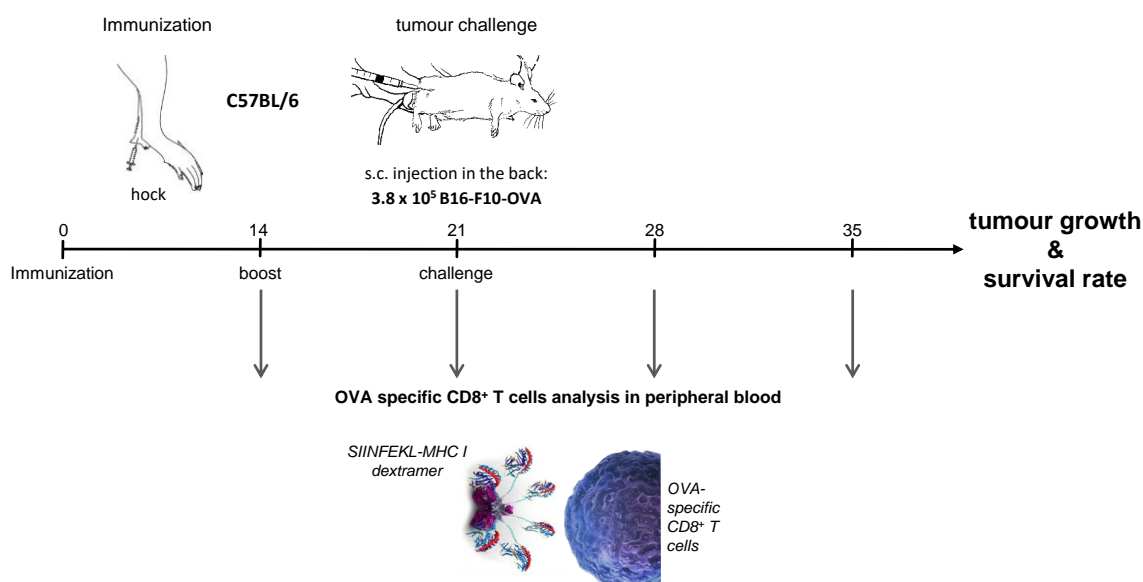
4.2.3. Anticancer activity of CpG- and OVA-IONP micelles

Once demonstrated the efficacy of the here developed nanosystems as potent immunostimulatory agents, the applicability of these vaccines as anticancer treatment was studied next. For this purpose, the previously described B16-F10-OVA mouse melanoma model was used. Since this tumour model expresses OVA protein on the

tumour cell surface, it is susceptible to be recognized and killed by high avidity OVA-specific CD8⁺ CTLs.

a) Prophylactic cancer treatment:

To investigate if the OVA- and CpG-IONP micelles could enhance protection against this highly aggressive melanoma challenge, 5 µg OVA and CpG ODNs free or in conjugation with IONP micelles were administered to C57BL/6 mice subcutaneously in the right hock on day 0 and 14 as prophylactic agents. Thus, on day 21, B16-F10-OVA cells were injected into the right back side and mice were monitored during 60 days (Scheme 4.2).



Scheme 4.2. Immunization schedule and scheme of antitumour prophylactic study. Five µg OVA and CpG ODNs free or in conjugation with IONP micelles (*ca.* 7 µg of magnetite) were injected in C57BL/6 mice subcutaneously in the right hock on day 0 and 14, as prophylactic agents. On day 21, B16-F10-OVA cells were injected into the right back side and mice were monitored during 60 days. Immune response was monitored by measuring the SIINFEKL-specific CD8⁺ T cells in peripheral blood during the vaccine injections and two weeks after tumour challenge. Tumour size and survival rate were studied over 60 days.

During 35 days after first vaccination, blood samples were taken every week and the immune response was monitored by measuring the SIINFEKL-dextramer positive CD8⁺ T cells (Figure 4.13). In concordance with the previous results, animals vaccinated with OVA- and CpG-IONP micelles induced higher number of SIINFEKL-specific CD8⁺ T cells compared with free OVA and CpG ODNs, even 35 days after the first immunization (Figure 4.13a-d). The maximum antigen-specific CD8⁺ cell response was observed 1

week after the second boost (day 21), and was at this moment when the co-administration of OVA and CpG loaded into IONP micelles showed statistically significant enhancement compared to the other immunization groups (Figure 4.13e).

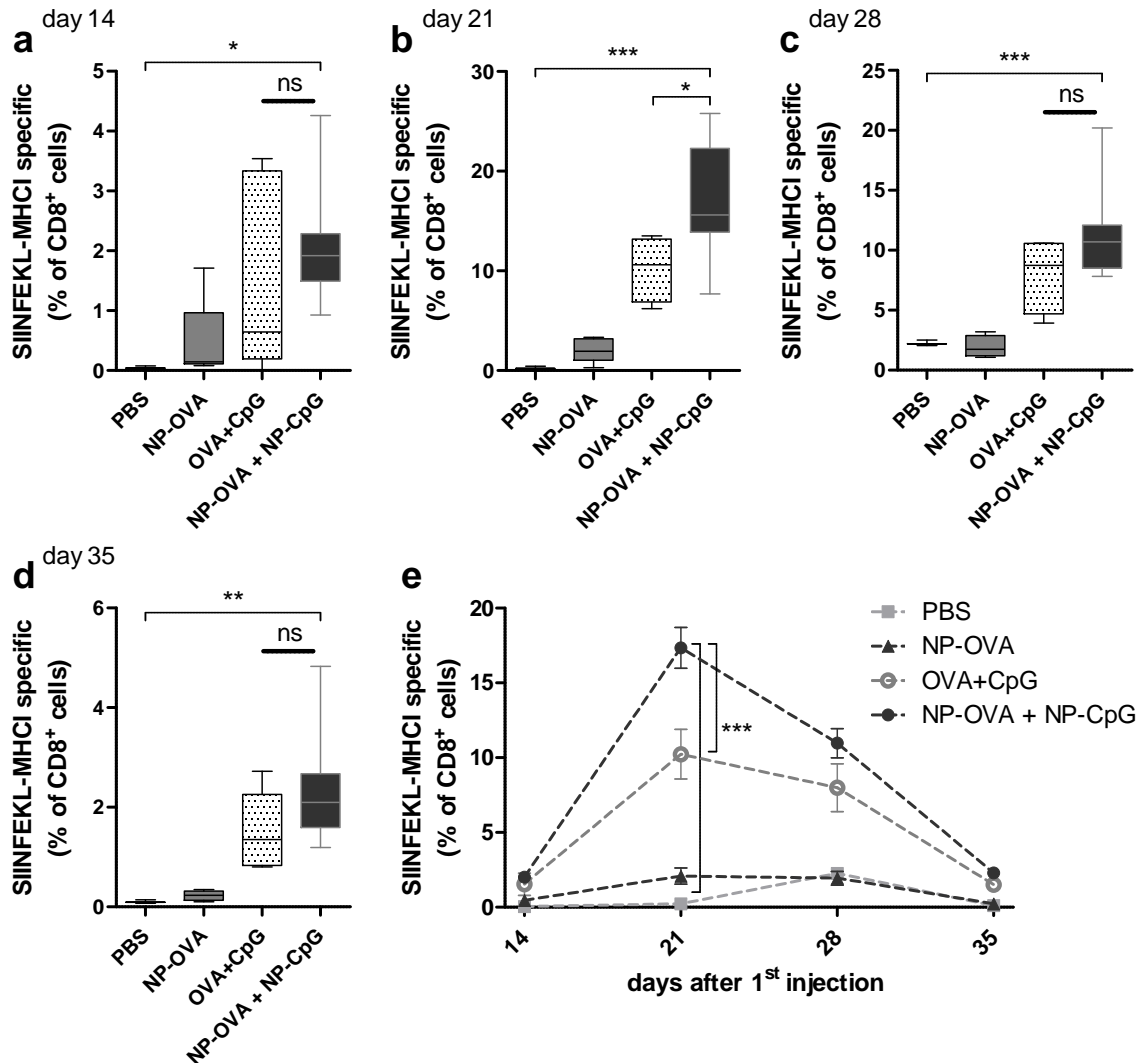


Figure 4.13. Monitoring SIINFEKL-specific CD8⁺ T cells allowed studying the immune response of the different prophylactic strategies. Five μg OVA and CpG ODNs free or in conjugation with IONP micelles (ca. 7 μg of magnetite) were injected in C57BL/6 mice subcutaneously in the right hock on day 0 and 14. On day 21, B16-F10-OVA cells were injected into the right back side of the animals. Analysis of SIINFEKL dextramer-positive CD8⁺ T cells in peripheral blood on day (a) 14, (b) 21, (c) 28 and (d) 35 after first immunization. (e) SIINFEKL-specific CD8⁺ T cell percentage over the time is shown. Data are presented as mean \pm SEM of 5 mice per group. * $P < 0.05$, ** $P < 0.01$, *** $P < 0.001$, ns = non-significant by (a-d) one-way ANOVA followed by Tukey's test and (e) two-way ANOVA followed by Bonferroni's test.

Thus, tumour cells were injected when the CD8⁺ T cells induced by OVA- and CpG-IONP micelles had higher capacity for recognizing and killing their antigen-bearing target cells *in vivo*.

Subcutaneous injection was chosen for administering the nanovaccines, since it is the most popular route in vaccination studies in mice and widely used for the evaluation of anticancer vaccines in many tumour models.^{95,96} Interestingly, if compared with the immunization assay showed in the previous section (Figure 4.10), some differences between subcutaneous injections into the flank or into the hock were observed. In terms of SIINFEKL-specific CD8⁺ T cells induction in peripheral blood, vaccination in the hock (a good alternative to footpad injection),⁹⁷ gave higher cell numbers specific for the injected antigen than immunizations performed into the flank (Figure 4.10 and 4.13 and Supporting Information, Figure S4.6). As showed in the chapter III, the injection into the hock drained several LNs including the inguinal and the popliteal ones, whereas the immunization in the flank did not reach to the popliteal LNs. Moreover, NPs injected into the hock reached also iliac and axillary LNs. The implanted tumour is drained by the mentioned LNs and therefore, tumour cells can potentially migrate to these organs as consequence of the metastasis process. Hence, hock immunization seemed the optimal route for vaccine injection.

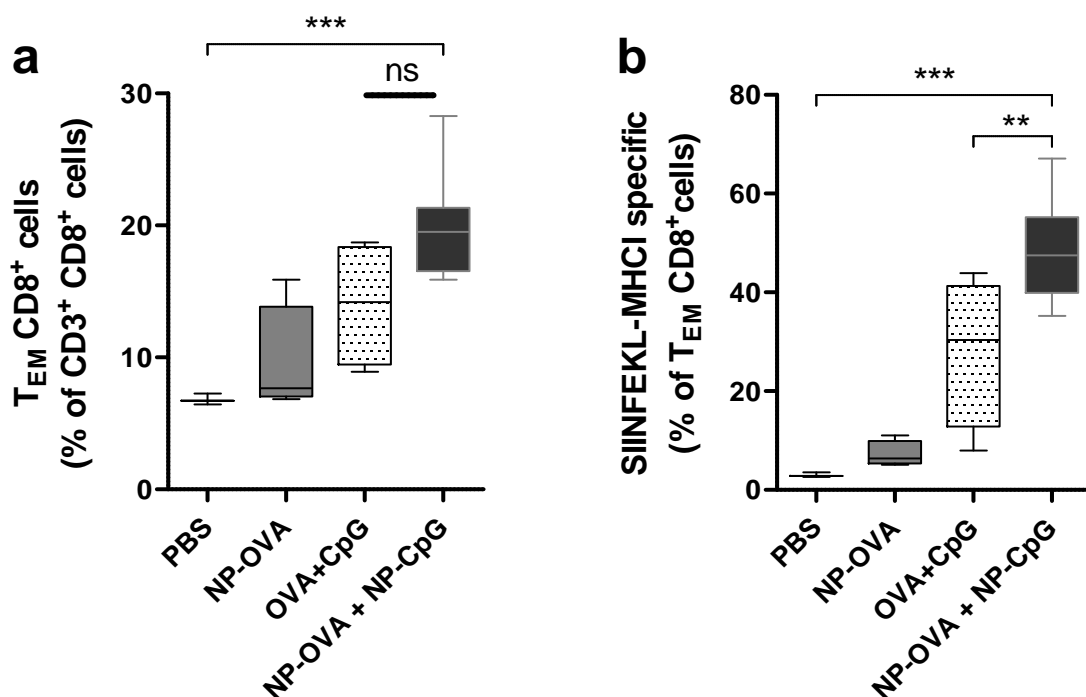


Figure 4.14. Co-administration of OVA-IONP micelles and CpG-IONP micelles previous to tumour challenge increased SIINFEKL-specific T_{EM} 28 days after first immunization. Five µg OVA and CpG ODNs free or in conjugation with IONP micelles (*ca.* 7 µg of magnetite) were injected in C57BL/6 mice subcutaneously in the right hock on day 0 and 14, as prophylactic agents. On day 21, B16-F10-OVA cells were injected into the right back side of the animals. One week after tumour challenge (day 28) (a) T_{EM} (CD8⁺CD44^{high}CD62L^{lo}) were analysed and (b) SIINFEKL dextramer-positive cell percentage was measured in that population. Data are presented as mean ± SEM of 5 mice per group. **P < 0.01, ***P < 0.001, ns = non-significant by one-way ANOVA followed by Tukey's test.

When analysing the CD8⁺ T_{EM} population described as CD44^{high}CD62L^{low}, it was observed that the administration of the nanovaccine formulation increased this cell percentage in peripheral blood, 1 week after tumour challenge (day 28) (Figure 4.14a). Moreover, the SIINFEKL-specific T_{EM} cell number was significantly enhanced when OVA- and CpG-IONP micelles were used for immunization compared to free molecules (Figure 4.14b). Therefore, although by day 28 OVA/CpG free molecules had similar SIINFEKL-specific CD8⁺ T cell percentage compared to antigen/adjuvant-loaded IONP micelles (*vide supra* Figure 4.13c), blood cells showing effector memory phenotype from mice administered with OVA- and CpG-IONP micelles still showed to have higher percentage of antigen-specific cells than with free OVA and CpG ODNs (Figure 4.14b).

These results were in agreement with the observed antitumour protection. The tumour growth was significantly delayed in animals immunized with OVA-IONP micelles and CpG-IONP micelles compared to in any other group, both in terms of tumour volume and proportion of tumour-free animals (Figure 4.15).

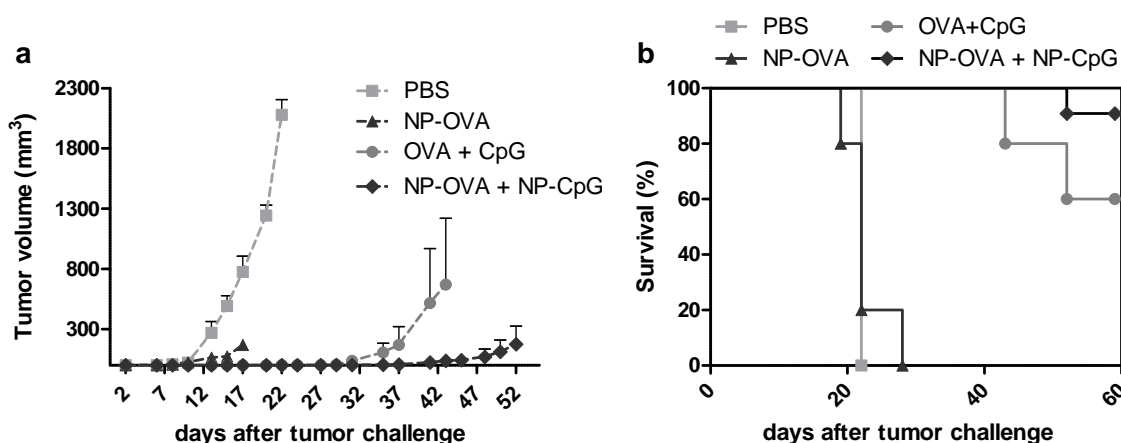


Figure 4.15. Administration of OVA-IONP micelles and CpG-IONP micelles as prophylactic agents enhanced tumour protection *in vivo*. Five µg OVA and CpG ODNs free or in conjugation with IONP micelles were injected in C57BL/6 mice subcutaneously in the right hock on day 0 and 14. On day 21, B16-F10-OVA cells were injected into the right back side and mice were monitored during 60 days. (a) Effect of prophylactic immunization on the growth of inoculated tumours and (b) survival rate in percentage. Data are presented as mean ± SEM of 5 mice per group.

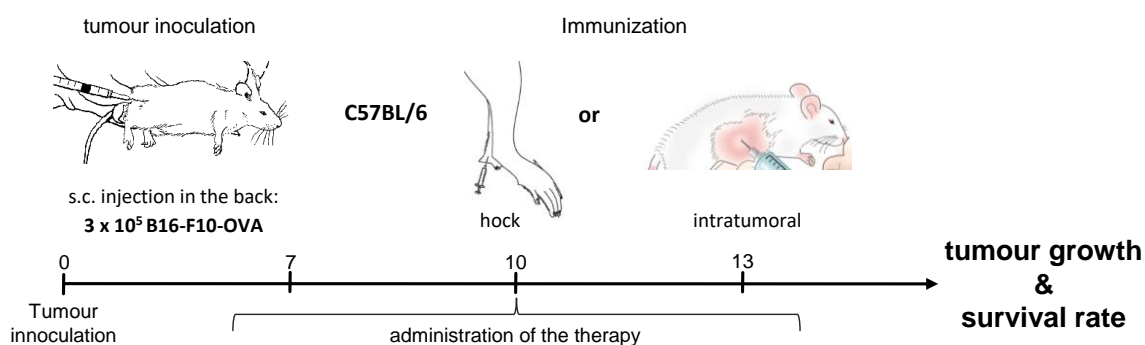
Interestingly, mice immunized with OVA-IONP micelles did not show big volume tumours; however, started to dye even sooner than control group presenting more aggressive tumour development. However, 73 % of the animals immunized with the OVA- and CpG-IONP nanovaccine were still tumour free 150 days after tumour challenge (Supporting Information, Figure S4.7a).

It is worth noting that the doses used in this prophylactic antitumour assay were very low compared to those used for anticancer vaccines in mice.^{79,98–100} The antigen dose required for triggering an efficient anticancer immune response is variable and depends on multiple factors. However, it is generally accepted that small amounts of antigenic agent incline the balance towards cell-mediated immunity, wanted for an optimal antitumour response, whereas higher doses preferentially induce humoral immunity.^{101,102} Of course, this pattern is not applicable to free soluble antigen administration, such as the TAAs, which are not able to induce potent immune response in absence of an adjuvant fraction.^{103,104} On the other hand, high adjuvant doses are generally required to induce strong CD8⁺ T cell immunity when employing vaccines.¹⁹

The incorporation of IONP micelles as delivery systems for the here chosen antigen/adjuvant allows decreasing the administered dose and still induce a potent antitumour cell mediated immune response.

b) Cancer therapy:

Finally, the therapeutic effect of the IONP-based anticancer vaccines was tested. For this purpose, B16-F10-OVA cells were inoculated as previously described and antigen/adjuvant carrying IONP-filled micelles were administered on days 7, 10 and 13 after tumour challenge (**Scheme 4.3**). In this last case, the OVA-IONP micelles formed by adsorption binding were used.



Scheme 4.3. Immunization schedule and scheme of the antitumour therapy study. B16-F10-OVA cells were injected in C57BL/6 mice subcutaneously into the right back side. Therapy was administered on days 7, 10 and 13 after tumour inoculation. Ten μg OVA and CpG ODNs free or in conjugation with IONP micelles (*ca.* 70 μg of magnetite) were injected subcutaneously in the right hock. OVA free intratumoural injection was included as control. Tumour size and survival rate were studied over 30 days.

The administration of CpG- and OVA-IONP micelles provided the best results for slowing down growth of established tumours (Figure 16a, b). The administration of OVA-IONP micelles without the adjuvant carrying micelle showed a similar effect as free antigen administered by intratumour injection. The mice treated with the IONP-based anticancer vaccine survived longer to the tumour challenge in comparison to the rest of the treatment groups (Figure 16c).

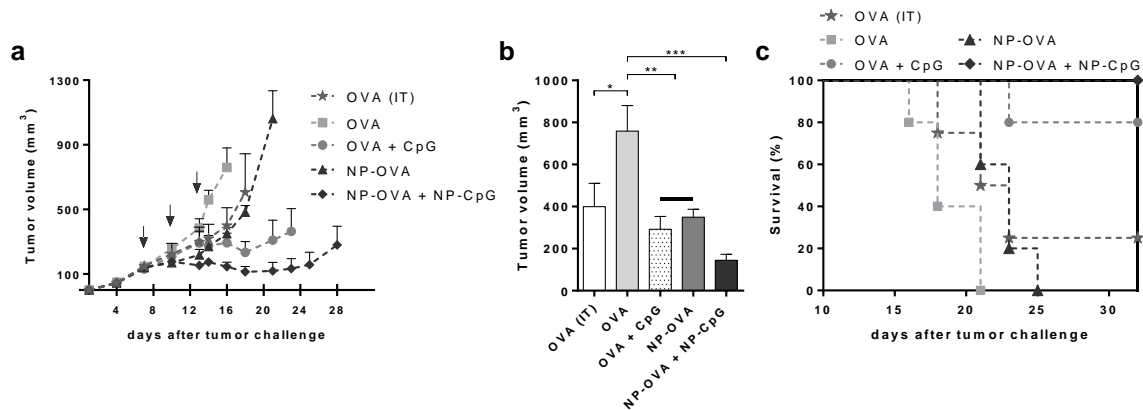


Figure 4.16. Administration of OVA-IONP micelles and CpG-IONP micelles as therapeutic agents slowed down tumour growth *in vivo*. Ten μg OVA and CpG ODNs free or in conjugation with IONP micelles were injected in C57BL/6 mice subcutaneously in the right hock on day 7, 10 and 13 after B16-F10-OVA cells injection into the right back side. OVA free intratumoural injection was included as control. (a) Effect of therapeutic immunization on the growth of inoculated tumours and (b) comparison of tumour volume on day 16. (c) Survival rate in percentage. Arrows represent injection of the therapy. Data are presented as mean \pm SEM of 5 mice per group. * $P < 0.05$, ** $P < 0.01$, *** $P < 0.001$ by one-way ANOVA followed by Tukey's test.

Overall, the here presented data are encouraging results in good agreement with earlier reports,^{105,106} and demonstrate that IONP micelles in combination with immunostimulatory moieties are promising candidates for anticancer vaccine development.

4.3. Conclusions

Through coordinated delivery of protein antigen and CpG ODN adjuvant using IONP-filled PEGylated micelles, potent immune responses were achieved both *in vitro* and *in vivo*. After encouraging *in vitro* results which showed enhanced activation of DCs and macrophages, *in vivo* studies showed that using the lipid-coated IONPs as delivery vehicle of CpG ODNs abolishes systemic *in vivo* release of pro-inflammatory cytokines and induces higher local activation of SLOs-resident immune cells. The OVA-IONP micelles enhanced by more than two orders of magnitude IgG OVA-specific antibody responses, demonstrating that the IONP-filled micelle is also an effective and versatile antigen vehicle for promoting strong humoral responses. Moreover, with the OVA-IONP micelles alone it was possible to induce production of OVA specific IgG2 antibodies, an isotype associated with Th1-type responses.

The results can be rationalised as resulting from the ability of IONP-based vaccines to directly target DCs in LNs. The use of similarly sized IONP micelles, in particular, most likely leads to better dual-targeting of CpG adjuvant and antigen (co-delivered on separate IONP micelles) to the same APCs in the SLOs. Consistent with this hypothesis, this coordinated co-delivery of adjuvant and antigen with the lipid-coated IONP vehicles enhanced humoral response and Th1-type cytokine secretion, which in turn resulted in stronger effector cytotoxic antigen-specific CD8⁺ CTL activation with enhanced cytolytic profiles, even with a low dose of adjuvant/antigen (5 µg/mice). The results obtained in this thesis show that through targeted delivery low amounts of antigen/adjuvant are able to induce robust humoral and cellular immunity *in vivo*. The overall low doses (<53 µg/mice) of IONP used for *in vivo* tracking and for eliciting antigen specific immunity makes this NP platform quite promising for developing ultrahigh performance nontoxic vaccines.

Apart from the passive targeting approach demonstrated in this thesis work, these magnetic NPs offer the opportunity for introducing new mechanisms for controlling the release, cellular fate, and biodistribution of antigen/adjuvant using external magnetic stimulated manipulations such as magnetic field guided localisation and of hyperthermia to enhance delivery and/or combined therapeutic effects. Although

none of these mechanisms have been exploited in cancer immunotherapy, a growing number of reports are already providing experimental demonstration of the potential of these magnetism-based mechanisms for precision drug delivery and combinatorial therapy in chemotherapy.

Taken together, these findings and the unique features that set magnetic particles apart from other delivery vehicles suggest that IONP-filled micelles can be expected to be a useful new vaccine technology to tackle infectious diseases and cancer.

4.4. Supporting Information of Chapter IV

CpG-IONP micelles induce higher amount of IL-12 cytokine than the same concentrations of free CpG ODNs in BMDCs. Although results are not statistically significant, the IL-12 production pattern is similar to other analysed cytokines (see Figure 4.4).

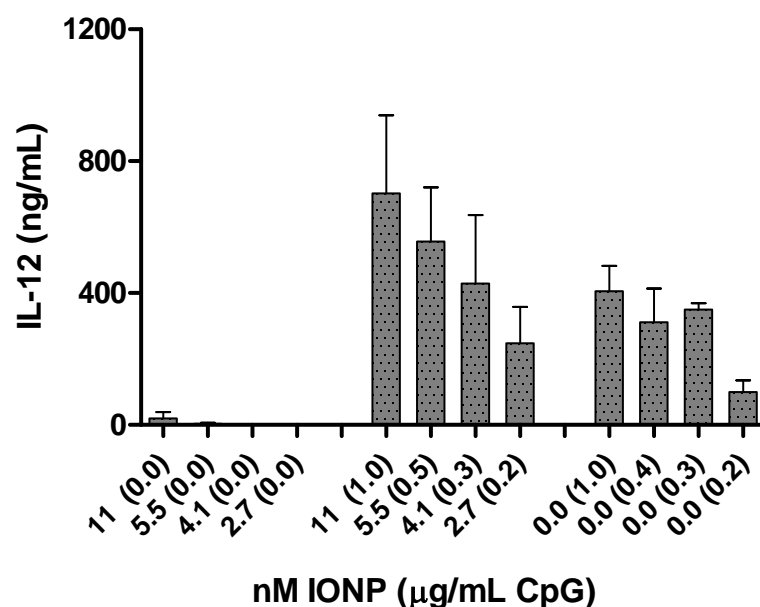


Figure S4.1. IL-12 cytokine production in BMDCs incubated for 24 h with different concentrations of IONP-filled micelles, CpG-IONP micelles or free CpG ODN. Data are presented as mean \pm SEM of three independent experiments.

Free CpG ODNs are considerably less immunostimulatory in J774A.1 macrophages and BMDCs than CpG-IONP micelles (see Figure 4.4).

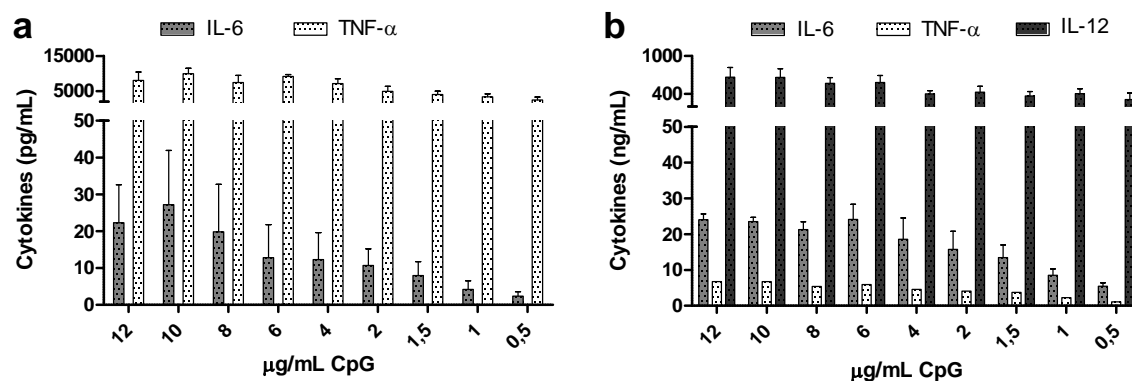


Figure S4.2. Cytokine production in (a) J774A.1 macrophages and (b) BMDCs after 24 h incubation at 37°C with free CpG ODNs. Data are presented as mean \pm SEM of three separate experiments.

The stimulation of BMDCs with free IONP micelles, CpG-IONP micelles or free CpG ODNs did not change the percentage of DCs expressing high levels of MHC class II.

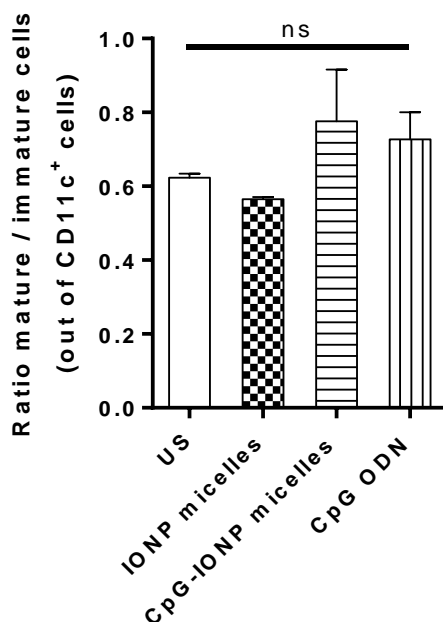


Figure S4.3. *In vitro* study of the ratio between mature (CD11c⁺, MHC class II^{high}) and immature (CD11c⁺, MHC class II^{low-intermediate}). BMDCs incubated for 24 h with control IONP micelles, CpG-IONP micelles and CpG ODN; 2.7 nM of IONP micelles and 0.2 µg/mL of CpG ODN. Data are presented as mean ± SEM of at least three independent experiments. ns = non-significant by two-way ANOVA followed by Bonferroni's test.

The *in vivo* stimulation of innate system after injection with free CpG or CpG-IONP micelles did not change the MHC class II expression levels in CD11c⁺ DCs neither the ratio between mature (CD11c⁺, MHC class II^{high}) and immature (CD11c⁺, MHC class II^{low-intermediate}) DCs.

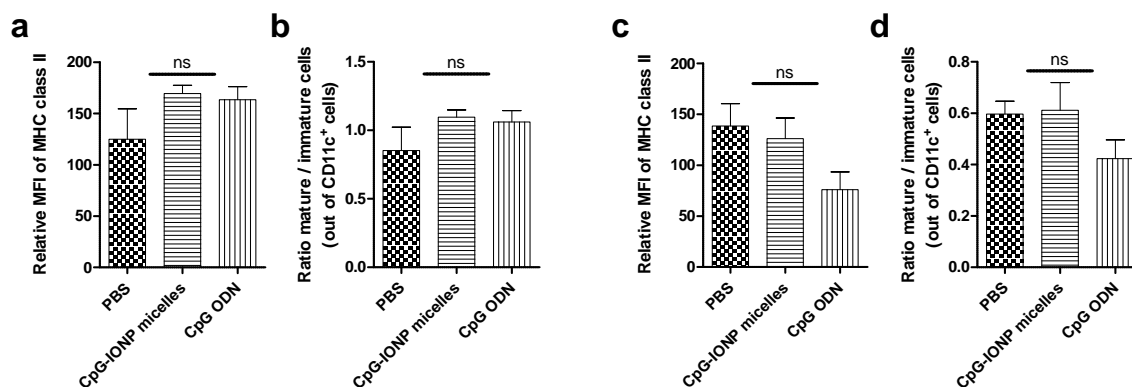


Figure S4.4. *In vivo* stimulation of innate system by injection of PBS as control, CpG-IONP micelles or CpG ODNs. 24 h after injection, (a, c) MHC class II MFI of CD11c⁺ DCs and (b, d) mature and immature DCs ratio was analysed in (a, b) spleen and (c, d) draining LN. Data are presented as mean ± SEM of 5 mice per group. ns = non-significant by one-way ANOVA followed by Tukey's test.

OVA-IONP micelles were not inducing the IFN- γ cytokine production in an unspecific manner, since there was no IFN- γ production when stimulating splenocytes over 48 h with the parent IONP-COOH micelles in the absence of OVA antigen.

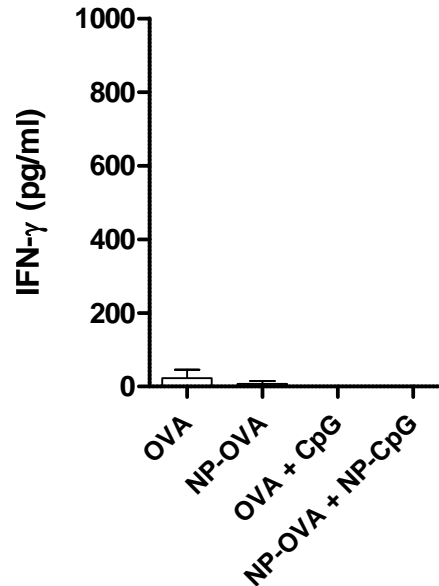


Figure S4.5. IFN- γ production after stimulation of splenocytes over 48 h with IONP-COOH micelles in the absence of OVA antigen. Data are presented as mean \pm SEM of 5 mice per group.

Subcutaneous immunization in the hock gave higher SIINFEKL-specific CD8⁺ T cell percentages in peripheral blood than subcutaneous injection in the flank, observing the maximum differences on day 28 after first immunization.

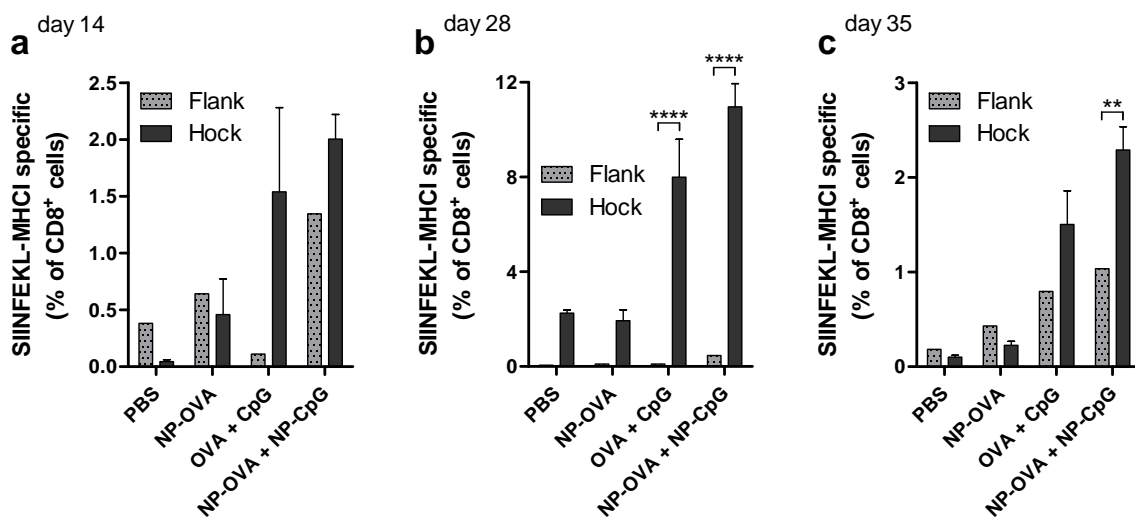


Figure S4.6. Five μ g OVA and CpG ODNs free or in conjugation with IONP micelles (ca. 7 μ g of magnetite) were injected in C57BL/6 mice subcutaneously in the flank or in the hock on day 0 and 14. Analysis of SIINFEKL dextramer-positive CD8⁺ T cells in peripheral blood on day (a) 14, (b) 28 and (c) 35 after first immunization. Data are presented as mean \pm SEM of 5 mice per group. ** $p < 0.01$, **** $p < 0.0001$, ns = non-significant by one-way ANOVA followed by Tukey's test.

Mice immunized with OVA- and CpG- IONP micelles were tumour free (73 % of the animals) even 150 days after challenge. Mice weight did not change between immunization groups during the tumour challenge, meaning that none of the procedures *in vivo* was deleterious for animal health.

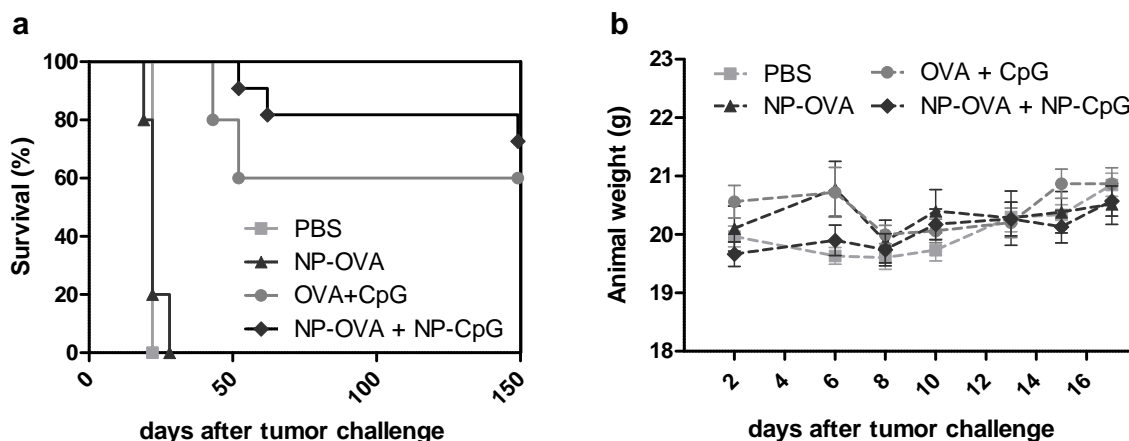


Figure S4.7. Five μg OVA and CpG ODNs free or in conjugation with IONP micelles were injected in C57BL/6 mice subcutaneously in the right hock on day 0 and 14, as prophylactic agents. On day 21, B16-F10-OVA cells were injected into the right back side. (a) Effect of prophylactic immunization on tumour growth over 150 days after challenge. (b) Animal weight was monitored after the tumour challenge. Data are presented as mean \pm SEM of 5 mice per group.

Body weight of mice treated with OVA- and CpG- IONP micelles did not change between immunization groups during the tumour therapy assay, meaning that none of the employed treatments was deleterious for animal health.

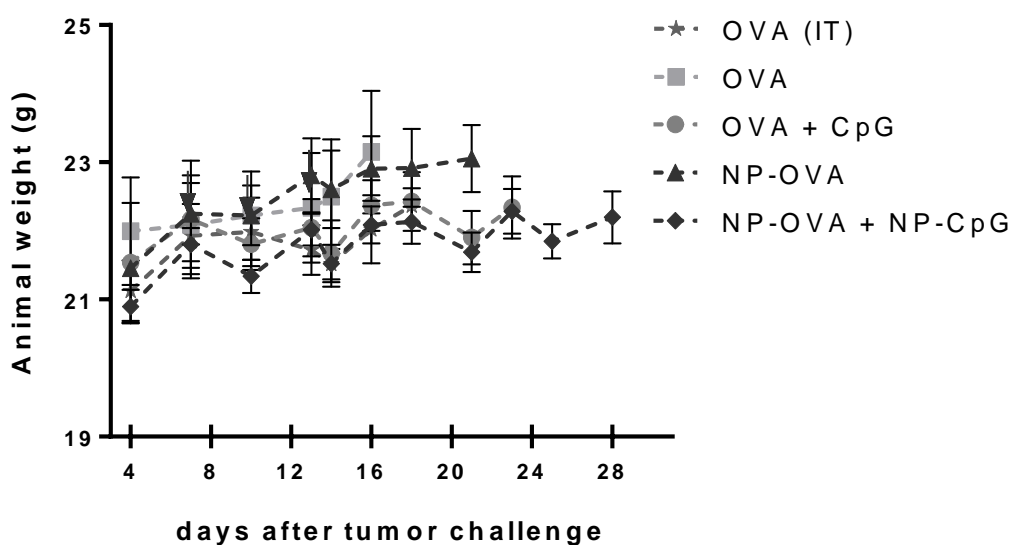


Figure S4.8. Ten μg OVA and CpG ODNs free or in conjugation with IONP micelles were injected in C57BL/6 mice subcutaneously in the right hock on day 7, 10 and 13 after B16-F10-OVA cells injection into the right back side. OVA free intratumoural injection was included as control. Animal weight was monitored after the tumour inoculation. Data are presented as mean \pm SEM of 5 mice per group.

Gating strategy followed for each flow cytometry assay shown in this chapter.

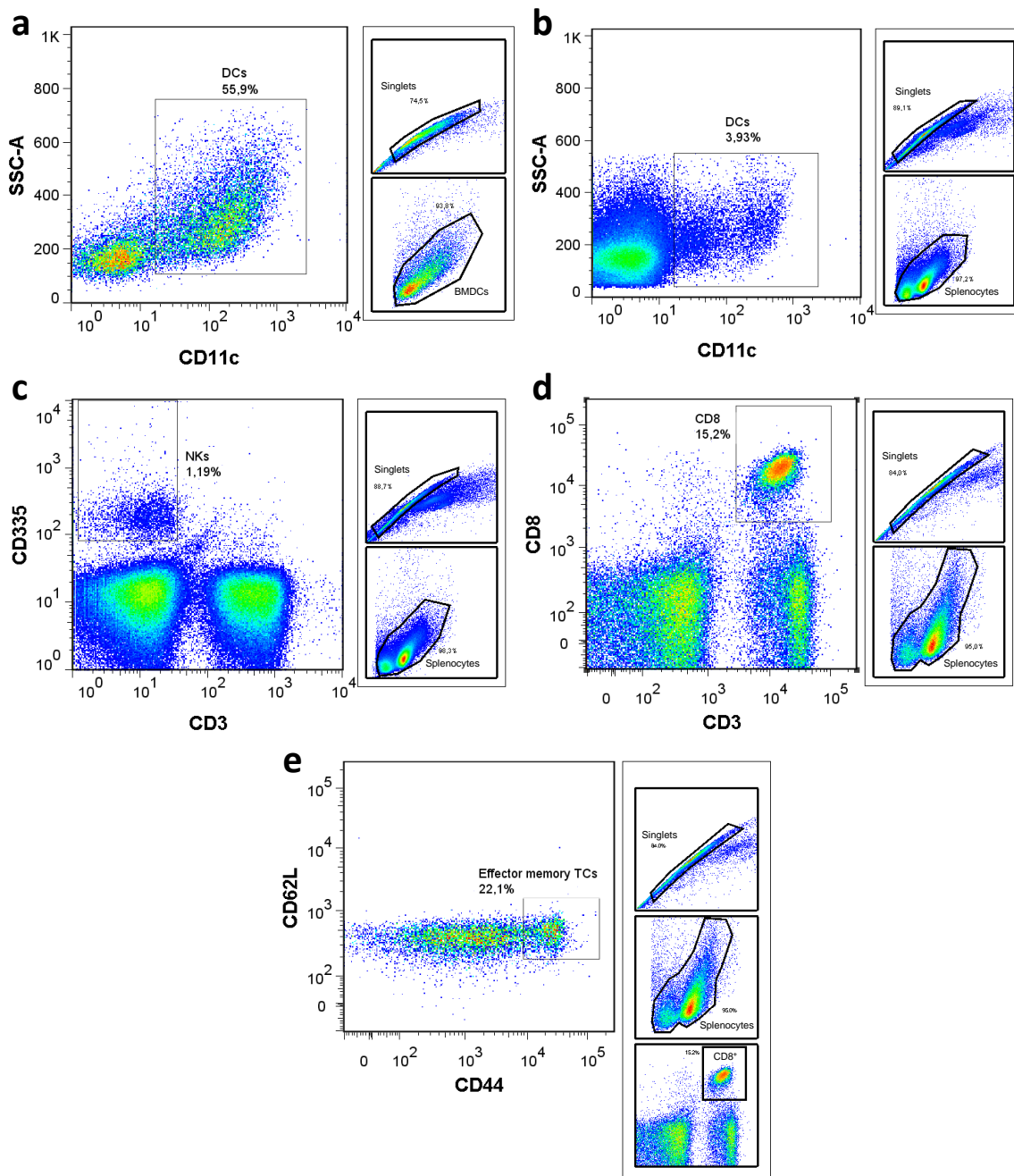


Figure S4.9. Cell gating strategies for the different flow cytometry assays shown in this chapter. (a) DC gating into the BMDCs, for maturation assays *in vitro*. For the assessment of the innate immune response (b) DC and (c) NK cells were gated into the splenocytes. (d) CD8⁺ T cell gating for both SIINFEKL-specific cells and intracellular IFN- γ and CD107a production analysis. (e) T_{EM} phenotype gating in CD8⁺ population.

References

1. Melero, I. *et al.* Therapeutic vaccines for cancer: an overview of clinical trials. *Nat. Rev. Clin. Oncol.* **11**, 509–524 (2014).
2. Coussens, L. M. & Werb, Z. Inflammation and cancer. *Nature* **420**, 860–7 (2002).
3. McLaughlin-Drubin, M. E. & Munger, K. Viruses associated with human cancer. *Biochim. Biophys. Acta* **1782**, 127–50 (2008).
4. Chithrani, B. D., Ghazani, A. A. & Chan, W. C. W. Determining the size and shape dependence of gold nanoparticle uptake into mammalian cells. *Nano Lett.* **6**, 662–668 (2006).
5. Uto, T. *et al.* Comparative activity of biodegradable nanoparticles with aluminum adjuvants: Antigen uptake by dendritic cells and induction of immune response in mice. *Immunol. Lett.* **140**, 36–43 (2011).
6. Akagi, T., Baba, M. & Akashi, M. Biodegradable Nanoparticles as Vaccine Adjuvants and Delivery Systems: Regulation of Immune Responses by Nanoparticle-Based Vaccine. *Adv. Polym. Sci.* **247**, 31–64 (2012).
7. Henriksen-Lacey, M., Korsholm, K. S., Andersen, P., Perrie, Y. & Christensen, D. Liposomal vaccine delivery systems. *Expert Opin. Drug Deliv.* **8**, 505–519 (2011).
8. Oh, N. & Park, J.-H. Endocytosis and exocytosis of nanoparticles in mammalian cells. *Int. J. Nanomedicine* **9**, 51–63 (2014).
9. Kuhn, D. A. *et al.* Different endocytotic uptake mechanisms for nanoparticles in epithelial cells and macrophages. *Beilstein J. Nanotechnol.* **5**, 1625–1636 (2014).
10. Kovacsovics-Bankowski, M., Clark, K., Benacerraf, B. & Rock, K. L. Efficient major histocompatibility complex class I presentation of exogenous antigen upon phagocytosis by macrophages. *Proc. Natl. Acad. Sci. U. S. A.* **90**, 4942–6 (1993).
11. Harding, C. V & Song, R. Phagocytic processing of exogenous particulate antigens by macrophages for presentation by class I MHC molecules. *J. Immunol.* **153**, 4925–33 (1994).
12. Shen, H. *et al.* Enhanced and prolonged cross-presentation following endosomal escape of exogenous antigens encapsulated in biodegradable nanoparticles. *Immunology* **117**, 78–88 (2006).
13. Uto, T. *et al.* Targeting of antigen to dendritic cells with poly(γ -glutamic acid) nanoparticles induces antigen-specific humoral and cellular immunity. *J. Immunol.* **178**, 2979–86 (2007).
14. Mohr, E. *et al.* IFN- γ produced by CD8 T cells induces T-bet-dependent and -independent class switching in B cells in responses to alum-precipitated protein vaccine. *Proc. Natl. Acad. Sci. U. S. A.* **107**, 17292–17297 (2010).

15. Korsholm, K. S. *et al.* Induction of CD8+ T-cell responses against subunit antigens by the novel cationic liposomal CAF09 adjuvant. *Vaccine* **32**, 3927–3935 (2014).
16. Steinman, R. M., Turley, S., Mellman, I. & Inaba, K. The induction of tolerance by dendritic cells that have captured apoptotic cells. *J. Exp. Med.* **191**, 411–6 (2000).
17. Steinman, R. M., Hawiger, D. & Nussenzweig, M. C. Tolerogenic dendritic cells. *Annu. Rev. Immunol.* **21**, 685–711 (2003).
18. Darrasse-Jèze, G. *et al.* Feedback control of regulatory T cell homeostasis by dendritic cells in vivo. *J. Exp. Med.* **206**, 1853–1862 (2009).
19. de Titta, A. *et al.* Nanoparticle conjugation of CpG enhances adjuvancy for cellular immunity and memory recall at low dose. *Proc. Natl. Acad. Sci. U. S. A.* **110**, 19902–7 (2013).
20. Demento, S. L. *et al.* TLR9-targeted biodegradable nanoparticles as immunization vectors protect against West Nile encephalitis. *J. Immunol.* **185**, 2989–2997 (2010).
21. Zhao, D. *et al.* Carbon Nanotubes Enhance CpG Uptake and Potentiate Antiglioma Immunity. *Clin. Cancer Res.* **17**, 771–782 (2011).
22. Lin, A. Y. *et al.* Gold Nanoparticle Delivery of Modified CpG Stimulates Macrophages and Inhibits Tumor Growth for Enhanced Immunotherapy. *PLoS One* **8**, (2013).
23. Thomas, S. N., Vokali, E., Lund, A. W., Hubbell, J. a. & Swartz, M. a. Targeting the tumor-draining lymph node with adjuvanted nanoparticles reshapes the anti-tumor immune response. *Biomaterials* **35**, 814–824 (2014).
24. Reddy, S. T. *et al.* Exploiting lymphatic transport and complement activation in nanoparticle vaccines. *Nat. Biotechnol.* **25**, 1159–64 (2007).
25. Manolova, V. *et al.* Nanoparticles target distinct dendritic cell populations according to their size. *Eur. J. Immunol.* **38**, 1404–1413 (2008).
26. Bachmann, M. F. & Jennings, G. T. Vaccine delivery: a matter of size, geometry, kinetics and molecular patterns. *Nat. Rev. Immunol.* **10**, 787–796 (2010).
27. Van Broekhoven, C. L., Parish, C. R., Demangel, C., Britton, W. J. & Altin, J. G. Targeting dendritic cells with antigen-containing liposomes: A highly effective procedure for induction of antitumor immunity and for tumor immunotherapy. *Cancer Res.* **64**, 4357–4365 (2004).
28. Bonifaz, L. C. *et al.* In vivo targeting of antigens to maturing dendritic cells via the DEC-205 receptor improves T cell vaccination. *J. Exp. Med.* **199**, 815–24 (2004).
29. Kwon, Y. J., James, E., Shastri, N. & Fréchet, J. M. J. In vivo targeting of dendritic cells for activation of cellular immunity using vaccine carriers based on pH-

- responsive microparticles. *Proc. Natl. Acad. Sci. U. S. A.* **102**, 18264–8 (2005).
30. Liu, K. *et al.* Immune tolerance after delivery of dying cells to dendritic cells in situ. *J. Exp. Med.* **196**, 1091–7 (2002).
 31. Probst, H. C., Lagnel, J., Kollias, G. & van den Broek, M. Inducible transgenic mice reveal resting dendritic cells as potent inducers of CD8⁺ T cell tolerance. *Immunity* **18**, 713–20 (2003).
 32. Wang, C. *et al.* Molecularly engineered poly(ortho ester) microspheres for enhanced delivery of DNA vaccines. *Nat. Mater.* **3**, 190–196 (2004).
 33. Pack, D. W. Timing is everything. *Nat. Mater.* **3**, 133–134 (2004).
 34. Wilson, N. S. *et al.* Most lymphoid organ dendritic cell types are phenotypically and functionally immature. *Blood* **102**, 2187–2194 (2003).
 35. Wilson, N. S. & Villadangos, J. A. Lymphoid organ dendritic cells: beyond the Langerhans cells paradigm. *Immunol. Cell Biol.* **82**, 91–98 (2004).
 36. Wilson, N. S., El-Sukkari, D. & Villadangos, J. A. Dendritic cells constitutively present self antigens in their immature state in vivo and regulate antigen presentation by controlling the rates of MHC class II synthesis and endocytosis. *Blood* **103**, 2187–2195 (2004).
 37. Sixt, M. *et al.* The Conduit System Transports Soluble Antigens from the Afferent Lymph to Resident Dendritic Cells in the T Cell Area of the Lymph Node. *Immunity* **22**, 19–29 (2005).
 38. Reddy, S. T., Swartz, M. A. & Hubbell, J. A. Targeting dendritic cells with biomaterials: developing the next generation of vaccines. *Trends Immunol.* **27**, 573–579 (2006).
 39. Swartz, M. A. The physiology of the lymphatic system. *Adv. Drug Deliv. Rev.* **50**, 3–20 (2001).
 40. Fifis, T. *et al.* Size-dependent immunogenicity: therapeutic and protective properties of nano-vaccines against tumors. *J. Immunol.* **173**, 3148–54 (2004).
 41. Oussoren, C., Zuidema, J., Crommelin, D. J. A. & Storm, G. Lymphatic uptake and biodistribution of liposomes after subcutaneous injection. *Biochim. Biophys. Acta - Biomembr.* **1328**, 261–272 (1997).
 42. Nishioka, Y. & Yoshino, H. Lymphatic targeting with nanoparticulate system. *Adv. Drug Deliv. Rev.* **47**, 55–64 (2001).
 43. Oussoren, C. & Storm, G. Liposomes to target the lymphatics by subcutaneous administration. *Adv. Drug Deliv. Rev.* **50**, 143–56 (2001).
 44. Reddy, S. T., Berk, D. A., Jain, R. K. & Swartz, M. A. A sensitive in vivo model for quantifying interstitial convective transport of injected macromolecules and nanoparticles. *J. Appl. Physiol.* **101**, 1162–1169 (2006).

45. Reddy, S. T., Rehor, A., Schmoekel, H. G., Hubbell, J. A. & Swartz, M. A. In vivo targeting of dendritic cells in lymph nodes with poly(propylene sulfide) nanoparticles. *J. Control. Release* **112**, 26–34 (2006).
46. Mellman, I. & Steinman, R. M. Dendritic cells: specialized and regulated antigen processing machines. *Cell* **106**, 255–8 (2001).
47. Cavanagh, L. L. & Von Andrian, U. H. Travellers in many guises: the origins and destinations of dendritic cells. *Immunol. Cell Biol.* **80**, 448–62 (2002).
48. Adema, G. J., de Vries, I. J. M., Punt, C. J. A. & Figdor, C. G. Migration of dendritic cell based cancer vaccines: in vivo veritas? *Curr. Opin. Immunol.* **17**, 170–4 (2005).
49. Sparwasser, T. *et al.* Bacterial DNA and immunostimulatory CpG oligonucleotides trigger maturation and activation of murine dendritic cells. *Eur. J. Immunol.* **28**, 2045–2054 (1998).
50. Henri, S. *et al.* The dendritic cell populations of mouse lymph nodes. *J. Immunol.* **167**, 741–748 (2001).
51. Lahoud, M. H. *et al.* DEC-205 is a cell surface receptor for CpG oligonucleotides. *Proc. Natl. Acad. Sci.* **109**, 16270–16275 (2012).
52. Martín-Fontecha, A. *et al.* Induced recruitment of NK cells to lymph nodes provides IFN- γ for TH1 priming. *Nat. Immunol.* **5**, 1260–1265 (2004).
53. Bajénoff, M. *et al.* Natural killer cell behavior in lymph nodes revealed by static and real-time imaging. *J. Exp. Med.* **203**, 619–31 (2006).
54. Ferlazzo, G. *et al.* Distinct roles of IL-12 and IL-15 in human natural killer cell activation by dendritic cells from secondary lymphoid organs. *Proc. Natl. Acad. Sci. U. S. A.* **101**, 16606–16611 (2004).
55. Habjanec, L., Halassy, B. & Tomašić, J. Comparative study of structurally related peptidoglycan monomer and muramyl dipeptide on humoral IgG immune response to ovalbumin in mouse. *Int. Immunopharmacol.* **10**, 751–759 (2010).
56. Liu, X., Wetzler, L. M. & Massari, P. The PorB porin from commensal *Neisseria lactamica* induces Th1 and Th2 immune responses to ovalbumin in mice and is a potential immune adjuvant. *Vaccine* **26**, 786–796 (2008).
57. Yang, Z., Chen, A., Sun, H., Ye, Y. & Fang, W. Ginsenoside Rd elicits Th1 and Th2 immune responses to ovalbumin in mice. *Vaccine* **25**, 161–169 (2007).
58. Germann, T., Rude, E. & Schmitt, E. The influence of IL12 on the development of Th1 and Th2 cells and its adjuvant effect for humoral immune responses. *Res. Immunol.* **146**, 481–6 (1995).
59. Vidarsson, G., Dekkers, G. & Rispens, T. IgG Subclasses and Allotypes: From Structure to Effector Functions. *Front. Immunol.* **5**, 520 (2014).

60. Schumaker, V. N., Calcott, M. A., Spiegelberg, H. L. & Mueller-Eberhard, H. J. Ultracentrifuge studies of the binding of IgG of different subclasses to the Clq subunit of the first component of complement. *Biochemistry* **15**, 5175–5181 (1976).
61. Visciano, M. L., Tagliamonte, M., Tornesello, M. L., Buonaguro, F. M. & Buonaguro, L. Effects of adjuvants on IgG subclasses elicited by virus-like Particles. *J. Transl. Med.* **10**, 4 (2012).
62. Nimmerjahn, F. Divergent Immunoglobulin G Subclass Activity Through Selective Fc Receptor Binding. *Science (80-.)*. **310**, 1510–1512 (2005).
63. Anderson, C. L. & Loone, R. J. Human leukocyte IgG Fc receptors. *Immunol. Today* **7**, 264–266 (1986).
64. Finkelman, F. D., Katona, I. M., Mosmann, T. R. & Coffman, R. L. IFN-gamma regulates the isotypes of Ig secreted during in vivo humoral immune responses. *J. Immunol.* **140**, 1022–1027 (1988).
65. Mosmann, T. R. & Coffman, R. L. TH1 and TH2 cells: different patterns of lymphokine secretion lead to different functional properties. *Annu. Rev. Immunol.* **7**, 145–173 (1989).
66. Huang, H. I. *et al.* Improved immunogenicity of a self tumor antigen by covalent linkage to CD40 ligand. *Int. J. Cancer* **108**, 696–703 (2004).
67. Ilyinskii, P. O. *et al.* Adjuvant-carrying synthetic vaccine particles augment the immune response to encapsulated antigen and exhibit strong local immune activation without inducing systemic cytokine release. *Vaccine* **32**, 2882–95 (2014).
68. Bioley, G., Lassus, A., Terrettaz, J., Tranquart, F. & Corthésy, B. Long-term persistence of immunity induced by OVA-coupled gas-filled microbubble vaccination partially protects mice against infection by OVA-expressing *Listeria*. *Biomaterials* **57**, 153–160 (2015).
69. Majewska-Szczepanik, M. *et al.* Epicutaneous immunization with ovalbumin and CpG induces TH1/TH17 cytokines, which regulate IgE and IgG2a production. *J. Allergy Clin. Immunol.* **138**, 262–273 (2015).
70. Yanase, N. *et al.* OVA-bound nanoparticles induce OVA-specific IgG1, IgG2a, and IgG2b responses with low IgE synthesis. *Vaccine* **32**, 5918–5924 (2014).
71. Beck, L. & Spiegelberg, H. L. The polyclonal and antigen-specific IgE and IgG subclass response of mice injected with ovalbumin in alum or complete Freund's adjuvant. *Cell. Immunol.* **123**, 1–8 (1989).
72. Yee, C. *et al.* Adoptive T cell therapy using antigen-specific CD8+ T cell clones for the treatment of patients with metastatic melanoma: in vivo persistence, migration, and antitumor effect of transferred T cells. *Proc. Natl. Acad. Sci. U. S. A.* **99**, 16168–73 (2002).

73. Sims, S., Willberg, C. & Klenerman, P. MHC-peptide tetramers for the analysis of antigen-specific T cells. *Expert Rev. Vaccines* **9**, 765–74 (2010).
74. Betts, M. R. *et al.* Sensitive and viable identification of antigen-specific CD8⁺ T cells by a flow cytometric assay for degranulation. *J. Immunol. Methods* **281**, 65–78 (2003).
75. Ackerman, A. L. & Cresswell, P. Cellular mechanisms governing cross-presentation of exogenous antigens. *Nat. Immunol.* **5**, 678–684 (2004).
76. Reis e Sousa, C. & Germain, R. N. Major histocompatibility complex class I presentation of peptides derived from soluble exogenous antigen by a subset of cells engaged in phagocytosis. *J. Exp. Med.* **182**, 841–851 (1995).
77. Hari, A. *et al.* Redirecting soluble antigen for MHC class I cross-presentation during phagocytosis. *Eur. J. Immunol.* **45**, 383–395 (2015).
78. Maurer, T. *et al.* CpG-DNA aided cross-presentation of soluble antigens by dendritic cells. *Eur. J. Immunol.* **32**, 2356 (2002).
79. Pouniotis, D. S., Esparon, S., Apostolopoulos, V. & Pietersz, G. A. Whole protein and defined CD8(+) and CD4(+) peptides linked to penetratin targets both MHC class I and II antigen presentation pathways. *Immunol. Cell Biol.* **89**, 904–13 (2011).
80. Szabo, S. J. *et al.* Distinct Effects of T-bet in T_H 1 Lineage Commitment and IFN gamma Production in CD4 and CD8 T Cells. *Science (80-.)*. **295**, 338–343 (2002).
81. Schoenborn, J. R. & Wilson, C. B. in *Advances in Immunology* 41–101 (Elsevier, 2007). doi:10.1016/S0065-2776(07)96002-2
82. Aktas, E., Kucuksezer, U. C., Bilgic, S., Erten, G. & Deniz, G. Relationship between CD107a expression and cytotoxic activity. *Cell. Immunol.* **254**, 149–154 (2009).
83. Seder, R. a, Darrah, P. a & Roederer, M. T-cell quality in memory and protection: implications for vaccine design. *Nat. Rev. Immunol.* **8**, 247–258 (2008).
84. Ikeda, H., Old, L. J. & Schreiber, R. D. The roles of IFN gamma in protection against tumor development and cancer immunoediting. *Cytokine Growth Factor Rev.* **13**, 95–109 (2002).
85. Kaech, S. M. & Ahmed, R. Memory CD8⁺ T cell differentiation: initial antigen encounter triggers a developmental program in naïve cells. *Nat. Immunol.* **2**, 415–422 (2001).
86. Wherry, E. J. *et al.* Lineage relationship and protective immunity of memory CD8 T cell subsets. *Nat. Immunol.* **4**, 225–234 (2003).
87. Haynes, B. F., Telen, M. J., Hale, L. P. & Denning, S. M. CD44 - a molecule involved in leukocyte adherence and T-cell activation. *Immunol. Today* **10**, 423–8 (1989).

88. Huet, S. *et al.* CD44 contributes to T cell activation. *J. Immunol.* **143**, 798–801 (1989).
89. MacDonald, H. R., Budd, R. C. & Cerottini, J. C. Pgp-1 (Ly 24) as a marker of murine memory T lymphocytes. *Curr. Top. Microbiol. Immunol.* **159**, 97–109 (1990).
90. Baaten, B. J. G. *et al.* CD44 regulates survival and memory development in Th1 cells. *Immunity* **32**, 104–115 (2010).
91. Kaech, S. M., Wherry, E. J. & Ahmed, R. Effector and Memory T-Cell Differentiation: Implications for Vaccine Development. *Nat. Rev. Immunol.* **2**, 251–262 (2002).
92. Gerberick, G. F., Cruse, L. W., Miller, C. M., Sikorski, E. E. & Ridder, G. M. Selective modulation of T cell memory markers CD62L and CD44 on murine draining lymph node cells following allergen and irritant treatment. *Toxicol. Appl. Pharmacol.* **146**, 1–10 (1997).
93. Krishnan, L. *et al.* Rapid clonal expansion and prolonged maintenance of memory CD8⁺ T cells of the effector (CD44^{high}CD62L^{low}) and central (CD44^{high}CD62L^{high}) phenotype by an archaeosome adjuvant independent of TLR2. *J. Immunol.* **178**, 2396–2406 (2007).
94. Oehen, S. & Brduscha-Riem, K. Differentiation of naive CTL to effector and memory CTL: correlation of effector function with phenotype and cell division. *J. Immunol.* **161**, 5338–46 (1998).
95. Mullins, D. W. *et al.* Route of immunization with peptide-pulsed dendritic cells controls the distribution of memory and effector T cells in lymphoid tissues and determines the pattern of regional tumor control. *J. Exp. Med.* **198**, 1023–34 (2003).
96. Okada, N. *et al.* Administration route-dependent vaccine efficiency of murine dendritic cells pulsed with antigens. *Br. J. Cancer* **84**, 1564–1570 (2001).
97. Kamala, T. Hock immunization: A humane alternative to mouse footpad injections. *J. Immunol. Methods* **328**, 204–214 (2007).
98. Basto, A. P. *et al.* Immune response profile elicited by the model antigen ovalbumin expressed in fusion with the bacterial OprI lipoprotein. *Mol. Immunol.* **64**, 36–45 (2015).
99. Aranda, F. *et al.* Adjuvant combination and antigen targeting as a strategy to induce polyfunctional and high-avidity T-cell responses against poorly immunogenic tumors. *Cancer Res.* **71**, 3214–3224 (2011).
100. Bourquin, C. *et al.* Targeting CpG Oligonucleotides to the Lymph Node by Nanoparticles Elicits Efficient Antitumoral Immunity. *J. Immunol.* **181**, 2990–8 (2008).

Chapter IV

101. Parish, B. Y. C. R. & Liew, F. Y. Immune response to chemically modified flagellin. III. Enhanced cell-mediated immunity during high and low zone antibody tolerance to flagellin. *J. Exp. Med.* **135**, 298–311 (1972).
102. Bretscher, P. A., Wei, G., Menon, J. N. & Ohmann-Bielefeldt, H. Establishment of Stable, Cell-Mediated Immunity That Makes 'Susceptible' Mice Resistant to *Leishmania major*. *Science (80-)*. **257**, 539–42 (1992).
103. Schreiber, T. H., Raez, L., Rosenblatt, J. D. & Podack, E. R. Tumor Immunogenicity and Responsiveness to Cancer Vaccine Therapy; The State of The Art. *Semin. Immunol.* **22**, 105–112 (2010).
104. Watson, A. M., Mylin, L. M., Thompson, M. M. & Schell, T. D. Modification of a tumor antigen determinant to improve peptide/MHC stability is associated with increased immunogenicity and cross-priming a larger fraction of CD8+ T cells. *J. Immunol.* **189**, 5549–60 (2012).
105. Lee, I. H. *et al.* Imageable antigen-presenting gold nanoparticle vaccines for effective cancer immunotherapy in vivo. *Angew. Chemie Int. Ed.* **51**, 8800–8805 (2012).
106. Li, H., Li, Y., Jiao, J. & Hu, H.-M. Alpha-alumina nanoparticles induce efficient autophagy-dependent cross-presentation and potent antitumour response. *Nat. Nanotechnol.* **6**, 645–50 (2011).

Summary of results

- Hydrophobic IONPs were successfully encapsulated using amphiphilic PEG-PLs with different functional end groups, resulting in IONP-filled micelles with a hydrodynamic diameter <40 nm. Different lipids were also included in the micelle formation without altering the rest of properties;
- IONP-filled micelles were able to anchor antigen (protein) and adjuvant (ODNs) moieties following simple attachment protocols applicable to a wide variety of biomolecules, without involving complicated chemical reactions;
- IONP-filled biofunctionalised micelles were successfully labelled using different imaging probes such as the fluorophore rhodamine B and the radioisotope ^{67}Ga . In this way, nanovaccines could be tracked both *in vitro* and *in vivo* using non-invasive multimodal imaging techniques (MRI/optical/nuclear);
- The delivery to specific tissues involved in the induction of immunity, such as LNs, was achieved and demonstrated by nuclear imaging techniques. Moreover, optical techniques such as FACS and fluorescence microscopy allowed the enhanced interaction with cells of the immune system and the delivery of the cargo into specific intracellular compartments/receptors to be observed;
- Biofunctionalised IONP-filled micelles elicited potent immune responses, clearly enhancing the effect of free antigen/adjuvant molecules and the commercially available adjuvant (alum). The observed immune response was based on Th1/Th2 balanced profile, i.e., a combination of humoral and cellular-based immunity optimal to attack tumour cells: 1) antibody production was enhanced; 2) pro-inflammatory cytokine induction was increased in SLOs resident immune cells but not systemically; and 3) antigen-specific CTLs were generated and their killing capabilities enhanced;
- IONP-filled micelles carrying antigen/adjuvant in separate formulations achieved a significant protection against tumour growth and an increased survival rate, in comparison to the administration of free biomolecules.

Experimental section

Materials

All experiments were carried out using commercially available reagents, without further purification, unless specified otherwise.

1. Synthesis of hydrophobic IONPs and IONP-filled micelles

Products employed in the synthesis of the hydrophobic IONPs are described next: Hexane (99%; LABSCAN), chloroform (water 0.005%; LABSCAN), diphenyl ether (99%; Sigma Aldrich), dibenzyl ether (>98%; Alfa Aesar), ethanol ($\geq 99.9\%$; Scharlau), 1,2-hexadecanediol (>98%; Tokyo Chemical Industry Co. Ltd), oleic acid (90%; Alfa Aesar), oleylamine (70%; Sigma Aldrich) and iron(III) acetylacetonate (99%; Strem Chemicals).

1,2-Dipalmitoyl-sn-glycero-3-phosphoethanolamine-N-[methoxy (polyethylene glycol)-2000] (ammonium salt) (DPPE-mPEG(2000)), 1,2-distearoyl-sn-glycero-3-phosphoethanolamine-N-[amino(polyethylene glycol)-2000] (ammonium salt) (DSPE-aPEG(2000)), 1,2-distearoyl-sn-glycero-3-phosphoethanolamine-N-[carboxy(polyethylene glycol)-2000] (ammonium salt) (DSPE-cPEG(2000)) and 1,2-dipalmitoyl-3-trimethylammonium-propane (chloride salt) (DOTAP) employed for preparing the IONP-filled micelles were purchased from Avanti Polar Lipids.

CpG ODNs sequence (TCCATGACGTTCTGATGC) was manufactured in the laboratories of The Midland Certified Reagent Company Inc. Albumin from chicken egg white was purchased from Sigma Aldrich and further purified to eliminate endotoxins using an ÄKTA purifier chromatography system, using a Superdex200, 10/300 GL column (GE Healthcare) and UNICORN 5.11 software.

1-Ethyl-3-[-3-dimethylaminopropyl]carbodiimide hydrochloride (EDC) and N-hydroxysulfosuccinimide (sodium salt) (NHSS) were purchased from Thermo Fisher Scientific.

2. Synthesis of labelled IONP-filled micelles

1,2-dipalmitoyl-sn-glycero-3-phosphoethanolamine-N-(lissaminerhodamine B sulfonyl) (ammonium salt) (DPPE-Rho) was purchased from Avanti Polar Lipids. FITC-labelled CpG ODNs were purchased from InvivoGen and Alexa647-labelled OVA from Molecular Probes (Thermo Fisher Scientific).

⁶⁷Ga citrate solution was purchased from Molypharma (Spain) and 1,4,7,10-tetraazacyclododecane-1,4,7,10-tetraacetic acid (DOTA) from Macrocyclics (Inc. Dallas, USA).

3. Reagents for *in vitro* and *in vivo* studies

Sodium chloride (99%), di-sodium hydrogen phosphate anhydrous (99%), potassium chloride (99,5%) and potassium di-hydrogen phosphate (99%) for phosphate-buffered saline (PBS buffer) were purchased from Panreac. PBS buffer (10 mM) was prepared by mixing NaCl at 137 mM, KCl at 2.7 mM, Na₂HPO₄ at 10 mM and KH₂PO₄ at 1.8 mM in nanopure water. After preparation, the buffer was filtered and autoclaved to ensure sterility.

Different cell culture media were used. Dulbecco's Modified Eagle's Medium (DMEM) with L-glutamine (Gibco®) was purchased from Life Technologies (Thermo Fisher Scientific) and RPMI-1640 medium without L-glutamine from Lonza. Media were supplemented with L-glutamine (2 mM; only if needed), heat inactivated fetal bovine serum (FBS; 10%) and Penicillin/Streptomycin (P/S; 100 µg/mL), all of them Gibco® and purchased from Life Technologies (Thermo Fisher Scientific).

4',6-Diamidino-2-phenylindole dihydrochloride (DAPI) was purchased from Invitrogen, LysoTracker Green from Molecular Probes (Thermo Fisher Scientific) and BD Cytfix/Cytoperm™ Plus Fixation/Permeabilization Kit from BD Biosciences. Primary anti-TLR 9 mouse monoclonal antibody and Alexa488-labelled goat polyclonal secondary antibody to mouse IgG were purchased from Abcam. All fluorescently labelled monoclonal antibodies and their respective isotype controls were purchased from BioLegend unless specified otherwise. The Fc blocking antibody was purchased

from BD Biosciences and bovine serum albumin ($\geq 98\%$, BSA) from Sigma Aldrich. Flow cytometry buffer was prepared by adding 1% of BSA and 0.1% of sodium azide (Sigma Aldrich) in 10 mM PBS.

Cell proliferation kit I (MTT) was purchased from Roche and dimethyl sulfoxide (99%, DMSO) from PanReac AppliChem. The ELISA kits for cytokine production analysis were purchased from: R&D Systems (IL-6 kit); PeproTech (IL-12 and TNF- α kit) and BioLegend (INF- γ kit). Goat anti-mouse total IgG-, IgG1-, IgG2a- and IgG2c-HRP conjugated antibodies were purchased from AbD Serotec (Bio-Rad).

Collagenase D and DNase I were purchased from Roche. 1 M EDTA was prepared by dissolving ethylenediaminetetraacetic acid (Sigma Aldrich) in nanopure water at pH = 8 (adjusted with sodium hydroxide). The solution was filtered and autoclaved for its use in cells.

Non-commercial red blood cell (RBC) lysis buffer was prepared by mixing 0.15 M NH_4Cl ($\geq 99.5\%$), 10 mM KHCO_3 (99.7%) and 0.1 mM Na_2EDTA (99%) in nanopure water (pH = 7.4, autoclaved; all of them purchased from Sigma Aldrich). Commercial RBC lysis buffer was purchased from BD Biosciences.

SIINFEKL OVA peptide (257–264) was purchased from Peptides International and Imject[®] Alum, purchased from Thermo Fisher Scientific, was prepared and used as described in the data sheet. Matrigel[®] Matrix was purchased from Corning.

J774A.1 cell line was purchased from ATCC and B16-F10-OVA melanoma cell line was a gift from Dr Pablo Sarobe (Center for Applied Medical Research (CIMA), University of Navarra). MycoAlert[™] Mycoplasma Detection Kit was purchased from Lonza and all cell lines were checked for contamination before use.

4. Animals for in vivo studies

Animals were cared for and handled in compliance with the Guidelines for Accommodation and Care of Animals (European Convention for the Protection of Vertebrate Animals Used for Experimental and Other Scientific Purposes) and internal guidelines, and all the experimental procedures were approved by the appropriate

local authorities. All animals were housed in ventilated cages and fed on a standard diet *ad libitum*.

Instrumentation

1. TEM

TEM studies were conducted on a JEOL JEM-2011 electron microscope operating at 200 kV. The samples were prepared by depositing a drop of IONPs solution onto a copper specimen grid coated with a carbon film and allowing it to dry. For IONP size determination using TEM, a minimum of 300 particles were measured using the *Image J* software.

2. DLS and zeta potential

Particle size analysis was measured with a NanoSizer (Malvern Nano-Zs, UK) with 173° scattering angle at 25 °C. For each sample, the correlation function was measured at least three times and the average value was used for data fitting.

Zeta potential measurements were performed with the mentioned NanoSizer instrument at 25 °C and with a cell drive voltage of 25 V using a Smoluchowski model.

3. UV-visible spectrophotometer and fluorospectrometer

UV-visible absorption spectra were recorded on a NanoDrop ND 1000 Spectrophotometer (NanoDrop Technologies) and on a V-630 Bio Spectrophotometer (JASCO Analytical Instruments).

The measurement of the absorbance in 96-well plates was performed on a TECAN Genios Pro 96/384 multifunction microplate reader.

The fluorescence spectra were recorded on a NanoDrop ND 3300 Fluorospectrometer (NanoDrop Technologies).

4. ICP-AES analysis

To determine the iron content in each sample, IONP-filled micelles were disintegrated by digestion at room temperature (RT) with nitric acid (70%, Fisher Scientific) over two days (100 μ L nitric acid and 40 μ L IONP-filled micelles). Digested sample was diluted with nanopure water up to 10 mL, in order to have 1% of nitric acid in the final sample for ICP-AES analysis.

ICP-AES studies were performed on a Perkin Elmer Optima 5300 DV (Perkin Elmer, Santa Clara, USA) at the SGIker analytical facility of the Universidad del País Vasco (UPV/EHU; Leioa, Spain), employing an RF forward power of 1400 W, with argon gas flows of 15, 0.2 and 0.75 L/min for plasma, auxiliary, and nebuliser flows, respectively. Using a peristaltic pump, sample solutions were taken up into a Gem Tip cross-Flow nebuliser and Scotts spray chamber at a rate of 1.50 mL/min. The instrument was operated in axial mode. To measure the iron content in the samples, three wavelengths (238.024, 239.562, 259.939 nm) were selected analysed in a fully quant mode (three points per unit wavelength). A range of calibration standards were prepared using single element 1000 mg/l stock solutions (Fisher Scientific UKLTD) and a Merck multi element standard (ICP Multi element standard solution, VICertipur®) was employed as a reference standard.

5. Flow cytometry

Flow cytometry experiments were carried out using a FACS Canto II (BD Bioscience) system, which has an excitation source composed of three lasers: violet (405 nm), blue (488 nm) and red (633 nm). Scattered light and fluorescence signals coming from the sample are directed by collection optics through spectral filters to the detectors. The collection optics in the used FACS Canto II was configured as follows: a trigon for the violet laser (450/50 nm and 510/50 nm bandpass filters); an octagon for the blue laser (530/30 nm, 585/42 nm, 695/40 nm and 780/60 nm bandpass filters); and a trigon for the red laser (660/20 nm and 780/60 nm bandpass filters). In each experiment, non-labelled and single labelled samples were included as control and as compensation samples, respectively. Collected data were analysed using the FlowJo, LCC software.

6. Fluorescence microscopy

Fluorescent cell images were obtained using a Zeiss Axio Observer wide field fluorescence microscope (Carl Zeiss, Germany) equipped with a Plan Apochromat 20x objective (numerical aperture of 0.8) and using bright field as contrast method for transmitted light channel. The Colibri LED module was used for fluorescence excitation (365 nm, 470 nm and 590 nm filters) and fluorescence emissions was collected with a high-efficiency multi-band pass Colibri filter set (bandpass filters of 402-448 nm and 500-557 nm, and a 615 nm longpass filter). AxioVision software was used to analyse and process obtained images.

Methods

1. Synthesis and characterisation of the IONP samples

a. Synthesis of hydrophobic IONPs

The synthesis of the oleic acid-coated IONPs (magnetite; Fe_3O_4) was carried out as described previously.¹ In order to get 6–7 nm IONPs by the thermal decomposition method, $\text{Fe}(\text{acac})_3$ (2 mmol), 1,2-hexadecanediol (10 mmol), oleic acid (6 mmol), oleylamine (6 mmol), and benzyl ether (20 mL) were mixed and magnetically stirred under a flow of nitrogen. The mixture was first heated to 200 °C for 2 h and then, still under nitrogen, brought to 300 °C for 1 h. The black-colored mixture was cooled to RT by removing the heat source. Under ambient conditions, ethanol (40 mL) was added to the mixture, and the material was precipitated and separated via centrifugation. The black product was dissolved in hexane (10 mL) containing oleic acid (0.05 mL) and oleylamine (0.05 mL). Centrifugation (3000g, 10 min) was applied to remove any undispersed residue. The product, *ca.* 7 nm Fe_3O_4 NPs, was then precipitated with ethanol, and isolated by centrifugation (3000g, 10 min). The dried powder was stored into plastic containers at RT until use.

The dried powder was redispersed in hexane or chloroform for TEM characterisation or micelle formation.

b. Synthesis of IONP-filled micelles

For the synthesis of IONP-filled micelles, different ratios of lipids and IONP to-lipid ratios were used to optimize the properties (e.g., size and charge) for subsequent attachment of CpG ODNs and OVA. The reported results were obtained with micelles prepared in the following way.² Hydrophobic magnetite NPs (1 mg) were dissolved in chloroform (500 μ L) with one of the following PEG-PLs mixtures:

- DPPE-mPEG(2000) (2 mg);
- DSPE-aPEG(2000) (2 mg);
- DPPE-mPEG(2000) (2 mg) and DOTAP (1 mg);
- DPPE-mPEG(2000) (1 mg) and DSPE-cPEG(2000) (1 mg).

After complete evaporation of the chloroform, the dried film was placed for 30 s in a water bath at 80 °C and hydrated by adding 500 μ L of nanopure water. The solution was transferred to an Eppendorf and centrifuged at 9700g for 5 min. The pellet, containing non-micelle enclosed IONPs, was discarded. The supernatant was passed through a 0.45 μ m filter and the resultant solution was centrifuged 3 times at 369 000g for 45 min in order to eliminate the empty micelles. Finally, the pellet containing IONP-filled micelles was dissolved in 400 μ L of nanopure water or PBS and stored at RT.

Hydrodynamic size and zeta potential of the IONP-filled micelles was characterised using the aforementioned NanoSizer and the iron content measured by ICP-AES as previously described.

c. Synthesis of fluorescently labelled IONP-filled micelles

For the preparation of fluorescent micelles, DPPE-Rho (at 1–5% of total moles of lipids) was added to the chloroform solutions containing the PEG PLs and hydrophobic IONPs and the entire synthesis protocol was conducted as previously described but protected from light. The UV-visible absorption spectra of the fluorescently labelled IONP-filled micelles were recorded on the V-630 Bio Spectrophotometer and the fluorescence spectra on the NanoDrop ND 3300.

d. Synthesis of radiolabelled IONP-filled micelles

Commercially available gallium citrate solution (specific activity =1.4 TBq/ μmol) was converted into $^{67}\text{GaCl}_3$ following a previously reported method.³ Briefly, the gallium citrate solution was passed through a light silica column cartridge (Sep-Pak, Waters) to selectively retain the radiometal. The cartridge was washed with ultrapure water (10 mL) and ^{67}Ga was finally eluted with HCl 0.1 M solution. The eluate was collected in different 100 μL fractions, and only those containing the maximum activity concentration were used in subsequent labelling experiments. The eluted ^{67}Ga chloride solution (100 μL , *ca.* 37 MBq) was then mixed with 50 μL of IONP micelle solution and diluted up to final volume of 350 μL in acetate buffer (pH = 3.8 ± 0.1). After incubation at 70 °C during 30 min, the reaction was cooled down to RT and the labelled NPs were separated via centrifugal filtration (6708g for 10 min) using Amicon Ultracel 100k (MWCO 100 kDa) centrifugal devices (Merck), and washed twice with phosphate buffered solution. The retentate was recovered from the filter by the addition of nanopure water or PBS (100 μL). The total radioactivity in the filtrates and retentates were measured in a CRC-25R dose calibrator (Capintec, USA) in order to determine the incorporation efficiency.

For stability studies, one batch of ^{67}Ga -IONP micelles was fractioned in different aliquots, which were incubated in the presence of DOTA chelating agent (10^6 moles of DOTA per mole of NP) at 37 °C. At different time points, the samples were filtered in order to separate the NPs from the ^{67}Ga complexed to DOTA, and radioactivity in the retentate and in the filtrate was measured in a 2470 WIZARD² Automatic Gamma Counter (PerkinElmer). The dissociation of ^{67}Ga (expressed in percentage) from the radiolabelled micelles at each time point was calculated as the ratio between the amount of radioactivity in the filter and the starting amount of radioactivity.

2. Synthesis and characterisation of the biofunctionalised samples

a. Attachment of CpG ODNs

Lyophilized CpG was resuspended in cell culture grade HyClone Water (Thermo Scientific) to a final concentration of 200 μM , aliquoted and stored at -20 °C until use.

The IONP-DOTAP micelle stock solution ([IONP] = 2 μ M) was mixed with CpG ODNs in a ratio of 66 mol of CpG ODNs per mole of NP, in a final volume of 500 μ L nanopure water. The mixture was stirred overnight at 700 rpm at RT. The unbound CpG ODNs were eliminated by ultrafiltration through a NanoSep 100k (MWCO 100 kDa) centrifugal device (Pall Life Sciences) at 1844g for 5 min (3 cycles) and by further ultracentrifugation (369 000g, 45 min, 4 cycles). The final pellet was resuspended in the same initial volume of nanopure water or PBS and stored at 4 $^{\circ}$ C.

b. Attachment of OVA protein

- *Covalent attachment.* To the solution of DSPE-cPEG(2000)-containing IONP micelles (stock [IONP] = 3 μ M), EDC and NHSS in 1:25:25 molar ratio were stirred for 2 h at RT for activation of the carboxylic acid groups. The excess of EDC/NHSS was eliminated by ultrafiltration through a NanoSep 100k (MWCO 100 kDa) centrifugal device (Pall Life Sciences) (1844g for 5 min, 3 cycles). The resulting activated IONP micelles were resuspended in the same initial volume and stirred overnight at RT with purified endotoxin-free OVA in a final volume of 300 μ L nanopure water. The unbound OVA was eliminated by ultrafiltration at 1844g for 5 min (4 cycles). The pellet was resuspended in the initial volume of nanopure water or PBS and stored at 4 $^{\circ}$ C.

- *Attachment by adsorption.* The protocol was conducted in the same way excluding the step where carboxylic acid groups were activated with EDC/NHSS linkers.

All experiments were carried out using the OVA-IONP micelles formed by covalent attachment, unless specified otherwise.

c. Characterisation of the CpG-IONP and OVA-IONP micelles

The Fe concentration in the samples was determined by ICP-AES analysis carried out as previously described.

The quantification of bound CpG ODNs was performed by hydrolysis of a known concentration of IONP micelle in the presence of 0.2 M NaOH. The mixture was stirred overnight at RT and ultracentrifuged (369 000g, 40 min) to pellet down the hydrolysed micelles. The UV-visible absorbance (λ_{\max} = 260 nm) of the supernatant was measured

Experimental section

using a NanoDrop ND 1000 Spectrophotometer and converted to concentration by comparison to a standard curve.

The amount of OVA bound to IONP-COOH micelles was quantified using the BCA protein assay reagent kit (Thermo scientific), after absorbance subtraction of the same concentration of parent IONP-COOH micelles. In this case, the absorbance measurements (550 nm) were performed in a 96-well plate with a TECAN Genios Pro microplate reader.

The UV-visible absorption spectra of samples were also measured using NanoDrop ND 1000 and a V-630 Bio Spectrophotometer and compared against solutions of free OVA/CpG and parent IONP micelles.

The size of the IONP-filled micelles was analysed by TEM and DLS using the NanoSizer. Superficial charge of the IONP-filled micelles was determined using the NanoSizer.

3. *In vitro* procedures and studies

a. Cellular uptake studies by flow cytometry

- *J774A.1 cell line.* J774A.1 cells were plated in 96-well plates (1×10^5 cells/well) and allowed to adhere overnight in DMEM medium supplemented as described before. Fluorescent IONP formulations containing the DPPE-Rho phospholipid were diluted in medium and added to cells, which were maintained at 37 °C, 5% CO₂ during 3 h. After the incubation with the formulations (*ca.* 0.15 μM of magnetite, equivalent to 7.72 μg per well), the medium was removed and cells were transferred to cytometer tubes by gentle pipetting in sterile PBS and pellet down by centrifugation (580g, 5 min, 4 °C). Cells were resuspended in a final volume of 200 μL of flow cytometry buffer. Rhodamine uptake was measured using the FACS Canto II cytometer and the data were analysed using the FlowJo, LCC software. J774A.1 cells were electronically gated based on the forward and side scatter parameters and the not-single events left out based on forward area and height scatter parameters. Rhodamine signal (585/42 nm) coming from the IONP-filled micelles was analysed within this population.

- *BMDC primary culture.* In order to obtain BMDCs BALB/c mice (6–12 weeks old) were sacrificed by cervical dislocation and intact femurs and tibiae of hind limbs were removed aseptically. Bones were washed in cold PBS and bone marrow was flushed with cold PBS using a syringe as described elsewhere.⁴ Clusters within the marrow were disaggregated to get a homogeneous cell suspension and after the erythrocytes were lysed with the non-commercial RBC lysis buffer, the cells were washed and resuspended in RPMI-1640 supplemented as previously described. On day zero cells were plated at a concentration of 2×10^6 cells per 100 mm bacteriological Petri dish (Falcon) in 10 mL of medium supplemented with 20 ng/mL of murine GM-CSF (Peprotech) and maintained in a humidified incubator with 37 °C and 5% CO₂. On day 3, 10 mL of complete RPMI-1640 medium containing GM-CSF (20 ng/mL) was added to each Petri dish. On day 6, half of the supernatant was collected, centrifuged and cell pellet resuspended in 10 mL of fresh complete RPMI-1640 with GM-CSF (10 ng/mL) and added again to each Petri dish. Finally, at day 8–9 of the differentiation process BMDCs were plated in 96-well plates (2×10^5 cells/well) in the presence of the fluorescent formulations (*ca.* 0.15 μ M of magnetite, equivalent to 7.72 μ g per well) and incubated overnight at 37 °C, 5% CO₂. As in the case of J774A.1 cell line, BMDCs were electronically gated based on the forward and side scatter parameters and the not-single events left out based on forward area and height scatter parameters. Within this population cells were gated based on double positive staining for CD11c (APC-labelled anti-CD11c, from BD Bioscience; 660/20 nm) and MHC class II (PerCP-Cy5.5-labelled anti-IA/IE; 695/40 nm) population markers and rhodamine uptake (585/42 nm) analysed within this population.

b. Cellular uptake studies by fluorescence microscopy

Cells were plated in an ibidi μ -Slide VI 0.4 (3×10^4 J774A.1 cells/channel and 9×10^4 BMDCs/channel) and allowed to adhere overnight in the presence of complete medium (DMEM for J774A.1 and RPMI-1640 for BMDC). The medium was changed and the cells were incubated with the solution containing CpG- or OVA-IONPs micelles labelled with rhodamine B for up to 3 h (*ca.* 0.11 μ M of magnetite, equivalent to 2.76 μ g per channel). The medium was removed and fresh medium containing LysoTracker

Experimental section

(1 μ M) was added. After 45 min, the medium was removed, the cells were washed twice with sterile PBS and the complete medium was added to preserve the cells.

To investigate if the CpG-IONPs micelles target TLR 9, the cells were seeded as above, but after the NP incubation step, the cells were treated as follows. The medium was removed and the adherent cells were fixed and permeabilised for 20 min with BD Cytotfix/Cytoperm fixation and permeabilisation kit at 4 °C. After being washed twice with BD Perm/wash buffer, the blocking buffer (10% FBS in PBS) was then added for 20 min at RT. The cells were incubated overnight at 4 °C with the primary anti-TLR 9 mouse antibody (10 μ g/mL) in blocking buffer. Then at RT, the cells were washed twice with sterile PBS. Alexa488-labelled goat anti-mouse secondary antibody (1 μ g/mL in blocking buffer, 1 h) was used for staining of the primary TLR 9 antibody. In all cases, nuclei were stained with DAPI (1 μ g/mL in medium for J774A.1 cells and 5 μ g/mL for BMDCs) for 15 min at 37 °C.

Cells were visualized using the Zeiss Axio Observer wide field fluorescence microscope: DAPI was visualised using the 365 nm excitation filter and the collection filter with a bandpass of 402-448 nm; the LysoTracker green fluorophore or the TLR 9 visualization was done using the 470 nm excitation filter and the signal collected with the 500-557 nm bandpass filter; and the rhodamine B was excited using the 590 nm filter and the signal collected with the 615 nm longpass filter. Brightfield and fluorescence images were collected and processed using AxioVision software.

c. Cytotoxicity studies by MTT assay

Cells were seeded (J774A.1: 3×10^4 cells/well in DMEM medium; BMDC: 2×10^5 cells/well in RPMI-1640 medium containing 20 ng/mL GM-CSF) in 96-well plates (100 μ L/well). For the J774A.1 macrophages, cells were allowed to adhere to the plate overnight. Then, medium was removed and cells were left untreated or treated with CpG-IONP micelles and the corresponding controls (IONP-DOTAP micelles and free CpG ODNs), diluted accordingly in medium, in triplicate. In the case of BMDC, samples to be tested were added directly to the DC containing wells (100 μ L/well) diluted accordingly in medium, in triplicate. After 24 h incubation at 37 °C cell supernatant was removed and frozen for subsequent cytokine analysis. The cell viability was measured using the

MTT assay. 100 μ L of MTT reagent (0.25 mg/mL in DMEM for J774A.1 or RPMI-1640 in the case of BMDCs) was added per well after the removal of the supernatant. Cells were incubated at 37 °C for 1 h, after which the medium was removed and the lysis solution (200 μ L of DMSO) was added. The absorbance of samples was measured using the microplate reader at 550 nm and data represented as the cell viability compared to untreated control wells. The experiments were repeated three times and expressed as mean \pm SEM.

d. Quantification of cytokine production by ELISA

The supernatants collected from the cell culture studies described in the previous section were analysed for cytokine production using sandwich ELISA following the manufacturer's instructions. A 4-parameter sigmoidal (logistic) standard curve was used to quantify the cytokine present (GraphPad Prism software). The measurement of each sample was conducted in duplicate and results were expressed as mean \pm SEM in pg/mL or ng/mL of three independent experiments.

e. BMDCs maturation assay by flow cytometry

BMDCs were counted and resuspended in complete RPMI-1640 medium at a final concentration of 2×10^5 cells per well (100 μ L) in 96-well plates. BMDCs were kept unstimulated or were stimulated with CpG-IONP micelles, the corresponding amount of parent IONP micelles or free CpG ODNs (2.7nM of magnetite and 0.2 μ g/mL of CpG ODNs, added in 100 μ L per well) and incubated overnight at 37 °C. BMDCs were stained with APC-labelled anti-CD11c (660/20 nm), PerCP-Cy5.5-labelled anti-IA/IE (695/40 nm), FITC-labelled anti-CD80 (530/30 nm), PE-labelled anti-CD86 (585/42 nm), and Pacific Blue-labelled anti-CCR7 antibodies (450/50 nm). The expression of the different molecules was analysed using the FACS Canto II flow cytometer. In this case, DCs gating strategy was done using only the population marker CD11c and maturation markers expression, including MHC class II (IA/IE), was analysed within this CD11c⁺ DC population. Isotype controls were included in each assay and were not included in the figures for clarity purposes. Results were expressed as mean \pm SEM of the MFI of each maturation marker of three independent experiments.

4. *In vivo* trafficking and biodistribution studies

a. CpG ODNs and OVA *in vivo* uptake by flow cytometry

BALB/c mice (6–8 weeks old) were subcutaneously injected into the right flank with FITC-labelled CpG-IONP micelles and Alexa647-labelled OVA-IONP micelles (100 μ L, 5 μ g of CpG, 5 μ g of OVA and *ca.* 31 μ g of IONP per mouse). 6 h after administration mice were sacrificed by cervical dislocation and spleens harvested and processed as described elsewhere⁵ and in darkness to avoid fluorophores quenching. 1×10^6 cells diluted in RPMI-1640 were placed per well in a round-bottom 96-well-plate. After washing twice cells with PBS, cells were stained with the markers for the different cells populations: APC-Cy7-labelled anti-CD11c (780/60 nm, trigon for the red laser), PerCP-Cy5.5-labelled anti-CD19 (695/40 nm) and PE-Cy7-labelled anti-F4/80 (780/60 nm, octagon for the blue laser). Cells were resuspended in a final volume of 200 μ L of flow cytometry buffer and the fluorescence of FITC (530/30 nm, CpG ODNs) and Alexa647 (660/20 nm, OVA) was analysed into each defined population. Results were expressed as mean \pm SEM of the MFI of CpG ODN/OVA of 4 mice per group of immunization, analysed individually and compared to PBS injected mice.

b. IONP-filled micelles biodistribution by SPECT/CT

SPECT/CT biodistribution studies were performed both in healthy BALB/c mice and in tumour bearing C57BL/6 mice (6–8 weeks old):

- *Healthy BALB/c mice.* Animals received injection of ⁶⁷Ga-IONP micelles suspended in PBS via different administration routes: subcutaneously on the inner side of the front forearm (30 μ L, 7.7 MBq in the left limb) or into the hock (the lateral tarsal region just above the ankle) (30 μ L, 7.3 MBq in the left limb) or in the flank (30 μ L, 6.4 MBq in the left side). The total amount of magnetite injected for each administration route was 8 μ g.

- *Tumour bearing C57BL/6 mice.* Animals were subcutaneously injected into the right back with 4×10^5 B16-F10-OVA cells diluted in a mixture of Matrigel[®] Matrix and PBS (volume ratio of cells and Matrigel[®] Matrix mixture 1:1). When tumour volume was *ca.* 100–150 mm³, mice were subcutaneously injected with biofunctionalised ⁶⁷Ga-

IONP micelles suspended in PBS in the flank or into the hock (50 μ L per mouse, in the right side of the animal). The total amount of magnetite injected for each administration was *ca.* 22 μ g of magnetite and the total radioactivity was 40–45 MBq.

In all cases, with the mouse under isoflurane anaesthesia (1.5–2% in oxygen), whole-body SPECT/CT scans were acquired at 3, 24 or 48 h post-injection. With the full ring detector, 360° of data were acquired by rotating the collimator 45° (45 steps, 1°/step). Data were collected in an energy acquisition window from 125–150 keV to 84–102 keV and acquisition times from 60 min (80 s/step) to 45 min (60 s/step). During image acquisition, mice were kept normothermic by the use of a heating blanket (Homeothermic Blanket Control Unit; Bruker BioSpin GmbH, Karlsruhe, Germany). After each SPECT scan, CT acquisitions were performed to provide anatomical information on each animal. The CT acquisition consisted of 220 views in 0.88° increments around the animal with 16 ms exposure per view. The X-ray tube settings were 70 kV and 32 mA. SPECT/CT images were acquired using the eXplore speCZT CT preclinical imaging system (GE Healthcare, USA). The system combines SPECT and CT on one gantry, allowing co-registration of the SPECT and CT data sets without additional postprocessing. The SPECT scanner uses a stationary, full ring of CZT detectors and interchangeable rotating cylindrical collimators. An 8-slit collimator was used with a field of view of 32 and 78 mm in the transaxial and axial directions, respectively. The SPECT images were reconstructed using the OSEM iterative algorithm (5 and 15 subsets, 3 and 5 iterations) into 128 \times 128 \times 32 array with a voxel size of 0.4 \times 0.4 \times 2.46 mm, and were not corrected for scatter and attenuation. The CT images were reconstructed using a cone beam filtered back-projection Feldkamp algorithm into 437 \times 437 \times 523 array with a voxel size of 0.2 \times 0.2 \times 0.2 mm. At the end of the scanning procedure, 24 or 48 h post-injection, the mice were culled by cervical dislocation and organs of interest removed for further *ex vivo* SPECT/CT imaging under the same conditions of the *in vivo* images. Analysis of the injected dose percentage per organ was performed by measuring their activity with a 2470 WIZARD² Automatic Gamma Counter (PerkinElmer).

5. *In vivo* immunization studies

a. Collection of blood serum

In order to analyse the production of circulating cytokines and anti-OVA IgG antibodies, blood was taken (25–50 μ L) via the facial vein using disposable precision glass capillary tubes soaked in heparin. Collected blood was diluted in PBS and centrifuged (13 000g, 5 min) to separate the serum (supernatant) from blood cells (pellet). Blood sera were stored at -20 °C until its analysis by ELISA.

b. Purification of peripheral blood cells

In order to analyse the circulating CD8⁺ T cells specific for the OVA epitope SIINFEKL, blood was taken (100 μ L) via the facial vein using the aforementioned capillary tubes and diluted up to 4 mL in cold PBS. After centrifugation (1028g, 5 min at 4 °C), the pellet was resuspended in 2 mL of commercial RBC lysis buffer and incubated at RT for 15 min. The lysis was quenched by addition of 2 mL of 5% FBS in PBS. The mixture was washed twice with PBS via centrifugation and resuspended in complete RPMI-1640, ready for further analysis.

c. Splenocytes and lymphocytes primary culture preparation

For the analysis of innate and adaptive immune responses induced *in vivo* after immunization, spleens and draining LNs were removed and processed for further analysis *ex vivo*. Organs were perfused with tissue dissociating mix (3–2.5 mL of collagenase/DNase I diluted in RPMI-1640 medium), cutted into small pieces (spleen) and incubated for 3 min at RT in a sterile Petri dish. The reaction was stopped with 36–30 μ L of 500 mM EDTA (diluted from stock solution in nanopure sterile water and diluted within the Petri dishes 1/85) and organs were dissociated with the plunger of a syringe. RBC lysis was performed in spleen cell suspensions, by adding 1 mL of the non-commercial RBC lysis buffer for 1 min and rapidly quenched with 10 mL of cold PBS. The resulting cell suspensions were recollected into 15 mL tubes, washed twice with cold PBS via centrifugation and resuspended in complete RPMI-1640, ready for the different studies.

d. Assessing innate immune responses *in vivo*

C57BL/6 mice (6–8 weeks old) were injected subcutaneously in both inner sides of the front forearms with the formulations diluted in PBS (20 μ L/forearm, 3.2 μ g of CpG and 38 μ g of IONP per mouse). Both pre-injection, and at various time points thereafter, blood was taken (25 μ L) via the facial vein as described before. Cytokines levels were measured in blood serum by standard sandwich ELISA and data analysed as described in the *in vitro* section. After the final blood collection (24 h after injection) mice were sacrificed by cervical dislocation and the spleen and axillary LN harvested and processed as described above, for further analysis of the maturation of DC and NK cells. Briefly, 1×10^6 cells diluted in RPMI-1640 were placed per well in a 96-well plate and divided into two different staining panels. For the DC maturation, cells were stained as described in the *in vitro* BMDCs maturation assays. In the case of NK panel, cells were stained with Brilliant Violet 421-labelled anti-CD3 (450/50 nm), PE-labelled anti-CD335 (NKp46; 585/42 nm) and APC-labelled anti-CD69 (660/20 nm) antibodies. NK cells population was defined as CD3 negative and CD335 positive, and CD69 expression was analysed into this defined population. Isotype controls were included in the assay but were excluded from the figures for clarity purposes. Results were expressed as mean \pm SEM of the MFI of each maturation markers of 4 mice per group.

e. Assessing adaptive immune responses *in vivo*

Two types of immunization studies were carried out in order to answer different questions: comparison between immunizations with free OVA and OVA-IONP micelles; and analysis of the immune activity of the nanovaccine composed of both the OVA- and CpG-IONP micelles.

- *OVA-IONP micelles immunization studies:* BALB/c mice (6–8 weeks old) were immunized twice with a 2 weeks interval between both injections. OVA free or OVA-IONP micelles dissolved in PBS (5 μ g of OVA and 53 μ g of IONP per mice) were injected via two different routes: subcutaneously into the inner side of the front forearms (20 μ L/forearm; 40 μ L per mouse) or into the flanks (20 μ L/side; 40 μ L per mouse). Blood was taken (50 μ L) via the facial vein at different time points (pre- and post-injection), and serum was analysed for the presence of anti-OVA IgG antibodies measured by

Experimental section

indirect ELISA. The results were expressed as the \log_{10} value of the reciprocal of the end point dilution that gave an optical density (O.D.) higher than the chosen cutoff, after the subtraction of background levels. Six weeks after the last immunization, mice were sacrificed by cervical dislocation and splenocytes harvested as described before. In order to analyse the IFN- γ production, 1×10^6 splenocytes were plated in 96-well plates and incubated for 48 h in the presence of different stimuli (OVA free or in conjugation with IONP micelles (10 $\mu\text{g}/\text{ml}$ OVA). Results were expressed as mean \pm SEM of 9 mice per each group of immunization from two independent studies, analysed individually and compared to unstimulated wells.

- *CpG- and OVA-IONP micelles immunization studies:* C57BL/6 mice (6–8 weeks old) were immunized subcutaneously in the flanks twice with an interval of 2 weeks between injections (200 μL , 5 μg of CpG, 5 μg of OVA and *ca.* 6.9 μg of IONP per mice). Blood was taken (100 μL) as previously described; serum was analysed for the presence of anti-OVA IgG antibodies and peripheral blood cells harvested for further analysis. 35 days after the first injection, mice were sacrificed by cervical dislocation and the splenocytes analysed for SIINFEKL-specific CD8⁺ T cells, extracellular and intracellular IFN- γ production and CD107a degranulation marker expression. The extracellular IFN- γ production was performed as previously described, but placing 8×10^5 cells/well and incubating the cells for 48 h with 10 $\mu\text{g}/\text{mL}$ of SIINFEKL peptide. For the analysis of the SIINFEKL-specific CD8⁺ T cells, 1×10^6 splenocytes or peripheral blood cells were stained with Brilliant Violet 421-labelled anti-CD3 (510/50 nm), PE.Cy7-labelled anti-CD8 (780/60 nm), APC-labelled anti-CD44 (660/20 nm), FITC-labelled anti-CD62L (530/30 nm) and PE-labelled (585/42 nm) H-2k^b-OVA_{257–264} dextramer (Immudex). SIINFEKL specific cell percentage was analysed in the CD8⁺ T cell population (CD3⁺ and CD8⁺ double positive) or in the effector memory CD8⁺ T cell population (inside CD3⁺ and CD8⁺ double positive population, cells showing a phenotype of CD44^{high} and CD62L^{low}). To study intracellular IFN- γ and the expression of the degranulation marker, 1×10^6 cells/well were placed in a 96-well plate in 100 μL of RPMI-1640 medium in the presence of BD Golgi Stop, the PE-labelled (585/42 nm) anti-CD107a antibody (LAMP-1 protein) and 10 $\mu\text{g}/\text{mL}$ SIINFEKL in RPMI-1640 medium. After 5 h of incubation at 37 °C, cells were washed twice and stained with the surface

markers Brilliant Violet 421-labelled anti-CD3 (450/50 nm), Brilliant Violet 510-labelled anti-CD4 (510/50 nm) and PE-Cy7-labelled anti-CD8 (780/60 nm). Then, cells were fixed and permeabilised as previously described (BD Cytofix/Cytoperm fixation and permeabilisation kit), after which intracellular cytokine staining was performed (APC-labelled anti-IFN- γ , 660/20 nm). T cells were gated based on double positive for CD3 and CD8 markers, excluding CD4⁺ cells. Results were represented as IFN- γ and CD107a double positive cell percentage of total CD3⁺ CD8⁺ T cells. Isotype controls were included in intracellular IFN- γ analysis by flow cytometry assay and were not included in the figures for clarity purposes. Results were expressed as mean \pm SEM of 5 mice per group of immunization, analysed individually and compared to unstimulated wells.

6. Tumour challenge

a. Assessing antitumour prophylactic effect

To study the prophylactic effect of the described systems, C57BL/6 mice (6–8 weeks old) were immunized as described above for the combination of CpG- and OVA-IONP micelles immunization studies with slight differences (40 μ L, subcutaneously in the right hock). One week after the second administration, 3.8×10^5 B16-F10-OVA cells diluted in PBS were injected in the right back. Blood was taken (100 μ L) at several time points after the first immunization and SIINFEKL-specific CD8⁺ T cells and T_{EM} cell percentages were analysed as previously described. Animals were monitored for tumour growth using an electronic digital caliper 779A series, from Starrett. Results were expressed as mean \pm SEM of 5 mice per group.

b. Assessing antitumour therapeutic effect

C57BL/6 mice (6–8 weeks old) were subcutaneously injected into the right back with 3×10^5 B16-F10-OVA cells diluted in a mixture of Matrigel[®] Matrix and PBS (volume ratio of cells and Matrigel[®] Matrix mixture 1:1). On day 7, 10 and 13 after tumour implantation (tumour volume *ca.* 100 mm³), mice were treated with the IONP formulations in the right hock (50 μ L, 10 μ g of CpG, 10 μ g of OVA and *ca.* 80 μ g of IONP per mice). Tumour growth was monitored using an electronic digital caliper 779A series, from Starrett. Results were expressed as mean \pm SEM of 5 mice per group.

References:

1. Sun, S. *et al.* Monodisperse MFe₂O₄ (M = Fe, Co, Mn) nanoparticles. *J. Am. Chem. Soc.* **126**, 273–279 (2004).
2. Carion, O., Mahler, B., Pons, T. & Dubertret, B. Synthesis, encapsulation, purification and coupling of single quantum dots in phospholipid micelles for their use in cellular and in vivo imaging. *Nat. Protoc.* **2**, 2383–2390 (2007).
3. Ščasnár, V. & van Lier, J. E. The use of SEP-PAK SI cartridges for the preparation of gallium chloride from the citrate solution. *Eur. J. Nucl. Med.* **20**, 273–273 (1993).
4. Lutz, M. B. *et al.* An advanced culture method for generating large quantities of highly pure dendritic cells from mouse bone marrow. *J. Immunol. Methods* **223**, 77–92 (1999).
5. Schmidt, S. T. *et al.* The administration route is decisive for the ability of the vaccine adjuvant CAF09 to induce antigen-specific CD8⁺ T-cell responses: The immunological consequences of the biodistribution profile. *J. Control. Release* **239**, 107–117 (2016).

Acknowledgements

First of all, I would like to express my gratitude to Professor Juan C. Mareque Rivas for giving me the opportunity to undertake my PhD thesis under his supervision. When looking back, I am very grateful for these five years of trust, assistance and dedication. I thank him for showing me how the world of science works and allowing me to grow as a researcher in all aspects. I am also thankful to Professor Miguel Trueba Conde for being my University Tutor; to Professor Adolfo Bornaetxea and Professor Xabier Artola for helping me with the translation of the abstract.

I also want to thank Professor Luis Liz Marzán, scientific director of CIC biomaGUNE, for allowing me to conduct the experimental work of this PhD at a centre of international excellence. The multi-disciplinary environment and the available equipment have allowed me to learn diverse techniques and gain extensive knowledge. This thesis would be never possible without the unconditional support of the specialised platforms at CIC biomaGUNE, specially the Radiochemistry and Nuclear Imaging Platforms (Vanessa) and the Animal Facility (Ander, Ainhoa, Clara and Sergio).

I want to thank to Dr. Dennis Christensen for allowing me to conduct a short stay at his laboratory and guiding me over the experiments performed at Statens Serum Institut, Copenhagen. I want also to express my gratitude to Dr. Signe Tandrup Schmidt for helping and supporting me during those three months.

I fell grateful for having fantastic laboratory colleagues over these five years that have help me in all the challenges that I have faced during the thesis. Special thanks go to: Luca, thanks to your experience and your generosity, you have helped me to become a better researcher and have given me new opportunities key for my professional career; Maca, who has helped me more than I could ever imagine, you are a friend that has always been there for listening; Malou, you have been my role model apart from becoming a compatriot and a friend forever; Aintzane, the person who has taught me so much about immunology and how to interpret it, you are an excellent friend and an example to follow; Nina, thanks for your patience and your excellent day-to-day work, this thesis would be never possible without you; Emmanuel, the most positive

Acknowledgements

man that I have ever known, I have the feeling that I still have a lot to learn from you; Silvia, your good mood and calmness make each day better at the laboratory and outside it; Idoia, although you are the most recent incorporation, your enthusiasm and positivity has transform the laboratory into a better place to work; Amaia, it has been a pleasure to carry out the PhD in parallel with you, I wish you the best in the future; also thanks to the rest of the colleagues and former members of the group: Anja, Javi, Ana, Giordano, Chus, Juan B. and Valentina.

Apart from the laboratory mates, I also want to thank people at CIC biomaGUNE that have helped me in one way or another, both professionally and personally: the guys from RQ, the coolest boys at the centre, Aitor, Xabi, Victor, M. Errasti, M. Gonzalez, Boguslaw and Unai, but also the marvellous girls Maria P., Olatz and specially Zuriñe for helping me both experimentally and personally; and finally, my beloved Eunice and funny Fernando, thank you all.

Out of the work circle, I would like to especially acknowledge my good friends: Mònica, mi alma gemela desde el primer momento que te oí hablar, estoy totalmente segura de que todavía tenemos mucho por vivir juntas; Pablo, quiero agradecerte todo lo que me has enseñado y lo que aún me queda por aprender de ti; Betta, por alentarme y enseñarme en mis primeros pasos en la ciencia; mi kuadrila adoptiva Olatz, Amaia, Ima y Naia, Los Cuatro Fantásticos, gracias por estar ahí cuando lo he necesitado; y Unayo, espero que sigas estando a mi lado por mucho tiempo.

And last but not least, I want to really thank the support of my family: Aitor, gracias por estar ahí en lo bueno y en lo malo y por tener la paciencia suficiente para aguantarme; mis tías y tíos y en especial a mis primas Ibone y Nerea, niretzako ahizpak bezala izateagatik; Aita, hemen ez egon arren, oso gertu sentitzen zaitudalako (mila kilometrora, bihotzetik gertu alegia); Iker, te admiro muchísimo y eres el hermano que ni en mis mejores sueños habría deseado; y finalmente Isabel, la mejor madre del mundo, lo único que puedo decir es que absolutamente todo lo que soy es gracias a ti.

Mila esker.

Curriculum Vitae

Ane Ruiz de Angulo Dorronsoro
ORCID ID: 0000-0001-6581-4038
(+34) 625 20 48 95
ruizdeangulo.a@gmail.com

Publications

- Alonso-de Castro, S.; Ruggiero, E.; **Ruiz-de-Angulo, A.**; Rezabal, E.; Mareque-Rivas, J. C.; Lopez, X.; López-Gallego, F.; Salassa, L. Riboflavin as bioorthogonal photocatalyst for the activation of a Pt^{IV} prodrug. *Chemical Science* **2017**, *8* (6), 4619–4625. [Impact factor: 9.14]
- **Ruiz-de-Angulo, A.**; Zabaleta, A.; Gómez-Vallejo, V.; Llop, J.; Mareque-Rivas, J. C. Microdosed lipid-coated ⁶⁷Ga-magnetite enhances antigen-specific immunity by image tracked delivery of antigen and CpG to lymph nodes. *ACS Nano* **2016**, *10* (1), 1602–1618. [Impact factor: 13.33]
- Cobaleda-siles, M.; Henriksen-Lacey, M.; **Ruiz-De-Angulo, A.**; Bernecker, A.; Vallejo, V. G.; Szczupak, B.; Llop, J.; Pastor, G.; Plaza-garcia, S.; Jauregui-osoro, M.; Meszaros, L. K.; Mareque-rivas, J. C. An iron oxide nanocarrier for dsRNA to target lymph nodes and strongly activate cells of the immune system. *Small* **2014**, *10* (24), 5054–5067. (Frontispiece) [Impact factor: 8.37]

Conference proceedings

Oral presentations

- **Ruiz-de-Angulo, A.**; Zabaleta, A.; Baz, Z.; Llop, J.; Mareque-Rivas, J. C. Traceable iron oxide based nanoparticles for antigen/adjuvant *in vivo* delivery to lymph nodes. *International Conference on Nanomedicine and Nanobiotechnology (ICONAN) 2016*, Paris, France.
- **Ruiz-de-Angulo, A.**; Mareque-Rivas, J. C. Traceable microdosed ⁶⁷Ga-magnetite-filled micelles for antigen/adjuvant delivery to lymph nodes. *Early Career Researchers Meeting of the British Society for NanoMedicine 2016*, Swansea, UK.

- **Ruiz-de-Angulo, A.**; Zabaleta, A.; Mareque-Rivas, J. C. Traceable iron oxide based nanoparticles for antigen/adjuvant *in vivo* delivery to lymph nodes. *1st Young Researchers Workshop on Biomaterials and Applications (bioMAPP) 2015*, San Sebastian, Spain.

Poster presentations

- **Ruiz-De-Angulo, A.**; Henriksen-Lacey, M.; Cobaleda-siles, M.; Mareque-Rivas, J. C. Iron oxide nanoparticles functionalized to activate immune responses. *The Ninth Elsinore Meeting On Infection Immunity 2013*, Elsinore, Denmark.

Other Contribution to Conference

- Oral presentation. Gómez Blanco, N.; Regueiro Figueroa, M.; **Ruiz-de-Angulo, A.**; de Blas, A.; Rodríguez Blas, T.; Mareque-Rivas, J. C. Theranostic nanomaterial: Dinuclear Gd(III) complex based magnetic resonance imaging and pH-controlled anticancer drug delivery. *9th International Conference on f-Elements (ICfE) 2015*, Oxford, UK.
- Oral presentations. *4th Early Stage Researchers Workshop in Nanoscience 2014*, Madrid, Spain:
 - Cobaleda-siles, M.; Henriksen-Lacey, M.; **Ruiz-De-Angulo, A.**; Mareque-Rivas, J. C. Iron oxide nanoparticles carrying dsRNA and targeting lymph nodes for immunotherapy.
 - Hernández Gil, J.; Cobaleda-siles, M.; **Ruiz-De-Angulo, A.**; Mareque-Rivas, J. C. Magnetic nanoparticles combined with Pt(IV) prodrugs and immunostimulatory dsRNA for theranostic applications.
 - Gómez Blanco, N.; Regueiro Figueroa, M.; **Ruiz-de-Angulo, A.**; de Blas, A.; Rodríguez Blas, T.; Mareque-Rivas, J. C. Nanosized materials based on dinuclear Gd(III) complexes as novel theranostic carriers.
- Poster presentation. Bermejo, I. A.; **Ruiz-de-Angulo, A.**; Martínez-Sáez, N.; Mareque-Rivas, J. C.; Busto, J. H.; Avenozza, A.; Peregrina, J. M.; Corzana, F. New

generation of cancer vaccines based on IONPs. *III Biennial Meeting of the Chemical Biology Group 2016*, Madrid, Spain.

- Poster presentation. Gómez Blanco, N.; Regueiro Figueroa, M.; **Ruiz-de-Angulo, A.**; de Blas, A.; Rodríguez Blas, T.; Mareque-Rivas, J. C. Theranostic nanomaterial: Dinuclear Gd(III) complex based magnetic resonance imaging and pH-controlled anticancer drug delivery. *XXXV Biennial Meeting of the Spanish Royal Society of Chemistry 2015*, A Coruña, Spain.

Short stays during the PhD

Host investigator	Institution	Period
Juan Bautista Blanco Canosa	Institute for Research in Biomedicine (Barcelona)	1-5 August 2016
Dennis Christensen	Statens Serum Institut (Copenhagen)	April 2015 – July 2015

Scientific formation

- **Course in experimental design for animal studies.** *Charles River Laboratories 2016*, CIC biomaGUNE, Spain. [Duration: 14 h]
- **PET/SPECT practical training.** *Nuclear Imaging Platform 2016*, CIC biomaGUNE, Spain. [Duration: 4 h]
- **Advanced training in Confocal Microscope.** *Optical Spectroscopy Platform 2015*, CIC biomaGUNE, Spain. [Duration: 4 h]
- **Initiation training in Radiochemistry Lab.** *Radiochemistry Platform 2015*, CIC biomaGUNE, Spain. [Duration: theoretical exam of 1 h]
- **Zeiss technology workshop.** *Carl Zeiss Iberia 2015*, Centro Nacional de Investigaciones Cardiovasculares (CNIC), Spain. [Duration: 26 h]
- **Recognition of Pain, Suffering and Distress in laboratory animals.** *Charles River Laboratories 2014*, online course. [Duration: 4 h]

- **Nuclear Image quantification in PMOD software.** *Image Analytics Platform 2014*, CIC biomaGUNE, Spain. [Duration: 4 h]
- **1st course in flow cytometry : techniques and application to clinic and research.** *Inbiomed Foundation & IDIVAL Foundation 2014*, Inbiomed Foundation, Spain. [Duration: 24 h]
- **Innovative tools and approaches for optimizing multicolour design: Resolving stem cell heterogeneity using flow cytometry panel discussion.** *BD Bioscience 2014*, University of Basque Country, Spain. [Duration: 6 h]

Fellowships

Grant	Awarding institution	Period
PREDOC grant (BFI-2012-270)	Basque Government	November 2012 – Present
EGONLABUR grant (EP_2015_1_3)	Basque Government	April 2015 – July 2015
CRUE CEPYME, company internship grant (MED034/2012)	Santander bank	July 2012 – September 2012
ERASMUS grant (E BARCELO 02)	Spanish Government	February 2011 – May 2011
AGAUR grant (MOBINT 2010-2011)	Government of Catalonia	February 2011 – May 2011

Tutoring of Bachelor and Master students

	Student name	Period
Bachelor student from Nantes Atlantic College of Veterinary Medicine, Food Science and Engineering	Emma Lafond-Thenaille	July 2016 – August 2016
Master student from University of the Basque Country	Idoia Mikelez Alonso	February 2016 – June 2016

eman ta zabal zazu



Universidad
del País Vasco

Euskal Herriko
Unibertsitatea

CIC 
bioma**GUNE**

Biomaterialetako Ikerkuntza Kooperatiboko Zentroa
Centro de Investigación Cooperativa en Biomateriales